NEUTRAL AND CATIONIC ORGANOANTIMONY(V) LEWIS ACIDS AS FLUORIDE RECEPTORS AND CATALYSTS

A Dissertation

by

MASATO HIRAI

Submitted to the Office of Graduate and Professional Studies of
Texas A&M University
in partial fulfillment of the requirements for the degree of

DOCTOR OF PHILOSOPHY

Chair of Committee,	François P. Gabbaï
Committee Members,	Marcetta Y. Darensbourg
	Oleg V. Ozerov
	Jodie L. Lutkenhaus
Head of Department,	Simon W. North

August 2016

Major Subject: Chemistry

ABSTRACT

It is known that SbF_5 and $SbCl_5$ are highly robust and show stronger acidic behavior than their boron counterparts, BF_3 and BCl_3, respectively. This effect is caused by the polarizability and the electropositivity of these heavy elements as well as a lowering of the element-centered σ* orbitals. These larger elements are also able to accept more ligands in their coordination sphere, thus promoting Lewis base coordination. However, antimony pentahalides violently react with water to generate the corresponding hydrohalic acids, which limits the scope of applications in which they can be employed. By replacing the Sb-X (X = F or Cl) bonds with carbon and/or oxygen substituents, this corrosive nature of antimony pentahalide species could be suppressed and become significantly more stable. As a drawback, displacement of electron-withdrawing halide substituents may also result in a decrease of Lewis acidity. It is therefore significant to design organoantimony(V) species that bear sufficient ligand functionalities to balance both reactivity and stability. In this dissertation, we will present our recent developments of both neutral and cationic organoantimony(V) compounds as sensors for small anions specifically in aqueouse media, reagents to activate molecules such as organic carbonyls, and potential ligands for heavy transition metals.

DEDICATION

For Grandma

ACKNOWLEDGEMENTS

I would first like to thank my high school chemistry teacher, Mr. Rudi Jansen, for his passion towards education and for introducing me to the enthusiastic world of chemistry (I would also like to use this opportunity to apologize for talking too much in class). I would also like to thank Prof. Marcetta Y. Darensbourg for not only serving as my PhD committee member but for consistently giving me advice and encouragement throughout my career as both an undergraduate and a graduate student. I would not have been where I am at today without the two of you and I am extremely grateful for that. I would also like to acknowledge my other two committee members Prof. Oleg V. Ozerov and Prof. Jodie L. Lutkenhaus for spending extensive amount of their valuable time for me.

I was incredibly fortunate for being able to work with members of the Gabbaï research group, past and present: Dr. Mitsukuni Tsunoda, Prof. Min Hyung Lee, Dr. Baofei Pan, Dr. Kewei Huang, Dr. Boris Vabre, Dr. Daniel Tofan, Dr. Guillaume Bélanger-Chabot, Lauren Leamer, Haifeng Yang, Anna Marie Christianson, Srobona Sen, Chang-Hong Chen, Elham Tabei, Mengxi (Moncy) Yang, Ying-Hao Lo, Di You, Gregory Day, Christina Lollar, Minji Kim, Merid Haile, Samantha Brewer, Andrian Maker, Xu Ye, Nilanjana Pati and Austin Williamson. I would particular like to thank Prof. Casey Wade, Dr. Tzu-Pin Lin, Dr. Haiyan Zhao and Dr. Iou-Sheng Ke for their mentorship in my earlier years of PhD, and Dr. Kantapat Chansaenpak and James (Stuart) Jones for being great friends and colleagues of mine since the beginning. My everlasting friendship goes

outside of lab as well. I could not have been able to complete my PhD without my former roommates and best friends Dr. Andrew Brown, John Patrick and Chandra-Mouli Palit. Thanks for hanging out with me whenever I needed a break. My special thanks also goes to the Phi Lambda Upsilon (PLU) 2012-2013 officers whom I had the privilege to work with: Dr. Natalie Harvey, Dr. Jessica DeMott, and Darrell Martin. The same respect applies to Dr. Amanda David who invited me to be a part of Organization for Cultural Diversity in Chemistry (OCDC).

My appreciation also goes to all of the wonderful professors and staff members who gave me sufficient advice and assistance: Prof. Abraham Clearfield, Prof. Donald J. Darensbourg, Prof. Kim R. Dunbar, Prof. Timothy R. Hughbanks, Prof. Dong-Hee Son, Prof. Coran M. H. Watanabe, Dr. Holly C. Gaede, Dr. Joanna G. Pellois, Dr. Nattamai Bhuvanesh, Dr. Joseph H. Reibenspies, Dr. Vladimir Bakhmoutov, Dr. K. P. Sarathy, Steve K. Silber, Dr. Gregory P. Wylie, Dr. Lisa Perez, Ron Carter, Sandy Horton, Valerie McLaughlin, Dennis Havemann, Curtis Lee, Melvin Williams, and Phillip Wymola. My extended gratitude goes to all of the assistants from the department who have become great friends of mine: Kim Holder, Angie Wilson, Andrezza Silva Mello Cesar An and Ethel Mejia.

Words cannot describe how thankful I am to my family back in Japan. My mom and dad gave me the freedom to study whatever I want and gave me the opportunity to go to school in the U.S. since I was 20 years old. I love you both dearly. My brother and I are completely the different but we understand each other the most. Although we do not converse as often, he is my only and the best brother a man could ask for. Thanks for

being such a cool bro. Many thanks goes to my friends back in my home country as well. My special gratitude goes to Natsuko Danjo who has continually encouraged me throughout the hard times. I have been using your Christmas gift every day.

I would also like to show my appreciation to the National Science Foundation, the Welch Foundation, Eastman Chemical, PLU and the Department of Chemistry for research funding and travel grants.

Finally, my greatest thanks goes to my research advisor, Prof. François P. Gabbaï. Working under him made me realize how much I love what I do in lab. I may not have been the best student but he never gave up on me and led me to where I am at right now. Not only do I respect him as an advisor, a professor or a chemist, I respect him as a person, a human being who cares so much about all of us and the department. I could not have asked for a better boss. Thank you so much Boss!

TABLE OF CONTENTS

Page

LIST OF FIGURES

Page

LIST OF TABLES

Page

CHAPTER I

INTRODUCTION TO ANTIMONY LEWIS ACIDS FOR MOLECULAR ANION RECOGNITION AND CATALYSIS

1.1 Introduction to organoantimony(V) Lewis acids

Background of group 15 Lewis acids. Group 15 compounds, also known as pnictogen compounds, are perhaps widely regarded as nucleophiles or Lewis bases in the +III oxidation state. For instance, amines and phosphines are few of the most commonly studied electron donors and have been readily applied in organic transformations and ligands for transition metals.[1] In the oxidation state of +V, however, these group 15 species are found to exhibit robust Lewis acidity, especially for heavier congeners. Unlike the tricoordinate group 13 species where the Lewis acidity arises from the vacant p_z-orbital, the electrophilic nature of group 15 compounds originates from the low-lying σ* orbital typically opposed to an electron-withdrawing substituent (Figure 1). This dissertation will particularly focus on the synthesis, characterization, and applications of both neutral and cationic organoantimony(V) Lewis acids.

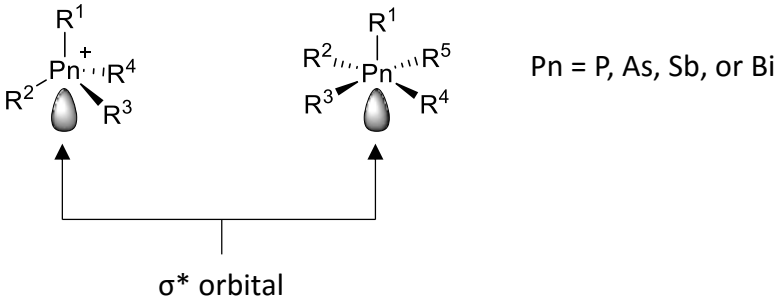

Figure 1. Lewis acidic sites (σ* orbitals) of tetracoordinate pnictogenium cations and pentacoordinate neutral pnictogen species.

Nitrogen, which is the lightest group 15 atom, at the oxidation state of +V form species that is often inert and rarely forms Lewis acid-base adducts. For instance, quaternary ammonium cations such as tetraalkylammonium, 1,1,3,3,5,5-hexamethylpiperidium, and bis(triphenylphosphine)iminium are sluggish electrophiles and widely utilized as inert cations. This lack of Lewis acidity of nitrogen-based compounds arises from the small size of the nitrogen atom which prevents the formation of hypervalent species.

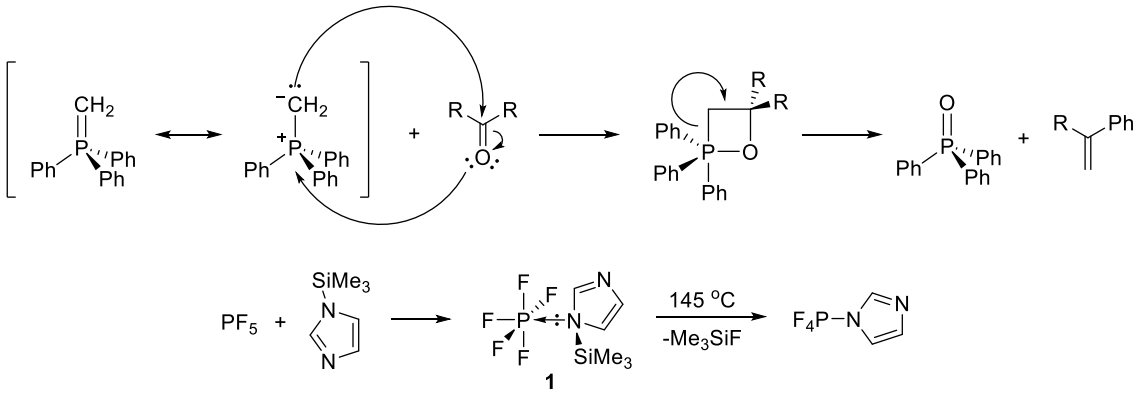

Figure 2. Top: the Wittig reaction and its mechanism. Bottom: the reaction of PF_5 and *N*-trimethylsilylimmidazol before and after heating.

Unlike nitrogen(V) compounds, phosphorus(V) species are more easily recognized as Lewis acids. One of the most notable examples is the Wittig reagent, a triphenyl phosphonium ylide that induces the conversion of aldehydes and ketones into alkenes (Figure 2, top).[2] This reagent, which can also be drawn as a zwitterionic triphenylalkylphosphonium carbanion, is electrophilic at the phosphorus center and plays a significant role in forming the oxaphosphetane intermediate. Soon after, neutral pentacoordinate phosphoranes bearing electron withdrawing substituents became documented as Lewis acids because of the low-lying σ* orbital. For instance, the phosphorus pentahalide species (PF_5 and PCl_5) forms hexacoordinate Lewis acid-base adducts with a number of nitrogen or oxygen bases and a few larger sulfur and phosphorus(III) donors.[3] An example that highlights the coordination chemistry and the reactivity of such adducts was reported by Schmutzler who showed that PF_5 and *N*-trimethylsilylimmidazole forms a simple Lewis acid-base adduct at ambient temperature which upon heating eliminates trimethylsilyl fluoride to afford pentacoordinate amidophosphorane **1** (Figure 2, bottom).[4] The phosphorus pentahalide species also forms adducts with halide anions. Hexafluorophosphate (PF_6^-), for example, is remarkably stable and has been readily employed as a non-coordinating anion whereas hexachlorophosphate (PCl_6^-) is less common because of its moisture sensitivity.

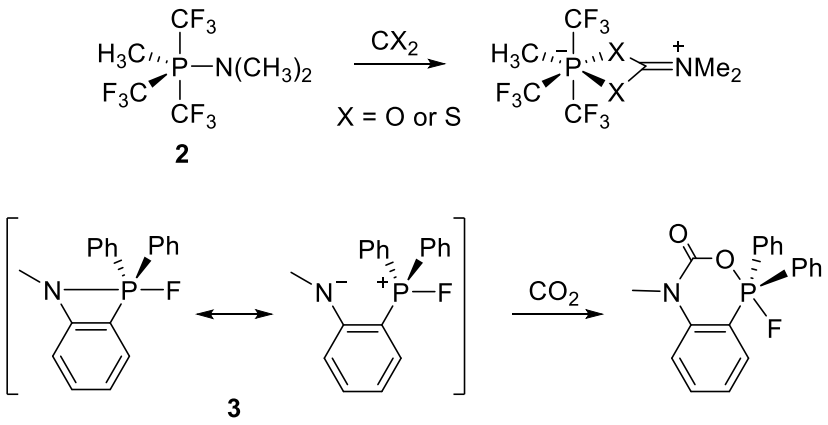

Figure 3. FLP reactions of amidophosphoranes **2** and **3** with CO_2 and/or CS_2.

Despite the precedence of Wittig reagents, the Lewis acidity of the phosphonium species has been less documented. Cavell, in 1977, reported a pentacoordinate amidophosphorane **2** that inserts CO_2 and CS_2 between the labile P-N bond to afford [**2**-CO_2] and [**2**-CS_2], respectively (Figure 3, top).[5] Although not mentioned in the original text, this is one of the earliest examples of CO_2 and CS_2 activation via the "Frustrated Lewis Pair" (FLP) reaction in which the phosphonium behaves as an acceptor of the terminal O and S while the amido group acts as a donor towards the electropositive carbon center. Stephan later reported an *ortho*-phenylene amidofluorophosphorane **3** that irreversibly binds CO_2 (Figure 3, bottom).[6] The resonance structure of **3** could be illustrated as a zwitterion with a formally cationic phosphorus center and an anionic nitrogen center. A variety of "free" phosphonium Lewis acids have also been reported in recent years and will be discussed later in this chapter.

Introduction to neutral antimony(V) compounds. The antimony species in the oxidation state of +V are categorized as the most powerful Lewis acids known to date. This is attributed to the large size of antimony atoms that allow high coordination numbers, and the electrostatic effect arising from the polarizability and electropositivity of antimony. One experiment that demonstrates the strong Lewis acidity of the antimony(V) species is reported by Gutmann in 1964.[7] In his work, Gutmann and his group measured the Lewis acidity of compounds such as BCl_3, $AlCl_3$, $SnCl_4$, PCl_5, and $SbCl_5$ by allowing them to react with tris(4-(dimethylamino)phenyl)methylium chloride, also known as "crystal violet" or "gentian violet"; a chromophore that changes color from violet to green or yellow concomitant with the coordination of the terminal dimethylamino moieties (Figure 4, top). The reactions in $POCl_3$. were monitored by UV-vis spectroscopy, and the estimated binding constants indicated that $SbCl_5$ is indeed the strongest Lewis acid among all, followed by $SnCl_4$, $AlCl_3$, BCl_3, and PCl_5. Gutmann also compared the chloride affinity of these species by carrying out potentiometric titrations with Et_4NCl [8] and spectrophotometric titrations with Ph_3CCl[9] in $POCl_3$. These experiments revealed similar trends. Another approach that has been applied to scale the strength of Lewis acids is to use theoretical methods to calculate the fluoride ion affinity (FIA) which compares the energy released upon binding fluoride ion in the gas phase (Figure 4, bottom).[10] The FIA calculations carried out by Krossing revealed that the value of SbF_5 (493 kJ/mol) greatly exceeds those of BCl_3, PF_5, and PCl_5 (405, 398, and 392 kJ/mol, respectively).[11, 12]

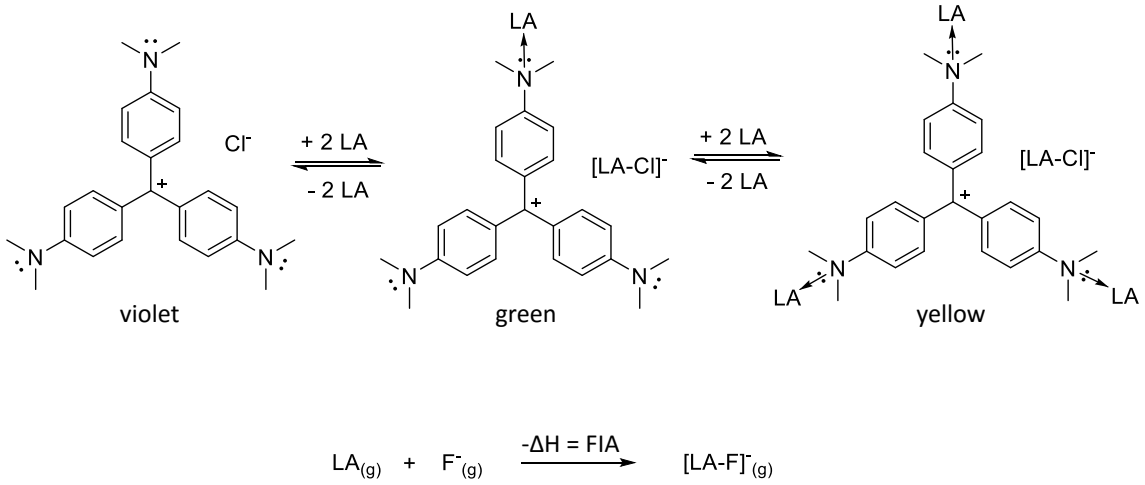

Figure 4. Top: reactions of crystal violet with Lewis acids along with the resulting color change. Bottom: reaction of a Lewis acid and fluoride ion in the gas phase.

In 1964, Olah showed that SbF_5 can react with a stoichiometric amount of fluorosulfuric acid (HSO_3F) to generate a superacid commonly known as a "magic acid" (Figure 5 A).[13-18] All Brønsted acids stronger than pure sulfuric acid are regarded as superacids and could be classified by the Hammett acidity function (H_0).[19] The H_0 values of sulfuric acid and magic acid are -12 and -19.2, respectively, indicating that the latter is 7 orders of magnitude stronger than the former.[20] Indeed, because of its high acidity and low nucleophilicity, magic acid rapidly reacts with alcohols,[21] carbonyls,[14] hydrides,[15, 22] hydroperoxide[23] and even saturated hydrocarbons[15] to afford stable carbocations. Similarly, the reaction of hydrogen fluoride (HF) and SbF_5 in a stoichiometric ratio of 2:1 affords fluoroantimonic acid (H_2FSbF_6); one of the most powerful superacids ever to be isolated (Figure 5 B).[24] Bickel and Hogeveen reported that H_2FSbF_6, which has a H_0 value of -31.3, can remove H_2 and methane from isobutane and neopentane, respectively, to afford carbenium ions.[25, 26] Moreover, $SbCl_5$ has been used as a halide ion acceptor to

promote heterolytic cleave of dihalogen bonds in the presence of a Lewis base, typically dialkyl sulfides, to afford stable halonium cations. Although these species have been known for over 20 years,[27] their reactivities have not been explored until later. Snyder in 2009 reported the synthesis of halodiethylsulfonium halopentachloroantimonate salts $[Et_2SX][XSbCl_5]$, also known as bromodiethylsulfonium bromopentachloroantimonate (BDSB) for the bromo species and chlorodiethylsulfonium hexachloroantimonate (CDSB) for the chloro species, by the reactions of $SbCl_5$ and diethyl sulfide (Et_2S) with X_2 (X = Cl or Br) in 1,2-dichloroethane at -30 ºC (Figure 5 C).[28, 29] In particular, BDSB, which could be prepared on a hundred-gram scale as a crystalline solid, is remarkably stable at ambient temperature and could be stored in an enclosed vial for over a week. The solid state structure of BDSB indicates a short S-Br distance of 2.170 Å and a sequestration of bromide to the antimonate anion, resulting in a cleavage of the Br-Br bond (Br-Br = 3.173 Å) and a large charge separation. Because of this, BDSB as well as CDSB are excellent halonium reagents that can promote polyene cyclizations.[29, 30]

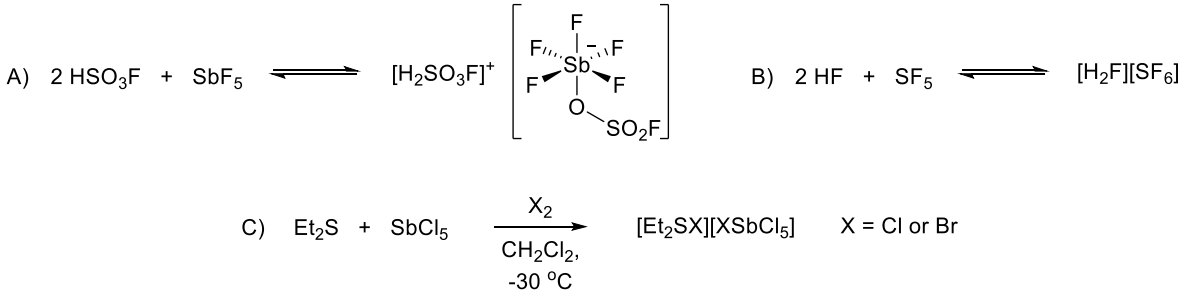

Figure 5. A) Formation of magic acid. B) Formation of fluoroantimonic acid. C) Heterolytic cleavage of X_2 (X = Cl or Br) by Et_2S and $SbCl_5$.

Although strongly Lewis acidic nature, antimony pentahalides are difficult to handle because they are highly corrosive and vigorously react with water to form the corresponding hydrohalic acids. In fact, $SbCl_5$ in particular can carbonize non-fluorinated plastics and etch stainless steel in the presence of moisture. The high reactivity, however, can be drastically suppressed by replacing the halide ligands with more inert organic and/or other oxygen, nitrogen, or sulfur-containing substituents. It is important to note that the stability and Lewis acidity of the organoantmimony(V) species greatly differ depending on the steric and electronic effects of the ligands.

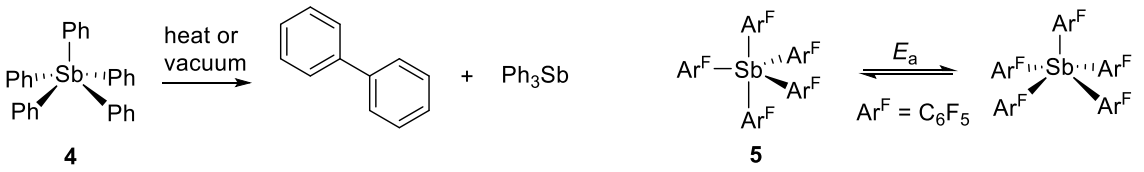

Figure 6. Left: reductive elimination of biphenyl upon heating of **4**. Right: equilibrium of geometrical change of **5** at 313 K.

An obvious example of an inert organoantimony(V) species is pentaphenyl stiborane (**4**), which was originally described in 1952 by Wittig (Figure 6, left).[31] In contrast to the antimony pentahalide species, **4** is reasonably stable in air at ambient temperature but decomposes at elevated temperature or under vacuum to reductively eliminate biphenyl to afford triphenylstibine. This instability is attributed to the weak Sb-C bond, arising from the lack of hybridization of the Sb s-orbital and the resulting Sb-C energy-level mismatch. The crystal structure of **4** was first reported in 1964 by Wheatley.[32] In the crystal, **4** surprisingly takes that of a distorted square pyramidal as

opposed to a typically favored trigonal bipyramidal for a pentacoordinate group 15 species. With the suspicion of a water molecule or some other small ligand molecules occupying the sixth coordination site about the antimony center, Cotton, in 1968, carefully reexamined the structure and found that **4** indeed adopts a distorted square pyramidal geometry.[33] Cotton conclusively adds that there is only a small difference in the potential energy between the square pyramidal and the trigonal bipyramidal geometries which may allow the former geometry to be favored in the solid state. It is worth stressing this unusual situation of Ph_5Sb since the penta-*p*-tolyl derivative has a trigonal bipyramidal structure in the solid state.[34] However, owing to its weak Lewis acidity and the possibility of a sterically hindered antimony center, Lewis acid-base adducts formed by **4** have not been reported. The more electron deficient pentakis(pentafluorophenyl)stiborane **5** was synthesized in 2012 by Romero (Figure 6, right).[35] This electron-deficient stiborane is air stable at ambient temperature and has been characterized by multi-nuclear NMR spectroscopy and single crystal X-ray diffraction analysis. In the crystal, stiborane **5** adopts a trigonal bipyramidal geometry as opposed to the distorted square pyramidal geometry found in **4**. Based on variable temperature NMR studies, the geometry of **5** in solution rapidly changes between square pyramidal and trigonal pyramidal at 313 K but the latter is favored at 183 K. The activation energy (E_a) associated with this dynamic process was estimated as only 24.4(4) $kJmol^{-1}$. Despite bearing strongly electron withdrawing substituents, Lewis acid-base adducts of **5** have also not been reported.

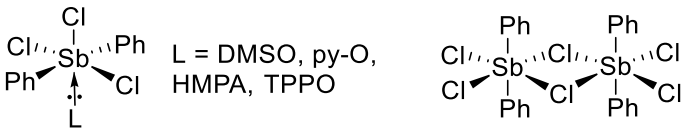

Figure 7. Left: Lewis acid-base adducts of **6** and with oxygen-based donors. Right: Ph_2SbCl_3 dimer formed under anhydrous conditions.

Interestingly, the diphenylantimony trihalide species, Ph_2SbX_3 (X = F, Cl or Br) are remarkably air stable at ambient temperature and are reported to form adducts with halide ions (Figure 7, left).[36] The Lewis acidity of diphenylantimony trichloride (Ph_2SbCl_3; **6**) in particular has been thoroughly studied and the crystal structures of Lewis pairs with nucleophiles such as DMSO, pyridine oxide (py-O), hexamethylphosphoramide (HMPA), triphenylphosphine oxide (TPPO), and even water have been reported.[37-40] Under anhydrous conditions, **6** exists as a dimer with two chlorine atoms asymmetrically bridging the two antimony centers (Figure 7, right).[41] Consequently, both antimony centers adopt an octahedral geometry as expected for a hexacoordinate antimony(V) species. On the other hand, triphenylantimony dichloride (Ph_3SbCl_2) is significantly less electrophilic and crystal structures of Lewis base adducts have not been reported.

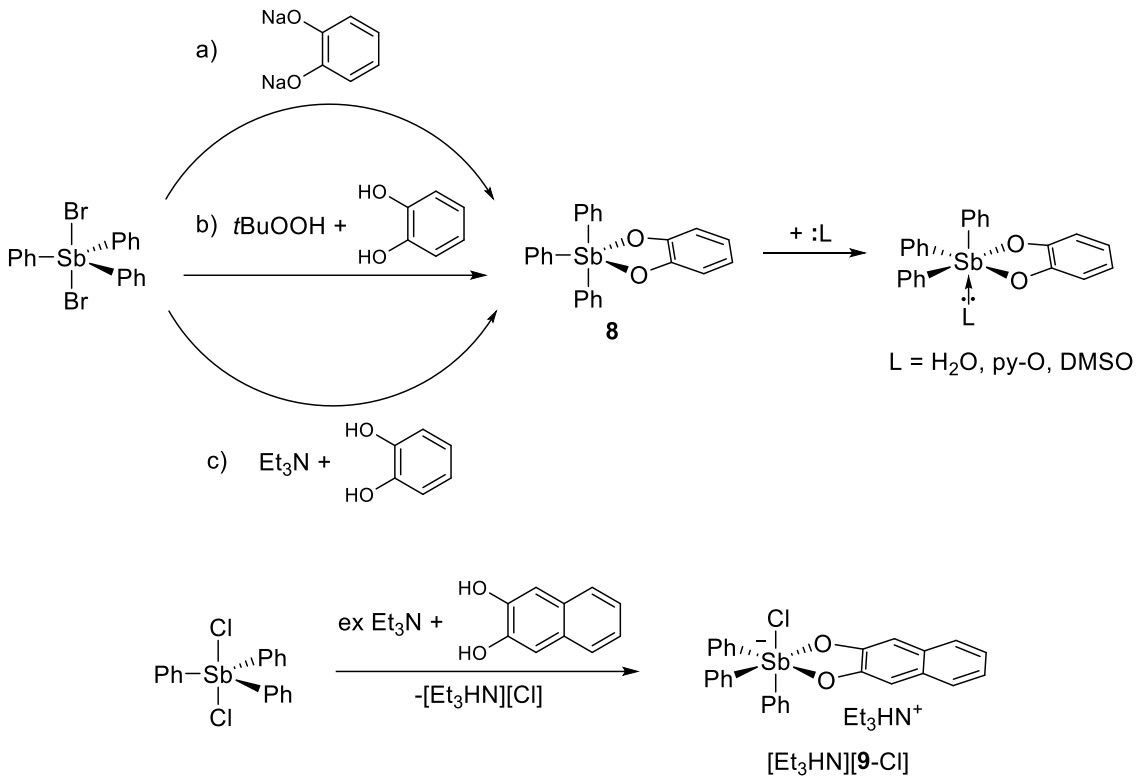

Figure 8. Top: three synthetic routes (shown as a, b, and c) for the preparation of **8** followed by the synthesis of its Lewis-base adducts. Bottom: synthesis of [Et_3HN][**9**-Cl].

Okawara, in 1969, reported organoantimony(V) compounds bearing a catecholate ligand. Both trimethylantimony catecholate **7** and triphenylantimony catecholate **8** have been prepared by the reaction of R_3SbBr_2 (R = Me or Ph) with sodium catecholate which was generated *in situ* with the reaction of sodium and catechol, in an acetone/benzene mixture (Figure 8, route a)[42] or by the reaction of R_3Sb and catechol in the presence of *t*ert-butyl hydroperoxide in toluene (Figure 8, route b).[43] Stiborane **8**, specifically, has also been prepared by the reaction of Ph_3SbCl_2 or Ph_3SbBr_2 and catechol in the presence of a base such as triethylamine or ammonia (Figure 8, route c). Although **7** decomposes over time in air or by light at ambient temperature, both **7** and **8** have been isolated as

stable adducts with oxygen donors including water, py-O, and DMSO which have been structurally characterized by single crystal X-ray diffraction analyses. A variety of glyconate and catecholate derivatives following the aforementioned procedures have been synthesized as well.[44, 45] Interestingly, an attempt to isolate triphenyantimony 2,3-naphthalenediolate by the reaction of Ph_3SbCl_2 and 2,3-napthalenediol with Et_3N (Figure 8, route c) was not successful and instead led to the formation of a chloride-bound antimonate anion as a triethylammonium salt ([Et_3HN][**9**-Cl]) (Figure 8, bottom).[46] The crystal structure of [**9**-Cl]$^-$ reveals a long Sb-Cl distance of 2.724(2) Å which is well in excess of the sum of the covalent radii of the two elements (Σ_ρ(Sb-Cl) = 2.41 Å), thus suggesting that the chloride ion is only weakly bound to the antimony center.

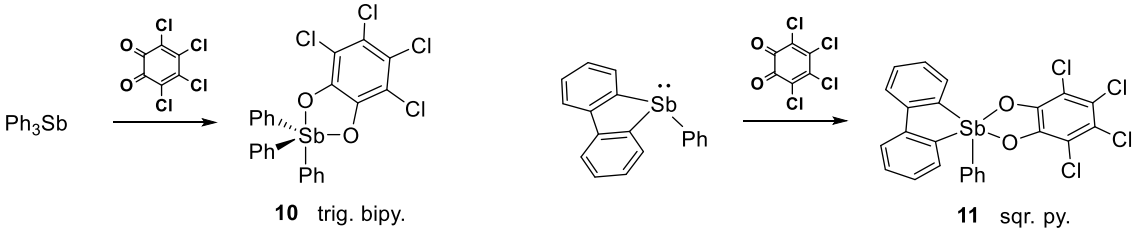

Figure 9. Synthesis of stiboranes **10** and **11**.

Derivatives of the triarylantimony catecholate species could also be accessed by two-electron oxidation of triarylstibines with *ortho*-benzoquinones.[46-53] For instance, the reaction of triphenylstibine (Ph_3Sb) with *ortho*-tetrachloroquinone (*o*-chloranil) affords triphenylantimony tetrachlorocatecholate **10**, which in the solid state adopts a distorted trigonal bipyramidal geometry about the antimony center as expected for a

pentacoordinate antimony(V) compound (Figure 9, left).[46] Similarly, the reaction of phenyl(2,2'-biphenylene)stibine with *o*-chloranil affords phenyl(2,2'-biphenylene)antimony tetrachlorocatecholate **11** (Figure 9, right). Unlike **10**, spirocyclic stiborane **11** in the solid state unexpectedly adopts a distorted square pyramidal geometry about the antimony center. Lewis acidities of both **10** and **11** have not been well documented in the literature and will be addressed later in this dissertation.

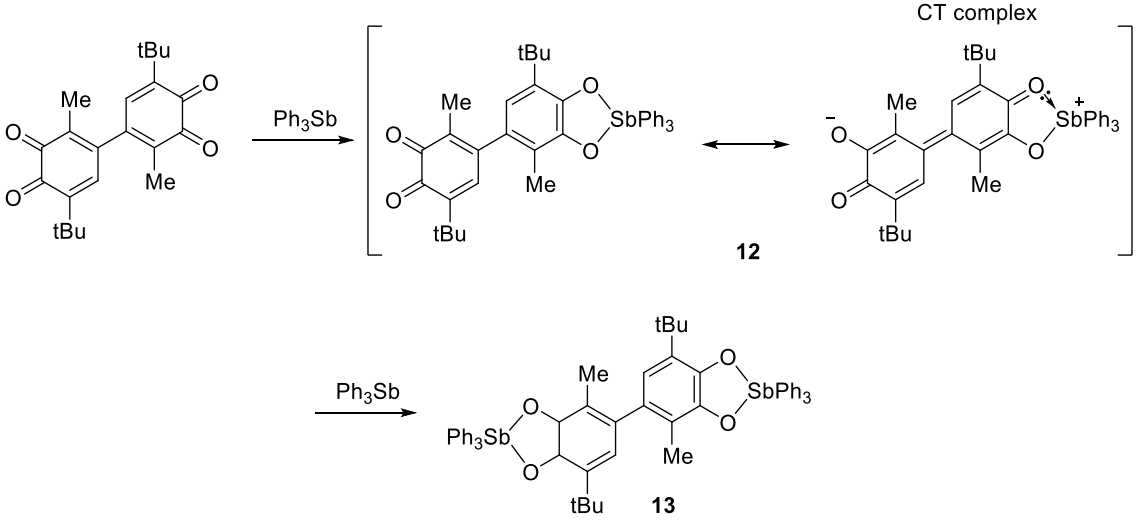

Figure 10. Oxidative addition of 4,4'-di-(3-methyl-6-*tert*-butyl-*o*-benzoquinone) to Ph_3Sb.

Abakumov, in 2005, showed that the reaction of 4,4'-di-(3-methyl-6-*tert*-butyl-*o*-benzoquinone) with Ph_3Sb proceeds as a sequential two-electron oxidative addition of each *o*-benzoquinone moiety to afford monostiborane **12** as a red solid, followed by distiborane **13** as a yellow solid.[47] The absorption spectrum of distiborane **13** in toluene at ambient temperature features a single intense band at 291 nm ascending from the two

catecholate moieties. In contrast, the UV-vis spectrum of monostiborane **12** displays three characteristic bands with maxima at 288, 400, and 505 nm under the same conditions. The authors propose that the unique low-energy absorption band (λ_{max} = 505 nm) of **12** originates from the charge transfer (CT) complex (Figure 10) which cannot be obtained for the di-*o*-quinone precursor and **13**.

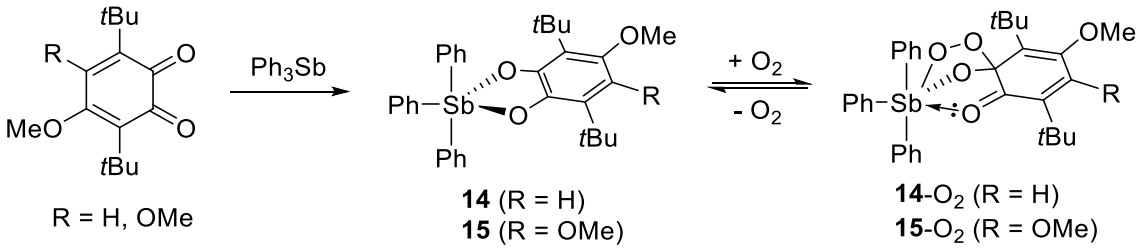

Figure 11. Synthesis of **14** and **15** and their reactions with molecular oxygen.

In 2006, Abakumova reported the reactions of Ph_3Sb with 4-methoxy-3,6-di-*tert*-butyl-*o*-benzoquinone and 3,6-di-*tert*-butyl-4,5-di-methoxy-*o*-quinone to afford the corresponding stiboranes **14** and **15**, respectively (Figure 11).[48] Both stiboranes were recrystallized in the presence of a donating solvent and the solid state structures revealed hexacoordinate antimony(V) compounds **14** and **15** with solvent molecules occupying the sixth coordination site. Strikingly, prolonged exposure of **14** and **15** to molecular oxygen led to the formation of the five-membered trioxastibolane species **14**-O_2 and **15**-O_2, respectively, and both of these species have been structurally characterized by single crystal X-ray diffraction analysis. In the crystal, the O-O distances are 1.475(2) Å for **14**-O_2 and 1.464(2) Å for **15**-O_2, which are closer to the corresponding bond lengths of the

peroxide species than that of molecular oxygen. These binding processes are reversible and repeated freeze-pump-warm cycles in the presence of donor solvents result in a release of free oxygen and regeneration of the solvent-coordinated stiboranes **14** and **15**.

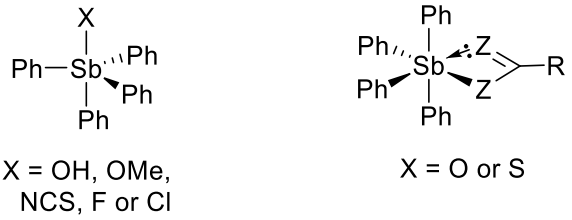

Figure 12. Coordination chemistry of Ph_4Sb^+ with small anions (left) and carboxylate anions (right) in the solid state.

Cationic organoantimony(V) Lewis acids. There are numerous examples of structurally characterized Lewis acid-base adducts of tetraphenylstibonium cation ($[Ph_4Sb]^+$) and Lewis basic anions reported in the literature.[54-73] In the solid state, small, basic anions such as hydroxide, methoxide,[54] isothiocyanate, fluoride,[56] and chloride[57] strongly interact with $[Ph_4Sb]^+$ to form strong covalent Sb-X (X = OH, OMe, NCS, F, or Cl) bonds, resulting in a trigonal bipyramidal geometry about the antimony center (Figure 12, left). Large and weakly basic iodide ions also coordinate to the Lewis acidic antimony center of $[Ph_4Sb]^+$ in the solid state; however, these are typically dissociated in polar solvents such as nitromethane.[64] The adducts of $[Ph_4Sb]^+$ formed with carboxylate and dithiocarbamate anions typically take that of a distorted octahedral geometry with the second O or S donor occupying the sixth coordination site (Figure 12, right).[74-77]

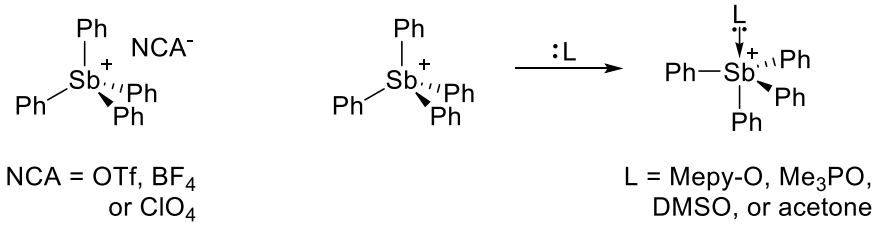

Figure 13. Lewis pair of $[Ph_4Sb]^+$ and non-coordinating anions and their adduct formation with neutral donors.

In contrast, $[Ph_4Sb]^+$ takes that of a tetrahedral geometry in the presence of less coordinating anions such as triflate (OTf^-),[78] tetrafluoroborate (BF_4^-),[79] tetraphenylborate (BPh_4^-)[80] or perchlorate (ClO_4^-)[81, 82] with no obvious interaction among the ionic pairs (Figure 13, left). With the fifth coordination site to avail, Burford, in his recent paper, demonstrated that sterically undemanding neutral donors such as 4-methylpyridine-*N*-oxide (Mepy-O) and triphenylphosphine oxide (Me_3PO) can indeed form adducts with $[Ph_4Sb]^+$ (Figure 13, right).[78] Sharutina and Pushilin similarly reported crystal structures of $[Ph_4Sb]^+$ bearing a molecule of DMSO and acetone, respectively.[74, 83] Our group has also studied the coordination chemistry and reactivity of tetraarylstibonium cation derivatives which will be discussed later in this chapter. The coordination chemistry of triarylstibonium dications has also been investigated, especially by the Burford group. These species are typically stabilized by monodentate or polydentate pyridine or phosphine oxide donors that saturate the coordination sites surrounding the antimony center. [84, 85]

1.2 Main-group Lewis acids as fluoride sensors

Introduction. Fluoride anions are frequently used as anabolic drugs as part of the treatment of osteoporosis, a disease which reduces bone density and increases the risk of broken bones.[86, 87]. Unfortunately, an overdose of such anions could severely impact human health by removing calcium from the tooth enamel to induce cavity formation and eventually causing dental fluorosis. [88] In advanced cases, excessive accumulation of fluoride in the bone may result in skeletal fluorosis,[89, 90] a severe illness that hardens the bones and joints and induces constant pain in the body. Because of these side-effects, the United States Environmental Protection Agency (EPA) has regulated such anions in drinking water and set the maximum contamination level of fluoride concentration to 4 ppm (200 μM).[91] Moreover, the U.S. Department of Health and Human Services has lowered the recommended fluoride level from 1.2 ppm to 0.7 ppm.[92] Recognition and capture of fluoride anions therefore has become a highly active research topic, especially in aqueous solutions.[93, 94] The reactivity of fluoride, however, is greatly suppressed in water via the formation of strong hydrogen bonds (ΔH^o = -504 kJ mol^{-1}), thus making it challenging to capture such anions in water.[95-97]

One of the modern methods to determine anion concentrations in water is to apply ion selective electrodes. Fluoride ions, in particular, require a crystal of lanthanum fluoride (LaF_3) doped with europium fluoride (EuF_2) as the sensing element.[98] However, this method requires equipment that is inportable which makes it inconvenient to carry. An alternative approach utilizes metal-ion complexes incorporating organic dyes.[99, 100] These complexes have a colorimetric response upon coordination of fluoride ions, which

is appealing from a practical point of view. Despite this method being relatively cheap, these transition metal complexes suffer from interferences from other anions such as chloride, phosphate and sulfate, inducing false positive responses.[101] Because of these drawbacks, a great deal of attention has been dedicated to develop molecular sensors that are selective towards fluoride ions.

Neutral monofunctional boranes as fluoride acceptors. Owing to their intrinsic Lewis acidity, triarylboranes have been widely utilized as acceptors to complex small nucleophilic anions such as fluoride to afford the corresponding borate anions. This reaction is driven by the donation of an electron pair of the anions into the unoccupied p_z-orbital of the boron center, thus forming a thermodynamically stable Lewis acid-base adduct. As a tradeoff, however, coordination of an anion to the tricoordinate boron atom induces a change in geometry from trigonal planar to tetrahedral and destabilizes the complex via forced steric repulsive interaction among the neighboring aryl groups (Figure 14). Consequently, the anion affinity of the triarylborane species is greatly governed by the steric and electronic properties of the aryl substituents incorporated in the boron center.

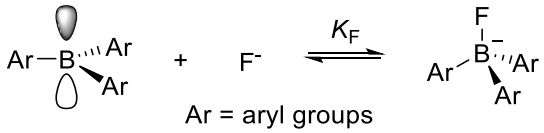

Figure 14. Fluoride binding of triarylboranes.

Despite these considerations, neutral monofunctional triarylboranes consisting of sterically bulky groups such as trimesitylborane (**16**)[102] and tri(9-anthryl)borane (**17**)[103]

effectively bind fluoride ions in aprotic organic solvents such as THF to afford the corresponding fluoroborate species (Figure 15). These binding processes could be monitored by UV-vis spectroscopy and the binding constants (K_F) have been estimated as 3.3×10^5 M^{-1} for **16** and 2.8×10^5 M^{-1} for **17**. Triarylborane **17,** in particular, has a distinct color change from orange to colorless upon fluoride complexation and could be used as a colorimetric fluoride ion sensor. These reactions are also found to be reversible with the addition of water to a THF solution of fluoroborate, thus indicating the instability of such fluoride adducts in the presence of water. Furthermore, because of the steric bulk of the ligands, both boranes **16** and **17** selectivity bind F^- over other larger anions such as Cl^-, Br^-, I^-, ClO_4^-, and BF_4^-.

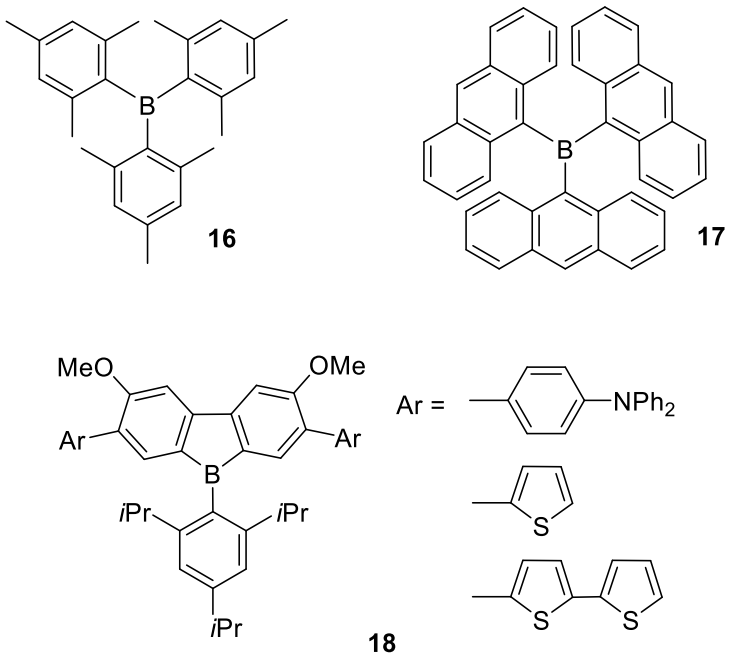

Figure 15. Triarylboranes **16**, **17** and **18**.

The electronic properties of the aryl substituents also greatly influence the anion affinity of triarylboranes. For instance, triarylboranes consisting of borafluorene moieties (**18**) prepared by Yamaguchi and Tamao display remarkable fluoride affinities which on average exceed the K_F value of **16** by one order of magnitude (Figure 15). These surprising Lewis acidities originate from the anti-aromatic character of the borafluorene moieties resulting in ground state destabilization of the molecule.

Neutral diboranes as fluoride acceptors. One of several strategies applied to increase the anion affinity of the triarylborane species is to prepare bifunctional diborane Lewis acids that promote chelation of guest anions. Several groups, including the Gabbaï group, have extensively studied bidentate diboranes with a naphthalene-based backbone. A prototypical example of such diboranes is 1,8-naphthalenediylbis(dimethylborane) (**19**), also known as a "hydride sponge", reported by Katz (Figure 16, top).[104, 105] The reaction of this diborane is not limited to hydride, but also fluoride and hydroxide ions to afford the corresponding chelate adducts. The naphthalene-based asymmetric diborane bearing a dimesityl boryl and a 9-thia-10-boranthracene moiety (**20**) has been isolated by our group and the fluoride affinity has been shown to exceed that of the monofunctional boranes such as trimesitylborane by more than four orders of magnitude in THF ($K_F > 5 \times 10^9$ M^{-1}) (Figure 16, bottom).[102] This bright yellow bidentate diborane is also a colorimetric fluoride sensor and the addition of fluoride ions to a THF solution of **20** leads to a loss of color, resulting from the population of the LUMO and the interruption of HOMO-2, HOMO-1, and HOMO to LUMO electronic transitions.

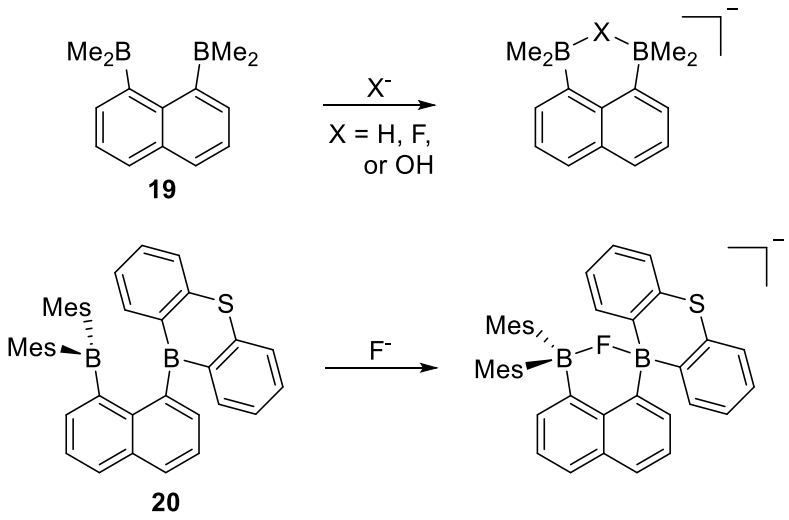

Figure 16. Reactions of diboranes **19** and **20** with small nucleophilic anions.

Bidentate diboranes based on *ortho*-phenylene units have also been readily investigated for chelating neutral electron-rich molecules and anions. An example of such diboranes is the 1,2-bis(bis(pentafluorophenyl)boryl)tetrafluorobenzene (**21**) which can efficiently chelate anions such as hydroxide, fluoride, methoxide, and chloride (Figure 17).[106, 107] Interestingly, the two boron centers of **21** can behave independently as monofunctional boranes as well. For example, crystallization in the presence of MeCN resulted in solvent molecules coordinating covalently to each boron center rather than bridging between the two (Figure 17).[108]

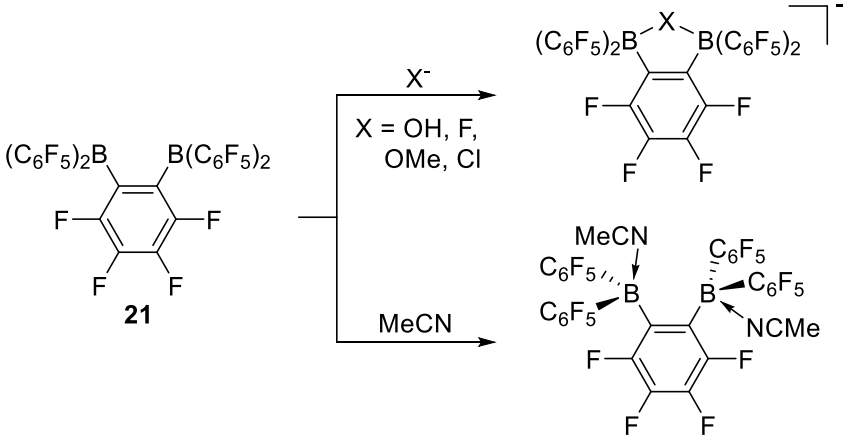

Figure 17. Reactions of diborane **21** with various anions and MeCN.

Anion complexations by cationic boranes. One of the most successful strategies employed to increase anion affinities is to incorporate cationic functionalities into the framework of triarylborane receptors. This approach is particularly effective because the presence of cationic groups introduces an enhancement of anion affinity via Coulombic and inductive effects [109] and also improves the solubility of the receptors in polar solvents including water.

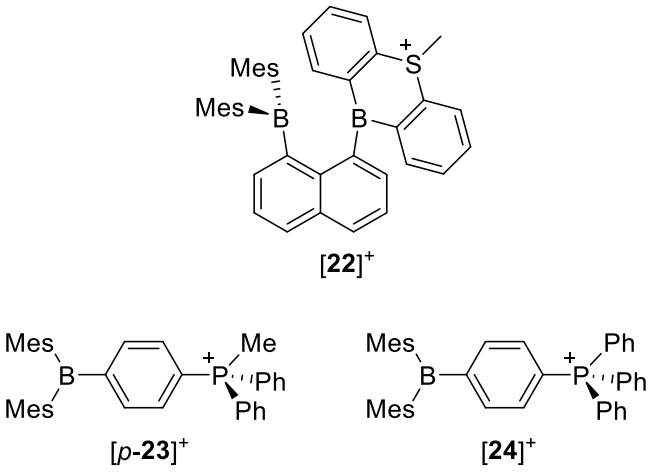

Figure 18. Sulfonium diborane [**22**]$^+$ and phosphonium boranes [*p*-**23**]$^+$ and [**24**]$^+$.

The Gabbaï group has previously shown that the cationic functionalities can drastically impact the anion affinity from a distant location from the Lewis acidic site. For example, the fluoride affinity of bidentate sulfonium diborane [**22**]$^+$ is significantly improved from its neutral counterpart **20** (Figure 18). The fluoride binding processes in $CHCl_3$ have been monitored by UV-vis spectroscopy confirming that [**22**]$^+$ stoichiometrically reacts with fluoride ions. This shows that the K_F of cationic diborane [**22**]$^+$ exceeds 10^5 M^{-1} and is thus at least four orders of magnitude greater than neutral diborane **19**. Other examples include cationic boranes [*p*-**23**]$^+$ and [**24**]$^+$ which both bear phosphonium moieties in the *para* position of a phenylene linker (Figure 18).[110, 111] These phosphonium boranes react quantitatively with fluoride ions to afford the corresponding zwitterions [*p*-**23**]-F and **24**-F. The fluoride titration of [*p*-**23**]$^+$ in $CHCl_3$ monitored by UV-vis spectroscopy revealed that the K_F is 6.5 (± 0.5) × 10^6 M^{-1} which exceeds those of both monodentate and bidentate neutral boranes by several orders of magnitude.

Furthermore, this phosphonium borane [*p*-**23**]$^+$ is compatible with an aqueous environment and readily binds fluoride in a 9/1 (v/v) H_2O/MeOH mixture at pH 4.9 as illustrated by K_F of 840 (± 50) M^{-1}. It is interesting to note that the complexation of fluoride results in a quenching of the green emission, thereby making [*p*-**23**]$^+$ a turn-off fluorescence sensor towards such anion. The fluoride affinity could also be greatly improved by introducing a more hydrophobic phosphonium moiety. For instance, phosphonium borane [**24**]$^+$, which bears a tetraarylphosphonium subunit, binds fluoride in 9/1 (v/v) H_2O/MeOH mixture at pH 4.6 with a K_F of 10 500 (± 1000) M^{-1} (Figure 18).

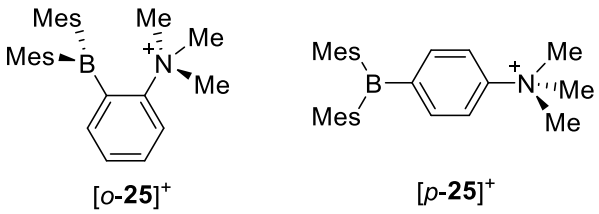

Figure 19. Ammonium boranes [*o*-**25**]$^+$ and [*p*-**25**]$^+$.

The proximity of the cationic group to the Lewis acidic site is also responsible for the selectivity and the affinity of small anions. In order to address this point, *ortho*- and *para*-isomers of ammonium boranes ([*o*-**25**]$^+$ and [*p*-**25**]$^+$) have been prepared as triflate salts, and the anion binding properties have been compared (Figure 19).[112] Both of these isomers quantitatively react with fluoride and cyanide ions in organic solvents to afford the corresponding zwitterionic ammonium fluoroborates [*o*-**25**]-F and [*p*-**25**]-F and cyanoborates [*o*-**25**]-CN and [*p*-**25**]-CN, respectively. However, the anion binding affinity of these two isomers largely differ in aqueous media. In a 6/4 (v/v) H_2O/DMSO

mixture containing HEPES buffer (6 mM) at neutral pH, [*p*-**25**]$^+$ readily binds cyanide ions with a binding constant (K_{CN}) of 3.9 (± 0.1) 10^8 M^{-1} while showing no affinity towards fluoride ions. In contrast, [*o*-**25**]$^+$ reacts with fluoride ions under the same conditions with a K_F of 910 (±50) M^{-1} and not with cyanide ions. The anion binding selectivity of these ammonium boranes is associated with the combination of both steric and electronic effects. Theoretical studies revealed that the energy of the LUMO of [*o*-**25**]$^+$ (E = -2.12 eV) is lower than that of [*p*-**25**]$^+$ (E = -2.02 eV) which gives rise to an increased Lewis acidity of [*o*-**25**]$^+$ as well as a higher binding affinity towards a less nucleophilic fluoride ion. Furthermore, the anion binding pocket of [*o*-**25**]$^+$ is congested due to the pendant trimethylammonium moiety, thereby preventing the complexation of a larger cyanide ion to the coordination site.

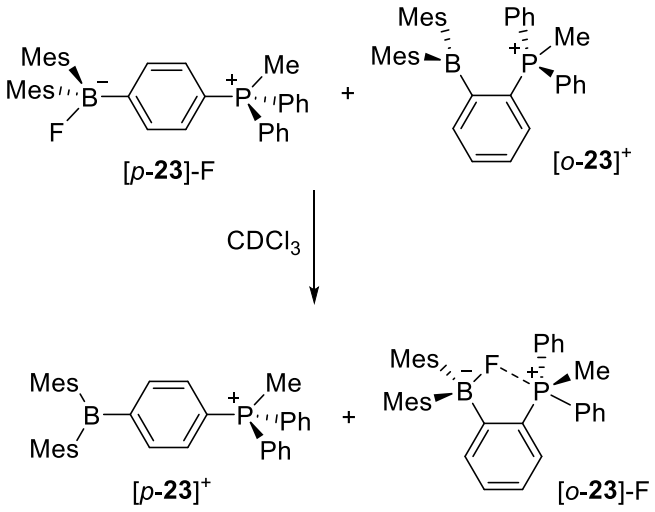

Figure 20. The competition experiment of [*p*-**23**]-F and [*o*-**23**]$^+$ in $CDCl_3$.

In the case of phosphonium boranes, the K_F of the *ortho*-isomer [*o*-**23**]$^+$ could not be measured in water due to its instability at a pH above 3.5 .[113] Instead, fluoride titration of [*o*-**23**]$^+$ has been carried out in a MeOH solution and the estimated K_F exceeds 10^6 M^{-1} which is at least four orders of magnitude greater than that of the *para*-isomer [*p*-**23**]$^+$ (K_F = 400 (± 50) M^{-1}). Indeed, the reaction of equimolar amounts of [*p*-**23**]-F and [*p*-**23**]$^+$ in $CDCl_3$ leads to quantitative formations of [*p*-**23**]$^+$ and [*o*-**23**]-F which were detected by multi-nuclear NMR spectroscopy (Figure 20). To better understand this difference in affinity, [*o*-**23**]-F has been characterized by single crystal X-ray diffraction and theoretical studies. In the solid state structure of [*o*-**23**]-F, the fluoride ion bridges the boron and the cationic phosphorus center with a remarkably short P-F contact of 2.66 Å ($\Sigma(P\text{-}F)_{vdW}$ = 3.45 Å). Moreover, the phosphorus center adopts a trigonal bipyramidal geometry with a F-P-C_{Ph} angle of 176.36°. Natural Bond Orbital (NBO) analysis identified an interaction of a fluoride lone pair donating into the σ*-orbital of the P-C_{Ph} bond which contributes 5.0 kcal/mol to the stability of the complex. These structural and theoretical results indicate that the high fluoride affinity of [*o*-**23**]$^+$ arises from both Coulombic and chelate effects, properties that are absent in the ammonium fluoroborate analog.

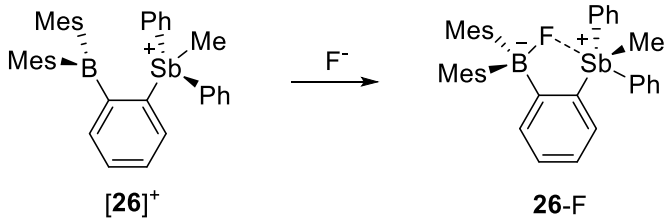

[**26**]$^+$ **26**-F

Figure 21. Reaction of stibonium borane [**26**]$^+$ with fluoride.

The effect of chelation has also been tested for heavier onium compounds. The *ortho*-stibonium borane complex [**26**]$^+$ reacts with a fluoride ion to afford the corresponding zwitterionic stibonium fluoroborate **26**-F (Figure 21).[114] The crystal structure of **26**-F confirms the formation of a B-F-Sb chelate motif similar to that found in [*o*-**23**]F, thereby indicating that [**26**]$^+$ also behaves as a bidentate Lewis acid. The B-F distance is longer in **26**-F (1.521 Å) than in [*o*-**23**]-F (1.476 Å), suggesting that the antimony atom pulls on the bridging fluoride from the boron center more than the phosphorus atom. Additionally, despite the larger size of the antimony atom, the Sb-F distance (2.45 Å) found in **26**-F is shorter than the P-F distance found in [*o*-**23**]-F (2.66 Å). Also, NBO analysis has been carried out on the optimized structure of [**26**]F. This calculation shows that the donor-acceptor interaction between the lone pair of fluoride and the σ*-orbital of the Sb-C_{Ph} bond contributes 15.2 kcal/mol to the stability, which is 10.2 kcal/mol greater than the P-F interaction in [*o*-**23**]F. Indeed, the reaction of [**26**]$^+$ with the equimolar amount of [*o*-**23**]F results in quantitative formation of [**26**]F and [*o*-**23**]$^+$ (Figure 22). These observations conclusively show that the stibonium moiety is more Lewis acidic than its phosphonium analog.

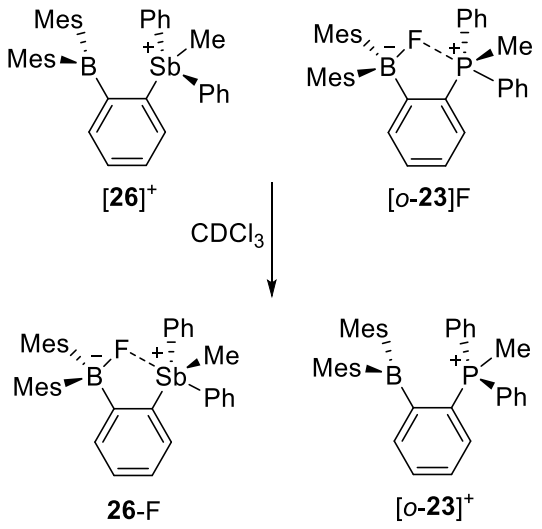

Figure 22. The competition experiment of [**26**]$^{+}$ and [*o*-**23**]F in $CDCl_3$.

Organoantimony(V) Lewis acids as fluoride acceptors. Fluoride adducts of organoantimony(V) Lewis acids are surprisingly rare, especially for the neutral stiborane species. One of the few examples of fluorophilic stiborane is **27**, which bears two α,α-bis(trifluoromethyl)benzyl ether bidentate moieties also known as "Martin's ligand".[115] The treatment of **27** with excess *n*-tetrabutylammonium fluoride (TBAF) in acetone afforded single crystals of the corresponding fluoride adduct TBA[**27**-F] (Figure 23). In the solid state of fluoroantimonate [**27**-F]$^{-}$, the fluoride ion is tightly bound to the antimony center with a short separation of 1.999(4) Å. It is noteworthy to point out that the fluoride ion and the oxygen atom are in an *anti*-relationship in the crystal. Variable temperature NMR (VT NMR) studies reveal that [**27**-F]$^{-}$ exists as multiple diastereoisomers in the solution at -40 ^{o}C (one of the isomers is shown in Figure 23, top). In contrast, one set of broad NMR signals is observed at ambient temperature, suggesting that fluoride only

weakly binds to the antimony center and that free **27** can undergo isomerization to create different coordination spheres for the incoming Lewis base. Indeed, treatment of fluoroantimonate [**27**-F]$^-$ in acetone with water at ambient temperature quantitatively results in the quantitative recovery of the free stiborane **27**. These experiments demonstrate that **27** is only mildly Lewis acidic and cannot sufficiently bind fluoride ions in aqueous media.

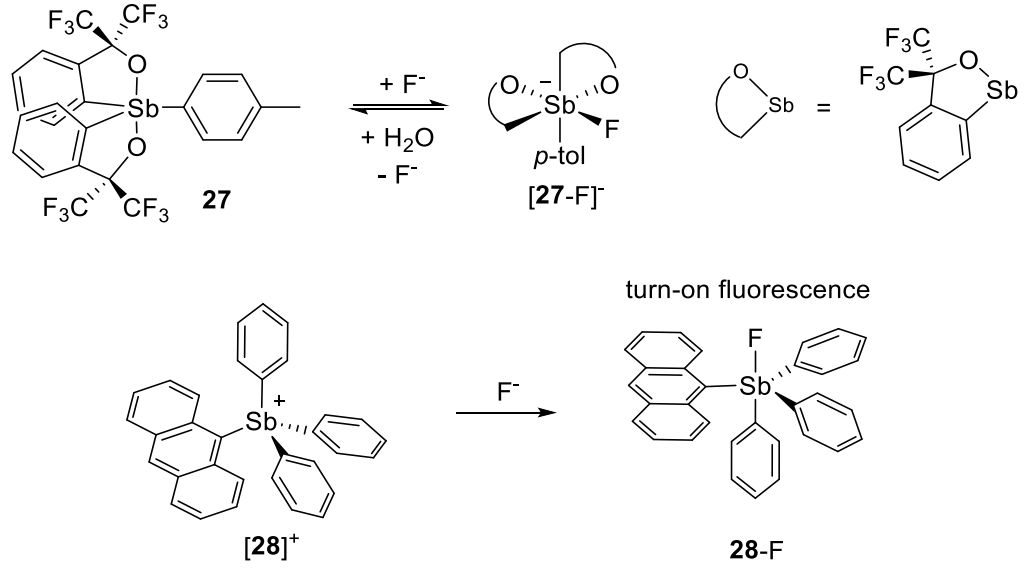

Figure 23. Top: reversible fluoride binding of **27**. Bottom: reaction of [**28**]$^+$ with a fluoride ion.

The fluoride affinity of stibonium cations are significantly more documented in the literature. Potratz, in 1956, demonstrated that tetraphenylstibonium sulfate salt ($[Ph_4Sb]_2[SO_4]$) is highly soluble in water and readily binds fluoride ions in a biphasic H_2O/CCl_4 mixture to afford Ph_4SbF which immediately transfers to the organic layer upon

formation.[116] The conversion of $[Ph_4Sb]^+$ to Ph_4SbF is rather quick and facile under these conditions. Rood took advantage of this fluorophilic property of $[Ph_4Sb]^+$ and utilized it as a carrier to extract and separate $^{18}F^-$, whose half-life is 110 min, from water containing H_2SO_4 at a pH as low as 3.[117] To parametrize the fluoride affinity of $[Ph_4Sb]^+$, our group carried out a spectrophotometric fluoride titration experiment in MeCN and estimated that the K_F exceeds 10^6 M^{-1}. The lighter pnictogenium analogs, $[Ph_4P]^+$ and $[Ph_4As]^+$, showed no signs of fluoride binding under the same conditions, exemplifying the fluorophilic nature of Ph_4Sb^+.

With these considerations in mind, our lab prepared a tetraarylstibonium cation bearing a 9-anthryl group as a fluorescent reporter for the application of photophysical fluoride sensing in water.[118] Analogous to $[Ph_4Sb]^+$, 9-anthryltriphenylstibonium cation $[\mathbf{28}]^+$ also readily binds fluoride ions in aqueous media to afford the corresponding fluorostiborane **28**-F which rapidly precipitates out of solution (Figure 23, bottom). It is important to note that $[\mathbf{28}]^+$ exists as a free stibonium cation at a pH below 5 as indicated by UV-vis spectroscopy. To investigate the fluoride ion affinity in an aqueous solution, spectrophotometric fluoride titration of $[\mathbf{28}]^+$ was carried out in a 9/1 (v/v) H_2O/DMSO mixture containing cetyltrimethylammonium bromide (10 mM) and pyridine (10 mM, pH = 4.8). After the addition of fluoride ions, their coordination to the antimony center was verified by the anthryl-based absorption band blue-shift and the marked increase of fluorescence intensity from Φ = 2.2% in $[\mathbf{28}]^+$ to Φ = 14.1% in **28**-F (λ_{ex} = 375 nm). The same experiment was carried out in the presence of other common anions such as Cl^-, Br^-,

I^-, NO_3^-, N_3^-, HCO_3^-, and HSO_4^- and no adequate signalling response was observed, thus indicating that [**28**]$^+$ is highly selective for fluoride anions in aqueous solution.

1.3 Organoantimony(V) Lewis acids as organic transformation catalysts

Introduction. The research of main-group catalysts has been attracting a great deal of attention as an alternative to transition metal complexes that are generally costly. In most cases, Lewis acids are involved in the binding of heteroatomic Lewis bases and polarize the electron density to facilitate heterolytic bond cleavage or directly activate the substrate towards nucleophilic attack. Some examples of Lewis acid-mediated organic transformations include Friedel-Crafts, Mukaiyama aldol, Sakurai, Diels-Alder, Michael, hydrosilylation, hydrodefluorination, and dehydrocoupling reactions.[119] Classical main-group catalysts that have been employed for these reactions include group 13 compounds such as BF_3, BCl_3, and $AlCl_3$ or group 14 compounds such as $SnCl_4$. Group 14 cations including trityl[120] and silylium[121] derivatives are also found to be effective catalysts. Many of these catalysts, however, are typically prone to hydrolysis and are difficult to handle in air.

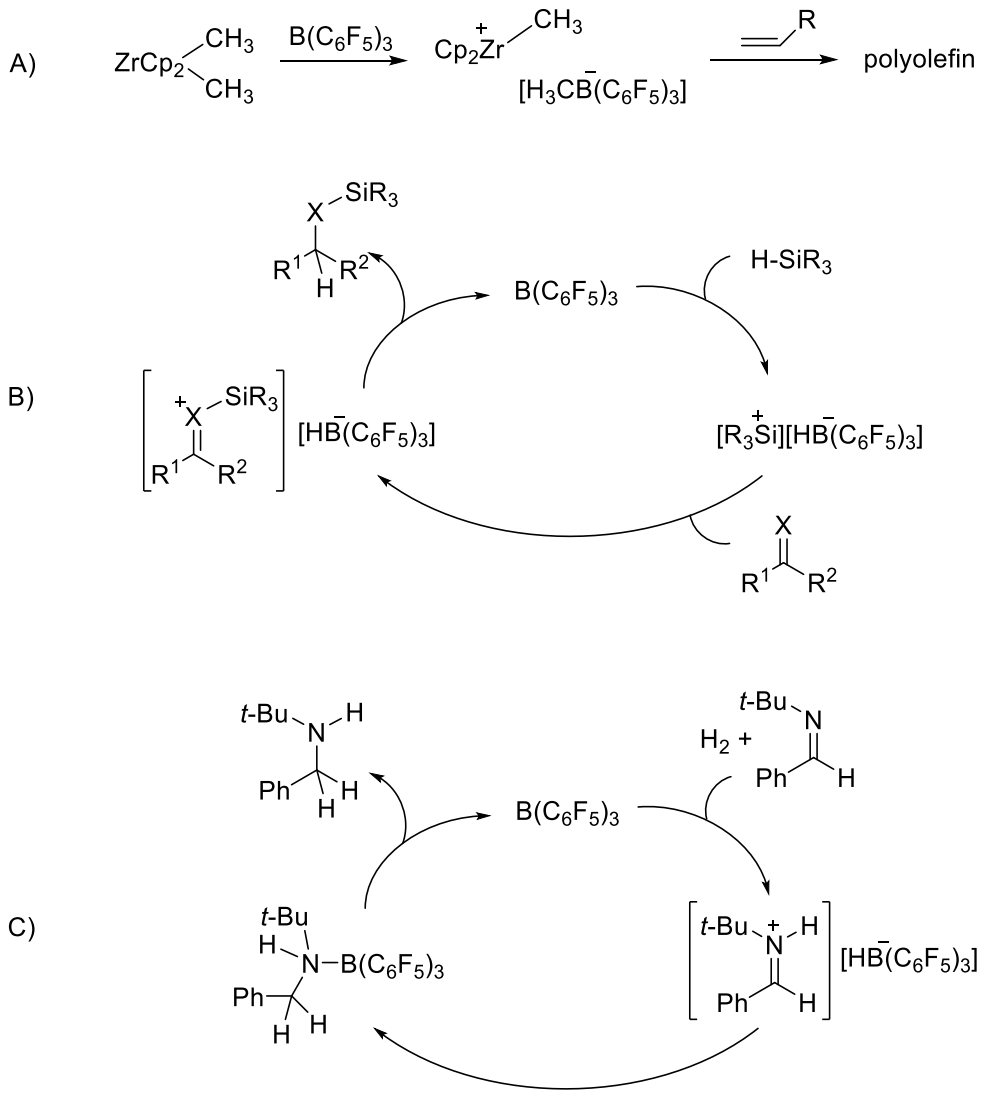

Figure 24. Reactions catalyzed by $(C_6F_5)_3B$: A) homogenous Ziegler-Natta olefin polymerization, B) hydrosilylation of imines, aldehydes, ketones, and esters, C) FLP-catalyzed hydrogenation of an imine.

Perhaps one of the most extensively investigated Lewis acid catalysts is tris(pentafluorophenyl)borane ($(C_6F_5)_3B$), which was originally prepared and described in 1963 by Massey and Park.[122, 123] Because of its versatility and relative air-stability, $(C_6F_5)_3B$ has gathered increasing popularity in recent years, and there has been over 2,000

publications related to this compound. By virtue of strongly electron withdrawing perfluorinated phenyl substituents, the Lewis acidity of $(C_6F_5)_3B$ judged by the Gutmann-Beckett method and the Childs method is comparable to that of BF_3 and slightly weaker than BCl_3.[124, 125] In 1994, Marks utilized $(C_6F_5)_3B$ as an activator or co-catalyst for homogeneous metallocene Ziegler-Natta polymerization catalysts which was previously achieved by methylalumoxane (Figure 24 A).[126] Shortly after, Piers reported $(C_6F_5)_3B$ as an efficient catalyst for hydrosilylation of aromatic aldehydes, ketones and esters (Figure 24 B).[127] In 2007, Stephan showed that $(C_6F_5)_3B$ can heterolytically cleave H_2 in the presence of a bulky phosphine such as tri-*tert*-butylphosphine (tBu$_3$P), resulting in the formation of phosphonium borate [tBu$_3$PH][HB$(C_6F_5)_3$].[128] Such FLP systems have been used in metal-free catalytic hydrogenation of imines (Figure 24 C), nitriles, aziridines, enamines,[129, 130] silyl enol ethers,[131] olefins,[132-134] polyarenes,[135] fulvenes,[136] and alkynes,[137] and most recently ketones and aldehydes.[138, 139]

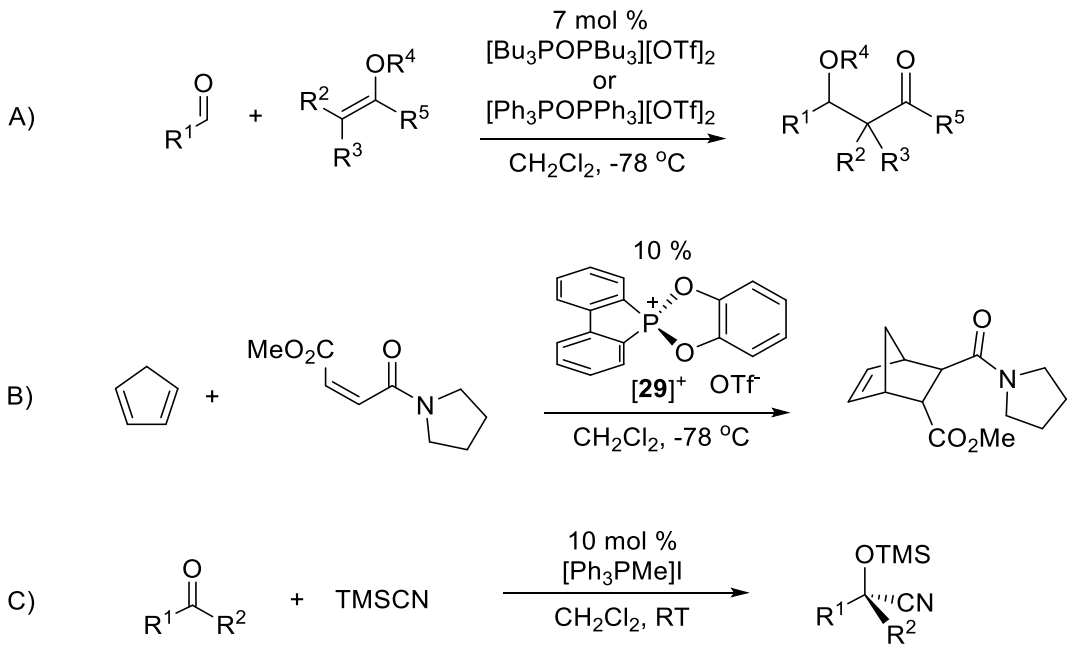

Figure 25. Phosphonium-catalyzed A) Mukaiyama-aldol, B) Diels-Alder, and C) cyanosilylation reactions.

Phosphonium and stibonium Lewis acids as catalysts. In contrast to group 13 and 14 Lewis acids, studies on the catalytic behavior of group 15 Lewis acids, such as phosphinum and stibonium cations, are less profound.[140, 141] Early examples of phosphonium catalysts were reported in 1989 by Matsui and Mukaiyama who showed that diphosphonium triflate salts $[Bu_3POPBu_3][OTf]_2$ and $[Ph_3POPPh_3][OTf]_2$ can effectively catalyze Mukaiyama-aldol reactions of aldehydes with silyl enol ethers and ketene silyl acetals (Figure 25 A).[142] They later updated that both of these catalysts are also effective for the formation of β-aminoesters from imines and ketene silyl esters.[143] These reactions typically gave high yields of the desired product when they took place in non-coordinating solvents such as CH_2Cl_2, but were less efficient in more polar or competing solvents such

as THF and MeCN. Thus, the authors postulate that the nucleophilic carbonyl substrate is activated by complexation to the Lewis acidic phosphorus center. Terada, in 2006, reported a geometrically strained alkoxyphosphonium [**29**]$^+$ as a catalyst for the Diels-Alder reaction of α, β-unsaturated amides and cyclopentadiene (Figure 25 B).[144] The catecholate ligand behaves as an electron withdrawing group to polarize the P-O bonds to enhance the Lewis acidity. In addition, Plumet reported a simple phosphonium cation [$MePh_3P$]$^+$ that can catalyze the addition of trimethylsilyl cyanide to aldehydes and ketones (Figure 25 C). It is important to note that the aforementioned phosphonium catalysts are all stable in air and moisture.

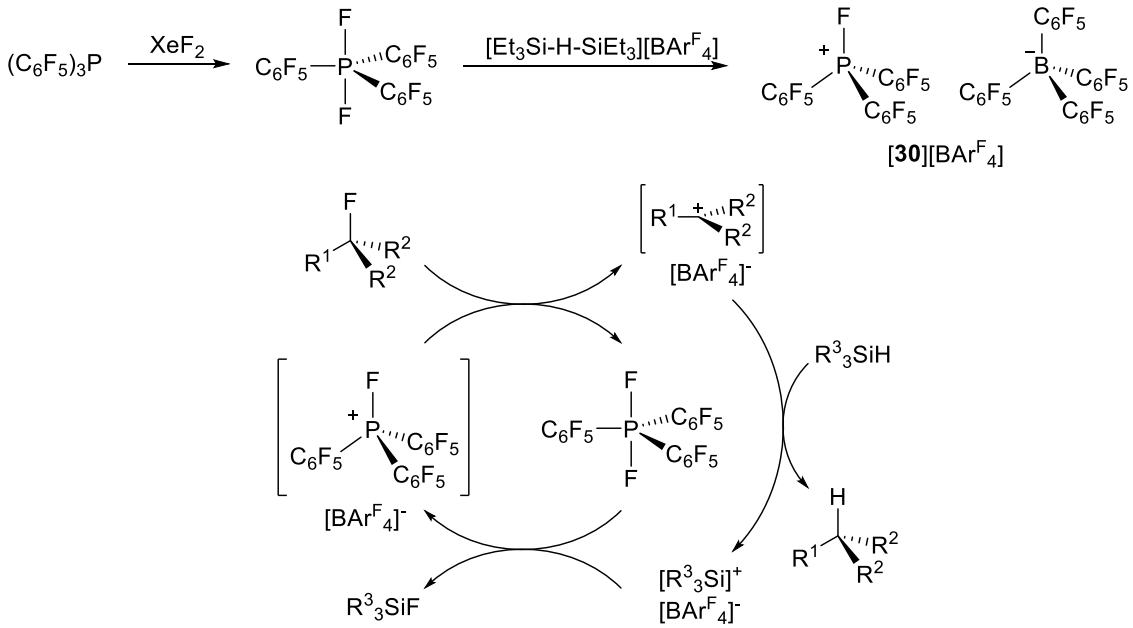

Figure 26. Top: synthesis of [**30**][BAr^F_4]. Bottom: proposed mechanism of the hydrodefluorination reaction catalyzed by [**30**][BAr^F_4].

In 2013, Stephan reported the synthesis and catalytic application of the highly electron deficient Lewis acid, fluoro-tris(pentafluorophenyl)phosphonium [**30**]$^+$ as a tetrakis(pentafluorophenyl)borate ($BAr^F{}_4^-$) salt.[145] This electrophilic phosphonium cation (EPC) was isolated by the reaction of $(C_6F_5)_3P$ and XeF_2 to afford $(C_6F_5)_3PF_2$, followed by fluoride abstraction with triethylsilylium $BAr^F{}_4$ ([Et_3Si-H-$SiEt_3$][$BAr^F{}_4$]), which was generated *in situ* by mixing neat Et_3SiH and trityl $BAr^F{}_4$ (Figure 26).[146] DFT calculations show that the LUMO is concentrated on the phosphorus center, occupying space opposite to the P-F bond. The three highly electron withdrawing and bulky pentafluorophenyl substituents provide steric protection around the phosphorus center, thus preventing aggregation of the compound. The original paper describes that [**30**]$^+$ is highly Lewis acidic and can activate alkyl C-F bonds via fluoride abstraction to afford **30**-F and highly reactive carbocations that were not detectable. Indeed, [**30**][$BAr^F{}_4$] was found to be an excellent catalyst for the hydrodefluorination of fluoroalkanes in the presence of equimolar amounts of Et_3SiH (catalyst loadings 1-10 mol %). Ever since this discovery, [**30**]$^+$ has been utilized as a catalyst for numerous organic transformations including olefin isomerization, Friedel-Crafts dimerization, hydrosilylation reactions,[147, 148] dehydrocoupling reactions,[149] hydroarylation and Markovnikov hydrothiolation of olefins, and ketone deoxygenation,[150] to name a few. The only drawback of [**30**]$^+$ is its moisture sensitivity, which leads to the formation of the hydroxyl adduct in the presence of water.

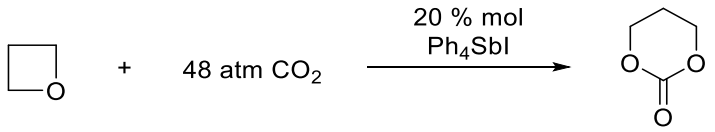

Figure 27. Cycloaddition of oxetane and carbon dioxide catalyzed by Ph_4SbI.

There are several antimony(V)-based catalysts reported in literature as well. In 1985, Baba and Matsuda reported that simple tetraphenylstibonium cations are catalytic active towards cycloaddition of oxetane and carbon dioxide.[151] The formation of the monomeric product was quantitative in the presence of 20 mol % Ph_4SbI at 100 °C under 48 atm of CO_2 (Figure 27, top). Lighter onium iodide species such as Bu_4NI, Ph_4PI, and Ph_4AsI exhibited no catalytic activity, thus indicating that iodide ion plays no critical role in the reaction. Moreover, Ph_4SbBr also did not promote the cycloaddition reaction, thereby revealing that $[Ph_4Sb]^+$ is the active catalyst and bromide ions coordinate to the antimony center to quench the Lewis acidity. Baba later showed that the same stibonium catalyst can promote cycloaddition of oxiranes with heterocumulenes such as isocyanates and carbodiimides as well (Figure 27, bottom).[152-154] Stibonium catalyst Ph_4SbI leads to the selective formation of isomer 1, unlike the classical LiBr catalyst which discriminatory affords isomer 2 (Figure 28). Mechanistic studies reveal that the α-cleavage of the epoxide substrate is kinetically more accessible because of less steric bulk surrounding the antimony center of the alkoxystiborane intermediate.[154]

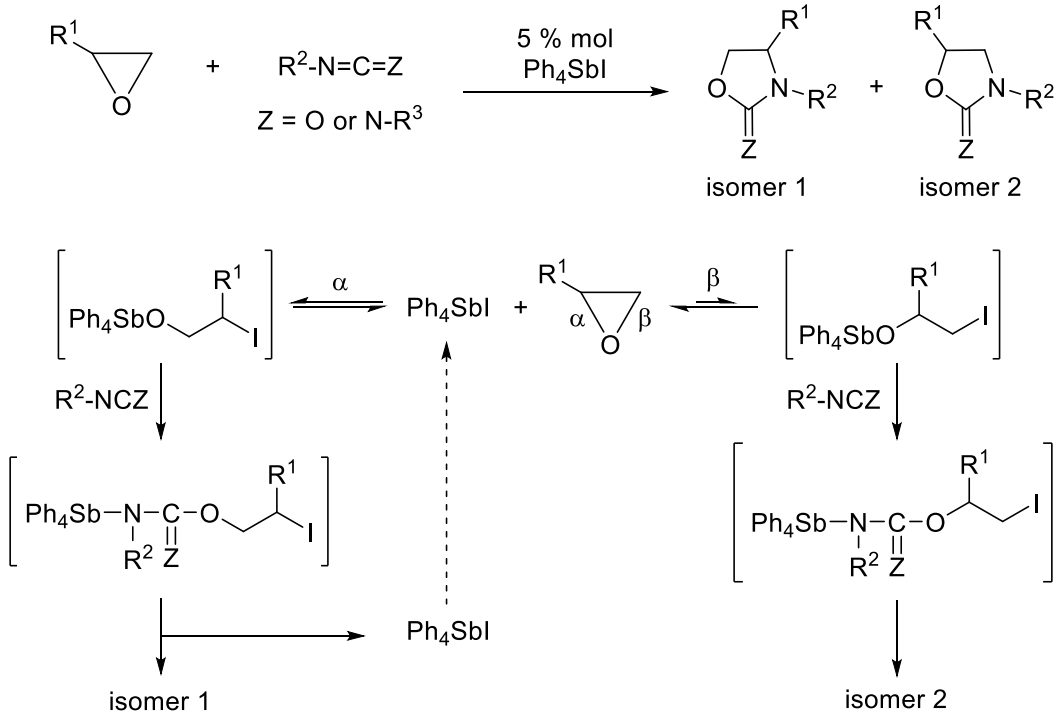

Figure 28. Cycloaddition of oxiranes with heterocumulenes catalyzed by Ph_4SbI and the proposed mechanism.

The triflate salt of Ph_4Sb^+ interestingly has a distinct behavior to its iodide analog and promotes the regio- and chemoselective reaction of oxiranes with amines.[155] In many cases, the product was selectively found as isomer 3 over isomer 4. The authors propose that the epoxide is activated by Ph_4Sb^+ and the amine subsequently attacks the less sterically hindered carbon center, leading to the formation of isomer 3. Mechanstic studies, however, have not been carried out.

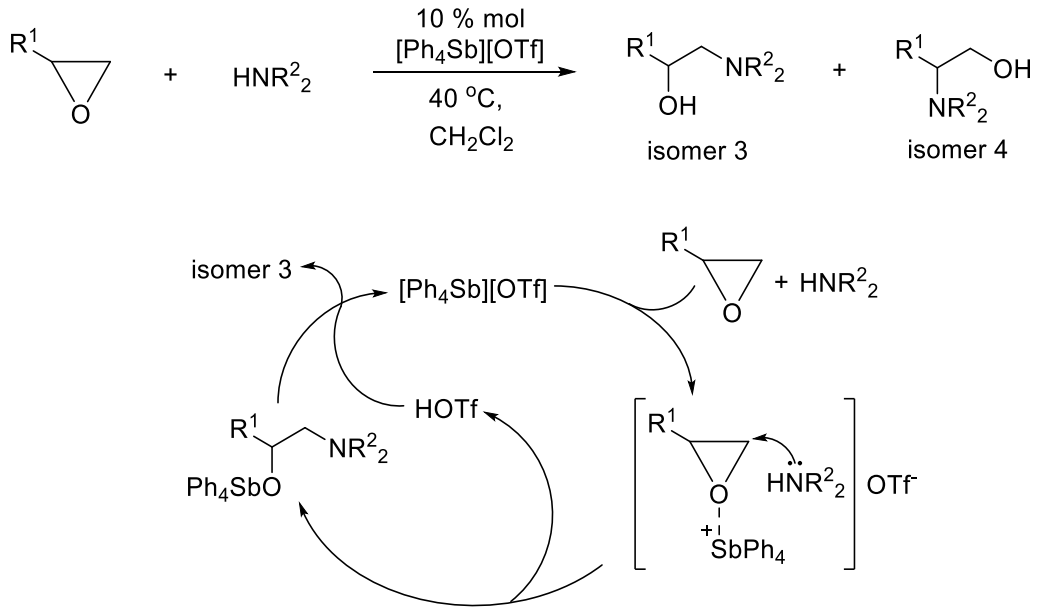

Figure 29. Cycloaddition of oxiranes with amines catalyzed by $[Ph_4Sb][OTf]$ and the proposed mechanism.

Xu, in 2015, reported an air-stable binuclear triphenylantimony(V) bearing an oxide bridge as a catalyst for Michael addition and allylation reactions.[156] This distibonium catalyst $[Ph_3SbOSbPh_3]^{2+}$ was prepared as both perfluorobenzenesulfonate ($[OSO_2C_6F_5]^-$) and perfluorooctanesulfonate ($[OSO_2C_8F_{17}]^-$). In the crystal structure of $[Ph_3SbOSbPh_3][OSO_2C_6F_5]_2$, the sulfonate anions strongly interact with the two antimony centers with Sb-O separations of 2.353(4) and 2.233(3) Å. In contrast, the crystal structure of $[Ph_3SbOSbPh_3][OSO_2C_8F_{17}]_2$ reveals that the sulfonate anions are well-separated from the distibonium complex. Instead, water molecules are coordinating and capping both antimony centers with Sb-O_{water} separations of 2.402(5) and 2.370(5) Å, thus showing that $[Ph_3SbOSbPh_3][OSO_2C_8F_{17}]_2$ is more electrophilic than $[Ph_3SbOSbPh_3][OSO_2C_6F_5]_2$.

Indeed, $[Ph_3SbOSbPh_3][OSO_2C_8F_{17}]_2$ exhibited higher reactivity and catalytic activity than $[Ph_3SbOSbPh_3][OSO_2C_6F_5]_2$ towards Michael addition and allylation reactions.

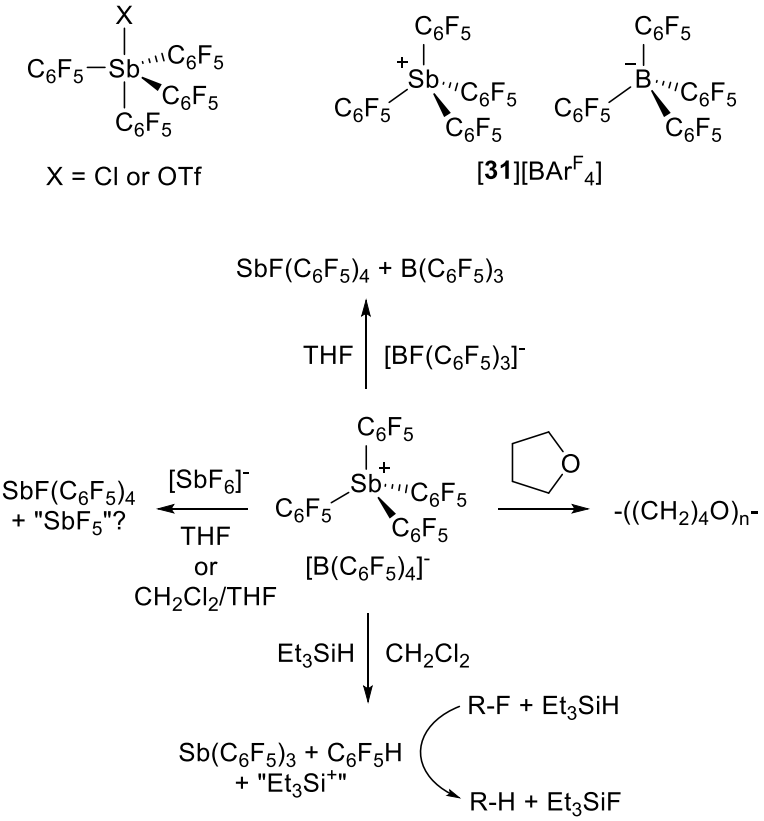

Figure 30. Top: stiboranes **31**-Cl and **31**-OTf and stibonium BAr^F_4 salt [**31**][BAr^F_4]. Bottom: reactivity of [**31**][BAr^F_4].

Our group has reported a highly electron deficient tetraarylstibonium cation, tetrakis(pentafluorophenyl)stibonium [**31**]$^+$, and investigated its coordination chemistry and reactivity.[157] The chloride complex **31**-Cl was synthesized by the reaction of 3.5 equivalents of C_6F_5Li and $SbCl_5$ in a mixture of hexanes and Et_2O at -78 ^oC, followed by filtration of the lithium salt and recrystallization. The crystal structure reveals a chloride

tightly bound to the antimony center (Sb-Cl = 2.4509(11) Å), leading to a trigonal bipyramidal geometry as expected for a pentacoordinate antimony(V) species. The reaction of **31**-Cl and trimethylsilyl triflate (TMSOTf) in MeCN cleanly affords **31**-OTf in good yields and was fully characterized. In the crystal, two independent molecules were found in the asymmetric unit. The crystal structure shows strong interactions within the ionic pair with Sb-O separations of 2.377(2) and 2.471(2) Å, despite triflate ion being less nucleophilic than chloride. Consequently, **31**-OTf also takes that of a trigonal bipyramidal geometry about the antimony center. With these observations in mind, $[\mathbf{31}]^+$ was also prepared with less coordinating anions. In toluene, the reaction of **31**-Cl and $[Et_3Si\text{-}H\text{-}SiEt_3][BAr^F{}_4]$ afforded $[\mathbf{31}][BAr^F{}_4]$ as a remarkably air-stable solid in quantitative yields. The crystal structure shows that $[\mathbf{31}]^+$ is well-separated from its counteranion and the antimony center adopts a tetrahedral geometry. The ^{19}F NMR signals of the $[\mathbf{31}]^+$ unit are more downfield from those of **31**-Cl and **31**-OTf, thereby supporting the ionic character of $[\mathbf{31}][BAr^F{}_4]$ in solution. To get a better insight into the electrophilicity of $[\mathbf{31}]^+$ and its adducts, the Gutmann-Beckett test was carried out and the ^{31}P NMR chemical shift was monitored in the presence of Et_3PO. The ^{31}P NMR resonances of the bound Et_3PO were detected as 73.0 ppm for **31**-OTf and 74.6 ppm for $[\mathbf{31}][BAr^F{}_4]$, thus indicating that the latter is more electrophilic. The reactivity of $[\mathbf{31}][BAr^F{}_4]$ was also investigated. In a solution of THF, the ^{19}F NMR resonances of $[\mathbf{31}]^+$ is much sharper, possibly due to coordination of a solvent molecule to the antimony center. Upon standing at ambient temperature, the THF solution undergoes polymerization which was not observed with **31**-OTf. The reactions of $[\mathbf{31}]^+$ with $(C_6F_5)_3BF^-$ and SbF_6^- in THF

or CH_2Cl_2 or a mixture of the two resulted in rapid formation of **31**-F and the corresponding base-free $(C_6F_5)_3B$ and SbF_5. While ^{19}F NMR signals of free $(C_6F_5)_3B$ were easily detected, the same did not apply for free SbF_5 due to the complex nature of the compound in solution. Stibonium $[\mathbf{31}]^+$ is also an activator of Et_3SiH for the hydrodefluorination reaction of fluoroalkanes such as 1-fluorooctane and trifluorotoluene. Unlike the case of fluorophosphonium $[\mathbf{30}]^+$, NMR studies reveal that $[\mathbf{31}]^+$ readily reacts with Et_3SiH to generate Et_3Si^+ as an active hydrodefluorination species[158] along with $(C_6F_5)_3Sb$ and C_6F_5H as reductive elimination products of unstable $(C_6F_5)_4SbH$.

1.4 Objectives

Despite their potential as stable yet robust Lewis acids, there are only limited reports on the reactivities of organoantimony(V) species. In this context, we decided to develop and investigate the synthesis and the characterization of both neutral and cationic organoantimony(V) Lewis acids for the applications in anion sensing or capturing, organic transformation catalysis as well as ligands to heavy transition metals. We will also study the effect of chelation which typically enhances the Lewis acidity, thus leading to an increased stability of the anion adduct and reactivity of electron-rich organic substrates.

CHAPTER II

LEWIS ACIDIC STIBORAFLUORENES FOR THE FLUORESCENCE TURN-ON SENSING OF FLUORIDE IN DRINKING WATER AT PPM CONCENTRATIONS*

2.1 Introduction

The complexation of fluoride anions in protic media is a topic of intense research because of applications in the field of drinking water analysis[92, 159] and ^{18}F-positron emission tomography.[160] Numerous organic compounds that interact with the anion via the formation of hydrogen bonds have been considered for this purpose.[161-171] However, the efficient capture of this anion in protic solvents typically necessitates the use of a Lewis acidic receptor.[93, 94, 172-175] While ample precedents show that group 13 Lewis acids are especially well suited for this purpose,[176-182] and recent advances in the chemistry of organo-group 15 compounds as Lewis acids[6, 145, 183-185] and fluorophores[186-190] have led us to question whether organoantimony (V) species may also be competent for the complexation and fluorescence sensing of fluoride ions in protic solvents.[114, 117, 191-195] With this objective in mind, we have recently investigated the 9-anthryltriphenylstibonium cation ([**28**]$^+$) and found that this cation captures fluoride in 9/1 vol. water/DMSO to afford the corresponding fluorostiborane **28**-F.[118] The fluorescence properties of [**28**]$^+$ as well as

* Reprinted in part with permission from: "Lewis acidic stiborafluorenes for the fluorescence turn-on sensing of fluoride in drinking water at ppm concentrations"; Hirai, M.; Gabbaï, F. P. *Chem. Sci.* **2014**, *5*, 1886-1893. Copyright 2014 by The Royal Society of Chemistry.

its fluoride affinity are such that sensing can be carried out at ppm or sub-ppm fluoride concentrations. We concluded from these initial experiments that the high fluoride affinity of [**28**]$^+$ arises from strong Coulombic effects which drive the ion pairing process. While the influence of such forces cannot be disputed, we have now decided to determine whether neutral organoantimony (V) compounds would be sufficiently Lewis acidic to complex fluoride anions in protic solvents. In this chapter, we present an initial validation of this idea.

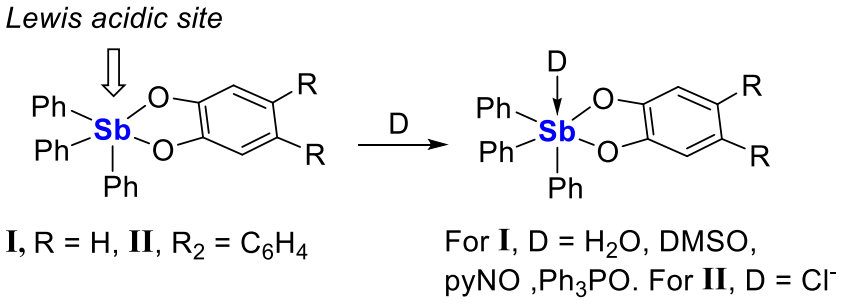

Figure 31. Reactions of triphenylcatecholate with various Lewis bases

In search of a class of Lewis acidic organoantimony species that we could employ in the present study, we were drawn by a number of reports dealing with Lewis adducts of triarylantimony catecholates such as **I**, which adopts a square pyramidal geometry[42, 196] and readily forms adducts with a number of Lewis bases including water,[42] DMSO, *N*-pyridine oxide,[197] and triphenylphosphine oxide.[43] Such compounds have also been shown to engage anions, as in the case of **II** which forms an adduct with chloride anions (Figure 31).[46]

2.2 Fluoride binding properties of spirocyclic stiboranes

Contending that spirocyclic stiboranes may exhibit greater structural stability and provide less hindered access to the antimony atom, we decided to investigate the Lewis acidic behavior of the stiborafluorene **32** and its tetrachloro-analog **11**, which has been previously reported.[46] Compound **32** was obtained in a 72% yield by reaction of the known (2,2'-biphenylene)phenylstibine[46] with *tert*-butyl hydroperoxide[197] and catechol in toluene at 0 °C. This compound has been fully characterized. Its ^{1}H NMR spectrum shows 9 distinct signals whose multiplicity suggests that the derivative adopts a *C*s symmetry. This view is confirmed by the crystal structure of the complex which shows that the biphenylene and catecholato groups are located at the base of the square pyramidal antimony atom, with the phenyl group defining the apex (Figure 32).

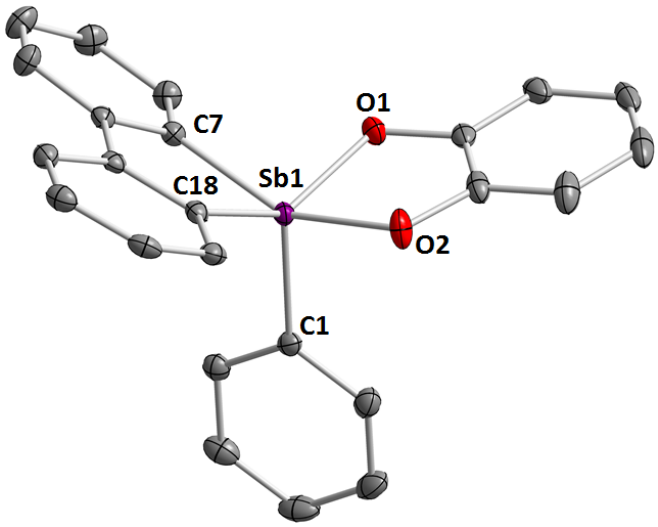

Figure 32. Crystal structure of **32**. Thermal ellipsoids are drawn at the 50 % probability level. The hydrogen atoms and the TAS cation are omitted for clarity. Selected bond lengths (Å) and angles (deg): Sb1-F1 1.973(4), Sb1-O1 2.105(4), Sb1-O2 2.082(4), Sb1-C1 2.131(6), Sb1-C7 2.128(6), Sb1-C18 2.141(6), F1-Sb1-C18 172.11(18), C1-Sb1-O1 168.21(19), O2-Sb1-C7 167.51(19), O1-Sb1-O2 78.65(16), C7-Sb1-C18 82.8(2).

The structures of these two compounds have been computationally optimized using DFT methods. The LUMO of these two complexes are localized on the stiborafluorene moieties and resemble that of the parent fluorenyl cation, with a larger contribution of the atom at the 9-position, in this case the antimony atom, which participates in the π-system via an orbital of σ*(Sb-C_{Ph}) character. The energy of the LUMO in **11** (-1.73 eV) is notably lower than that of **32** (-1.50 eV), an effect that we assign to the perchlorination of the catechol group in **11** (Figure 34).

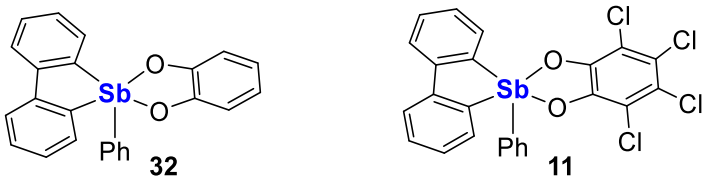

Figure 33. Chemical structures of **32** and **11**.

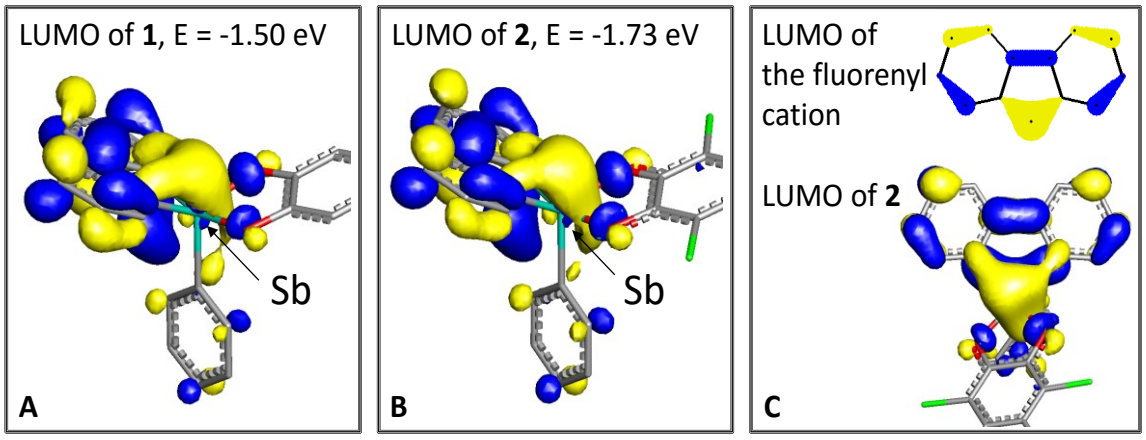

Figure 34. Contour plot and energy of the LUMO in **32** (panel A) and **11** (panel B) (Isodensity = 0.036). Panel C shows the similarity existing between the LUMO of the fluorenyl cation and that of **11**.

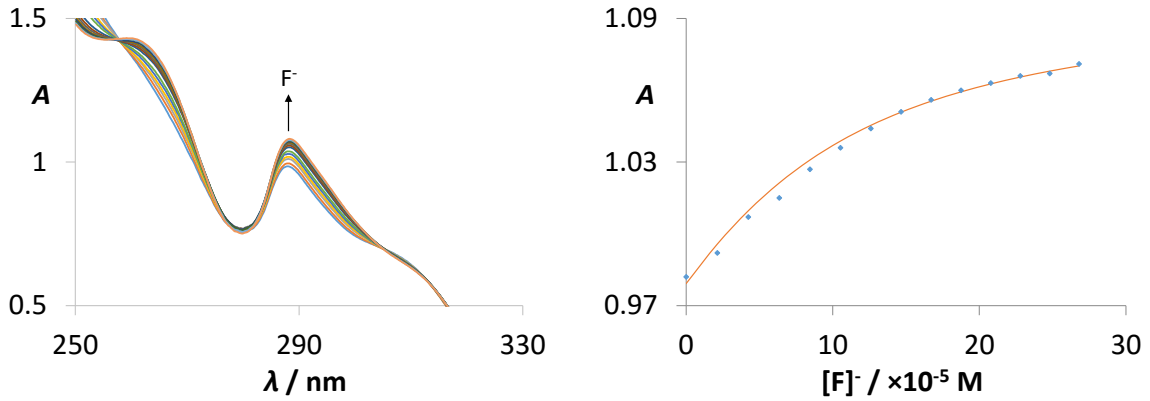

Figure 35. Left: absorption spectra in 7/3 vol. THF/water showing the conversion of **11** (7.2×10^{-5} M) into [**11**-F]$^-$ upon addition of fluoride anions. Right: the experimental and the calculated 1:1 fluoride binding isotherm for **11**. The data were measured at 287.4 nm and fitted with K = 13 500 (± 1 400) M^{-1} (ε(**11**) = 13 600 $M^{-1}cm^{-1}$ and ε([**11**-F]$^-$) = 15 300 $M^{-1}cm^{-1}$).

With these compounds in hand, we decided to investigate their fluoride anion affinity in aqueous solutions. To this end, we carried out a spectrophotometric fluoride titration experiment in 7/3 vol. THF/water solution (Figure 35). While no changes are observed in the UV-Vis spectrum of **32** upon incremental addition of TBAF, we observed clear evidence of fluoride anion binding in the case of **11**. Indeed, the intensity of the band centered at 287.4 nm increases with the fluoride anion concentration. While the origin of these small spectral changes is difficult to assign, they can be fitted to a 1:1 binding isotherm affording a stability constant of 13 500 (± 1400) M^{-1} for [**11**-F]$^-$.[102] Formation of [**11**-F]$^-$ was confirmed by an end-of-titration electrospray ionization mass spectroscopy (ESI-MS) measurement which showed the molecular ion at m/z = 614.7764 amu. It is worth noting that neutral Lewis acids including boranes such as Mes_3B[102, 198] or fluorosilanes such as Ph_3SiF fail to complex fluoride under such conditions, a difference

that underscores the unusual Lewis acidic properties of the stiborafluorene **11**. Also, the contrasting behavior of **32** and **11** demonstrates that the perchlorinated and thus more electron withdrawing catecholate group in **11** effectively increases the Lewis acidity of the antimony center. This conclusion is consistent with the lower energy calculated for the LUMO of **11** when compared to **32** (Figure 34).

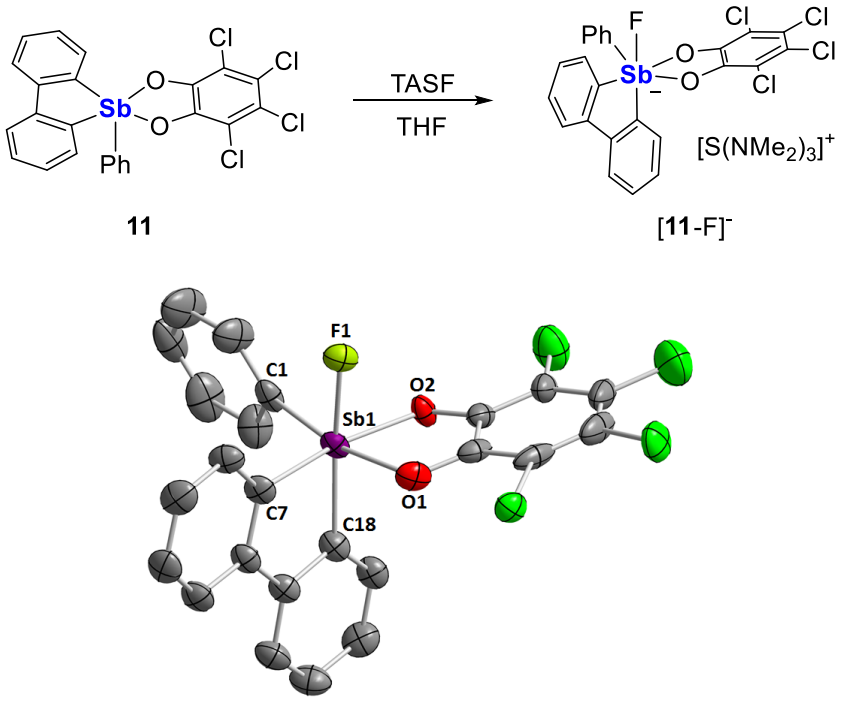

Figure 36. Top: Synthesis of TAS[**11**-F]. Bottom: Crystal structure of TAS[**11**-F]. Thermal ellipsoids are drawn at the 50 % probability level. The hydrogen atoms and the TAS cation are omitted for clarity. Selected bond lengths (Å) and angles (deg): Sb1-F1 1.973(4), Sb1-O1 2.105(4), Sb1-O2 2.082(4), Sb1-C1 2.131(6), Sb1-C7 2.128(6), Sb1-C18 2.141(6), F1-Sb1-C18 172.11(18), C1-Sb1-O1 168.21(19), O2-Sb1-C7 167.51(19), O1-Sb1-O2 78.65(16), C7-Sb1-C18 82.8(2).

The anionic complex [**11**-F]$^-$ can be easily obtained as a tris(dimethylamino)sulfonium (TAS) salt by reaction with TASF in THF. The ^{1}H NMR

resonances of [**11**-F]$^-$ show a loss of the *C*s symmetry with the hydrogen atoms of the biphenylene backbone becoming unequivalent. The ^{19}F NMR spectrum of this complex features a single resonance at -102.8 ppm for [**11**-F]$^-$ corresponding to the antimony-bound fluoride anions. ESI-MS of this salt shows the molecular peak of [**11**-F]$^-$ at 614.7764 amu. The crystal structure of the salt TAS[**11**-F] shows that the anion and the cation are well separated. The anionic component [**11**-F]$^-$ displays an antimony atom in a slightly distorted octahedral geometry (Figure 36). The fluoride anion, arbitrarily denoted as an axial ligand, is located trans from a phenylene ring of the biphenylene backbone. The tetrachlorocatecholate and the phenyl group both lie in the equatorial plane. The fluorine antimony distance for [**11**-F]$^-$ is 1.973(4) Å, which is slightly longer than the average Sb-F bond length in SbF_6^- (1.844 Å).[199]

Although the above results demonstrate that stiborafluorenes are competent molecular recognition units for fluoride anions, the photophysical response accompanying fluoride binding is very weak. This lack of an adequate signaling response makes compounds such as **11** poorly suited for sensing applications. In order to overcome this limitation, we questioned whether the tetrachlorocatecholate ligand of **11** could be replaced by a 1,2-dihydroxybenzene derivative with comparable electron-withdrawing properties, yet more prevalent photophysical properties. These consideration led us to consider alizarin red (1,2-dihydroxyanthraquinone),[200-202] a chromophore that has been previously used in tandem with phenyl boronic acid for the fluorescence detection of fluoride anions.[203-205] The alizarin red chromophore could be conveniently incorporated into the stiborafluorene platform by the route depicted in Figure 37 to afford compound

33 as a dark yellow derivative. The proton spectrum of **33** confirms the presence of the 1,2-dihydroxyanthraquinone. Despite the unsymmetrical nature of the 1,2-dihydroxyanthraquinone ligand, only four C-H resonances from the stiborafluorene backbone are observed, which is suggestive of a fluxional structure. Although we have not been able to obtain a crystalline sample of this complex, we assume that it adopts a square pyramidal geometry analogous to that observed for **32** and **11**. DFT calculations reveal that the HOMO and LUMO of **33** are based on the 1,2-dihydroxyanthraquinone ligand. The LUMO+1 of **33** is localized on the stiborafluorene moiety and resembles the LUMO of **32** and **11** with a large lobe on the antimony atom (Figure 38). The energy of this stiborafluorene-based orbital (-1.61 eV) suggest that the anthraquinone backbone exerts an electron withdrawing effect intermediate between that of the catecholate and tetrachlorocatecholate ligands.

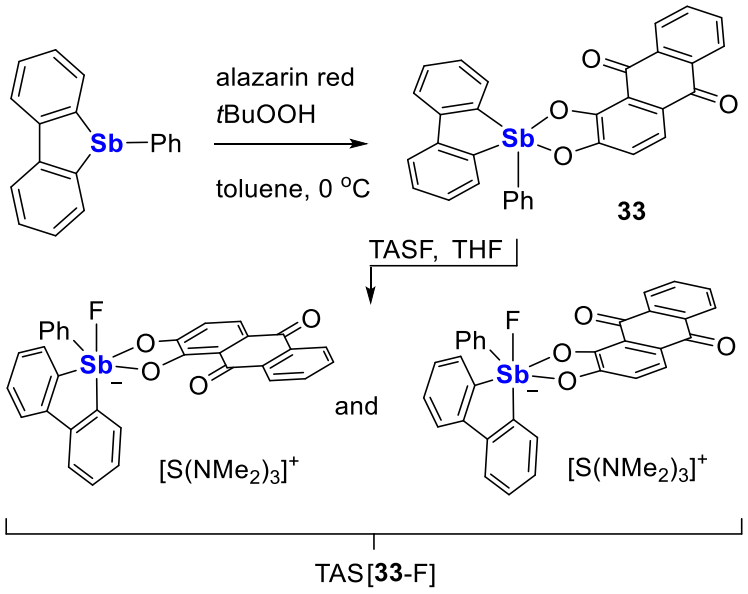

Figure 37. Synthesis of **33** and TAS[**33**-F].

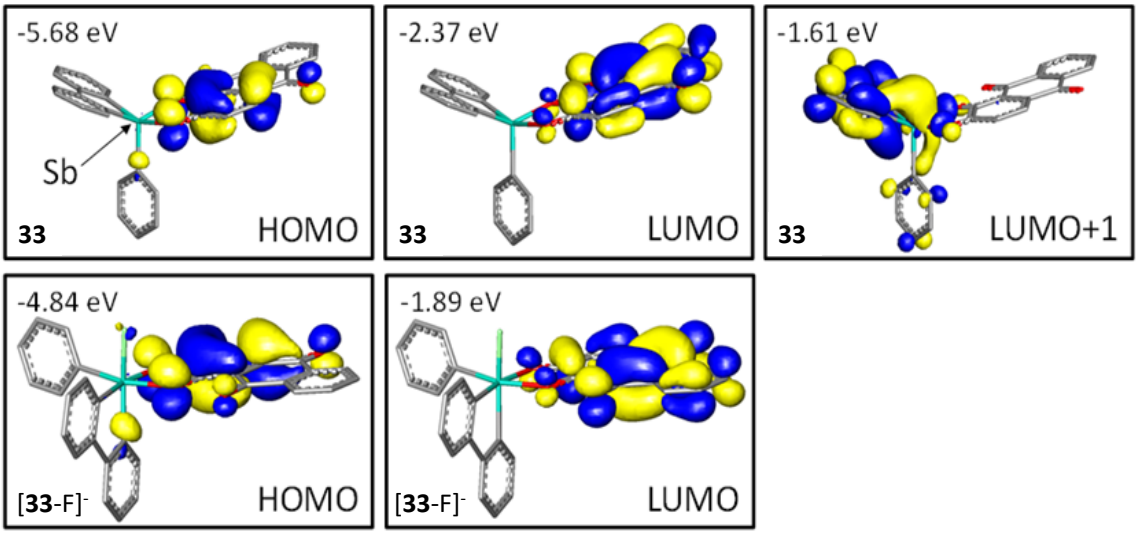

Figure 38. Contour plot of the relevant orbitals in **33** and [**33**-F]$^-$ (Isodensity = 0.036).

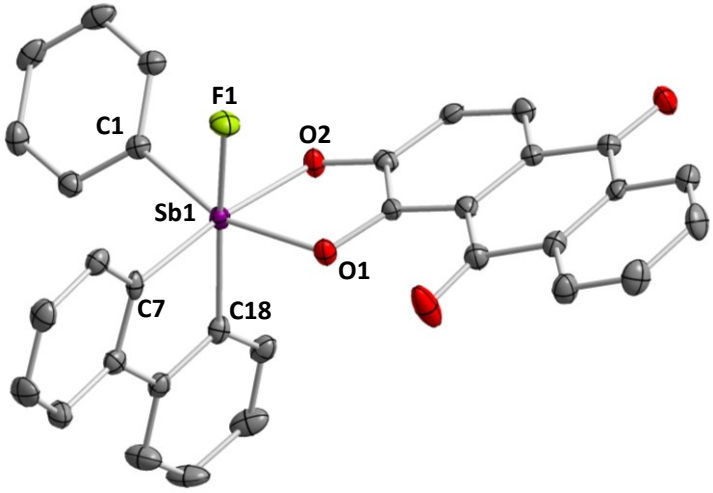

Figure 39. Structure of the crystallized enantiomer of TAS[**33**-F]. Thermal ellipsoids are drawn at the 50 % probability level. The hydrogen atoms and the TAS cations are omitted for clarity. Selected bond lengths (Å) and angles (deg) with the corresponding metrical parameters for the second independent molecule in brackets: Sb1-F1 1.978(4) [1.979(2)], Sb1-O1 2.077(3) [2.082(3)], Sb1-O2 2.100(3) [Sb2-O6 2.100(2)], Sb1-C1 2.126(4) [2.127(4)], Sb1-C7 2.132(4) [2.128(4)], Sb1-C18 2.141(4) [2.138(4)], F1-Sb1-C18 172.14(12) [170.05(12)], C1-Sb1-O2 160.53(12) [162.58(12)], C7-Sb1-O1 172.36(12) [171.80(12)], O1-Sb1-O2 77.61(10) [77.90(10)], C7-Sb1-C18 82.02(15) [81.96(14)].

Complex [**33**-F]$^-$ can be isolated as a crystalline TAS salt when generated from **33** and TASF in THF (Figure 37). This salt has been isolated and fully characterized. Its composition has been verified by elemental analysis. When this compound is dissolved in CD_3CN and analyzed by ^{19}F NMR spectroscopy, two signals are observed at -107.3 and -112.3 ppm with a 1:1 intensity ratio. We speculate that these two signals, which are close to those measured for [**11**-F]$^-$ (-102.8 ppm), arise from the existence of diastereomers that differ by the orientation of the unsymmetrical 1,2-dihydroxyanthraquinone with respect to the Sb-Ph bond (Figure 39). Due to complication, both ^1H and ^{19}F NMR spectra are shown in Figure 47. Crystallization of TAS[**33**-F] lead to the isolation of single crystals which contain the two enantiomers of one of the diastereomers (Figure 39). In these crystals, the two enantiomers, which are not related by crystallographically imposed symmetry, are found in the asymmetric unit. Their structures are, as expected, very similar with an octahedral geometry at antimony and with Sb-F bond lengths of 1.978(2) and 1.979(2) Å comparable to those in [**11**-F]$^-$.

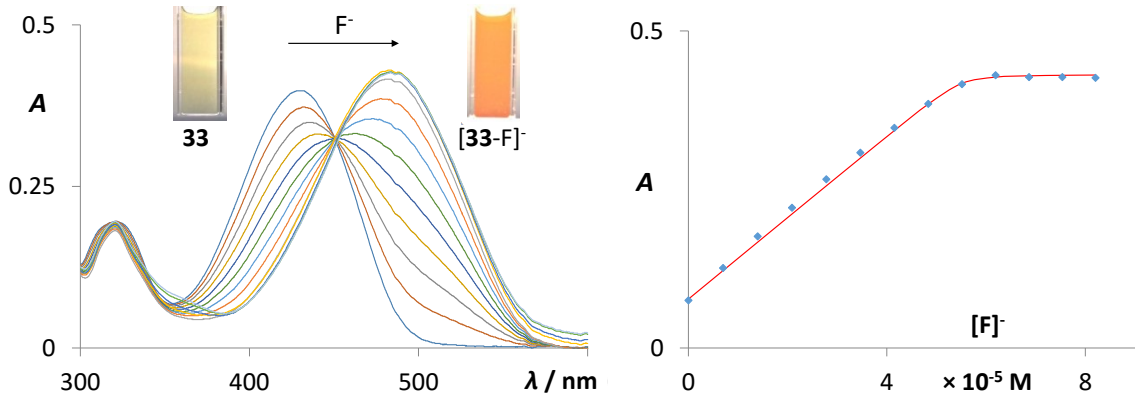

Figure 40. Left: spectral changes in the UV-Vis absorption spectrum of **33** (5.5×10^{-5} M in CH_2Cl_2) upon addition of fluoride. The inset on the top right shows the fluorescence spectra of **33** (5.0×10^{-6} M in CH_2Cl_2) before and after addition of a stoichiometric amount of fluoride ($\lambda_{excitation}$= 482 nm). Right: the experimental and the calculated 1:1 fluoride binding isotherms for **33** at 483 nm. The data were fitted with $K > 10^7$ M^{-1} (ε(**33**) = 1400 $M^{-1}cm^{-1}$ and ε([**33**-F]$^-$ = 7850 $M^{-1}cm^{-1}$)).

In a solution of dry CH_2Cl_2, the absorption spectrum of **33** is dominated by a broad absorption band at λ_{max} = 430 nm arising from the 1,2-dihydroxyanthraquinone chromophore. The energy of this band is similar to that observed in other alizarin containing derivatives.[200-205] TD-DFT calculations show that this absorption band corresponds to the HOMO to LUMO transition (λ_{max}(calculated) = 435 nm, f = 0.2598). Incremental addition of fluoride ions induces a notable redshift of the low energy band as shown in Figure 40. This phenomenon is ascribed to the conversion of **33** into [**33**-F]$^-$, whose formation is essentially quantitative as indicated by the shape of the 1:1 binding isotherm (Figure 40). Inspection of the spectra also shows that the energy of the absorption band shifts by 50 nm upon conversion of **33** (λ_{max} = 430 nm) into [**33**-F]$^-$ (λ_{max} = 482 nm). This redshift is accompanied by a marked colorimetric response which can be readily detected with the naked eye when the reaction is carried out at mM concentrations.

Using the same level of theory as for **33**, the structure of [**33**-F]$^-$ has been optimized using DFT methods and subsequently subjected to TD-DFT calculations (Table 1 and Table 2). These calculations show that the frontiers orbitals remain centered on the alizarin chromophore, with the same atomic distribution as in the case of **33** (Figure 38). These calculations also show that their energy is perturbed by the presence of an antimony-bound fluoride anion. This perturbation is reflected by the narrower HOMO-LUMO gap and the calculated wavelength of λ_{max}(calculated) = 484 nm (f = 0.2824) (vs the experimental value of λ_{max} = 482 nm). These theoretical results show that the redshift observed upon conversion of **33** into [**33**-F]$^-$ originates from the conversion of the stiborane into a negatively charged, electron-rich fluoroantimonate, which destabilizes the alizarin-based HOMO and narrows the HOMO-LUMO gap by 0.36 eV from 3.31 eV in **33** to 2.95 eV in [**33**-F]$^-$ based on the computed energy of the frontier orbitals. These calculations are in good agreement of with the experimentally observed 50 nm (or 0.31 eV) redshift observed upon fluoride binding. The redshift observed upon formation of the fluoroantimonate [**33**-F]$^-$ bears a parallel to the chemistry of some organoboron-based fluoride sensors, for which conversion of the neutral boron center into an electron-rich fluoroborate moiety also results in a redshift of the absorption band of the appended chromophore.[206, 207]

Table 1. TD-DFT calculation output showing the nature of the low energy excitation for **33** in CH_2Cl_2.

Excitations	Energy	Oscillator strength	MO→MO transition	Contributions
E_a	2.8526 eV (434.63 nm)	0.2598	133→134	0.69855

Table 2. TD-DFT calculation output showing the nature of the low energy excitation for [**33**-F]$^-$ in CH_2Cl_2.

Excitations	Energy	Oscillator strength	MO→MO transition	Contributions
E_a	2.5633 eV (483.69 nm)	0.2824	138→139	0.70012

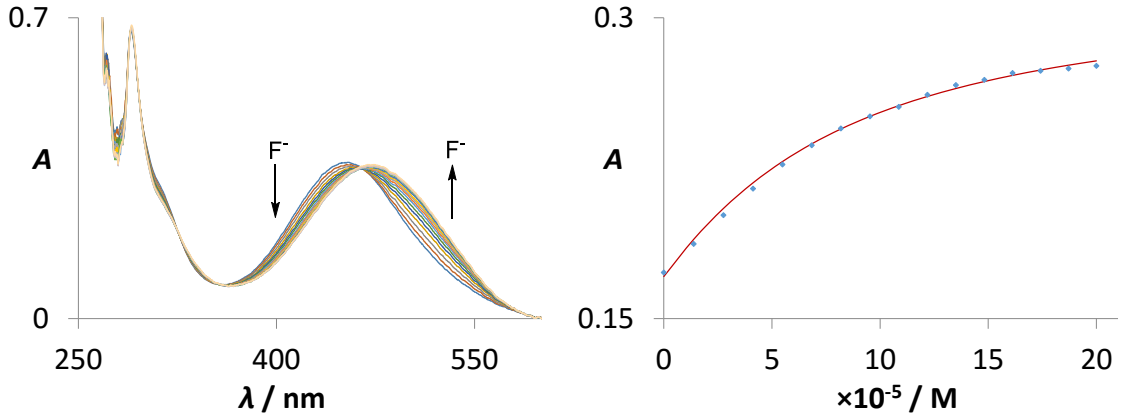

Figure 41. Left: Spectral changes in the UV-Vis absorption spectrum of **33** (3.8×10^{-5} M in 7/3 vol. THF/water) upon addition of fluoride. Right: The experimental and the calculated 1:1 fluoride binding isotherms for **33** at 510 nm. The data were fitted with K = 16 100 M^{-1} (ε(**33**) = 4500 $M^{-1}cm^{-1}$ and ε([**33**-F]$^-$ = 8350 $M^{-1}cm^{-1}$)).

A spectrophotometric titration carried out in 7/3 vol. THF/water shows that the stability constant of [**33**-F]$^-$ (16 100 (± 1100) M^{-1}) is close to that of [**11**-F]$^-$ (13 500 (± 1400) M^{-1}) (Figure 41). The aliquot after titration was analyzed by ESI-MS which showed the molecular peak of [**33**-F]$^-$ at m/z = 607.0655 amu. Under these conditions, however, the redshift of the low energy band is not as marked as in neat CH_2Cl_2, a difference that we assign to the coordination of water to the antimony atom.

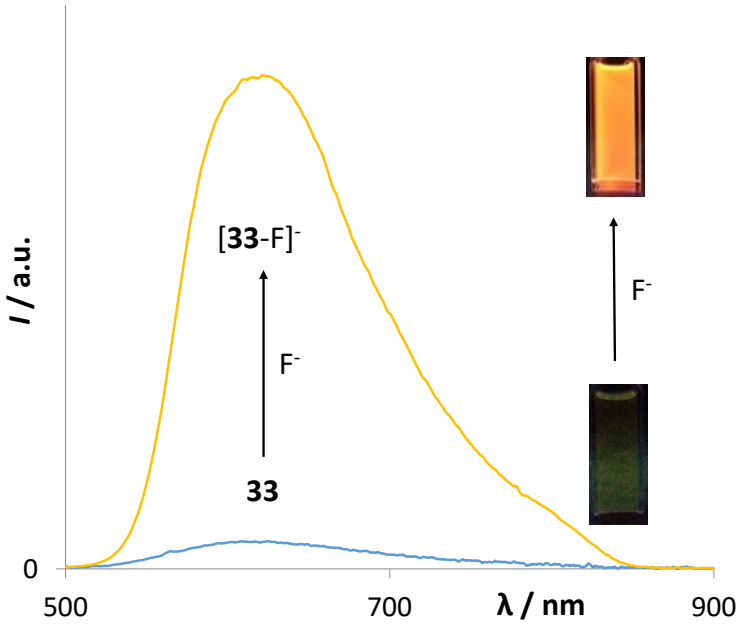

Figure 42. The fluorescence spectra of **33** (5.0×10^{-6} M in CH_2Cl_2) before and after addition of a stoichiometric amount of fluoride ($\lambda_{excitation}$= 482 nm). The fluorescent images were taken using a solution of **33** (5.5×10^{-5} M) in CH_2Cl_2, before and after addition of fluoride, illuminated with a hand-held UV lamp.

We have also tested the fluorescence properties of **33**. The fluorescence spectra of this compound in CH_2Cl_2 show a broad emission at 616 nm, characteristic of the alizarin red chromophore (Figure 42).[203-205] With a quantum yield of Φ = 0.2 % ($\lambda_{excitation}$= 482 nm), this emission is very weak. Gratifyingly, we found that addition of fluoride to the solution results in a drastic fluorescence increase from Φ = 0.2 % for **33** to Φ = 3.0 % for [**33**-F]$^-$. The intensity increases linearly with the first equivalent of fluoride indicating quantitative formation of [**33**-F]$^-$. The fluorescence turn-on response observed during this anion binding reaction is assigned to the increased rigidity of the hexacoordinate antimony complex [**33**-F]$^-$.

2.3 Spirocyclic stiboranes as fluoride sensors in water/CH_2Cl_2 mixture

The anion binding properties of complex **33** have been evaluated under biphasic conditions. We first layered a CH_2Cl_2 solution of **33** (1 mL, [**33**] = 5.0×10^{-4} M) with an aqueous solution (5 mL) containing tetrapropylammonium bromide (TPABr; 20 mM) as a phase transfer agent. We found that tetrapropylammonium bromide is a better choice than tetramethyl- and tetraethyl-ammonium bromide which do not efficently support fluoride phase transfer. We also observed that tetra-*n*-butylammonium bromide is too lipophilic and promotes uncontrolled hydroxide transfer to the organic phase, leading to neutralization of the Lewis acidic receptor. Upon shaking of this biphasic mixture, the color of the CH_2Cl_2 layer changes from pale yellow to dark red, a phenomenon assigned to hydroxide binding to the antimony center of **33**. Gratifyingly, we found that this interfering reaction could be prevented by simply buffering the water layer at pH 4.68 using a citric acid/citrate (10 mM). Using these conditions, we decided to interrogate the system with low concentrations of fluoride and we observed that ppm concentrations of this anion can be readily assessed with the naked eye. Indeed, addition of 1.9 ppm of fluoride (1.0×10^{-4} M KF) to the water layer results in a distinct darkening of the CH_2Cl_2 layer from yellow to pale orange (Figure 43). A further intensification of the color is observed when the KF concentration is raised to 3.8 ppm (2.0×10^{-4} M KF). Formation of [**33**-F]$^-$ was confirmed by UV-Vis and fluorescence measurements as well as by ^{19}F NMR measurements (13 200 scans) of the CH_2Cl_2 layer which shows the two expected peaks at -107.2 and -112.4 ppm. No color change was observed in the presence of other

anions such as Cl^-, Br^-, NO_3^-, HCO_3^-, $H_2PO_4^-$ and HSO_4^-, which indicates that **33** is highly selective for fluoride anions.

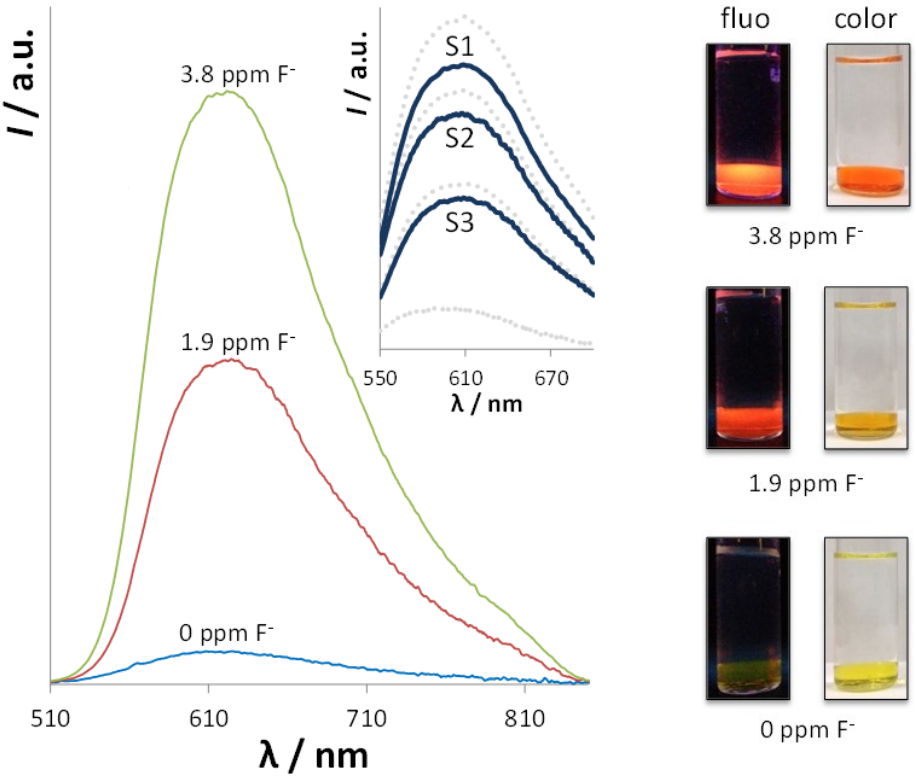

Figure 43. Left: Fluorescence spectra ($\lambda_{excitation}$ = 482 nm) of solutions of **33** (5.0×10^{-6} M) in CH_2Cl_2. For each measurement, the solution was prepared by the 100-fold dilution of a 5.0×10^{-4} M solution of **33** which had been layered with an aqueous solution of KF (0, 1.9 and 3.8 ppm) containing TPABr (20 mM) and a citrate buffer (10 mM, pH 4.68). Drinking water analysis data: each fluorescence spectrum is obtained with a solution of **33** in CH_2Cl_2 (5.0×10^{-5} M) after layering with a standard fluoride solution or an unknown sample. The spectra drawn with dotted lines correspond to the standard fluoride solutions (0, 0.4, 0.7 and 1.0 ppm, from bottom to top). The spectra obtained for the unknown samples are drawn with solid lines (S1 = H-E-B® Baby Purified Water (with fluoride added); S2 = Nursery® Water; S3 = College Station Tap Water. Right: Naked-eye fluorescence and colorimetric response associated with the formation of [**33**-F]$^-$ at a concentration of 5.0×10^{-4} M.

2.4 Determination of fluoride concentrations of water samples

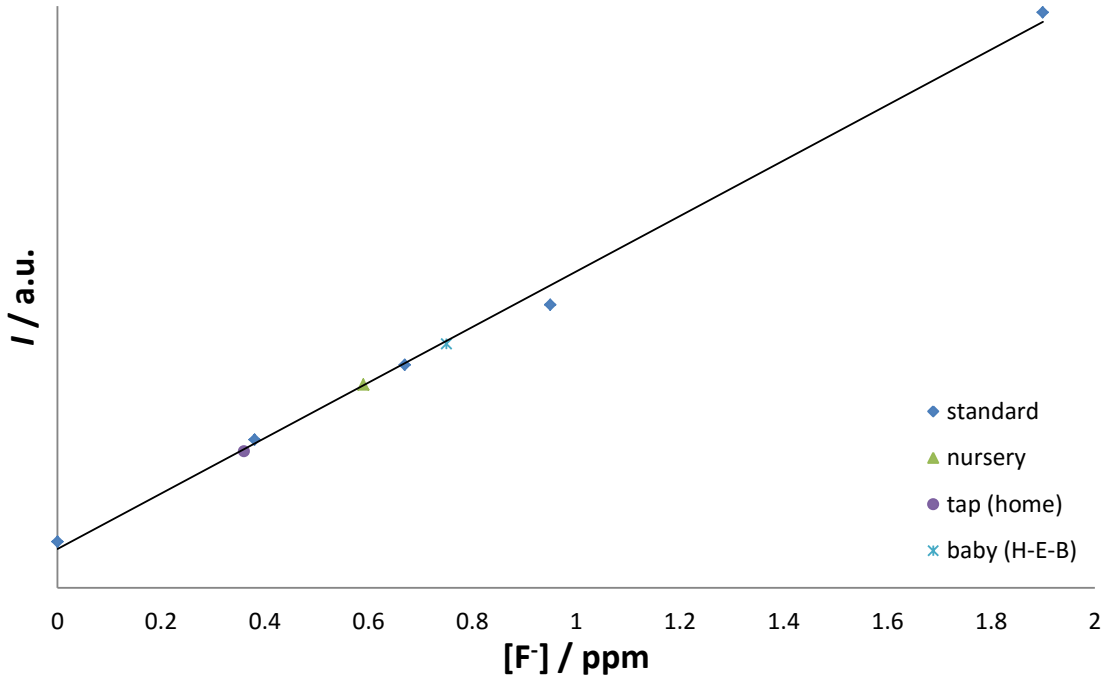

Figure 44. Drinking water analysis. Fluorescence intensity of a solution of **33** in CH_2Cl_2 (1 mL, 5.0×10^{-5} M) measured at 610 nm ($\lambda_{excitation}$ = 482 nm). For each measurement, a 5 mm NMR tube was filled with a solution of **33** in CH_2Cl_2 (1.0 mL, 5.0×10^{-5} M) and layered with an aqueous solution containing TPABr (20 mM) and a citrate buffer (10 mM, pH 4.6). To obtain a calibration curve, the aqueous layer was doped with different amounts of fluoride (0, 0.4, 0.7, 1.0, 1.9 ppm). After vigorous shaking (1 min), the tube was inserted into the cavity of the fluorometer such that only the CH_2Cl_2 layer was position in the optical path. The plot shows that the fluorescence intensity increases linearly with the fluoride concentration in the 0-1.9 ppm range. Drinking water samples (Nursery® Water, H-E-B® Baby Purified Water, and tap water of College Station) where combined with TPABr (20 mM) and buffered with citrate (10 mM, pH 4.6). The resulting solutions were transferred into a 5 mm NMR tube filled with a solution of **33** in CH_2Cl_2 (1.0 mL, 5.0×10^{-5} M). The fluorescence intensity was measured as described above for the standard.

These fluoride sensing results suggest that **33** may be well suited for real-life applications. To put this possibility to a test, we have investigated the use of **33** for tap

water and bottled water analysis (Figure 44). Using biphasic conditions analogous to those described above, we analyzed several drinking water samples. We found that the tap water in College Station contains 0.4(±0.05) ppm of fluoride, which is close to the concentration of 0.44 ppm documented in the most recent water quality report. We also assayed two different brands of fluoridated water marketed for infant consumption. In the first water sample, sold by the H-E-B® supermarket chain as H-E-B® Baby Purified Water (with fluoride added), we found a fluoride concentration of 0.8(±0.1) ppm which is in good agreement with the maximum fluoride content of 1 ppm advertised on the label. The second water sample was Nursery® Water with an advertised maximum concentration of 0.7 ppm. For this water sample, our method provided a concentration of 0.6(±0.7) ppm, again in good agreement with the level of fluorination advertised on the label.

2.5 Conclusion

The results presented in this paper show that neutral organoantimony(V) species may be sufficiently Lewis acidic to overcome the high hydration energy of the fluoride anion. This is the case of compounds **11** and **33** which are readily converted into the corresponding fluoroantimonate anions [**11**-F]$^-$ and [**33**-F]$^-$. While fluoride binding to the antimony center does not necessarily trigger a strong photophysical response as in the case of **11**, the incorporation of an alizarin chromophore in **33** imparts some advantageous turn-on properties. These turn-on properties along with its elevated fluoride affinity make this derivative a useful water compatible fluoride sensor which can be used for the determination of sub-ppm concentrations of fluoride ions in bottled and tap waters.

2.6 Experimental section

General considerations. Because of poor gastrointestinal uptake, oral LD50 values for antimony compounds (eg. 0.5g/kg for SbCl3 and 1.1g/kg for SbCl5 in rat) are relatively high. However, antimony compounds are very toxic when administered intravenously. We have therefore handled these compounds with great caution and recommend any experimentalist to do the same. N,N,N'N'-tetramethylethylenediamine (tmeda) was purchased from Aldrich and distilled from powdered CaH2 and stored under N2. Biphenyl and [S(NMe2)3][Me3SiF2] (TASF) were purchased from Aldrich and used as received. Antimony trichloride ($SbCl_3$), triphenyl stibine (Ph_3Sb), n-butyl lithium (2.3 M in hexane), 1,2-dihydroxyanthraquinone (alizarin red) were purchased from Alfa Aesar. Tetrachloro-o-benzoquinone was purchased from Acros Organics. (2,2'-Biphenylene)phenylstibine and stiborane **11**[46] were prepared according to the reported procedure. All preparations were carried out under an atmosphere of dry N_2 employing either a glovebox or standard Schlenk techniques. Solvents were dried by passing through an alumina column (pentane, CH_2Cl_2) or refluxing under N_2 over Na/K (Et_2O and THF). All other solvents were ACS reagent grade and used as received. NMR spectra were recorded on a Varian Unity Inova 500 FT NMR (499.42 MHz for ^1H, 469.86 MHz for ^{19}F, 125.60 MHz for ^{13}C) spectrometer at ambient temperature. Chemical shifts are given in ppm and are referenced to residual ^1H and ^{13}C solvent signals and external $BF_3 \cdot Et_2O$ for ^{19}F. Elemental analyses were performed by Atlantic Microlab (Norcross, GA). The pH measurements were carried out with a Radiometer PHM290 pH meter equipped with a VWR SympHony electrode. Electronic absoption spectra were recorded at ambient

temperature using an Ocean Optics USB4000 spectrometer with an Ocean Optics ISS light source. Emission spectra were recorded at ambient temperature using a PTI QuantaMaster™ 30 fluorescence spectrofluorometer. Electrospray ionization mass spectra were recorded on Applied Biosystems PE SCIEX QSTAR.

Computational details. Density functional theory (DFT) structural optimizations with the *Gaussian 09* program.[208] In all cases, the structures were optimized using the B3LYP functional[209, 210] and the following mixed basis set: Sb, aug-cc-pVTZ-PP;[211] Cl, 6-311g(d); F, 6-31g(d'); [212] C/O/H, 6-31g.[213] Each structure was subsequently subjected to TD-DFT calculation using the B3LYP functional and the SMD implicit solvation model with CH_2Cl_2 as a solvent. The orbitals plotted in Figure 34 and Figure 38 as well as their energies are obtained from the TD-DFT output (with solvation). For all optimized structures, frequency calculations were carried out to confirm the absence of imaginary frequencies. The molecular orbitals were visualized and plotted in Jimp 2 program.[214] The LUMO of the fluorenyl cation show in Figure 34 was generated using the The Simple Huckel Molecular Orbital Theory Calculator program available at http://www.chem.ucalgary.ca/SHMO/.

Crystallographic measurements. The crystallographic measurements were performed at 110(2) K using a Bruker APEX-II CCD area detector diffractometer, with a graphite-monochromated Mo-Kα radiation (λ = 0.71069 Å). A specimen of suitable size and quality was selected and mounted onto a nylon loop. The semi-empirical method SADABS was applied for absorption correction. The structure was solved by direct methods, which successfully located most of the non-hydrogen atoms. Subsequent

refinement on F^2 using the SHELXTL/PC package (version 6.1) allowed location of the remaining non-hydrogen atoms. All H-atoms were geometrically placed and refined using a standard riding model.

Table 3. Crystal data, data collections, and structure refinements for **32** and TAS[**11**-F].

Crystal data	**32**	TAS[**11**-F]
Empirical formula	C24 H17 O2 Sb	C30 H31 Cl4 F N3 O2 S Sb
Formula weight	459.13	780.19
Temperature	110(2) K	110(2) K
Wavelength	0.71073 Å	0.71073 Å
Crystal system	Monoclinic	Monoclinic
Space group	P2(1)/c	P2(1)/c
Unit cell dimensions	a = 9.8268(8) Å	a = 10.0011(8) Å
	b = 14.9773(12) Å	b = 21.4018(18) Å
	c = 13.5372(11) Å	c = 16.9437(11) Å
	α = 90°	α = 90°
	β = 111.26°	β = 93.69°
	γ = 90°	γ = 90°
Volume	1856.9(3) Å^3	3061.9(4) Å^3
Z	4	4
Density (calculated)	1.642 Mg/m^3	1.692 Mg/m^3
Absorption coefficient	1.502 mm^{-1}	1.359 mm^{-1}
F(000)	912	1568
Crystal size	0.55 x 0.38 x 0.34 mm^3	0.28 x 0.22 x 0.22 mm^3
Theta range for data collection	2.11 to 29.67°.	1.71 to 28.36°.
Index ranges	-13<=h<=13, -20<=k<=20, -18<=l<=18	-13<=h<=13, -28<=k<=28, -22<=l<=22
Reflections collected	23397	38078
Independent reflections	4996 [R(int) = 0.0265]	7649 [R(int) = 0.0292]
Absorption correction	Semi-empirical from equivalents	Semi-empirical from equivalents
Max. and min. transmission	0.6292 and 0.3617	0.7542 and 0.7021
Refinement method	Full-matrix least-squares on F^2	Full-matrix least-squares on F^2
Data / restraints / parameters	4996 / 0 / 244	7649 / 0 / 385
Goodness-of-fit on F^2	1.128	1.055
Final R indices [I>2sigma(I)]	R1 = 0.0200, wR2 = 0.0482	R1 = 0.0693, wR2 = 0.1890
R indices (all data)	R1 = 0.0223, wR2 = 0.0490	R1 = 0.0800, wR2 = 0.1988
Largest diff. peak and hole	0.453 and -0.638 e.Å^{-3}	3.313 and -3.658 e.Å^{-3}

[a] $R1 = \Sigma||Fo| - |Fc||/\Sigma|Fo|$. [b] $wR2 = \{[\Sigma w(Fo^2 - Fc^2)^2]/[\Sigma w(Fo^2)^2]\}^{1/2}$.

Table 4. Crystal data, data collection, and structure refinement for TAS[**33**-F].

Crystal data	TAS[**33**-F]
Empirical formula	C38 H37 F N3 O4 S Sb
Formula weight	772.52
Temperature	110(2) K
Wavelength	0.71073 Å
Crystal system	P2(1)2(1)2(1)
Space group	Orthothombic
Unit cell dimensions	a = 14.7131(16) Å
	b = 16.7493(18) Å
	c = 27.433(3) Å
	α = 90°
	β = 90°
	γ = 90°
Volume	6760.4(13) Å^3
Z	8
Density (calculated)	1.518 Mg/m^3
Absorption coefficient	0.929 mm^{-1}
F(000)	3152
Crystal size	0.28 x 0.20 x 0.08 mm^3
Theta range for data collection	1.57 to 28.33°.
Index ranges	-19<=h<=19, -22<=k<=22, -36<=l<=36
Reflections collected	84322
Independent reflections	16829 [R(int) = 0.0494]
Max. and min. transmission	0.9294 and 0.7809
Refinement method	Full-matrix least-squares on F^2
Data / restraints / parameters	16829 / 0 / 860
Goodness-of-fit on F^2	1.064
Final R indices [I>2sigma(I)]	R1 = 0.0582, wR2 = 0.1483
R indices (all data)	R1 = 0.0683, wR2 = 0.1557
Absolute structure parameter	0.78(2)
Largest diff. peak and hole	7.932 and -1.704 e.Å^{-3}

[a] $R1 = \Sigma||Fo| - |Fc||/\Sigma|Fo|$. [b] $wR2 = \{[\Sigma w(Fo^2 - Fc^2)^2]/[\Sigma w(Fo^2)^2]\}^{1/2}$.

The NMR data was reported according to the following numbering scheme:

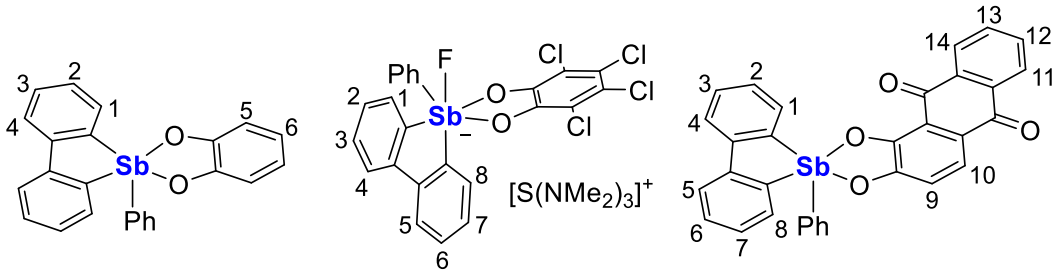

32 TAS[**11**-F] **33**

Synthesis of 32. To a suspension of (2,2'-biphenylene)phenylstibine (285.7 mg, 81 μmol) and catechol (110.1 mg, 81 μmol) in toluene (15 mL) at 0 ºC was added a toluene solution (5 mL) of *tert*-butyl hydroperoxide (70 wt. % in water, 104.0 mg, 0.081 mmol) dropwise over a period of 15 min. After stirring the mixture at reduced temperature for 15 min, the solvent was removed under vacuum and washed with two portions of methanol (5 mL each) to afford **32** as a yellow product (268.6 mg, 72% yield). Large yellow single crystals of **32** were obtained by slow diffusion of pentane into a chloroform solution at ambient temperature. ^{1}H NMR (499.42 MHz, $CDCl_3$): δ 8.08 (d, H_4, $^{3}J_{H\text{-}H}$ = 7.5 Hz; 2H), 8.02 (d, *o*-SbPh, $^{3}J_{H\text{-}H}$ = 7.5 Hz; 2H), 7.64 (pseudo dt, H_1, $^{3}J_{H\text{-}H}$ = 7.0 Hz, $^{4}J_{H\text{-}H}$ = 2.0 Hz; 2H), 7.57 (pseudo td, H_2 or H_3, $^{3}J_{H\text{-}H}$ = 7.5 Hz, $^{4}J_{H\text{-}H}$ = 1.5 Hz; 2H), 7.51 (pseudo td, H_2 or H_3, $^{3}J_{H\text{-}H}$ = 7.5 Hz, $^{4}J_{H\text{-}H}$ = 1.5 Hz; 2H), 7.45 (pseudo td, *p*-SbPh, $^{3}J_{H\text{-}H}$ = 7.5 Hz, $^{4}J_{H\text{-}H}$ = 1.5 Hz; 1H), 7.38 (pseudo td, H_2, $^{3}J_{H\text{-}H}$ = 7.0 Hz, $^{4}J_{H\text{-}H}$ = 2.0 Hz; 2H), 6.97 (m, 2H, H_6), 6.68 (m, 2H, H_5). ^{13}C{^{1}H} NMR (125.60 MHz, $CDCl_3$): δ 147.66 (*o*-C_6H_4) , 140.78,

135.11, 133.96, 132.89, 132.51, 132.29, 132.19, 129.77, 129.71, 122.75, 118.97. The NMR spectra of this compound are provided in Figure 45 as a measure of purity.

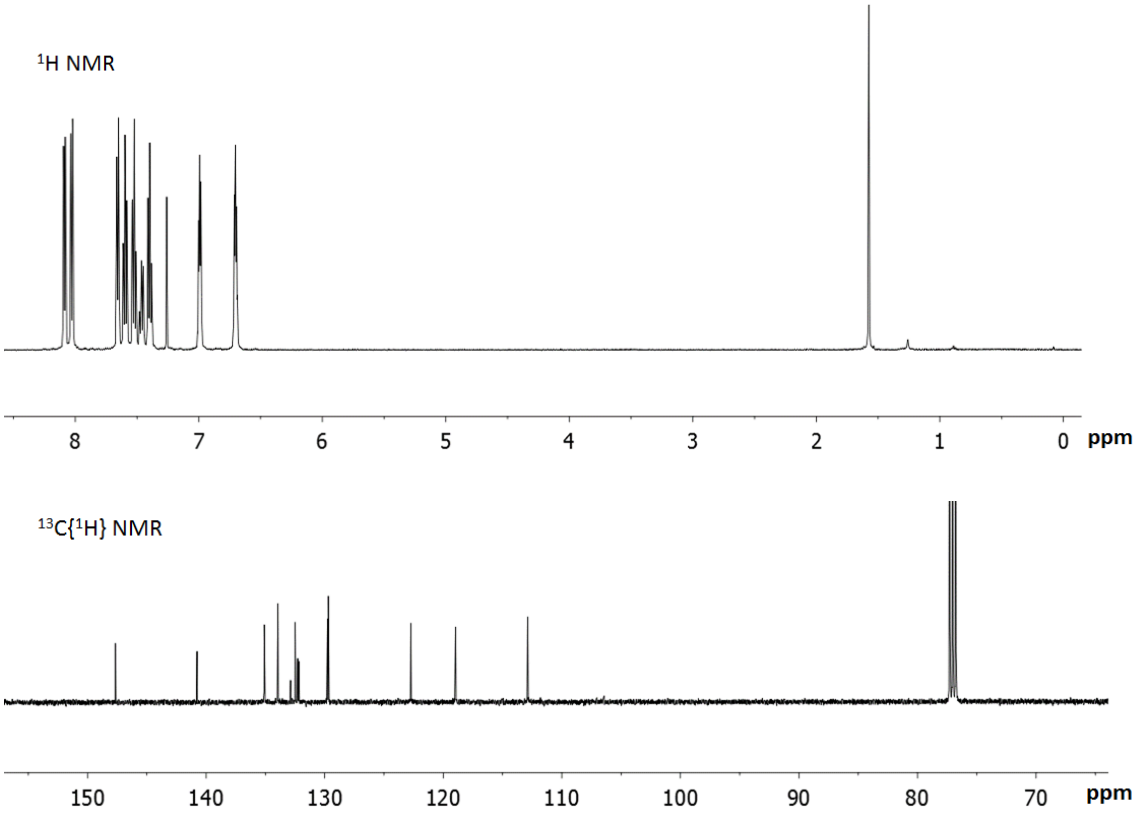

Figure 45. ^{1}H and ^{13}C{^{1}H} NMR spectra of **32**.

Synthesis of TAS[11-F]. To a solution of **11** (41.8 mg, 70 μmol) in THF (3 mL) was added a solution of TASF (19.3 mg, 70 μmol) in THF (3 mL) at ambient temperature. After stirring for 10 min, the solvent was evaporated under vacuum and the remaining solid was washed with two portions (5 mL each) of diethyl ether to afford TAS[**11**-F] as a white solid (54.6 mg, 84% yield). Colorless single crystals of TAS[**11**-F] were obtained by slow diffusion of pentane into a THF solution at ambient temperature. ^{1}H NMR (499.42

MHz, CD_3CN): δ 8.07 (d, $^3J_{H\text{-}H}$ = 7.5 Hz; 1H), 8.04 (d, $^3J_{H\text{-}H}$ = 8.0 Hz; 1H), 7.93 (d, *J* = 7.5 Hz; 1H), 7.61 (dd, $^3J_{H\text{-}H}$ = 8 Hz, J_2 = 2 Hz; 2H), 7.56 (dt, J_1 = 7.5 Hz, J_2 = 1.5 Hz; 1H), 7.44 – 7.40 (m, 2H), 7.39 (dd, J_1 = 8 Hz, J_2 = 2 Hz; 1H), 7.35 – 7.25 (m, 4H), 2.82 (s, $N(CH_3)_2$;18H). $^{13}C\{^1H\}$ NMR (125.60 MHz, CD_3CN): δ 150.34, 150.50, 149.89, 149.52, 144.65, 142.87, 142.63, 142.02, 140.85, 140.83, 134.87, 134.78, 133.43, 132.03, 131.36, 130.55, 129.98, 129.90, 129.68, 123.93, 123.80, 117.83, 116.81, 116.27, 116.25, 39.36 ($N(CH_3)_2$). ^{19}F NMR (469.86 MHz, CD_3CN): δ -102.8 (s). Elemental analysis calculated (%) for $C_{30}H_{31}Cl_4FN_3O_2SSb$: C, 46.18; H, 4.01; N, 5.39; found C, 46.90; H, 4.20; N, 5.36.

Synthesis of 33. To a suspension of (2,2'-biphenylene)phenylstibine (177.4 mg, 0.5 mmol) and alizarin red (94%, 128.9 mg, 0.5 mmol) in toluene (15 mL) at 0 ºC was added a toluene solution (5 mL) of *tert*-butyl hydroperoxide (70 wt. % in water, 64.9 mg, 5.0×10^{-4} mol) dropwise over a period of 15 min. After stirring the mixture at reduced temperature for an hour, the solvent was removed under vacuum and washed with two portions (5 mL each) of methanol followed by two portions of diethyl ether (5 mL each) to afford **33** as a dark yellow product (160.8 mg, 55% yield). ^1H NMR (499.42 MHz, $CDCl_3$): δ 8.34 (d, H_{11}, $^3J_{H\text{-}H}$ = 7.5 Hz; 1H), 8.26 (broad, H_4 + H_5 + H_{14}; 3H), 8.06 (d, *o*-SbPh, $^3J_{H\text{-}H}$ = 7.5 Hz; 2H), 7.84 (d, H_{10}, $^3J_{H\text{-}H}$ = 8.5 Hz; 1H), 7.75 - 7.58 (m, *m*-SbPh + H_1 +H_3 + H_6 + H_8 + H_{13}; 7H), 7.50 (t, *p*-SbPh, $^3J_{H\text{-}H}$ = 8.5 Hz; 1H), 7.43 (m, H_2 + H_7 + H_{12}; 3H), 7.28 (d; merged with $CDCl_3$ resonance, H_9; 1H). $^{13}C\{^1H\}$ NMR (125.60 MHz, $CDCl_3$): δ 183.40 (*C*=O), 182.83 (*C*=O), 154.21, 149.4, 140.76, 135.17, 135.04, 133.92, 133.76, 133.28, 133.01, 132.98, 132.76, 131.57, 130.75, 130.23, 130.11, 126.78, 126.69,

125.28, 123.01, 120.08, 118.62, 116.65. The NMR spectra of this compound are provided in Figure 46 as a measure of purity.

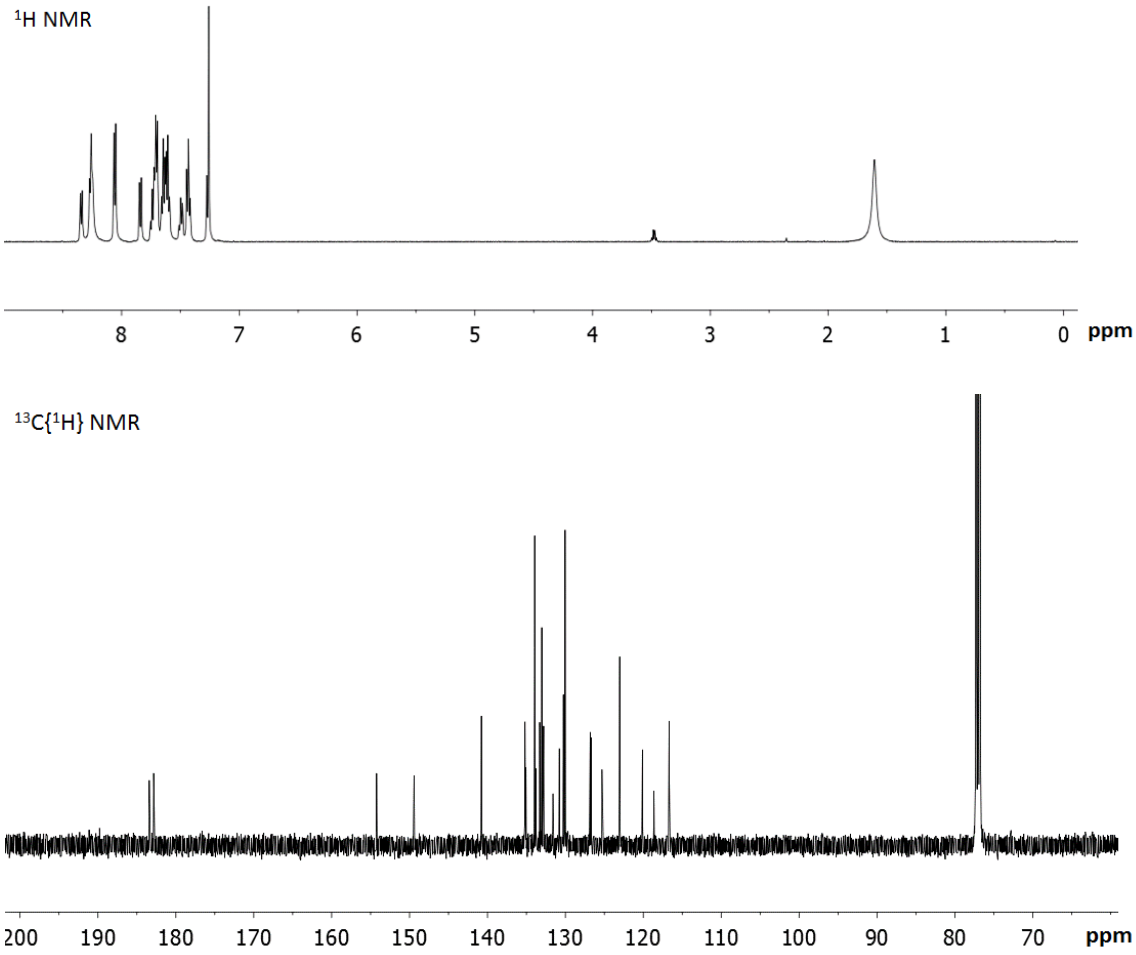

Figure 46. ^{1}H and ^{13}C{^{1}H} NMR spectra of **33**.

Synthesis of TAS[33-F]. To a solution of **33** (44.8 mg, 76 μmol) in THF (3 mL), a solution of TASF (20.9 mg, 76 μmol) in THF (3 mL) was added dropwise at ambient temperature. After stirring for 15 min, the solvent was removed under vacuum and the remaining solid was washed with two portions of diethyl ether (5 mL each) to afford

TAS[**33**-F] as a dark red solid (54.0 mg, 92% yield). Single crystals of TAS[**33**-F] were obtained as dark red platelets by slow diffusion of diethyl ether into a dimethyl formamide solution at ambient temperature. Ratio of diastereoisomer based on integration of the ^{19}F NMR signals, 54:46. ^{1}H NMR (499.42 MHz, $CDCl_3$): δ 8.28 (d, $^{3}J_{H\text{-}H}$ = 8.0 Hz; 1H), 8.18 (d, $^{3}J_{H\text{-}H}$ = 8.0 Hz; 1H), 8.13 – 7.95 (m, 9H), 7.84 – 7.69 (m, 5H), 7.66 - 7.60 (m, 4H), 7.58 – 7.21 (m, 18H), 7.17 (t, $^{3}J_{H\text{-}H}$ = 7.5 Hz; 1H), 7.01 (d, $^{3}J_{H\text{-}H}$ = 8.5 Hz; 1H), 6.61 (d, J = 8.5 Hz; 1H), 2.82 (s, N(CH_3)$_2$; 18H). $^{13}C\{^{1}H\}$ NMR (125.60 MHz, $CDCl_3$): δ 183.67, 183.24, 183.22, 182.99, 160.18, 154.83, 154.27, 149.86, 144.79, 142.5, 141.81, 141.53, 140.36, 136.81, 135.26, 135.02, 134.48, 134.26, 133.78, 133.67, 133.38, 133.18, 132.96, 132.76, 131.34, 130.65, 130.53, 129.81, 129.36, 129.21, 129.11, 129.03, 128.95, 127.3, 126.85, 126.64, 124.32, 123.24, 123.19, 123.12, 120.50, 119.52, 115.41, 115.29, 38.72 (N(CH_3)$_2$). ^{19}F NMR (469.86 MHz, CD_3CN): δ -107.9 (s), -111.9 (s). Elemental analysis calculated (%) for $C_{38}H_{37}FN_3O_4SSb$: C, 59.07; H, 4.83; N, 5.44; found C, 58.62; H, 4.86; N, 5.33. The spectra of ^{1}H (aryl region) and ^{19}F NMR in $CDCN_3$ are shown in Figure 47.

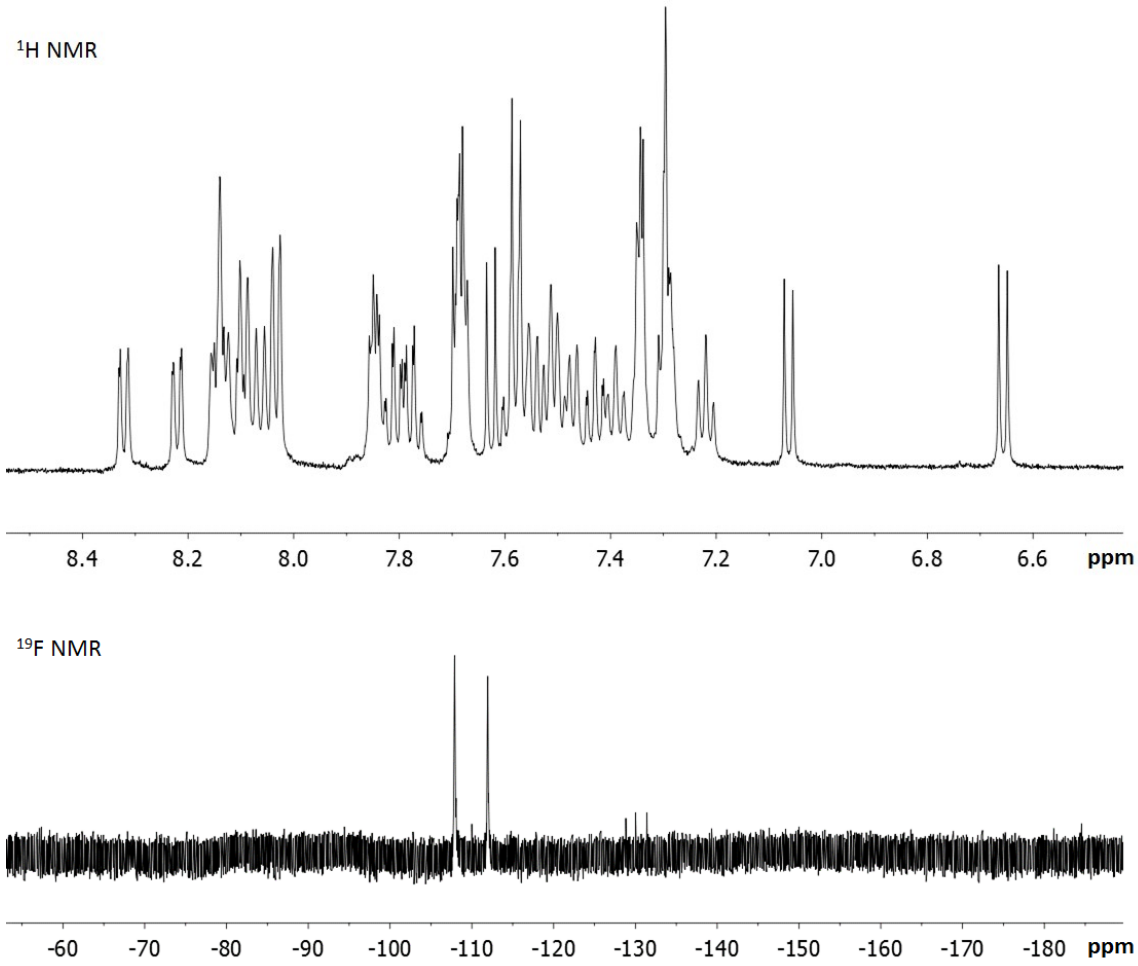

Figure 47. ^{1}H (aryl region) and ^{19}F NMR spectra of TAS[**33**-F].

Fluoride ion complexation in water/CH_2Cl_2 biphasic mixture. In a typical experiment, a solutions of **33** in CH_2Cl_2 (1.0 mL, 5.0×10^{-4} M) was layered with an aqueous solution (5 mL) containing TPABr as a phase transfer agent and a citrate buffer (10 mM, pH 4.68). In two separate experiment, 25 µL and 50 µL of a concentrated KF solution (0.02 M) were added to the aqueous layer, leading to a final fluoride concentration of 1.9 ppm (1.0×10^{-4} M) and 3.8 ppm (2.0×10^{-4} M), respectively. After shaking these

mixtures for 5 minutes, the colors of the organic layer changed from yellow to pale orange for the solution containing 1.9 ppm of fluoride and to orange for the solution containing 3.8 ppm of fluoride. After separating the two layers, 50 μL aliquots of the CH_2Cl_2 were diluted to a total volume of 3 mL to make a 5×10^{-6} M solution. The UV-Vis spectra of these solutions were recorded and showed a redshift of the lowest energy absorption band from $\lambda_{max} = 423$ nm (vs 430 nm in dry CH_2Cl_2) to $\lambda_{max} = 475$ nm (vs 482 nm in dry CH_2Cl_2) (Figure 40 and Figure 48). The fluorescence spectra were also recorded and showed an increase in a broad intensity band at $\lambda_{max} = 616$ nm. Both UV-Vis and fluorescence measurements support the formation of [**33**-F]$^-$ which was also confirmed by recording the ^{19}F NMR spectrum of the CH_2Cl_2 layer obtained with 3.8 ppm of fluoride. Analogous experiments with NaCl, NaBr, $NaNO_3$, $NaHCO_3$, NaH_2PO_4, $NaHSO_4$ (4.0×10^{-4} M) did not result in a no visible color change.

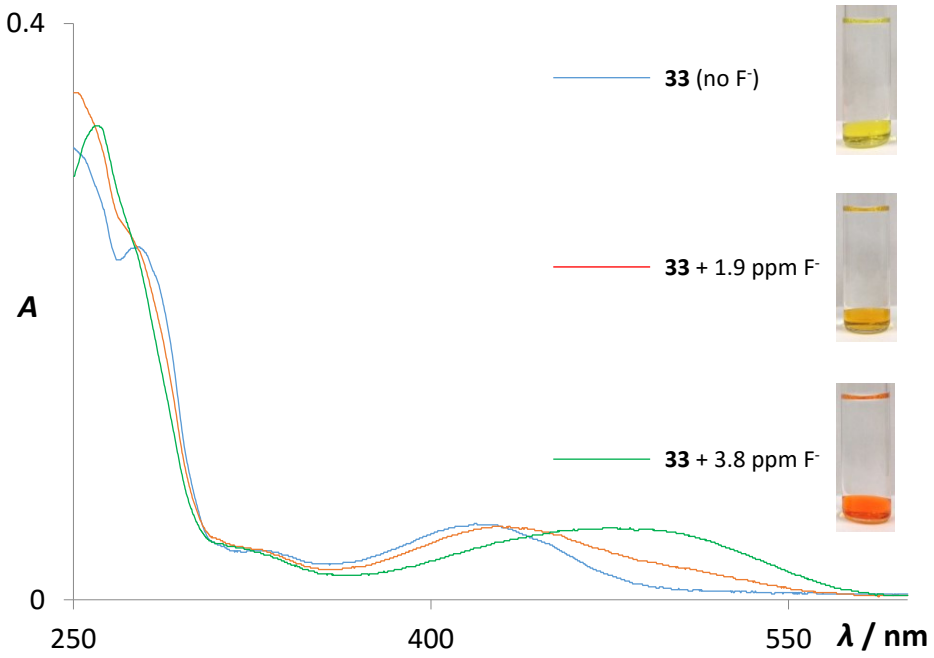

Figure 48. UV-Vis absorption spectra of solutions of **33** (5×10^{-6} M) in CH_2Cl_2. For each measurement, the solution was prepared by the 100-fold dilution of a 5×10^{-4} M solution of **33** which had been layered with an aqueous solution of KF (0, 1.9 and 3.8 ppm) containing TPABr (20 mM) and a citrate buffer (10 mM, pH 4.68).

Drinking water analysis. In a typical experiment, a 5 mm NMR tube was filled with a solution of **33** in CH_2Cl_2 (1.0 mL, 5.0×10^{-5} M) were layered with an aqueous solution containing TPABr (20 mM) and a citrate buffer (10 mM, pH 4.6). To obtain a calibration curve, the aqueous layer was doped with different amounts of fluoride (0, 0.4, 0.7, 1.0, and 1.9 ppm). After vigorous shaking (1 min), the tube was inserted into the cavity of the fluorometer such that only the CH_2Cl_2 layer was position in the optical path. The exact positioning of each tube in the cavity of the fluorometer was facilitated by the use of a custom made insert. The fluorescence intensity was recorded at λ_{max} = 610 nm ($\lambda_{excitation}$ = 482 nm). A plot shows that the fluorescence intensity at λ_{max} = 610 nm

increases linearly with the fluoride concentration in the 0-1.9 ppm range (Figure S8). Drinking water samples (Nursery® Water, H-E-B® Baby Purified Water, and tap water of College Station) where combined with TPABr (20 mM) and buffered with citrate (10 mM, pH 4.6). The resulting solutions were transferred into a 5 mm NMR tube filled with a solution of **33** in CH_2Cl_2 (1.0 mL, 5.0×10^{-5} M). The fluorescence intensity was measured as described above and correlated to a fluoride concentration using the calibration described above. The measurements were reproduced two times.

CHAPTER III

SQUEEZING FLUORIDE OUT OF WATER WITH A NEUTRAL BIDENTATE ANTIMONY(V) LEWIS ACID*

3.1 Introduction

Owing to its small size, the fluoride anion enjoys a high hydration energy of 504 kJ/mol. Model studies suggest that this stabilization arises from the formation of hydrogen bonds with as many as seven water molecules that can simultaneously reside in the first solvation shell of the anion.[97] Owing to the stability of this solvation shell, fluoride ions tend to be inert and thus difficult to capture in aqueous media. This inertness constitutes one of the main limitations encountered in the design of water compatible fluoride sensors and captors for applications in drinking water analysis[92, 159] and ^{18}F positron emission tomography,[160] respectively. The most successful approaches reported to date are based on the use of cationic compounds whose fluoride affinity is enhanced by Coulombic effects.[118, 177, 215-218] This is for example the case of cationic boranes which have been shown to bind fluoride in water.[110-112, 182, 219] By contrast, neutral boranes cannot overcome the elevated hydration energy of the fluoride anion and are thus incompetent for fluoride complexation in aqueous media.[102, 103, 220, 221] As part of our ongoing interest in this chemistry, we have recently become interested in antimony(V) Lewis acids[42, 43, 84, 114,

---

* Reprinted in part with permission from: "Squeezing Fluoride out of Water with a Neutral Bidentate Antimony(V) Lewis Acid"; Hirai, M.; Gabbaï F. P. *Angew. Chem. Int. Ed.* **2015**, *54*, 1205-1209. Copyright 2015 by John Wiley & Sons, Inc.

[117, 118, 157, 184, 191-194, 222, 223] such as **A**, a neutral stiborane that displays stronger Lewis acidities than non-fluorinated triarylboranes.[224] This higher Lewis acidity is reflected by the fact that **A** bind fluoride in 7:3 THF:H_2O vol. solution with stability constants *K* in the range of 10^4 M^{-1} while boranes show no affinity for the anion under such conditions. Despite the strength of the binding, the use of these molecules in solutions that contain a high water content (>50 % H_2O) has not been established. Potential problems include coordination of water to the vacant antimony binding site compounded with the strong hydration of the fluoride anion which competes with antimony coordination.[40, 42, 225] Faced with these difficulties, we have decided to investigate strategies to increase the fluoride affinities of these antimony species. Lessons learned from the chemistry of boron-based fluoride receptors have shown that chelating diboranes of type **B** display a markedly enhanced affinity for fluoride anions.[102, 104, 105, 226-229] Inspired by these earlier results, we have now decided to investigate the synthesis and properties of bidentate distiboranes.

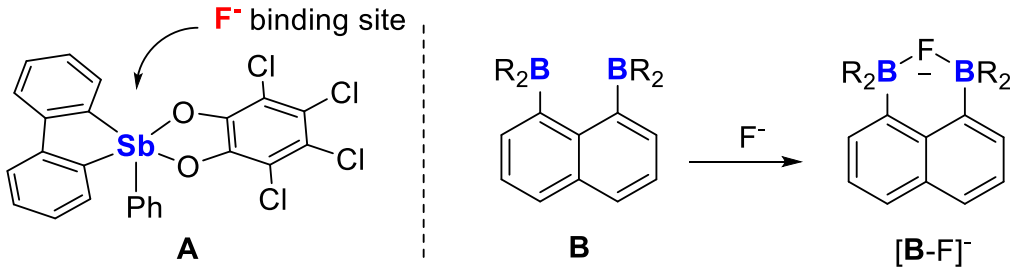

Figure 49. Left: depiction of the anion binding site of stiborane **A**. Right: reaction of diborane **B** with fluoride ion.

3.2 Synthesis and characterization of distibine and distiborane

Toward this end, we first prepared 4,5-bis(diphenylstibino)-9,9-dimethylxanthene (**34**) by the reaction of 4,5-dilithio-9,9-dimethylxanthene-1.5(tmeda)[230] and two equivalents of diphenylantimony chloride. This compound was isolated as a white solid in 60 % yield. Its ^{1}H NMR spectrum in $CDCl_3$ indicates that all four phenyl groups are equivalent. The ^{1}H NMR spectrum also shows the expected dimethylxanthene backbone resonances including three resonances consistent with an ABC spin system arising from the aromatic backbone hydrogen nuclei. These spectroscopic characteristics suggest that distibine **34** has C_2 symmetry. This geometry is confirmed by the crystal structure of **34** which also shows that the two antimony centers are separated by 4.1517(4) Å (Figure 50).[231]

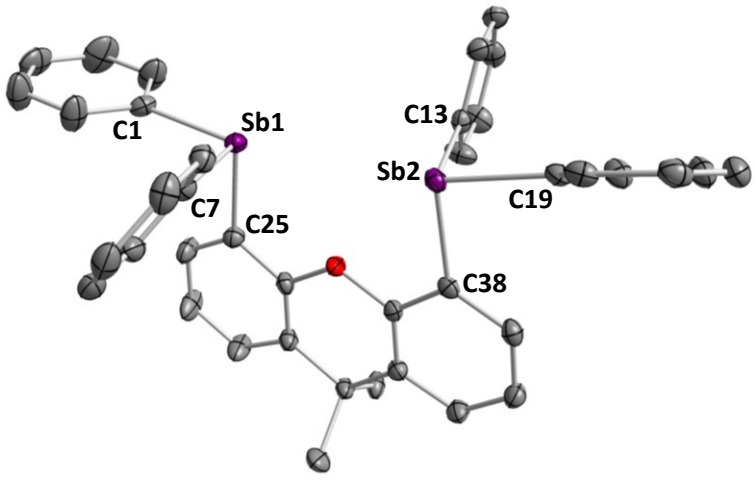

Figure 50. Crystal structure of **34**. Displacement ellipsoids are scaled to the 50% probability level. Hydrogen atoms are omitted for clarity. Selected bond lengths (Å) and angles (deg): Sb1-C1 2.153(3), Sb1-C7 2.146(2), Sb1-C25 2.153(2), Sb2-C13 2.149(2), Sb2-C19 2.157(2), Sb2-C38 2.161(2), C1-Sb1-C7 97.14(9), C1-Sb1-C25 94.18(9), C7-Sb2-C25 93.27(9), C13-Sb2-C19 93.87(9), C13-Sb2-C38 94.72(9), C19-Sb2-C38 94.72(9).

The reaction of **34** with one equivalent of *o*-chloranil in THF followed by a MeOH wash affords monooxidized stibine-stiborane complex **35** as an off-white solid in 91 % yield. In the ^{1}H NMR spectrum in $CDCl_3$, we observe two sets of phenyl resonances along with the asymmetrical set of xanthene signals. The two methyl resonances appear as a sharp singlet at 1.71 ppm. Pale yellow single crystals of **35** were obtained as plates by slow diffusion of pentane to a toluene solution and were subjected to X-ray diffraction analysis. In the solid state structure, we can verify that only one of the antimony centers has been oxidized by *o*-chloranil. The unoxidized antimony center retains its trigonal pyramidal geometry while the oxidized antimony center adopts a distorted trigonal bipyramidal geometry with a τ-value of 0.59. The separation between the two antimony centers is 4.325(13) Å which is slightly elongated from that of distibine **34** (4.152 Å).

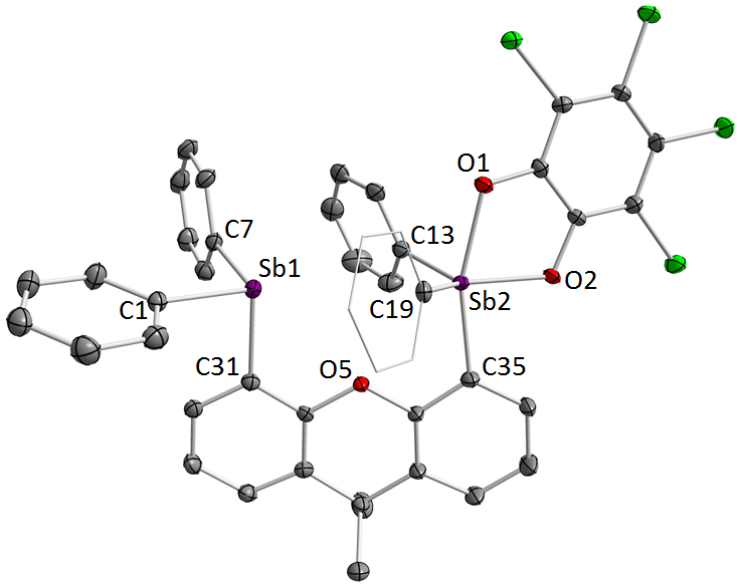

Figure 51. Crystal structure of **35**. The hydrogen atoms and a molecule of toluene are omitted for clarity.

Alternatively, both antimony centers of distibine **34** can undergo clean oxidation using two equivalents of *o*-chloranil to afford the corresponding distiborane **36** in 84 % yield (Figure 52). This distiborane has been fully characterized. In the ^{1}H NMR spectrum in $CDCl_3$, the phenyl groups were observed as two broad signals at room temperature, indicating rapid rotation of the phenyl groups in solution. Oxidation of the two antimony centers induces a downfield shift of the dimethylxanthene ABC aromatic spin system resonances which appear at 7.68, 7.11 and 6.78 ppm (d) in **36** *vs.* 7.44, 7.00 and 6.91 ppm in **34**.

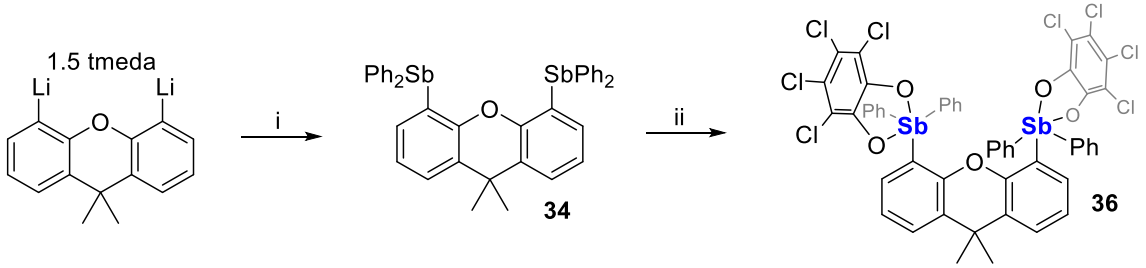

Figure 52. Synthesis of **34** and **36**. i) 2 eq Ph_2SbCl, Et_2O, -78°C ; ii) 2 eq *o*-chloranil, THF, RT.

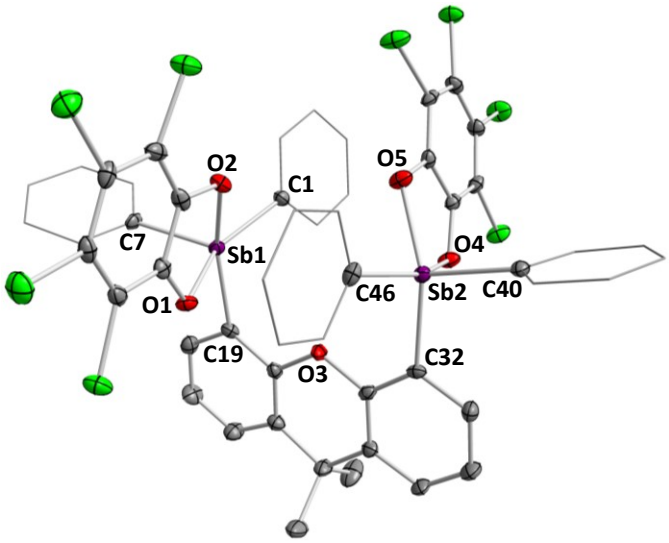

Figure 53. Solid state structure of the crystallized **36**. Thermal ellipsoids are drawn at the 50 % probability level. The hydrogen atoms and toluene molecules are omitted for clarity. Selected bond lengths (Å) and angles (deg): Sb1-C1 2.115(3), Sb1-C7 2.103(3), Sb1-C19 2.129(3), Sb1-O1 2.0551(18), Sb1-O2 2.0360(18), Sb2-C32 2.134(3), Sb2-C40 2.093(3), Sb2-C46 2.110(3), Sb2-O4 2.0389(18), Sb2-O5 2.0554(18), O1-Sb1-O2 78.46(7), C1-Sb1-C7 102.92(10), C1-Sb1-C19 101.51(10), C7-Sb1-C19 101.51(10), O4-Sb2-O5 78.60(7), C32-Sb2-C40 103.43(10), C32-Sb2-C46 101.35(10), C40-Sb2-C46 107.67(10).

Oxidation of the two antimony centers also results in a notable increase of the Sb-Sb separation from 4.1517(4) Å in **34** to 4.7805(7) Å in **36** (Figure 53).[231] This increase reflects the larger steric bulk of the stiborane units, which both adopt a distorted square pyramidal geometry with an average τ-value of 0.08. In the crystal, the molecule has a C_2 symmetry, with the square bases of each pyramid oriented in a face-to-face fashion. This unique arrangement generates a cavity flanked on either side by Lewis acidic antimony(V) atoms. Compound **36** has also been investigated computationally using Density Functional Theory (DFT) methods (B3LYP functional with the mixed basis sets: aug-cc-pVTZ-pp for Sb, 6-311g(d) for Cl, 6-31g for C, O and H). The electrostatic potential

surface of **36** shows an accumulation of positive character at each antimony center. Accordingly, the LUMO is concentrated on the two antimony atoms which both contribute via orbitals of Sb-C_{Ph} σ* character (Figure 54).

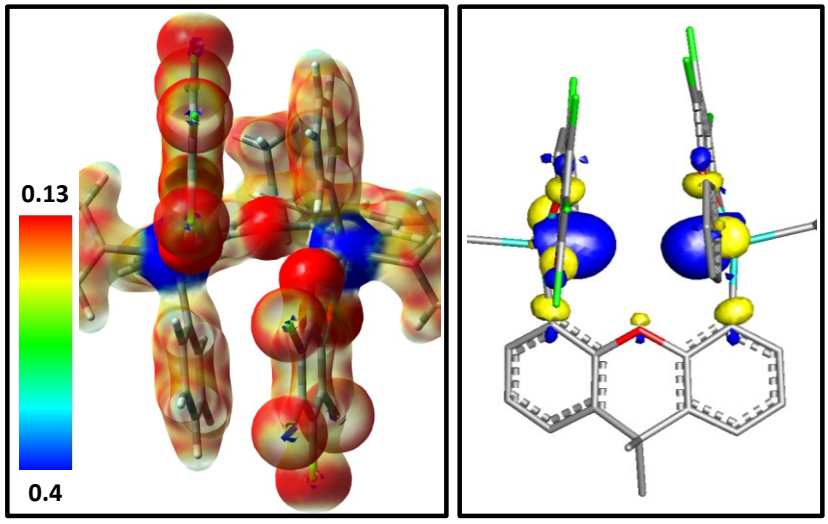

Figure 54. Left: electrostatic potential surface of **36** (isovalue = 0.05). Right: Contour plot of the LUMO of **36** (isovalue = 0.05).

3.3 Fluoride binding property of distiborane in water

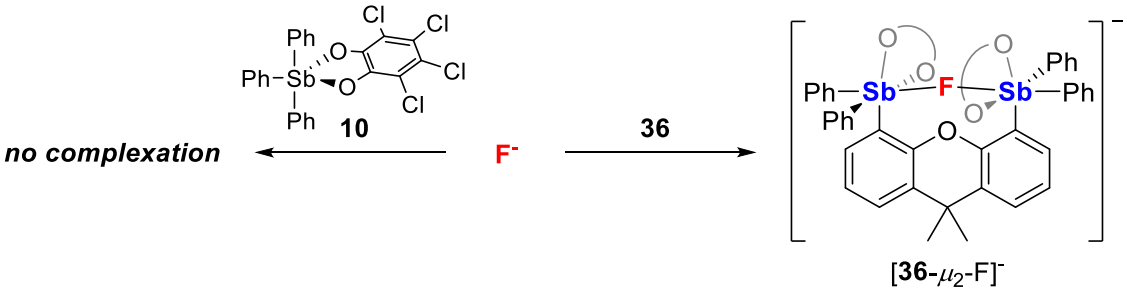

Figure 55. The reaction of fluoride with **36** and **10** in 9.5:0.5 H_2O:THF vol. solution at pH 4.36 (0.045 M Triton X-100/citrate buffer).

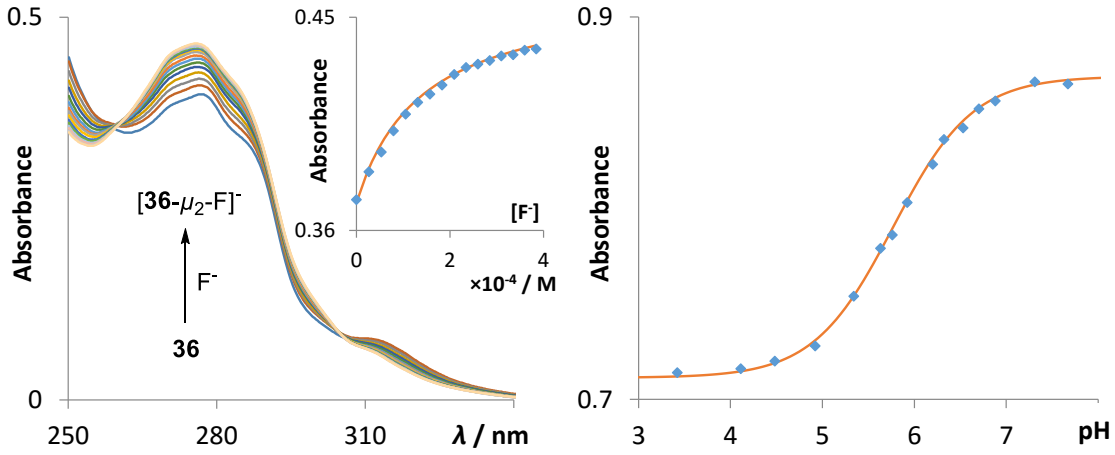

Figure 56. Left: Spectral changes in the UV-vis absorption spectra of **36** (4.2×10^{-5} M) in 9.5:0.5 H_2O:THF vol. solution at pH 4.36 (0.01 M citrate, 0.045 M Triton X-100) upon incremental addition of fluoride. The inset shows the experimental and the calculated 1:1 binding isotherms for **36** at 280.8 nm. The data were fitted with $K = 700$ (± 30) M^{-1} (ε(**36**) = 8 850 $M^{-1}cm^{-1}$ and ε([**36**-μ_2-F]$^-$) = 11 000 $M^{-1}cm^{-1}$). Right: Spectrophotometric acid-base titration curve of **36** in 9.5:0.5 H_2O:THF vol. solution (0.01 M sodium phosphate, 0.045 M Triton X-100). The absorbance was measured at 280.8 nm. The data were fitted to K_{Sb} = [[**36**-μ_2-OH]$^-$][H^+]/[**36**] (eq. 1) with ε(**36**) = 9 700 $M^{-1}cm^{-1}$ and ε([**36**-μ_2-OH]$^-$) = 11 850 $M^{-1}cm^{-1}$, and the pK_{Sb} values estimated as 5.77 (± 0.08).

With this compound in hand, we decided to investigate its anion binding property and compare them to those of $Ph_3Sb(O_2C_6Cl_4)$ (**10**), a known derivative which was prepared as a monofunctional model compound for the purpose of this study.[46] To make our study more relevant to applications that involve aqueous fluoride sources, we decided to evaluate these molecules in solutions containing a high water content. We found that both **36** and **10** could be dissolved in 9.5:0.5 H_2O:THF vol. mixtures in the presence of Triton X-100 (0.045 M), a neutral surfactant often employed as a detergent in biomedical experiments.[232] To probe the behaviour of these two compounds in this solution, we first studied their possible neutralization by hydroxide anions. To this end, we monitored the

UV-vis spectrum of these two compounds as a function of pH. We found that the spectrum of the monofunctional derivative **10** remained unchanged upon elevation of the pH from 4 to 6, at which point the band at 308.5 nm undergoes a progressive quenching. Fitting of the titration data to a simple acid-base equilibrium (Figure 57) affords pK_{Sb} = 7.40 (± 0.08) (Figure 58).

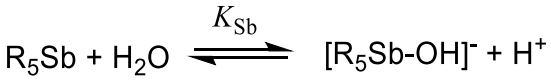

Figure 57. Equation of acid-base equilibrium of stiboranes.

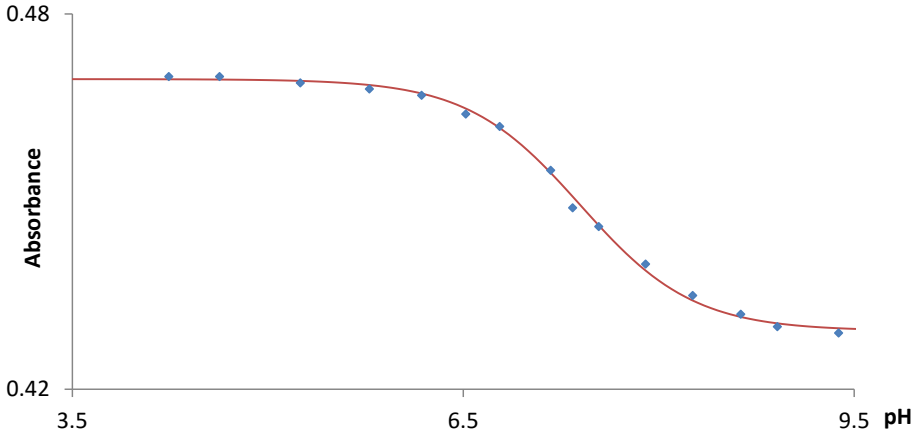

Figure 58. Spectrophotometric acid-base titration curve of **10** in 9.5:0.5 H_2O:THF vol. solution containing Triton X-100 (0.045 M) and sodium phosphate (0.01 M). The absorbance was measured at 308.5 nm. The data were fitted to $K_{Sb} = [[\mathbf{10}\text{-OH}]^-][H^+]/[\mathbf{10}]$ with ε(**10**) = 8 750 $M^{-1}cm^{-1}$ and ε([**10**-OH]$^-$) = 8 000 $M^{-1}cm^{-1}$, and the pK_{Sb} values estimated as 7.40 (± 0.08).

When the same experiment was carried out with **36**, neutralization started to occur at lower pH leading to a pK_{Sb} of 5.77 (± 0.08) (Figure 56 Right).[233] These measurement

are important because they indicate that **36** is more acidic than **10** by almost two orders of magnitudes. These measurements clearly demonstrate the increase in acidity imparted by the bifunctional nature of **36**. Next, we decided to verify if a similar trend would be observed in the fluoride binding properties of these two compounds. Using the 9.5:0.5 H_2O:THF vol. mixture described above buffered at pH 4.34 with citrate (0.01 M), we found that incremental addition of fluoride to a solution of **10** ($4.3\ 10^{-5}$ M) did not result in any changes of the UV-vis spectrum thus indicating that monofunctional **10** does not complex fluoride anions under these conditions. By contrast, when the same experiment was repeated with **36** (4.2×10^{-5} M), addition of fluoride induced a notable change of the UV-vis spectrum, suggesting the formation of a fluoride complex for which a stability constant of 700 (± 30) M^{-1} can be calculated. To our knowledge, compound **36** is the first neutral main group Lewis acid to capture fluoride anions in water.[102, 198, 234] The formation of [**36**-μ_2-F]$^-$ in these solutions was confirmed by ESI-MS which shows an intense molecular peak at *m/z* 1268.7729 amu. No change in the UV-vis spectrum was observed in the presence of other common anions such as Cl^-, Br^-, HCO_3^-, NO_3^-, HSO_4^- and $H_2PO_4^-$, pointing to the selectivity of anion binding.

3.4 Reaction of the distiborane with fluoride ions

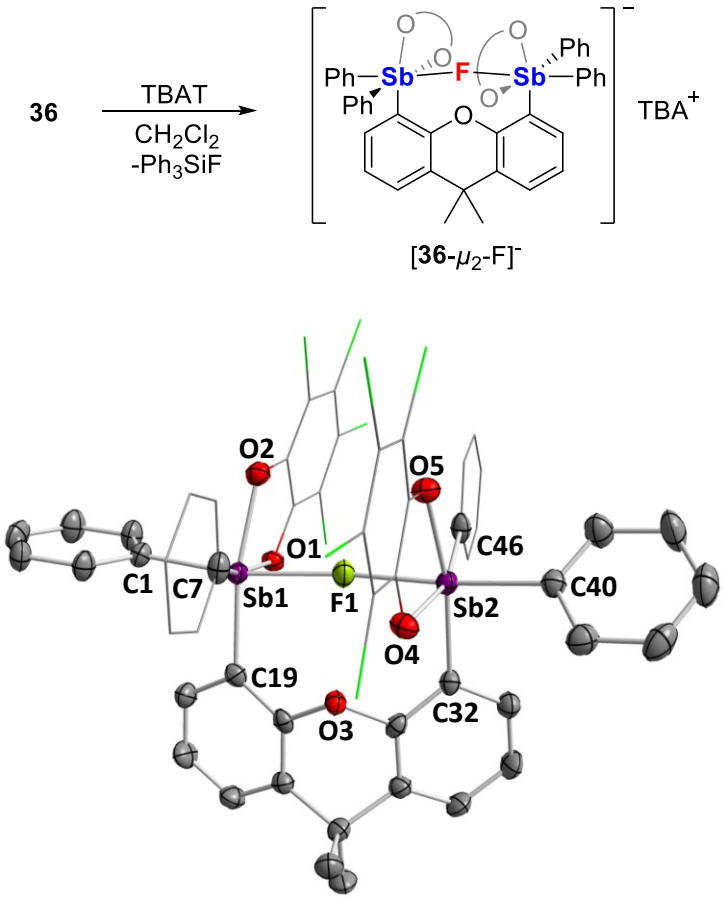

Figure 59. Top: Synthesis of [TBA][**36**-μ_2-F], TBAT = [nBu$_4$N][Ph$_3$SiF$_2$], TBA$^+$ = [nBu$_4$N]$^+$. Bottom: solid state structure of the crystallized [**36**-μ_2-F]$^-$. Thermal ellipsoids are drawn at the 50 % probability level. The hydrogen atoms, TBA cation, and THF molecules are omitted for clarity. Selected bond lengths (Å) and angles (deg): Sb1-F1 2.1684(17), Sb2-F1 2.1621(18), Sb1-C1 2.147(3), Sb1-C7 2.137(3), Sb1-C19 2.162(3), Sb1-O1 2.074(2), Sb1-O2 2.071(2), Sb2-C32 2.145(3), Sb2-C40 2.141(3), Sb2-C46 2.132(3), Sb2-O4 2.041(2), Sb2-O5 2.070(2), Sb1-F1-Sb2 165.45(9), C1-Sb1-F1 167.78(9), C7-Sb1-O1 164.12(10), C19-Sb1-O2 164.81(9), C40-Sb2-F1 172.89(9), C32-Sb2-O5 165.90(9), C46-Sb2-O4 163.45(10).

To confirm that the bidentate nature of **36** is responsible for its increased fluoride anion affinity, we endeavoured to isolate a salt containing the anion [**36**-μ_2-F]$^-$. The tetra-*n*-butylammonium salt of this anion [**36**-μ_2-F]$^-$ could be easily obtained by reaction of **36** with TBAT ([*n*Bu$_4$N][Ph$_3$SiF$_2$]) in CH_2Cl_2 (Figure 59, top). While the ^{1}H NMR spectrum shows all the expected resonances, the presence of an antimony bound fluoride anion is revealed by a ^{19}F NMR signal at -26.5 ppm. The solid state structure obtained by single crystal X-ray diffraction[231] shows that the two antimony centers adopt a distorted octahedral geometry, similar to those of other hexacoordinate antimonate species[194, 224] including SbF_6^- (Figure 59, bottom).[199] Furthermore, the crystal structure confirmed that the fluoride atom is indeed bound to both antimony centres. In agreement with the bridging nature of the fluoride ligand, the Sb-F bonds in **36** (Sb1-F1 2.1684(17) Å, Sb2-F1 2.1622(18) Å) are significantly longer than the Sb-F bond in [**10**-F]$^-$ (1.973(4) Å), which was isolated as tetra-*n*-butylammonium salt for the purpose of this study (Figure 60).[231] The Sb1-F1-Sb2 angle (165.45(9)°) indicates a slight bending at the fluorine atoms. A similar Sb-F-Sb motif is found in $Sb_2F_{11}^-$, a highly stable inorganic anion which is compatible with strongly acidic environments.[17, 235, 236] Additionally, the Sb1-Sb2 distance significantly decreases from 4.7805(7) Å in **36** to 4.2957(12) Å in [**36**-μ_2-F]$^-$, thus illustrating the flexibility of the xanthene backbone and its ability to clamp down on the anionic guest. Strikingly, the distance between F1 and O3 of the xanthene backbone is 2.602 Å, which is well within the sum of the van der Waals radii of the two elements (3.05 Å).[237] Given the fact that an interaction between an oxygen atom and a fluorine atom

should be repulsive, we propose that the compression observed in the F1-O3 distance is reflective of the strength of the fluoride chelate effect.

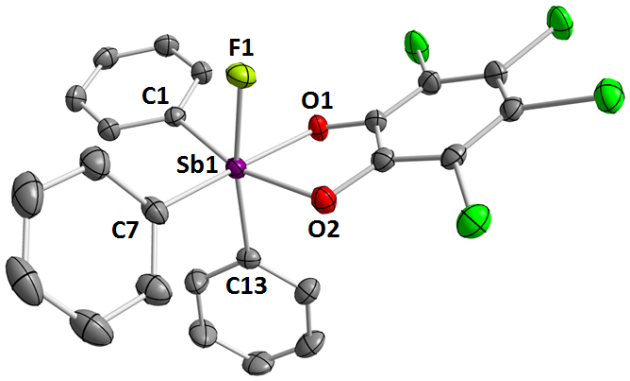

Figure 60. Crystal structure of [**10**-F]$^-$. Thermal ellipsoids are drawn at the 50 % probability level. The hydrogen atoms, TBA cation, and to THF molecules are omitted for clarity. Selected bond lengths (Å) and angles (deg): Sb1-F1 1.9877(13), Sb1-C1 2.142(2), Sb1-C7 2.137(2), Sb1-C13 2.155(2), Sb1-O1 2.0930(15), Sb1-O2 2.1026(16), F1-Sb1-C13 170.38(7), F1-Sb1-C1 87.71(7), C1-Sb1-O2 `64.09(7), C1-Sb1-C7 101.46(9), C7-Sb1-O1 166.42(7), C13-Sb1-O2 89.34(8), O1-Sb1-O2 77.73(6).

The structure of [**36**-μ_2-F]$^-$ strongly support the notion that the higher fluoride affinity of **36** originates from its ability to chelate the fluoride anion. This view is supported by the computed fluoride ion affinity (FIA) of **36** and **10** (FIA = 359.88 kJ/mol for **36** and 192.23 kJ/mol for **10**) which shows that the chelate Sb-F-Sb motif in [**36**-μ_2-F]$^-$ is stabilized by more than 160 kJ/mol when compared to the terminal Sb-F bond of [**10**-F]$^-$. Accordingly, NMR spectroscopy shows that [**10**-F]$^-$ reacts with **36** to afford [**36**-μ_2-F]$^-$. A similar reaction is obtained upon mixing **36** with [(Mes$_2$B)C$_6$H$_4$(FPPh$_2$Me)]I thus indicating that **36** is more Lewis acidic that the cationic borane [*p*-(Mes$_2$B)C$_6$H$_4$(PPh$_2$Me)]$^+$ which we have previously used to complex fluoride in water.[110]

Because the computed FIA of **36** is lower than that of $B(C_6F_5)_3$ (413.30 kJ/mol),[11, 238, 239] we also decided to test the stability of [**36**-μ_2-F]$^-$ in the presence of this perfluorinated borane. As anticipated from the FIAs, the addition of $B(C_6F_5)_3$ to a solution of [TBA][**36**-μ_2-F] in $CDCl_3$ affords quantitative formation of **36** and $[BF(C_6F_5)_3]^-$. This reaction occurs without decomposition of **36** thus indicating that fluoride binding by **36** is reversible.

3.5 Conclusion

In conclusion, we report a neutral bidentate distiborane which readily overcomes the hydration of fluoride anions in water. Fluoride complexation, which is highly selective, is driven by the formation of a Sb-F-Sb chelate motif, the existence of which has been established crystallographically. Finally, the importance of bifunctionality is established by a comparison with a monofunctional analog which shows that the bidentate distiborane is more acidic by at least two orders of magnitudes.

3.6 Experimental section

General considerations. *Antimony is potentially toxic and should be handled with caution.* *N,N,N'N'*-tetramethylethylenediamine (tmeda) was purchased from Sigma Aldrich and distilled from powdered CaH_2 and stored under N_2. 9,9-Dimethylxanthene, antimony trichloride ($SbCl_3$), triphenyl stibine (Ph_3Sb) *n*-butyl lithium (2.2 M in hexane) were purchased from Alfa Aesar. $SbCl_3$ and Ph_3Sb were used to generate Ph_2SbCl by simple ligand exchange at RT. Tetrachloro-*o*-benzoquinone was purchased from Acros Organics. Tetra-*n*-butylammonium difluorotriphenylsilicate (TBAT) was purchased from TCI and used as received. Triphenyl(tetrachlorocatecholato)antimony(V)[46] and 4,5-dilithio-9,9-dimethylxanthene·1.5(tmeda)[230] were prepared according to the reported procedures. All preparations were carried out under an atmosphere of dry N_2 employing either a glovebox or standard Schlenk techniques. Solvents were dried by passing through an alumina column (pentane and CH_2Cl_2) or by refluxing under N_2 over Na/K (hexanes, Et_2O, and THF). All other solvents were ACS reagent grade and used as received. NMR spectra were recorded on a Varian Unity Inova 400 FT NMR (399.508 MHz for ^1H, 100.466 MHz for ^{13}C) or Varian Unity Inova 500 FT NMR (499.42 MHz for ^1H, 469.86 MHz for ^{19}F, 125.60 MHz for ^{13}C) spectrometer at ambient temperature. Chemical shifts are given in ppm and are referenced to residual ^1H and ^{13}C solvent signals and external $BF_3·Et_2O$ for ^{19}F. Elemental analyses were performed by Atlantic Microlab (Norcross, GA). Electronic absoption spectra were recorded at ambient temperature using an Ocean Optics USB4000 spectrometer with an Ocean Optics ISS light source. Electrospray ionization mass spectra were recorded on Applied Biosystems PE SCIEX QSTAR.

Computational details. Density functional theory (DFT) structural optimizations with the *Gaussian 09* program.[208] In all cases, the structures were optimized using the B3LYP functional;[209, 210], and the following mixed basis set: Sb, aug-cc-pVTZ-PP;[240] Cl, 6-311g(d); F, 6-31g(d');[212] C/O/H, 6-31g.[213] For all optimized structures, frequency calculations were carried out to confirm the absence of imaginary frequencies. The molecular orbitals were visualized and plotted in Jimp 2 program.[214]

Crystallographic measurements. The crystallographic measurements were performed at 110(2) K using a Bruker APEX-II CCD area detector diffractometer, with a graphite-monochromated Mo-Kα radiation (λ = 0.71073 Å). A specimen of suitable size and quality was selected and mounted onto a nylon loop. The semi-empirical method SADABS was applied for absorption correction. The structure was solved by direct methods, which successfully located most of the non-hydrogen atoms. Subsequent refinement on F^2 using the SHELXTL/PC package (version 6.1) allowed location of the remaining non-hydrogen atoms. All H-atoms were geometrically placed and refined using a standard riding model.

Table 5. Crystal data, data collection, and structure refinement for **34** and **35**.

Crystal data	**34**	**35**
Empirical formula	C39 H32 O Sb2	C48.50 H35.50 Cl4 O3 Sb2
Formula weight	760.15	1051.57
Temperature	110(2) K	110(2) K
Wavelength	0.71073 Å	0.71073 Å
Crystal system	Monoclinic	Triclinic
Space group	P2(1)/n	P-1
Unit cell dimensions	a = 17.288(2) Å	a = 10.9051(6) Å
	b = 11.4864(16) Å	b = 13.2640(8) Å
	c = 18.044(3) Å	c = 20.993(8) Å
	α = 90°	α = 81.480(1)°
	β = 117.34	β = 74.214(1)°
	γ = 90°	γ = 78.566(1))°
Volume	3182.8(8) Å^3	2403.5(2) Å^3
Z	4	2
Density (calculated)	1.586 Mg/m^3	1.453 Mg/m^3
Absorption coefficient	1.727 mm^{-1}	1.384 mm^{-1}
F(000)	1504	1041
Crystal size	0.18 x 0.15 x 0.10 mm^3	0.24 x 0.18 x 0.09 mm^3
Theta range for data collection	1.35 to 28.27°.	1.57 to 28.47°.
Index ranges	-22<=h<=23, -15<=k<=15, -23<=l<=23	-14<=h<=14, -17<=k<=17, -23<=l<=23
Reflections collected	35867	33839
Independent reflections	7584 [R(int) = 0.0415]	12917 [R(int) = 0.0291]
Absorption correction	Semi-empirical from equivalents	Semi-empirical from equivalents
Max. and min. transmission	0.8463 and 0.7463	0.883 and 0.782
Refinement method	Full-matrix least-squares on F^2	Full-matrix least-squares on F^2
Data / restraints / parameters	7584 / 0 / 379	12917 / 0 / 847
Goodness-of-fit on F^2	1.107	1.025
Final R indices [I>2sigma(I)]	R1 = 0.0245, wR2 = 0.0618	R1 = 0.0399, wR2 = 0.0846
R indices (all data)	R1 = 0.0304, wR2 = 0.0713	R1 = 0.0631, wR2 = 0.0943
Largest diff. peak and hole	0.529 and -0.407 e.Å^{-3}	1.077 and -0.594 e.Å^{-3}

[a] $R1 = \Sigma||Fo| - |Fc||/\Sigma|Fo|$. [b] $wR2 = \{[\Sigma w(Fo^2 - Fc^2)^2]/[\Sigma w(Fo^2)^2]\}^{1/2}$.

Table 6. Crystal data, data collection, and structure refinement for **36** and [TBA][**36**-F].

Crystal data	**36**	[TBA][**36**-F]
Empirical formula	C65 H48 Cl8 O5 Sb2	C75 H83 Cl8 F N O7 Sb2
Formula weight	1436.13	1656.52
Temperature	110(2) K	110(2) K
Wavelength	0.71073 Å	0.71073 Å
Crystal system	Triclinic	Triclinic
Space group	P-1	P-1
Unit cell dimensions	a = 11.133(2) Å	a = 13.095(5) Å
	b = 15.901(3) Å	b = 13.461(5) Å
	c = 17.820(4) Å	c = 20.993(8) Å
	α = 91.32°	α = 88.776(4)°
	β = 107.80°	β = 86.789(4)°
	γ = 99.72°	γ = 83.113(4)°
Volume	2951.1(10) $Å^3$	3668(2) $Å^3$
Z	2	2
Density (calculated)	1.616 Mg/m^3	1.500 Mg/m^3
Absorption coefficient	1.329 mm^{-1}	1.084 mm^{-1}
F(000)	1432	1686
Crystal size	0.18 x 0.12 x 0.11 mm^3	0.12 x 0.11 x 0.08 mm^3
Theta range for data collection	2.140 to 27.103°.	1.89 to 28.38°.
Index ranges	-14<=h<=14, -20<=k<=20, -22<=l<=22	-17<=h<=17, -18<=k<=17, -27<=l<=27
Reflections collected	33839	44559
Independent reflections	12917 [R(int) = 0.0330]	17879 [R(int) = 0.0475]
Absorption correction	Semi-empirical from equivalents	Semi-empirical from equivalents
Max. and min. transmission	0.868 and 0.796	0.9183 and 0.8809
Refinement method	Full-matrix least-squares on F^2	Full-matrix least-squares on F^2
Data / restraints / parameters	12917 / 0 / 526	17879 / 0 / 847
Goodness-of-fit on F^2	1.091	1.025
Final R indices [I>2sigma(I)]	R1 = 0.0520, wR2 = 0.1755	R1 = 0.0399, wR2 = 0.0846
R indices (all data)	R1 = 0.0640, wR2 = 0.1846	R1 = 0.0631, wR2 = 0.0943
Largest diff. peak and hole	0.604 and -0.494 e.$Å^{-3}$	1.077 and -0.594 e.$Å^{-3}$

[a] $R1 = \Sigma||Fo| - |Fc||/\Sigma|Fo|$. [b] $wR2 = \{[\Sigma w(Fo^2 - Fc^2)^2]/[\Sigma w(Fo^2)^2]\}^{1/2}$.

Table 7. Crystal data, data collection, and structure refinement for [TBA][**10**-F].

Crystal data	[TBA][**10**-F]
Empirical formula	C40 H51 Cl4 F N O2 Sb
Formula weight	860.37
Temperature	110(2) K
Wavelength	0.71073 Å
Crystal system	Monoclinic
Space group	P2(1)/n
Unit cell dimensions	a = 13.471(2) Å
	b = 20.709(4) Å
	c = 15.224(3) Å
	α = 90°
	β = 106.746(2)°
	γ = 90°
Volume	4067.0(13) Å^3
Z	4
Density (calculated)	1.405 Mg/m^3
Absorption coefficient	0.980 mm^{-1}
F(000)	1768
Crystal size	0.15 x 0.15 x 0.12 mm^3
Theta range for data collection	1.78 to 29.65°.
Index ranges	-18<=h<=18, -28<=k<=27, -20<=l<=20
Reflections collected	44060
Independent reflections	10780 [R(int) = 0.0439]
Max. and min. transmission	Semi-empirical from equivalents
Refinement method	0.8915 and 0.8670
Data / restraints / parameters	Full-matrix least-squares on F^2
Goodness-of-fit on F^2	10780 / 0 / 446
Final R indices [I>2sigma(I)]	1.029
R indices (all data)	R1 = 0.0338, wR2 = 0.0743
Absolute structure parameter	R1 = 0.0474, wR2 = 0.0814
Largest diff. peak and hole	1.896 and -0.776 e.Å^{-3}

[a] $R1 = \Sigma||Fo| - |Fc||/\Sigma|Fo|$. [b] $wR2 = \{[\Sigma w(Fo^2 - Fc^2)^2]/[\Sigma w(Fo^2)^2]\}^{1/2}$.

Synthesis of 34. A solution of Ph_2SbCl (3.52 g, 11.2×10^{-3} mol) in Et_2O (20 mL)/THF (10 mL) was added dropwise to a suspension of 4,5-dilithio-9,9-dimethylxanthene·1.5(tmeda) (2.24 g, 5.6×10^{-3} mol) in Et_2O (30 mL) at -78 ºC. After stirring at this temperature for an hour, the solution was slowly warmed up to ambient temperature and stirred for an additional 12 hours. After adding a drop of water to quench the reaction, the solvent was removed *in vacuo* and CH_2Cl_2/hexanes (20 mL/10 mL) was added to the residue. The resulting mixture was stirred over anhydrous $MgSO_4$ for 30 min before filtering over Celite. The filtrate was concentrated *in vacuo* and washed with MeOH (15 mL) to afford the product as a white solid in 60 % yield (2.55 g, 3.4×10^{-3} mol). Single crystals of **34** were obtained as colorless blocks by slow diffusion of pentane into a THF solution at ambient temperature. ^{1}H NMR (399.508 MHz, $CDCl_3$): δ 7.44 (dd, 2H, $^3J_{H\text{-}H}$ = 7.8 Hz, $^4J_{H\text{-}H}$ = 1.2 Hz, xanthene-C*H*), 7.39 – 7.33 (m, 8H, Sb*Ph*), 7.31 – 7.22 (m, 12H, Sb*Ph*), 7.00 (pseudo t, 2H, $^3J_{H\text{-}H}$ = 7.6 Hz, xanthene-C*H*), 6.91 (dd, 2H, $^3J_{H\text{-}H}$ = 7.2 Hz, $^4J_{H\text{-}H}$ = 1.2 Hz, xanthene-C*H*), 1.68 (singlet, 6H, xanthene-C*H*$_3$). ^{13}C{^{1}H} NMR (100.466 MHz, $CDCl_3$): δ 153.60, 138.87, 136.69, 133.69, 134.94, 129.84, 128.89, 128.49, 127.18, 126.99, 124.55, 34.87 (xanthene-*C*H$_3$), 32.55 (xanthene-*C*H$_3$). m.p. 132 ºC. Elemental analysis calculated (%) for $C_{39}H_{32}OSb_2$: C, 61.62; H, 4.24; found C, 61.34; H, 4.39.

Synthesis of 35. To a stirred solution of **34** (0.341 g, 4.5×10^{-4} mol) in THF (5 mL) at -78 ºC was added a solution of *o*-chloranil (0.114 g, 4.5×10^{-4} mol) in THF (3 mL) dropwise over 10 min. After stirring for 30 min at ambient temperature, the solvent was removed *in vacuo* and washed with two portions of methanol (5 mL each) to afford the

product as a pale yellow solid in 91 % yield (0.411 g, 4.1×10^{-4} mol). Single crystals of **35** were obtained as yellow plates by slow diffusion of pentane into a THF solution at ambient temperature. ^{1}H NMR (399.508 MHz, $CDCl_3$): δ 7.90 (d, 2H, $^{3}J_{H\text{-}H}$ = 7.9 Hz, xanthene-C*H*), 7.64 (dd, 2H, $^{3}J_{H\text{-}H}$ = 7.9 Hz, $^{1}J_{H\text{-}H}$ = 2.0 Hz, xanthene-C*H*), 1.74 (s, 6H, xanthene-C*H*$_3$). ^{13}C{^{1}H} NMR (100.466 MHz, $CDCl_3$): δ150.29, 135.25, 134.17 (broad), 133.77, 132.39, 131.75, 130.95, 129.13, 128.23, 124.14, 35.80, 30.51 (xanthene-*C*H$_3$). Elemental analysis calculated (%) for $C_{45}H_{32}Cl_4O_3Sb_2$: C, 53.72; H, 3.21; found C, 53.56; H, 3.26.

Synthesis of 36. To a stirred solution of **34** (0.350 g, 4.6×10^{-4} mol) in THF (5 mL) was added a solution of *o*-chloranil (0.226 g, 9.2×10^{-4} mol) in THF (3 mL) dropwise over 10 min. After stirring for 30 min, the solvent was removed *in vacuo* and washed with two portions of methanol (10 mL each) to afford the product as a pale yellow solid in 86 % yield (0.496 g, 4.0×10^{-4} mol). Single crystals of **36** were obtained as yellow blocks by slow diffusion of pentane into a toluene solution at ambient temperature. ^{1}H NMR (399.508 MHz, $CDCl_3$): δ 7.68 (dd, 2H, $^{3}J_{H\text{-}H}$ = 7.6 Hz, $^{4}J_{H\text{-}H}$ = 1.6 Hz, xanthene-C*H*), 7.60 (broad, 8H, *o*-Sb*Ph*), 7.24 (broad, 12H, Sb*Ph*), 7.11 (pseudo t, 2H, $^{3}J_{H\text{-}H}$ = 8.0 Hz, xanthene-C*H*), 6.78 (dd, 2H, $^{3}J_{H\text{-}H}$ = 7.2 Hz, $^{4}J_{H\text{-}H}$ = 1.6 Hz, xanthene-C*H*), 1.82 (s, 6H, xanthene-C*H*$_3$). ^{13}C{^{1}H} NMR (100.466 MHz, $CDCl_3$): δ152.24, 144.08, 134.22 (broad), 132.83, 131.75 (broad), 131.49, 129.34 (broad), 129.13, 125.19, 124.76, 120.43, 116.59, 35.07, 32.16 (xanthene-*C*H$_3$). m.p. 172 ºC (dec.). Elemental analysis calculated (%) for $C_{51}H_{32}Cl_8O_5Sb_2$: C, 48.93; H, 2.58; found C, 49.05; H, 2.72. The purity of **36** was confirmed by NMR spectroscopy. Both ^{1}H and ^{13}C{^{1}H} NMR spectra are shown in Figure 61 as a measurement of purity.

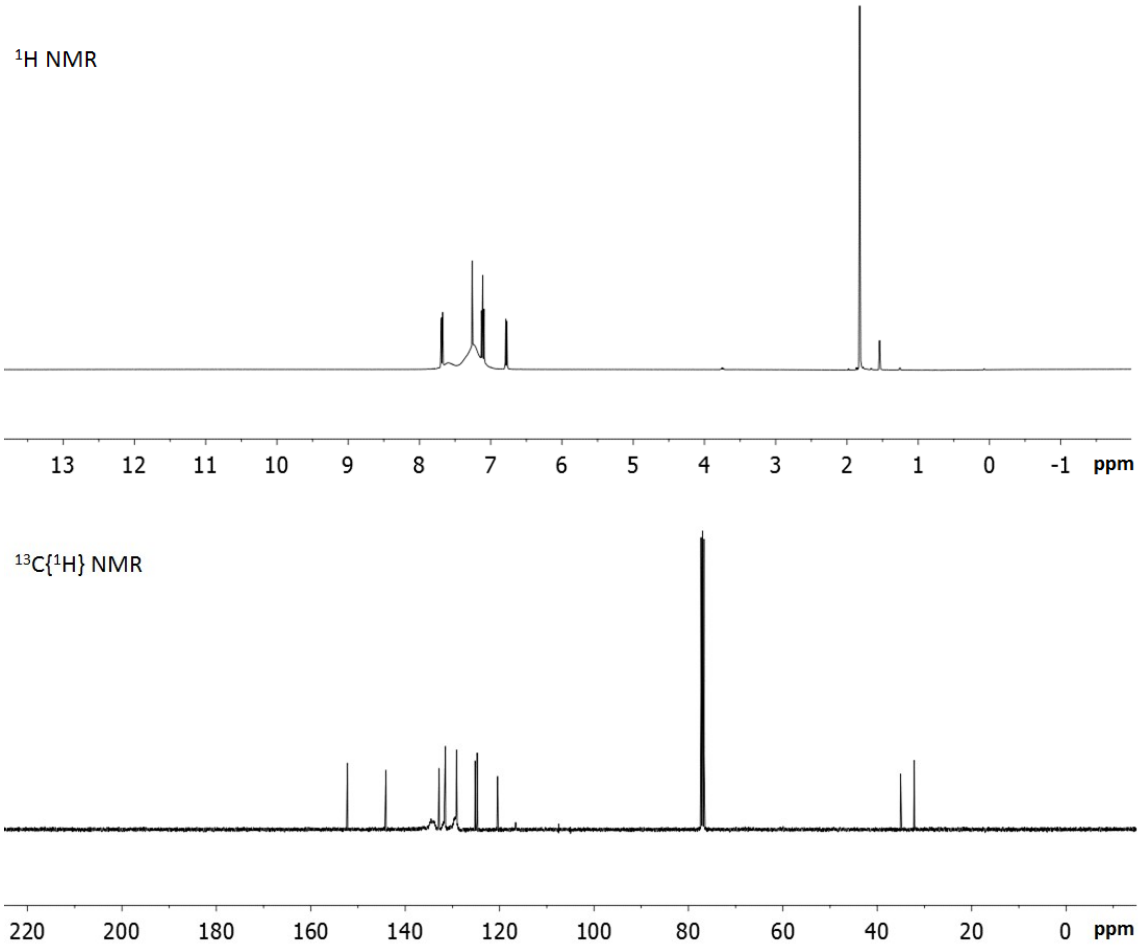

Figure 61. ^{1}H and ^{13}C{^{1}H} NMR spectra of **36**.

Synthesis of [TBA][36-μ_2-F]. To a solution of **36** (0.103 g, 8.2×10^{-5} mol) in dichloromethane (10 mL) was added a solution of TBAT (0.044 g, 8.2×10^{-5} mol) in dichloromethane (5 mL). After stirring for 15 min, the mixture was treated with water (10 mL). The organic layer was separated, dried with anhydrous $MgSO_4$ and filtered over Celite. Removal of the solvent *in vacuo* afforded [TBA][**36**-μ_2-F] as a white solid which was washed with two portions of Et_2O (5 mL each). This procedure afforded [TBA][**36**-μ_2-F] in 91 % yield (0.113 g mg, 7.5×10^{-5} mol). Single crystals of [TBA][**36**-μ_2-F] were

obtained as colorless blocks by slow diffusion of Et_2O into a MeCN solution at ambient temperature. ^{1}H NMR (499.42 MHz, $CDCl_3$): δ 7.65 (d, 4H, $^3J_{H\text{-}H}$ = 7.5 Hz, *o*-Sb*Ph*), 7.44 (dd, 2H, $^3J_{H\text{-}H}$ = 7.5 Hz, $^4J_{H\text{-}H}$ = 1.5 Hz, xanthene-C*H*), 7.24 (pseudo t, 2H, $^3J_{H\text{-}H}$ = 7.5 Hz, xanthene-C*H*), 7.11 (m, 14 H, Sb*Ph*), 6.91 (t, 2H, $^3J_{H\text{-}H}$ = 7.5 Hz, *p*-Sb*Ph*), 6.69 (dd, 2H, $^3J_{H\text{-}H}$ = 7.5 Hz, $^4J_{H\text{-}H}$ = 1.5 Hz, xanthene-C*H*), 2.52 (m, 8H, TBA-CH_2), 1.76 (s, 6H, xanthene-CH_3), 1.23 (broad, 8H, TBA-CH_2), 1.12 (m, 8H, TBA-CH_2), 0.89 (t, 12H, $^3J_{H\text{-}H}$ = 7.2 Hz, TBA-CH_3). ^{13}C{^{1}H} NMR (125.60 MHz, $CDCl_3$): δ 158.35, 147.25, 146.42, 135.96, 134.22, 134.09, 132.72, 132.32, 128.51, 128.40, 127.95, 127.69, 125.30, 123.10, 117.55, 117.22, 115.23, 115.18, 58.85 (TBA-*C*H_2), 36.78 (xanthene-*C*H_3), 26.94, 23.85 (TBA-*C*H_2), 19.66 (TBA-*C*H_2), 13.71 (TBA-*C*H_3). ^{19}F NMR (469.86 MHz, $CDCl_3$): δ -26.5 (s). m.p. 240 ºC (dec.). Elemental analysis calculated (%) for $C_{67}H_{68}Cl_8FNO_5Sb_2$: C, 53.17; H, 4.53; N, 0.93; found C, 53.16; H, 4.66; N, 0.94. HRMS (ESI-TOFMS): *m/z* calculated for $C_{51}H_{32}Cl_8FO_5Sb_2^-$ 1270.7764, found 1270.7752.

Synthesis of [TBA][10-F]. To a solution of **10** (0.099 g, 1.7×10^{-4} mol) in dichloromethane (10 mL) was added a solution of tetra-*n*-butylammonium triphenyldifluorosilicate (TBAT; 0.089 g, 1.7×10^{-4} mol) in dichloromethane (5 mL). After stirring for 15 min, the mixture was treated with water (10 mL). The organic layer was separated, dried with anhydrous $MgSO_4$ and filtered over Celite. Removal of the solvent *in vacuo* afforded [TBA][**10**-F] as a solid which was washed with two portions of Et_2O (5 mL each). This procedure afforded [TBA][**10**-F] in 84 % yield (0.12 g, 1.4×10^{-4} mol). Single crystals of [TBA][**10**-F] were obtained as colorless blocks by slow diffusion of Et_2O into a CH_2Cl_2 solution at ambient temperature. ^{1}H NMR (499.42 MHz, $CDCl_3$): δ

7.84 (dd, 4H, $^{3}J_{H\text{-}H}$ = 6.2 Hz, $^{4}J_{H\text{-}H}$ = 2.0 Hz, *o*-Sb*Ph*), 7.42 (dd, 2H, $^{3}J_{H\text{-}H}$ = 7.5 Hz, $^{4}J_{H\text{-}H}$ = 1.0 Hz, *o*-Sb*Ph*), 7.34 – 7.30 (m, 6H), 7.20 – 7.14 (m, 3H, *p*-Sb*Ph*), 2.71 (broad, 8H, TBA-C*H*$_2$), 1.27 (broad, 8H, TBA-C*H*$_2$), 1.13 (m, 8H, TBA-C*H*$_2$), 0.87 (t, 12H, $^{3}J_{H\text{-}H}$ = 7.2 Hz, TBA-C*H*$_3$). $^{13}C\{^{1}H\}$ NMR (125.60 MHz, $CDCl_3$): δ 148.99, 145.81, 145.57, 135.24, 134d.27, 128.58, 128.17, 127.88, 116.79, 115.14, 58.14 (TBA-*C*H$_2$), 23.81 (TBA-*C*H$_2$), 19.61 (TBA-*C*H$_2$), 13.76 (TBA-*C*H$_3$). ^{19}F NMR (469.86 MHz, $CDCl_3$): δ -84.6 (s). m.p. 164 ^{o}C (dec.). Elemental analysis calculated (%) for $C_{40}H_{51}Cl_4FNO_2Sb$: C, 55.84; H, 5.97; N, 1.63; found C, 55.93; H, 5.98; N, 1.72.

CHAPTER IV

1-PYRENYL- AND 3-PERYLENYL-ANTIMONY(V) DERIVATIVES FOR THE FLUORESCENCE TURN-ON SENSING OF FLUORIDE IONS IN WATER AT SUB-PPM CONCENTRATIONS

4.1 Introduction

Fluoridation of drinking water and toothpaste is a regular practice in the U.S. because of the beneficial effects of fluoride anions in dental health.[241] Such anions are also commonly used as a part of anabolic drugs for treating osteoporosis, a disease which reduces bone density and increases the risk of broken bones.[86, 87] Excessive consumption of fluoride salts, however, can trigger dental fluorosis[88] or more seriously skeletal fluorosis,[89, 90] an incurable disease that hardens and deform the bones causing constant pain throughout the body. Because of these side effects, the amount of fluoride in drinking water is typically regulated in the U.S. and the maximum contaminant level has been set to 4 ppm by the Environmental Protection Agency (EPA).[91] Moreover, the U.S. Department of Health and Human Services has recently lowered the recommended level of fluoride in drinking water from 1.2 to 0.7 ppm.[92] It follows that sensing technologies that are portable, water compatible and competent in this concentration range have become particularly coveted. An additional impetus from this research comes from the presence of fluoride in sarin gas, a nerve agent used in chemical warfare or UF_6 which is used for the purpose of uranium enrichment.[179, 242]

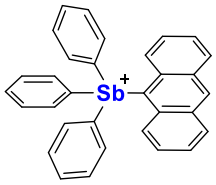

[**28**]$^+$

Figure 62. Previously reported turn-on fluorescent fluoride sensor [**28**]$^+$.

While the complexation and sensing of fluoride anions in aqueous media is complicated by their high hydration energy of 504 kJmol^{-1}, several groups[93, 94, 176, 177, 216-218, 243-245] including ours have introduced the use of Lewis acidic compounds as fluoride binding platforms.[110-112, 180, 182, 219] Examples of such systems include a phosphinum borane such as [*p*-$Ph_3PC_6H_4BMes_2$]$^+$ that binds fluoride anions in 9/1 (v/v) water/MeOH mixtures.[111] Although competent in the ppm range, fluoride complexation by this compound results in a turn-off colorimetric response, making it poorly suited for analytical applications. Faced with this limitation, we turned our attention toward a different type of Lewis acid and considered derivatives that incorporate an antimony(V) center.[42, 43, 46, 78, 84, 85, 114, 157, 184, 192, 194, 197, 223, 224, 246-250] These studies were prompted by the long known fact that tetraphenylstibonium is able to bind fluoride in biphasic water/CCl_4 mixtures to afford the corresponding fluorostiborane Ph_4SbF.[117, 191] Building on this earlier knowledge, we reported the 9-anthryltriphenlystibonium cation [**28**]$^+$ and found that it could be use in 9/1 (v/v) water/DMSO for the sub-ppm sensing of fluoride anions.[118] Sensing, which occurs by conversion of [**28**]$^+$ into the corresponding fluorostiborane, is accompanied by a substantial increase in the fluorescence quantum yield of the anthryl reporter. Although this new platform came with the advantage of displaying a turn-on

fluorescence response as observed for related silicon and bismuth compounds,[251, 252] the 9-anthryl fluorophore requires excitation in the UV part of the spectrum which may be inconvenient for the development of portable devices. The fluorescence quantum yield of the fluoride adduct is also somewhat low (~14.1%). With the aim of further improving the properties of such fluoride anion binding platforms, we decided to consider replacing the 9-anthryl substituent with other polycyclic aromatic moieties that display higher quantum yields and longer excitation wavelengths. In this paper, we describe the results of these undertakings and show that the use of the 3-perylenyl chromophore leads to a new water-compatible antimony-based fluoride sensor which displays a large turn-on fluorescence upon binding of the analyte.

4.2 Synthesis and characterization of tetraaryl stibonium bromide salts

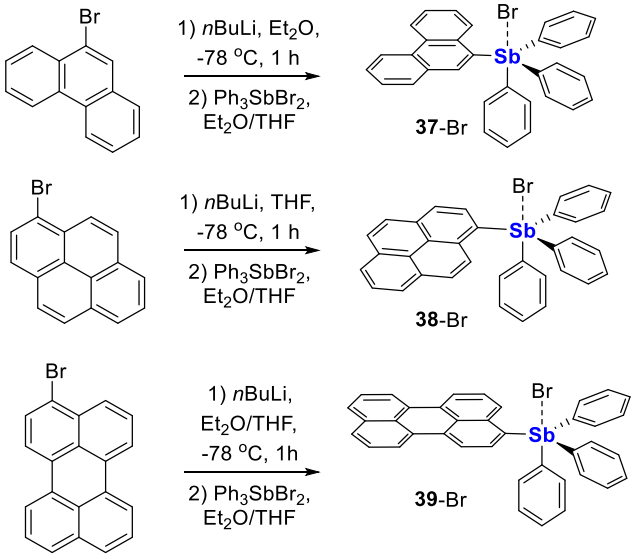

Figure 63. Synthesis of stibonium bromide salts [**37**]Br, [**38**]Br and [**39**]Br.

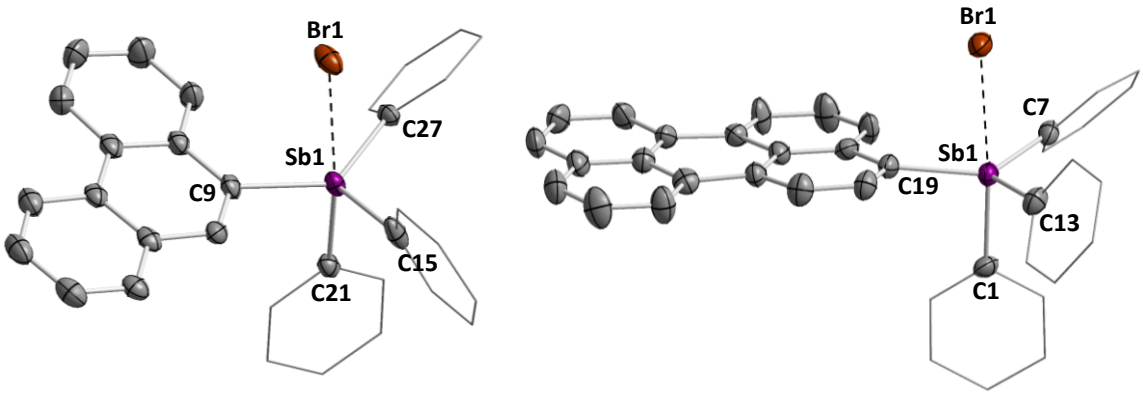

Figure 64. Solid-state structure of [**37**]Br (left) and [**39**]Br (right). Thermal ellipsoids are drawn at the 50% probability level. The hydrogen atoms are omitted for clarity. Selected bond lengths (Å) and angles (deg) for [**37**]Br: Sb1-Br1 2.9072(5), Br1-Sb1-C21 169.80(8), C9-Sb1-C15 108.31(13), C9-Sb1-C27 131.71(12), C15-Sb1-C27 115.27(12). Selected bond lengths (Å) and angles (deg) for [**39**]Br (the metrical parameters of the second independent salt are given in brackets): Sb1-Br1 2.9211(11) [2.8817(11)], Br1-Sb1-C1 173.50(18) [177.4(2)], C7-Sb1-C13 114.5(3) [115.5(3)], C7-Sb1-C19 130.1(3) [115.0(3), 130.1(4)], C13-Sb1-C19 112.0(3) [111.7(3), 126.7(3)].

For the purpose of this study, we decided to prepare the phenanthrene, pyrene, and perylene analogs of [**28**]$^{+}$. We were particularly interested in use of perylene which as a pure substance in ethanol exhibits a quantum yield of 94% exceeding that of anthracene (Φ_{FL} = 27%) by three orders of magnitude.[253] The tetraarylantimony(V) bromides **37**–Br, **38**–Br and **39**–Br were isolated as air-stable solids in 17, 32 and 22% yield, respectively, by the reaction of Ph_3SbBr_2 with 9-phenanthryllithium, 1-pyrenyllithium, and 3-perylenyllithium, respectively, as described in Figure 63.[118] The ^{1}H NMR spectra of these compounds serve to confirm the successful incorporation of the aryl fluorophores. These spectra also show that all three phenyl groups are equivalent in $CDCl_3$ solution, suggesting rapid equilibration of the trigonal bipyramidal geometry of these bromide derivatives as previously described for Ph_4SbBr.[64] Electrospray ionization mass spectrometry (ESI-MS)

measurements of these tetraarylantimony(V) bromides showed a molecular ion at *m/z* = 529.0912, 553.0911, and 603.1067 amu corresponding to the halide–free stibonium cations $[\mathbf{37}]^+$, $[\mathbf{38}]^+$, and $[\mathbf{39}]^+$, respectively. Single crystals of **37**–Br and **39**–Br were successfully grown and subjected to X-ray diffraction analyses. For both compounds, the coordination geometry of the antimony atom is trigonal bipyramidal. The chromophore occupies one of the equatorial sites while the bromide anion is axially coordinated *trans* from a phenyl substituent. In both structures, the bromide ligand interacts weakly with the antimony center as illustrated by Sb–Br separations of 2.9072(5) Å for **37**–Br and 2.9211(11) Å for **39**–Br, which are both well above the sum of the covalent radii of the two elements (Sb–Br = 2.59 Å) (Figure 64).[254] Although single crystals of **38**–Br were not obtained, we assumed that it adopts a structure similar to that of both **37**–Br and **39**–Br. The elongated Sb–Br bond distances measured in these compounds serve as a reminder that tetraarylantimony(V) bromides adopt a solid state structure that is intermediate between that of a bromostiborane and a stibonium bromide.[64, 255, 256] In organic solutions, conductivity measurements carried out on Ph_4SbBr leave no doubt to the ionic character of this class of compounds.[255, 257] In aqueous solutions (*vide infra*), there is no evidence of association with the bromide anion even when an excess of cetyltrimethylammonium bromide (CTAB) is used as a surfactant. Hence, while the solid state structures display elongated Sb–Br bonds, these antimony(V) compounds fully dissociate into stibonium once dissolved in aqueous solutions.

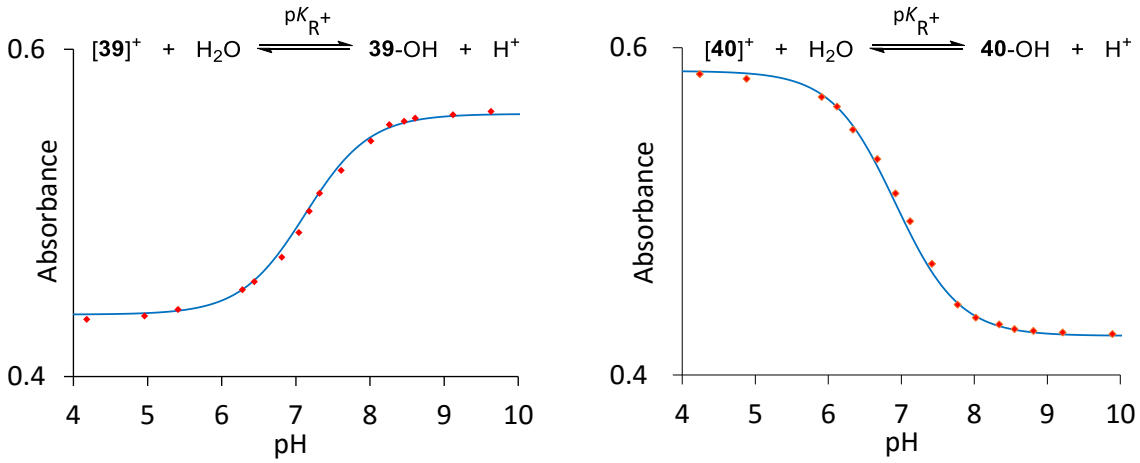

Figure 65. Spectrometric acid-base titration curve for [**38**]Br and [**39**]Br in 9/1 (v/v) H_2O/DMSO containing CTAB (10 mM) and sodium phosphate (10 mM). For [**38**]Br (left), the absorbance was measured at 350 nm and fitted to K_{R^+} = [**38**-OH][H^+]/[[**38**]$^+$] with ε([**38**]Br) = 15 320 M^{-1} cm^{-1}, ε(**38**-OH) = 21 200 M^{-1} cm^{-1}, and pK_{R^+} = 7.12 ± 0.06. For [**39**]Br (right), the absorbance was measured at 434 nm and fitted to K_{R^+} = [**39**-OH][H^+]/[[**39**]$^+$] with ε([**39**]Br) = 23 800 M^{-1} cm^{-1}, ε(**39**-OH) = 16 200 M^{-1} cm^{-1}, and pK_{R^+} = 6.94 ± 0.06.

With these new derivatives at our disposal, we moved to investigate their behavior in aqueous media. We first examined the water compatibility and pH stability range of [**37**]$^+$, [**38**]$^+$, and [**39**]$^+$ using UV-vis spectroscopy. To this end, spectrophotometric acid-base titrations were carried out on dilute solutions of each stibonium cation dissolved in 9/1 (v/v) water/DMSO mixtures containing 10 mM of cetyltrimethylammonium bromide (CTAB) as an additive to prevent precipitation during the titration experiment. These solutions, which also contained 10 mM of sodium phosphate added to obtain less abrupt

pH variations, were prepared with an initial pH in the 3-4 range. A hydroxide solution was progressively added. After each addition, the pH of the solution as well as the absorption spectrum of the stibonium cation was recorded. In the case of [**37**]$^+$, evidence of decomposition was obtained in the UV spectrum when the pH reached a value of 6. For this reason, this cation was no longer studied. By contrast, we found that stiboniums [**38**]$^+$ and [**39**]$^+$ reversibly bind hydroxide under these conditions (Figure 65). In the absorption spectra of [**38**]$^+$ and [**39**]$^+$, the addition of hydroxide anions induces a discrete blue shift, suggesting the complexation of such anions to the antimony centers. Furthermore, the absorption spectra of both [**38**]$^+$ and [**39**]$^+$ hardly fluctuate below pH of 5, thereby suggesting that both species exist as base–free cations under these conditions. The absorbance data obtained for [**38**]$^+$ and [**39**]$^+$ as a function of pH was fitted to the following equation:

$$K_{Sb} = \frac{[\mathrm{Ar_4SbOH}][\mathrm{H^+}]}{[\mathrm{Ar_4Sb^+}]}$$

affording the pK_{Sb} values of 7.12 ± 0.06 for [**38**]$^+$ and 6.94 ± 0.06 for [**39**]$^+$, which are comparable to that measured previously for [**28**]$^+$ (pK_{Sb} = 7.07 ± 0.05) (Figure 65). These pK_{Sb} values, which can be regarded as the pH values at which the stibonium cations are 50% neutralized by hydroxide binding, indicate that fluoride binding should be carried out at slightly acidic pH in order to avoid any interference from hydroxide anions. The similarity of the pK_{Sb} values also suggests that [**38**]$^+$, [**39**]$^+$ and [**28**]$^+$ have similar Lewis acidity and should therefore bind fluoride anions with very similar binding constants.

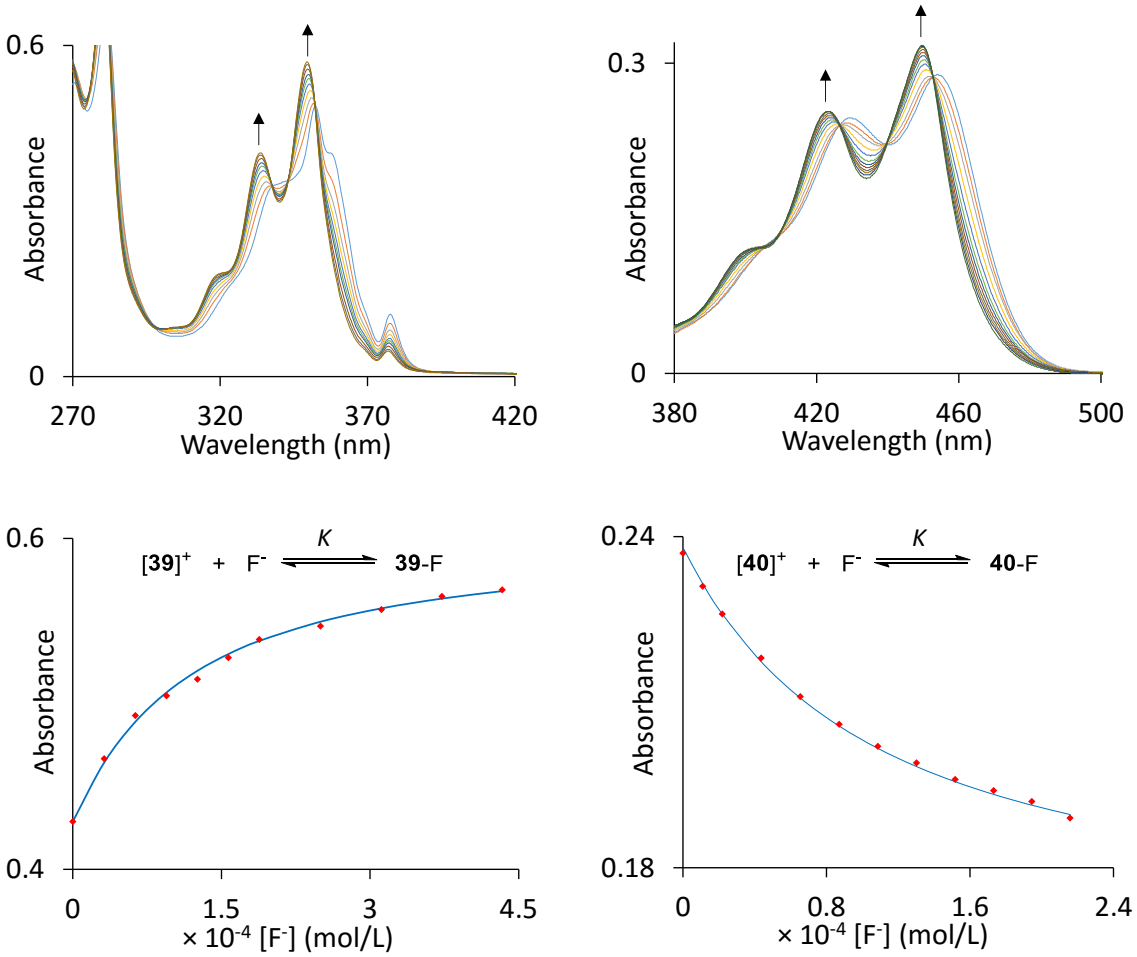

Figure 66. Top: spectral changes in the UV-vis absorption spectrum of [**38**]Br (left; 2.8 × 10^{-5} M) and [**39**]Br (right; 1.0 × 10^{-5} M) in 9/1 (v/v) H_2O/DMSO containing CTAB (10 mM) at pH 4.8 (pyridine buffer) upon incremental addition of fluoride. Bottom: the experimental and the calculated 1:1 fluoride binding isotherms of [**38**]Br (left) at 351 nm and [**39**]Br (right) at 436 nm. The data were fitted with K = 10 000 ± 800 M^{-1} for [38]Br (ε([**38**]Br) = 15 320 M^{-1} cm^{-1} and ε([**38**–F] = 21 500 M^{-1} cm^{-1})) and 10 000 ± 500 M^{-1} for [**39**]Br (ε([**39**]Br) = 23 800 M^{-1} cm^{-1} and ε([**39**–F] = 16 650 M^{-1} cm^{-1})).

Fluoride anion titrations of [**38**]$^+$ and [**39**]$^+$ were undertaken in 9/1 (v/v) water/DMSO mixtures containing 10 mM of CTAB. The pH of these solution was adjuted to 4.8 using a 10 mM pyridine buffer. Incremental addition of fluoride to these solutions

induces a gradual blue shift of the fluorophore-based absorption bands, suggesting progressive conversion into the corresponding fluorostiboranes **38**–F and **39**–F, respectively (Figure 66, top). The absorption data was modeled on the basis of a 1:1 binding isotherm affording fluoride binding constants (K) of 10 000 ± 800 M^{-1} for [**38**]$^+$ and 10 000 ± 500 M^{-1} for [**39**]$^+$ (Figure 66, bottom). These values are very close to that measured for [**28**]$^+$ under similar conditions (K = 12 000 ± 1100 M^{-1}).

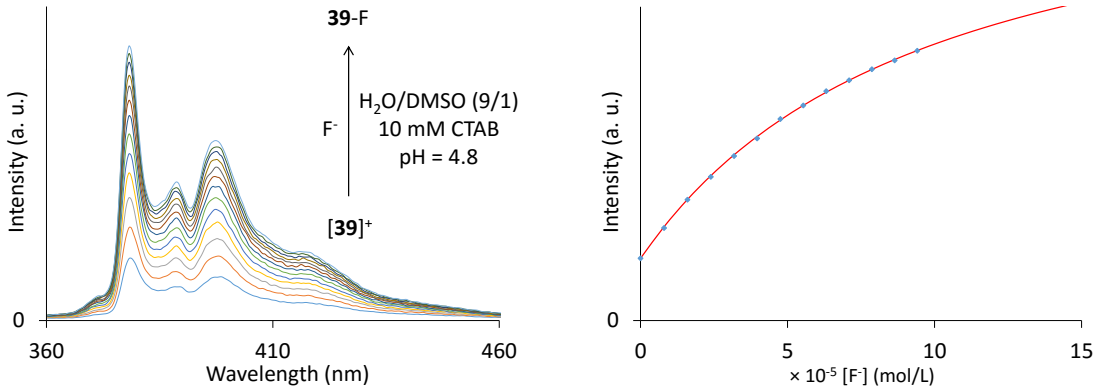

Figure 67. Left: change in fluorescence spectra of [**38**]Br (7.0×10^{-6} M) in 9/1 (v/v) H_2O/DMSO containing CTAB (10 mM) at pH 4.8 (pyridine buffer) upon incremental addition of fluoride. Right: plot of fluorescence intensity increase at λ_{fluo} = 379 nm of [**38**]Br after successive addition of fluoride anions.

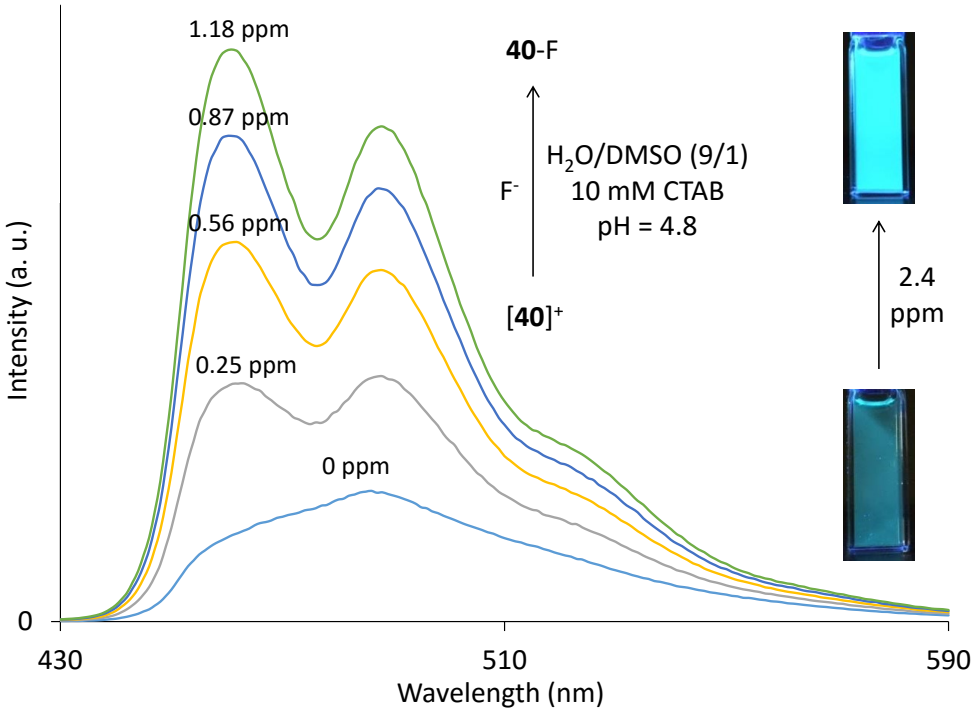

Figure 68. Fluorescence emission spectral changes (λ_{ex} = 423 nm) observed upon incremental addition of fluoride anions to [**39**]Br (5.0×10^{-6} M) in 9/1 (v/v) H_2O/DMSO. The inset shows the visible fluorescence changes under 9/1 (v/v) H_2O/DMSO at pH 4.8 (10 mM CTAB/pyridine buffer) under a hand-held UV lamp after addition of 2.4 ppm of fluoride.

Similar to stibonium [**28**]$^+$, stibonium [**38**]$^+$ is only weakly fluorescent with a pyrene-based emission band centered at 379 nm and Φ_{FL} = 0.5%. The conversion of [**38**]$^+$ into **38**–F led to a noticeable photophysical change with Φ_{FL} of 5.2% (Figure 67). Despite this 10–fold increase, the fluorescence quantum yield is still rather low and hard to detect with the naked eye. By contrast, conversion of [**39**]$^+$ (Φ_{FL} = 7.3%) into **39**–F resulted in a substantial enhancement of fluorescence intensity with a characteristically strong perylene-based emission (Φ_{FL} = 59.2%) spanning the 440-570 nm spectral window and

easily observable with the naked eye (Figure 68). For potential practical applications, it is important to note that the excitation of **39**–F is achieved in the visible region (λ_{ex} = 423 nm) which is considerably lower in energy compared to its 9-anthryl analog [**28**]$^+$ (λ_{ex} = 375 nm). The photophysical properties of stibonium cations [**38**]$^+$ and [**39**]$^+$ and fluorostiboranes **38**–F and **39**–F are summarized in Table 8. As for [**28**]$^+$, no response was observed in the presence of other anions including Cl^-, Br^-, NO_3^-, HCO_3^-, HSO_4^-, and $H_2PO_4^-$, which allows us to conclude that both [**38**]$^+$ and [**39**]$^+$ are highly selective for fluoride anions in aqueous solution.

Table 8. Photophysical properties of stibonium cations [**28**]$^+$, [**38**]$^+$ and [**39**]$^+$ and fluorostiboranes **28**–F, **38**–F and **39**–F in 9/1 (v/v) water/DMSO mixture containing 10 mM of CTAB and 10 mM of pyridine as a buffer to maintain the pH to 4.8.

	λ_{ex} (nm)	λ_{fluo} (nm)	Φ_{FL} (%)
[**28**]$^+$	375	425	2.2
28–F	375	425	14.1
[**38**]$^+$	348	379	0.5
38–F	348	379	5.2
[**39**]$^+$	423	486	7.3
39–F	423	463	59.2

4.4 Isolation of fluorostiboranes

To verify the formation of **38**–F and **39**–F, the two fluorostiboranes were isolated by treating **38**–Br and **39**–Br with KF in MeOH. Shortly after mixing, **38**–F and **39**–F precipitated leading to their isolation in 71% and 77% yields, respectively. These fluorostiboranes were fully characterized and their compositions were confirmed by elemental analyses. In the ^{19}F NMR spectra, the resonances appear as singlets at -77.5 ppm for **38**–F and -79.0 ppm for **39**–F, whose values are comparable to that of the 9-anthryl analog (δ = -75.8 ppm). Crystal structures of **38**–F and **39**–F were also determined by single crystal X-ray diffraction analyses (Figure 70).[258] In the crystals, the fluoride anions are tightly bound to the antimony centers in the axial position, forming short Sb–F bonds of 2.0933(14) Å for **38**–F and 2.0498(17) Å for **39**–F.

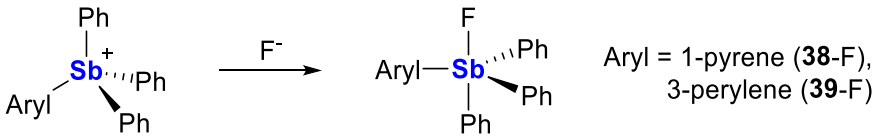

Figure 69. Reactions of tetraarylstibonium cations with fluoride ions

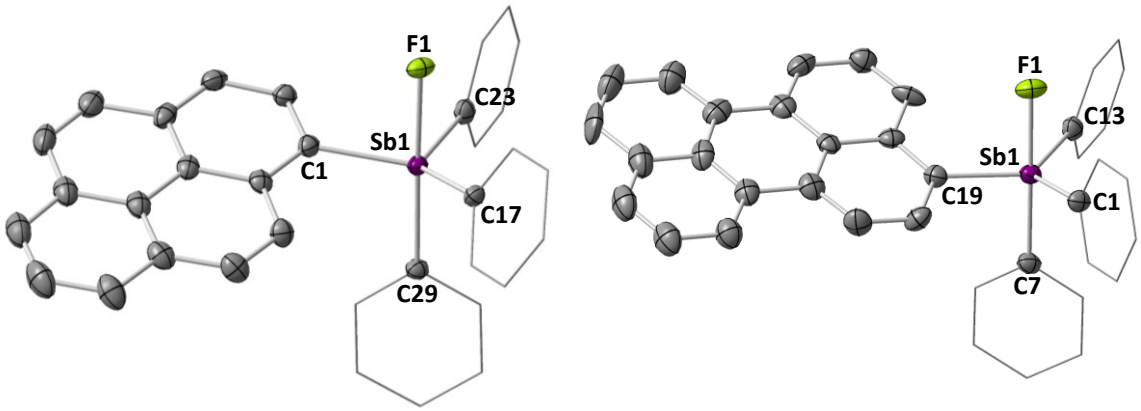

Figure 70. Solid-state structures of **38**-F (left) and **39**-F (right). Thermal ellipsoids are drawn at the 50% probability level. The hydrogen atoms are omitted for clarity. Selected bond lengths (Å) and angles (deg) for **38**-F: Sb1-F1 2.0933(14), F1-Sb1-C29 176.75(8), C1-Sb1-C17 109.02(10), C1-Sb1-C23 123.85(10), C17-Sb1-C23 122.75(10). Right: The hydrogen atoms are omitted for clarity. Selected bond lengths (Å) and angles (deg) for **39**-F: Sb1-F1 2.0498(17), F1-Sb1-C7 178.04(9), C1-Sb1-C13 123.36(12), C1-Sb1-C19 126.74(15), C13-Sb1-C19 107.61(15).

4.5 Determination of fluoride concentration of tap and bottled water samples by fluorescent tetraarylstibonium sensor

To complete this study, we investigated the use of stibonium [**39**]$^+$ as a fluoride sensor for the analysis of tap water (from the city of College Station) and a bottled water from the Ozarka® Brand (Natural Spring Water with added fluoride). We first generated a standard curve by carrying out a spectrophotometric fluoride titration on a solution consisting of a DMSO solution of **39**–Br (0.3 mL, 5×10^{-5} M), an aqueous CTAB (10 mM) solution (1.7 mL) buffered at pH 4.8 (pyridine buffer, 10 mM) and distilled water doped with increasing amounts of fluoride (1 mL) (Figure 71). Water testing was carried out by adding 1 mL of the water sample instead of the distilled water portion. The resulting mixture was stirred for 5 min before an emission spectrum was recorded (λ_{ex} =

423 nm). We found that the fluoride concentrations in the selected water samples are 0.48 ± 0.03 ppm for the City of College Station tap water and 0.74 ± 0.06 ppm for the Ozarka® Brand bottled water. These numbers agree with the reported values for these water samples and are in good agreement with those determined using ion chromatography (Table 9).

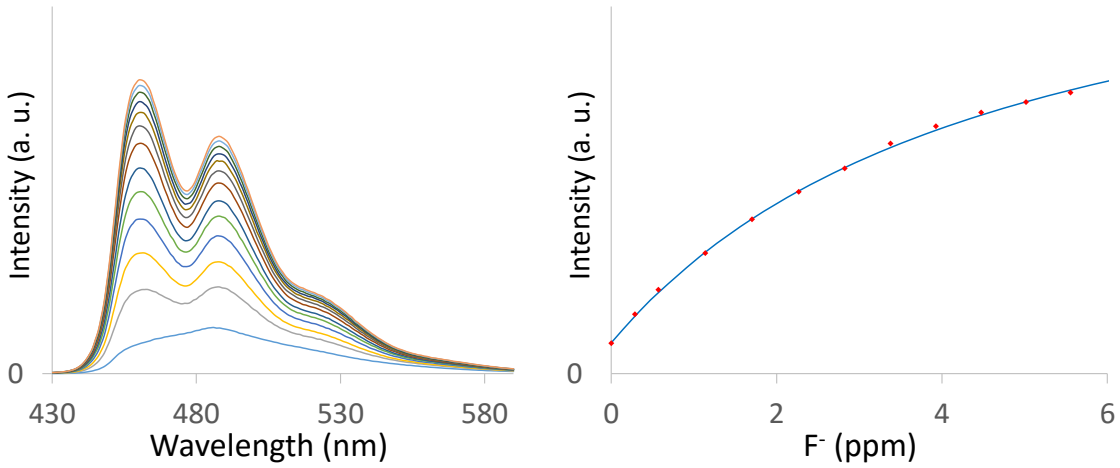

Figure 71. Left: spectral changes in the emission spectrum of **39**-Br upon incremental addition of fluoride anions. Right: plot of fluorescence intensity increase at λ_{fluo} = 461 nm of **39**-Br after successive addition of fluoride anions.

Table 9. Fluoride concentrations of College Station tap water and Ozarka® (added fluoride) water determined by [**39**]$^+$ and IC, and the reported values from water quality reports.

Sample	Em_{461}	F^- ppm (by [**39**]$^+$)	F^- ppm (by IC)	F^- ppm (reported)
Tap water	189912	0.48 (±0.03)	0.45	0.48
Ozarka® (added fluoride)	243366	0.74 (±0.06)	0.73	0.72

4.6 Conclusion

In summary, we have now been able to generalize the approach that we introduced in 2012 using [**28**]$^+$ as a fluoride sensor.[118] We have shown that our synthetic methods can be extended to the use of other polycyclic aromatic fluorophores including the 1-pyrenyl and 3-perylenyl units. These compounds are water stable and complex fluoride anions in aqueous solutions with elevated binding constants. The most important outcome of this study is undoubtedly the isolation as well as the optical and anion binding properties of the 3-perylenyl derivative [**39**]$^+$. Fluoride anion binding by this stibonium cation results in a highly emissive fluorostiborane which can be excited in the visible part of the spectrum. Last but not least, it is also sufficiently stable and selective to be used for measuring sub-ppm concentrations of fluoride anions in drinking water samples.

4.7 Experimental section

General considerations. *Antimony is potentially toxic and should be handled with caution.* Triphenylantimonydibromide,[259] 1–Bromopyrene,[260] and 3–Bromoperylene[261] were prepared according to reported procedures. 9–Bromophenanthrene, KF and n-BuLi (2.2 M in hexane) were purchased from Alfa Aesar. All preparations were carried out under an atmosphere of dry N_2 employing either a glovebox or standard Schlenk techniques. Solvents were dried by passing through an alumina column (pentane and CH_2Cl_2) or by refluxing under N_2 over Na/K (Et_2O and THF). All other solvents were ACS reagent grade and used as received. NMR spectra were recorded on a Varian Unity Inova 300 FT NMR (299.960 MHz for ^{1}H, 75.432 MHz for ^{13}C, 282.206 MHz for ^{19}F)

spectrometer at ambient temperature. Chemical shifts are given in ppm and are referenced to residual ^{1}H and ^{13}C solvent signals and external $BF_3 \cdot Et_2O$ for ^{19}F. Elemental analyses were performed by Atlantic Microlab (Norcross, GA). Electronic absorption spectra were recorded at ambient temperature using Shimadzu UV-2501PC UV-vis Recording Spectrophotometer. Emission spectra were recorded at ambient temperature using a PTI QuantaMaster™ 30 fluorescence spectrofluorometer. Electrospray ionization mass spectra were recorded on Applied Biosystems PE SCIEX QSTAR. Thermogravimetric analysis was carried out using TA Instruments TGA Q500. Ion chromatographs were recorded on Thermo Scientific Dionex ICS-900. The pH measurements were carried out with a Radiometer PHM290 pH meter equipped with a VWR SympHony electrode. The fluoride binding constants (K) were calculated using a method reported previously.[118] TGA indicated that the KF used in this work contained 3 wt% of water. All stoichiometries involving KF were adjusted accordingly.

Crystallography. The crystallographic measurements were performed at 110(2) K using a Bruker APEX-II CCD area detector diffractometer, with a graphite-monochromated Mo-K_α radiation ($\lambda = 0.71069$ A). A specimen of suitable size and quality was selected and mounted onto a nylon loop. The semi-empirical method SADABS was applied for absorption correction. The structure was solved by direct methods, which successfully located most of the non-hydrogen atoms. Subsequent refinement on F^2 using the SHELXTL/PC package (version 6.1) allowed location of the remaining non-hydrogen atoms. All H-atoms were geometrically placed and refined using a standard riding model.[262, 263]

Table 10. Crystal data, data collection, and structure refinement for **37**-Br and **38**-F.

Crystal data	**37**-Br	**38**-F
Empirical formula	C32 H24 Br Sb	C35 H28 F O Sb
Formula weight	610.17	605.32
Temperature	110(2) K	110(2) K
Wavelength	0.71073 Å	0.71073 Å
Crystal system	Monoclinic	Monoclinic
Space group	P2(1)/n	P 21/c
Unit cell dimensions	a = 10.568(2) Å	a = 19.8623(15) Å
	b = 17.691(3) Å	b = 8.0961(6) Å
	c = 13.565(3) Å	c = 17.4657(13) Å
	α = 90°	α = 90°
	β = 101.529(2)°	β = 108.3120(10)°
	γ = 90°	γ = 90°
Volume	2484.9(8) $Å^3$	2666.4(3) $Å^3$
Z	4	4
Density (calculated)	1.631 Mg/m^3	1.508 Mg/m^3
Absorption coefficient	2.737 mm^{-1}	1.069 mm^{-1}
F(000)	1208	1224
Crystal size	0.18 x 0.14 x 0.12 mm^3	0.18 x 0.15 x 0.08 mm^3
Theta range for data collection	1.916 to 29.745°.	2.16 to 29.86°.
Index ranges	-14<=h<=14, -24<=k<=24, -18<=l<=18	-27<=h<=27, -10<=k<=11, -24<=l<=23
Reflections collected	29716	33283
Independent reflections	6726 [R(int) = 0.0628]	7216 [R(int) = 0.0492]
Absorption correction	Semi-empirical from equivalents	Semi-empirical from equivalents
Max. and min. transmission	0.681 and 0.500	0.9194 and 0.8309
Refinement method	Full-matrix least-squares on F^2	Full-matrix least-squares on F^2
Data / restraints / parameters	6726 / 0 / 307	7216 / 0 / 346
Goodness-of-fit on F^2	1.019	1.03
Final R indices [I>2sigma(I)]	R1 = 0.0364, wR2 = 0.0724	R1 = 0.0362, wR2 = 0.0789
R indices (all data)	R1 = 0.0638, wR2 = 0.0816	R1 = 0.0471, wR2 = 0.0838
Largest diff. peak and hole	1.548 and -2.006 e.$Å^{-3}$	2.360 and -1.156 e.$Å^{-3}$

[a] $R1 = \Sigma||Fo| - |Fc||/\Sigma|Fo|$. [b] $wR2 = \{[\Sigma w(Fo^2 - Fc^2)^2]/[\Sigma w(Fo^2)^2]\}^{1/2}$.

Table 11. Crystal data, data collection, and structure refinement for **39**-Br and **39**-F.

Crystal data	**39**-Br	**39**-F
Empirical formula	C76 H52 Br2 Sb2	C38 H26 F Sb
Formula weight	1368.49	623.34
Temperature	110(2) K	110(2) K
Wavelength	0.71073 Å	0.71073 Å
Crystal system	Monoclinic	Monoclinic
Space group	P c	P 21/c
Unit cell dimensions	a = 18.230(4) Å	a = 19.121(3) Å
	b = 11.474(3) Å	b = 8.2771(15) Å
	c = 16.730(4)) Å	c = 17.338(3) Å
	α = 90°	α = 90°
	β = 114.509(3)°	β = 99.910(2)°
	γ = 90°	γ = 90°
Volume	3184.2(13) Å^3	2703.0(8) Å^3
Z	2	4
Density (calculated)	1.427 Mg/m^3	1.532 Mg/m^3
Absorption coefficient	2.145 mm^{-1}	1.054 mm^{-1}
F(000)	1360	1256
Crystal size	0.13 x 0.11 x 0.08 mm^3	0.24 x 0.16 x 0.06 mm^3
Theta range for data collection	1.775 to 27.314°.	1.081 to 28.264°.
Index ranges	-23<=h<=23, -14<=k<=14, -21<=l<=21	-25<=h<=25, -11<=k<=11, -22<=l<=23
Reflections collected	36102	30936
Independent reflections	14271 [R(int) = 0.0441]	6568 [R(int) = 0.0423]
Absorption correction	Semi-empirical from equivalents	Semi-empirical from equivalents
Max. and min. transmission	0.7455 and 0.6128	0.893 and 0.839
Refinement method	Full-matrix least-squares on F^2	Full-matrix least-squares on F^2
Data / restraints / parameters	14271 / 0 / 716	6568 / 0 / 434
Goodness-of-fit on F^2	0.714	1.091
Final R indices [I>2sigma(I)]	R1 = 0.0357, wR2 = 0.0911	R1 = 0.0410, wR2 = 0.0849
R indices (all data)	R1 = 0.0507, wR2 = 0.1032	R1 = 0.0551, wR2 = 0.0924
Largest diff. peak and hole	0.582 and -0.390 e.Å^{-3}	1.142 and -0.801 e.Å^{-3}

[a] $R1 = \Sigma||Fo| - |Fc||/\Sigma|Fo|$. [b] $wR2 = \{[\Sigma w(Fo^2 - Fc^2)^2]/[\Sigma w(Fo^2)^2]\}^{1/2}$.

Synthesis of 37-Br. *n*-Butyllithium (2.65 M) in hexanes (0.8 mL, 2.1 mmol) was slowly added to a solution of 9-bromophenanthrene (0.547 g, 2.1 mmol) in Et_2O (10 mL) at -78 ºC. After stirring for 1 h, the solvent was decanted off using a cannula fitted with a filter tip. The remaining white solid was washed with two portions of Et_2O (5 mL each). The lithium salt was suspended in Et_2O (20 mL) and cooled down to -78 ºC. This mixture was slowly transferred to a solution of Ph_3SbBr_2 in THF (5 mL) via cannula. After stirring at room temperature for 1 h, an off-white solid precipitated out. The solid was collected by filtration and washed with two portions of Et_2O (5 mL each) to obtain **37**-Br in 17% yield (0.220 g). Single crystals of **37**-Br suitable for X-ray diffraction analysis were obtained by slow diffusion of pentane over a THF solution at ambient temperature. ^{1}H NMR (299.960 MHz, $CDCl_3$): δ 8.78 (d, 1H, $^3J_{H\text{-}H}$ = 6.0 Hz), 8.73 (d, 1H, $^3J_{H\text{-}H}$ = 6.0 Hz), 8.01 (s, 1H), 7.97-7.93 (m, 6H; *o*-Sb*Ph*), 7.81-7.60 (m, 4H; phenanthryl *H*), 7.57-7.41 (m, 10H; *m*- and *p*-Sb*Ph* + phenanthryl *H*). $^{13}C\{^1H\}$ NMR (75.432 MHz, $CDCl_3$): δ 137.36, 135.93, 134.84, 134.49, 131.54, 131.47, 131.38, 131.25, 131.00, 129.70, 129.52, 129.34, 128.58, 127.53, 127.45, 127.35, 123.73, 122.83. The detailed assignments of the $^{13}C\{^1H\}$ NMR resonances can be found in Figure 72 along with the ^{1}H NMR spectrum as a measurement of purity prior to titration. Elemental analysis calculate (%) for $C_{32}H_{24}BrSb$: C, 62.99; H, 3.96; found C, 62.88; H, 3.92.

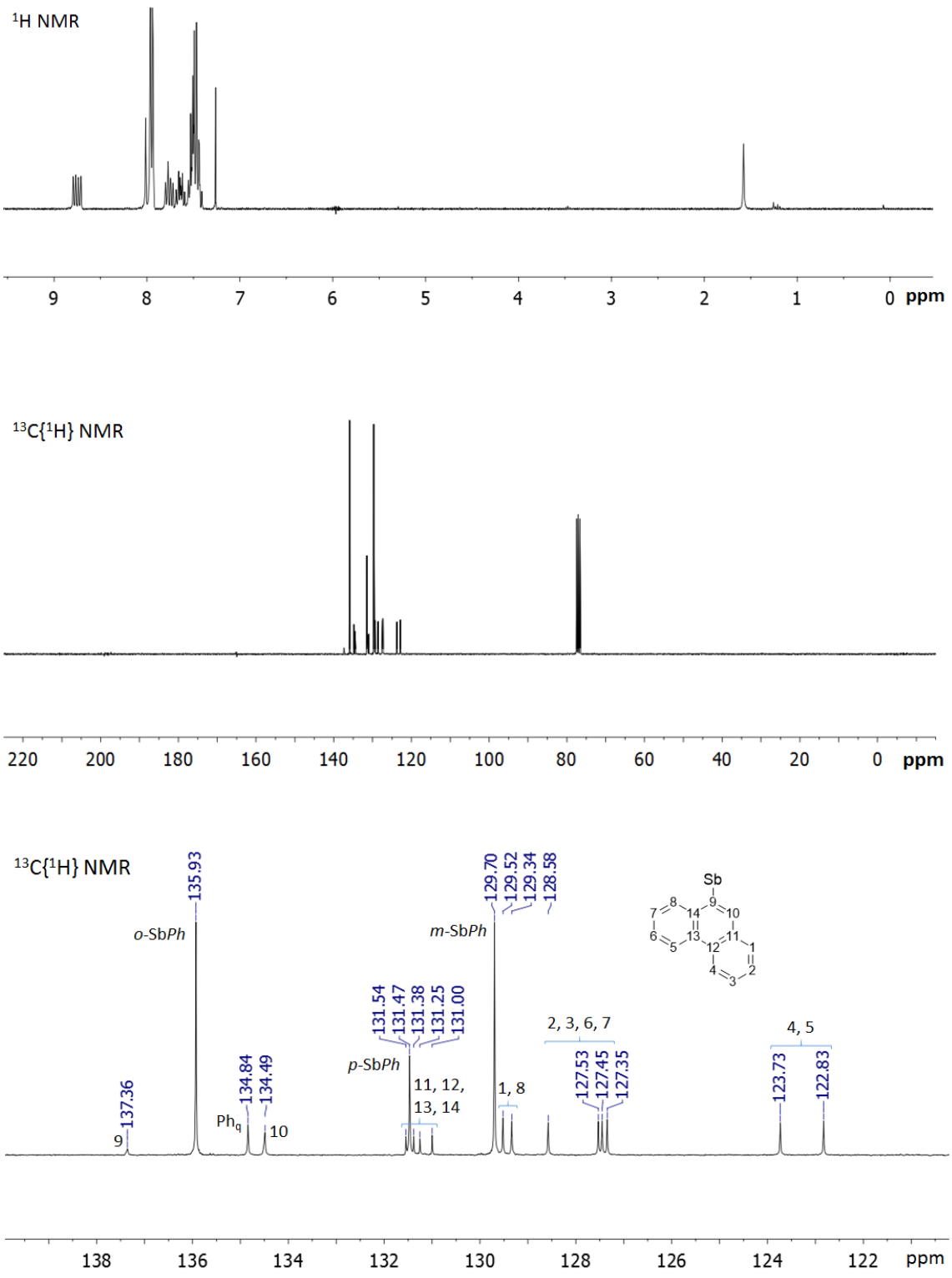

Figure 72. ^{1}H and ^{13}C{^{1}H} spectra of **37**-Br in $CDCl_3$ at room temperature.

Synthesis of 38-Br. *n*-Butyllithium (2.2 M) in hexanes (1.2 mL, 3.2 mmol) was slowly added to a solution of 1-bromopyrene (0.751 g, 2.7 mmol) in THF (5 mL) at -78 ^{o}C. After stirring for 1 h, the solvent was decanted off using a cannula fitted with a filter tip. The remaining brown solid was washed with two portions of Et_2O (5 mL each). The lithium salt was suspended in Et_2O (20 mL) and cooled down to -78 ^{o}C. This mixture was slowly transferred to a solution of Ph_3SbBr_2 in THF (5 mL) via cannula. After stirring at room temperature for 3 h, an off-white solid precipitated out of solution. The solid was collected by filtration and washed with two portions of Et_2O (5 mL each) to obtain **38**-Br in 32% yield (0.542 g). ^{1}H NMR (299.960 MHz, $CDCl_3$): δ 8.32-8.00 (m, 10H; pyrenyl *H*), 7.97-7.92 (pseudo d, 6H, $^{3}J_{H\text{-}H}$ = 6.0 Hz; *o*-Sb*Ph*), 7.56-7.51 (t, 3H, $^{3}J_{H\text{-}H}$ = 6.0 Hz; *p*-Sb*Ph*), 7.50-7.45 (pseudo t, 6H, $^{3}J_{H\text{-}H}$ = 7.5 Hz; *m*-Sb*Ph*). $^{13}C\{^{1}H\}$ NMR (75.432 MHz, $CDCl_3$): δ 136.00, 134.09, 133.29, 132.49, 131.51, 131.08, 130.97, 130.89, 130.55, 129.74, 129.55, 129.29, 127.27, 126.84, 126.63, 126.43, 126.20, 125.72, 125.64, 124.43. The detailed assignments of the $^{13}C\{^{1}H\}$ NMR resonances can be found in Figure 73 along with the ^{1}H NMR spectrum as a measurement of purity prior to titration. Elemental analysis calculated (%) for $C_{34}H_{24}BrSb$: C, 64.39; H, 3.81; found C, 64.37; H, 3.76.

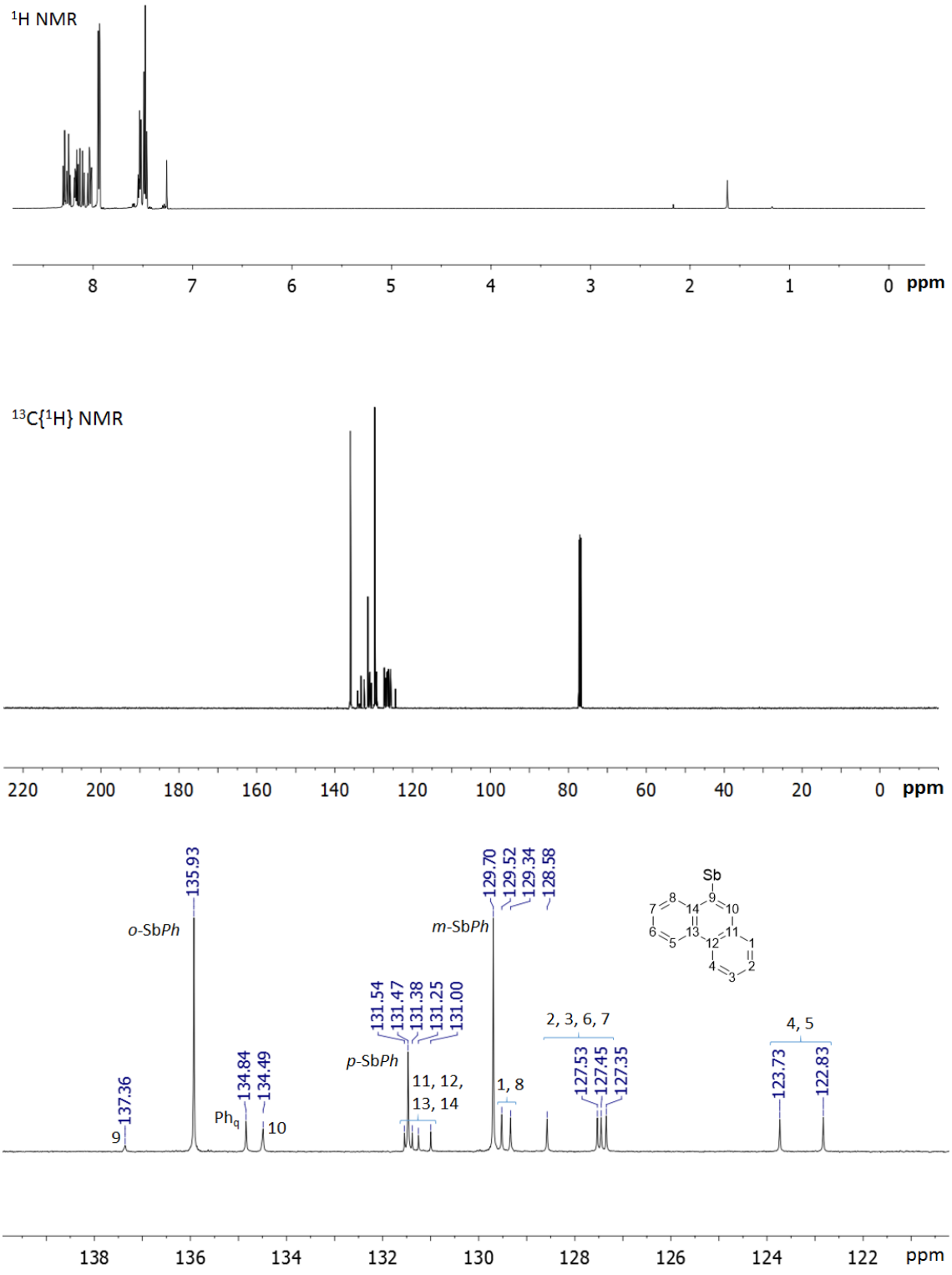

Figure 73. ^{1}H and ^{13}C{^{1}H} NMR spectra of **38**-Br in $CDCl_3$ at room temperature.

Synthesis of 38-F. A MeOH solution (1 mL) of KF (74 mg, 1.3×10^{-3} mol, 5 eq) was added to a MeOH solution (3 mL) of **38**-F (162 mg, 2.5×10^{-4} mol, 1 eq). After letting the mixture stand for an hour at ambient temperature, diffraction-quality single crystals of **38**-F were obtained as pale yellow plates in 71% yield (70 mg, 1.3×10^{-4} mol). ^{1}H NMR (299.960 MHz, $CDCl_3$): δ 8.29-7.97 (m, 9H), 7.92 (d, 1H, $^{3}J_{H\text{-}H}$ = 3.0 Hz; Pyrenyl *H*), 7.82 (broad, 6H; *o*-Sb*Ph*), 7.55-7.33 (m, 9H; *m*- and *p*-Sb*Ph*). $^{13}C\{^{1}H\}$ NMR (75.432 MHz, $CDCl_3$): δ 136.75, 136.46), 134.13, 132.51, 131.87, 131.15, 130.70, 130.49, 129.35, 129.02, 128.51, 128.44, 128.17, 127.35, 126.19, 125.66, 125.61, 125.35, 124.97, 124.55. ^{19}F NMR (282.206 MHz, $CDCl_3$): δ -77.5 (s). The detailed assignments of The detailed assignments of the $^{13}C\{^{1}H\}$ NMR resonances can be found in Figure 74. Elemental analysis calculated (%) for $C_{34}H_{24}FSb$: C 71.23, H 4.22; found C 71.38, H, 4.25.

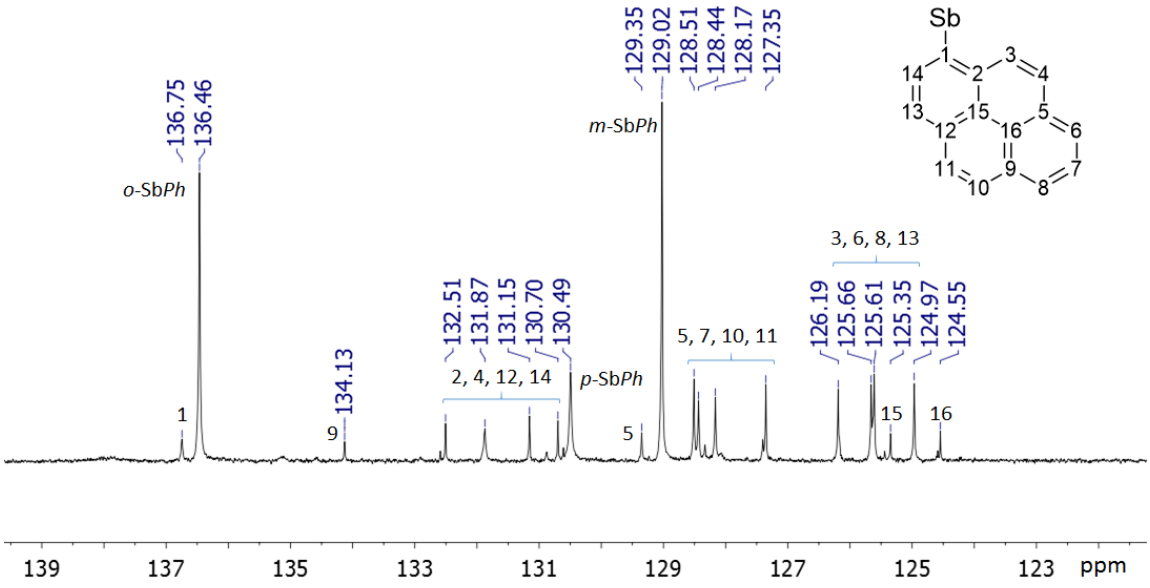

Figure 74. $^{13}C\{^{1}H\}$ NMR spectrum of **38**-F in $CDCl_3$ at room temperature.

Synthesis of 39-Br. *n*-Butyllithium (2.2 M) in hexanes (0.9 mL, 1.9 mmol) was slowly added to a solution of 3-bromoperylene (0.622 g, 1.9 mmol) in a Et_2O (10 mL)/THF (1 mL) mixture at -78 ºC. After stirring for 1 h, the solvent was decanted off using a cannula fitted with a filter tip. The remaining orange lithium salt was washed with two portions of Et_2O (5 mL each). The lithium salt was then dissolved in Et_2O (15 mL)/THF (5 mL) mixture and cooled down to -78 ºC. This mixture was slowly transferred to a pre-cooled solution (-78 ºC) of Ph_3SbBr_2 (0.963 g, 1.9 mmol) in Et_2O (10 mL)/THF (5 mL) via cannula. After stirring at ambient temperature for 3 h, an orange solid precipitated out of solution. The solid was recovered by filtration and extracted with two portions of MeOH (10 mL each). After concentrating the MeOH solution volume down to approximately 1 mL, Et_2O (10 mL) was added slowly to afford an orange solid. This solid was isolated by filtration and successively washed with two portions of Et_2O (5 mL) to afford **39**-Br in 22% yield (0.283 g). Diffraction-quality single crystals of **39**-Br were obtained as orange blocks by slow diffusion of Et_2O into a CH_2Cl_2 solution at ambient temperature. ^{1}H NMR (299.960 MHz, $CDCl_3$): δ 8.23-8.16 (m, 4H; perylene), 7.92 (pseudo d, 6H, $^3J_{H\text{-}H}$ = 5.9 Hz; *m*-Sb*Ph*), 7.79 (d, 1H, $^3J_{H\text{-}H}$ = 3.0 Hz; perylene), 7.75 (d, 1H, $^3J_{H\text{-}H}$ = 5.8 Hz; perylene), 7.72 (d, 1H, $^3J_{H\text{-}H}$ = 5.8 Hz; perylene), 7.71 (d, 1H, $^3J_{H\text{-}H}$ = 3.0 Hz; perylene), 7.55-7.46 (m, 11H; *o*- and *p*-Sb*Ph* and perylene), 7.37 (pseudo t, 1H, $^3J_{H\text{-}H}$ = 5.8 Hz; perylene). $^{13}C\{^1H\}$ NMR (75.432 MHz, $CDCl_3$): δ135.92, 134.95, 134.61, 134.49, 134.09, 133.52, 132.50, 131.47, 130.53, 130.17, 130.06, 129.69, 129.17, 128.54, 128.36, 127.97, 127.84, 126.79, 126.71, 121.57, 121.12, 121.01, 120.18. The detailed assignments of the $^{13}C\{^1H\}$ NMR resonances can be found in Figure 75 along with the ^{1}H

NMR spectrum as a measurement of purity prior to fluoride titration. Elemental analysis calculated (%) for $C_{38}H_{26}BrSb$: C 66.70, H 3.83; found C 66.88, H 3.89.

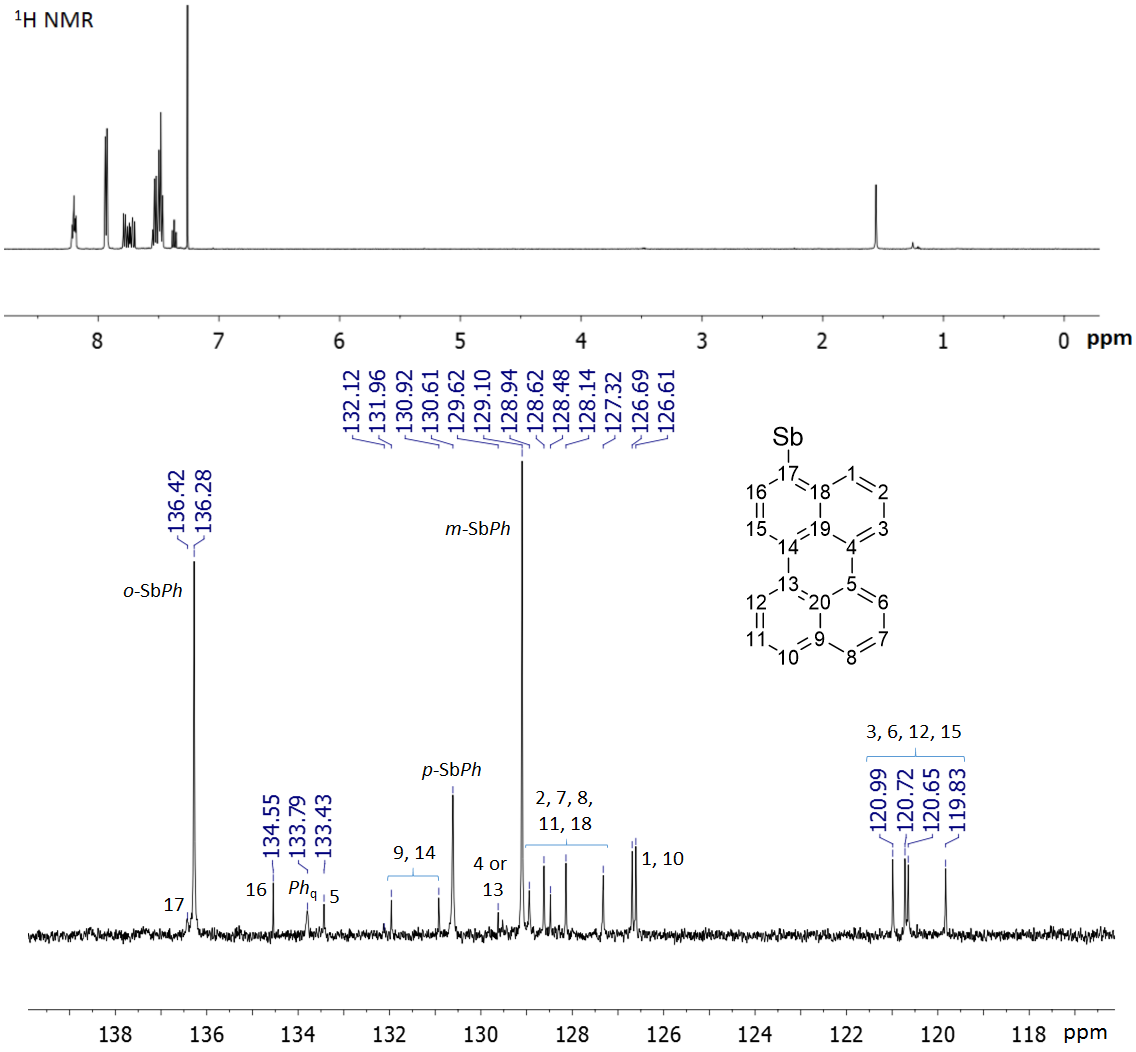

Figure 75. ^{1}H and $^{13}C\{^{1}H\}$ NMR spectra of **39**-Br in $CDCl_3$ at room temperature.

Synthesis of 39-F. KF (51 mg, 7.3×10^{-4} mol, 5 eq) was added to a MeOH solution (3 mL) of **39**-Br (121 mg, 1.8×10^{-4} mol, 1 eq). The resulting suspension was stirred for 30 min then filtered. The remaining dark yellow solid was washed with two portions of MeOH (2 mL each) followed by Et_2O (5 mL) to afford **39**-F in 77% yield (85 mg, 1.4×10^{-4} mol). Diffraction-quality single crystals of **39**-F were obtained as orange blocks by slow diffusion of pentane into a $CDCl_3$ solution at ambient temperature. ^{1}H NMR (299.960 MHz, $CDCl_3$): δ 8.19-8.13 (m, 4H; perylenyl *H*), 7.80 (broad, 6H; *o*-Sb*Ph*), 7.76-7.65 (m, 4H; perylenyl *H*), 7.23 (pseudo t, 1H, $^3J_{H\text{-}H}$ = 6.0 Hz; perylenyl *H*), 7.51-741 (m, 11H; *m*- and *p*-Sb*Ph* + perylenyl *H*), 7.29 (t, 1H, $^3J_{H\text{-}H}$ = 6.0 Hz; perylenyl *H*). ^{13}C{^{1}H} NMR (75.432 MHz, $CDCl_3$): δ 136.28, 134.55, 133.79, 133.43, 131.96, 130.92, 130.61, 129.62, 129.10, 128.94, 128.62, 128.48, 128.14, 127.32, 126.69, 126.61, 120.99, 120.72, 120.65, 119.83. Four of the quaternary carbon signals associated with the perylenyl group could not be found. The detailed assignments of the ^{13}C{^{1}H} NMR resonances can be found in . ^{19}F NMR (282.206 MHz, $CDCl_3$): δ -78.7 (s). Elemental analysis calculated (%) for $C_{38}H_{26}FSb$: C 73.22, H 4.20; found C 73.38, H 4.29.

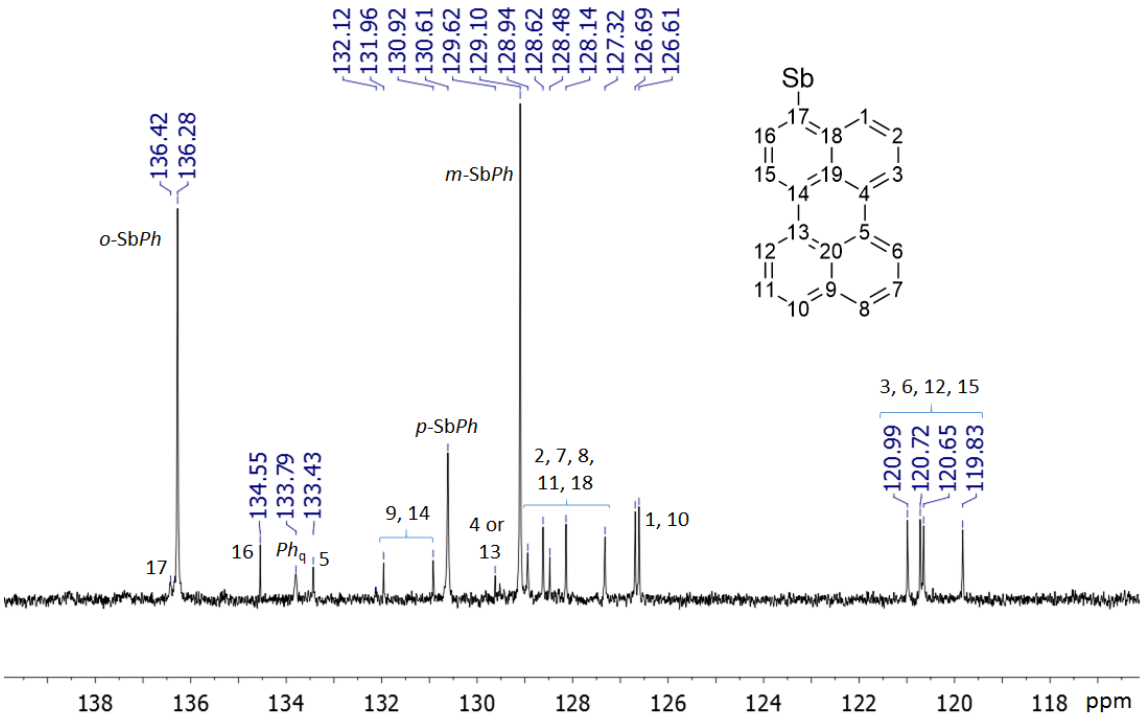

Figure 76. $^{13}C\{^{1}H\}$ NMR spectrum of **39**-F in $CDCl_3$ at room temperature.

Anion selectivity test. A 0.05 M water solution of NaX (5 µL, 16.7 eq; X^- = Cl^-, Br^-, NO_3^-, HCO_3^-, HSO_4^-, and $H_2PO_4^-$) was added to a 9/1 H_2O/DMSO solution of **38**-Br or **39**-Br (3 mL, 5×10^{-6} M, 1 eq) containing CTAB (10 mM) at pH 4.8 (10 mM pyridine). After stirring for 5 min, the fluorescence spectrum was recorded. In all cases, the fluorescence intensities remained unchanged, indicating the lack of binding of these anions toward $[\mathbf{38}]^+$ and $[\mathbf{39}]^+$.

CHAPTER V

PROMOTING THE HYDROSILYLATION OF BENZALDEHYDE BY USING A DICATIONIC ANTIMONY-BASED LEWIS ACID: EVIDENCE FOR THE DOUBLE ELECTROPHILIC ACTIVATION OF THE CARBONYL SUBSTRATE*

5.1 Introduction

Electrophilic phosphonium cations are attracting an increasing interest as Lewis acids for the complexation of small anions or for the activation of various organic reactions.[148, 149] The unique Lewis acidic properties displayed by these saturated derivatives arise from the ability of phosphorus to exceed the octet rule, a phenomenon facilitated by the introduction of electron withdrawing ligands.[145, 147-150, 264-266] Another methods that has been explored as a means to achieve greater Lewis acidity is based on the incorporation of two electrophilic moieties positioned to cooperatively interact with an incoming nucleophile. This is for example the case with the phosphonium borane derivative [*o*-**23**]$^+$ which acts as a bidentate Lewis acid toward fluoride.[113] The Stephan group has recently investigated the Lewis acidic properties of the bis-fluorophosphonium species ([**40**]$^{2+}$) and found that the proximity of the two group 15 cations leads to enhanced

* Reprinted in part with permission from: "Promoting the Hydrosilylation of Benzaldehyde by Using a Dicationic Antimony-Based Lewis Acid: Evidence for the Double Electrophilic Activation of the Carbonyl Substrate"; Hirai, M.; Cho, J.; Gabbaï F. P. *Chem. Eur. J.* **2016**, *22*, 6537-6541. Copyright 2016 by John Wiley & Sons, Inc.

catalytic activity in a range of reactions including Friedel Crafts, hydrosilylation, and hydrodefluorination reactions.[266, 267]

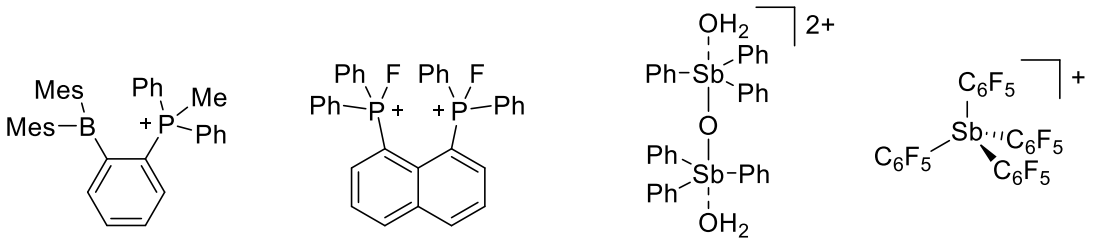

[*o*-**23**]$^{+}$ [**40**]$^{2+}$ [**41**]$^{2+}$ [**31**]$^{+}$

Figure 77. Phosphonium borane [*o*-**23**]$^{+}$, bis(fluorophosphonium) [**40**]$^{2+}$, distibonium [**41**]$^{2+}$, and tetrakis(pentafluorophenyl)stibonium [**31**]$^{+}$.

Organoantimony(V) derivatives are another class of Lewis acidic derivatives drawing attention.[84, 85, 114, 117, 118, 191] Such derivatives including [**41**]$^{2+}$[156] and [**31**]$^{+}$[157] are emerging as air stable Lewis acids which can be used to promote C-C bond forming reactions or to activate strong element-fluorine bonds. As part of our contribution to the chemistry of these new Lewis acids, we have also synthesized bidentate distiboranes such as **36** and found evidence of strong cooperativity between the two Lewis acidic centers in the binding of fluoride anions.[249] Encouraged by these ongoing developments, we have now decided to test whether bidentate antimony derivatives could also be used as organic catalysts for the double electrophilic activation of organic carbonyls as illustrated in **III**.[268-273] In this paper, we present a series of results which support this possibility.

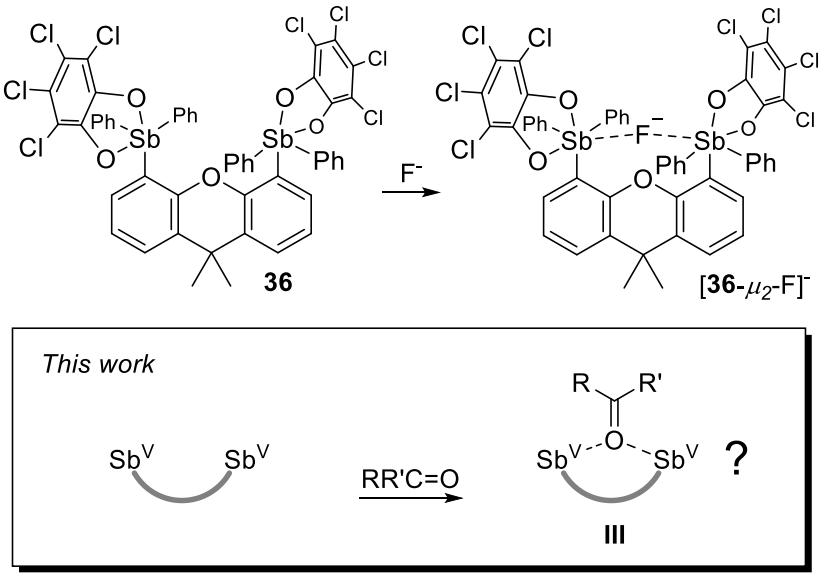

Figure 78. Top: reaction of distiborane **36** with fluoride ion. Bottom: proposed binding mode of carbonyl substrates with bidentate organoantimony(V) species.

5.2 Synthesis and characterization of *o*-phenylene-based distibonium salts

To initiate our study, we decided to target a bifunctional antimony Lewis acid with a binding pocket that is readily substrate-accessible. This consideration led us to target the *ortho*-phenylene derivative [**42**]$^{2+}$ which features two Lewis acidic antimony sites predisposed to interact with incoming nucleophiles. Distibonium salts [**42**][OTf]$_2$ and [**42**][BF_4]$_2$ could be conveniently generated by treatment of *o*-phenylene-bis(diphenylstibine)[274] with methyl trifluoromethylsulfonate (MeOTf) and trimethyloxonium tetrafluoroborate ([Me_3O][BF_4]), respectively (Figure 79). Both [**42**][OTf]$_2$ and [**42**][BF_4]$_2$ have been fully characterized and their compositions have been verified by elemental analyses. The ^{1}H NMR spectrum of [**42**][OTf]$_2$ and [**42**][BF_4]$_2$ in CD_2Cl_2 shows a diagnostic methyl resonance at 2.18 and 2.17 ppm, respectively,

indicative of the formation of the methylstibonium moiety. Both [**42**][OTf]$_2$ and [**42**][BF$_4$]$_2$ are very soluble in CH_2Cl_2, THF, and CH_3CN and sparingly soluble in $CHCl_3$. Salt [**42**][BF$_4$]$_2$ is stable over prolonged periods of time and shows no tendency toward decomposition by fluoride transfer from the BF_4^- anion to the Lewis acidic antimony center. For comparison, we also prepared the monofunctional model compound [Ph$_3$MeSb][OTf][275] and [Ph$_3$MeSb][BF$_4$][276] which have both been previously described.

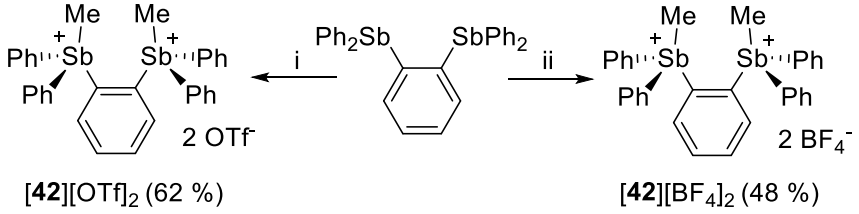

Figure 79. Synthesis of [**42**][OTf]$_2$ and [**42**][BF$_4$]$_2$. i) 4 eq MeOTf, toluene, 90 ^{o}C; ii) 2.05 eq [Me$_3$O][BF$_4$], 1:2 $C_2H_4Cl_2$:toluene, 90 ^{o}C.

With these compounds in hand, we first decided to quantitatively examine their Lewis acidity by applying the Gutmann-Beckett method which relies on the ^{31}P NMR chemical shift change observed upon coordination of Et$_3$PO to a Lewis acid.[277] In the case of monofunctional Lewis acids [Ph$_3$MeSb][OTf] and [Ph$_3$MeSb][BF$_4$], CH_2Cl_2 solutions of Et$_3$PO (7.5×10^{-2} M) containing a 8-fold excess of the stibonium salt feature a broad ^{31}P NMR signal at 57.0 ppm, downshifted from the free Et$_3$PO (δ = 51.0 ppm) by +6.0 ppm. This suggests that these two salts display similar Lewis acidity despite the differing counteranions. When the same measurement was repeated with the distibonium salts [**42**][OTf]$_2$ and [**42**][BF$_4$]$_2$ using CH_2Cl_2 solutions of Et$_3$PO (7.5×10^{-2} M) containing a

four-fold excess of the distibonium, the ^{31}P NMR chemical shift of the phosphine oxide is observed at 61.4 ppm and 62.2 ppm, respectively (Figure 92 and Figure 93). These resonances are significantly more downfield that those observed with the simple stibonium salts [Ph_3MeSb][OTf] and [Ph_3MeSb][BF_4] indicating that the distibonium salts [**42**][OTf]$_2$ and [**42**][BF_4]$_2$ are more Lewis acidic and more effectively polarize the P=O bond of Et_3PO (Figure 94 and Figure 95). This suggests that this greater Lewis acidity arises from the preorganization of the two stibonium moieties and their ability to simultaneously interact with the oxygen atom of the phosphine oxide. Last, we note a small influence of the counteranions for the bifunctional derivatives, with the BF_4^- salt displaying a slightly higher Lewis acidity than its triflate counterpart.

While we failed to crystallize the abovementioned Et_3PO adducts, single crystals of the distibonium salt [**42**][OTf]$_2$ were obtained as colorless blocks by diffusion of Et_2O into a CH_2Cl_2 solution (Figure 80).[278] In the crystal, one of the triflate anions is well separated from the distibonium complex. In contrast, the other triflate anion bridges the two antimony centers resulting in Sb1-O1 and Sb2-O2 separations of 2.8541(12) and 2.9838(13) Å, respectively. These Sb-O distances are shorter than the Sb-O separation of 3.1518(16) Å found in the monofunctional analog [Ph_3MeSb][OTf], the structure of which was also determined for the purpose of this study (Figure 87).[278] In turn, coordination of the triflate anion in [**42**][OTf]$_2$ cannot be overlooked and likely diminishes the Lewis acidity of the antimony centers. Next, we moved to the crystallization of [**42**][BF_4]$_2$.[278] In all attempts that involved a variety of solvents or solvent mixtures, this salt only precipitated in a powder form. In a few cases, we observed that precipitation of [**42**][BF_4]$_2$

was accompanied by formation of a small number of single crystals. Analysis of these crystal indicate that they correspond to the hydrate [**42**-OH_2][BF_4]$_2$ which probably results from the presence of adventitious water in the solvent (Figure 81). The water molecule interacts with one of the antimony centers (Sb2) as indicated by a Sb2-O1 distance of 2.938(3) Å. The other antimony atom interacts with a tetrafluoroborate anion as indicated by the Sb1-F4 contact of 3.066(6) Å.

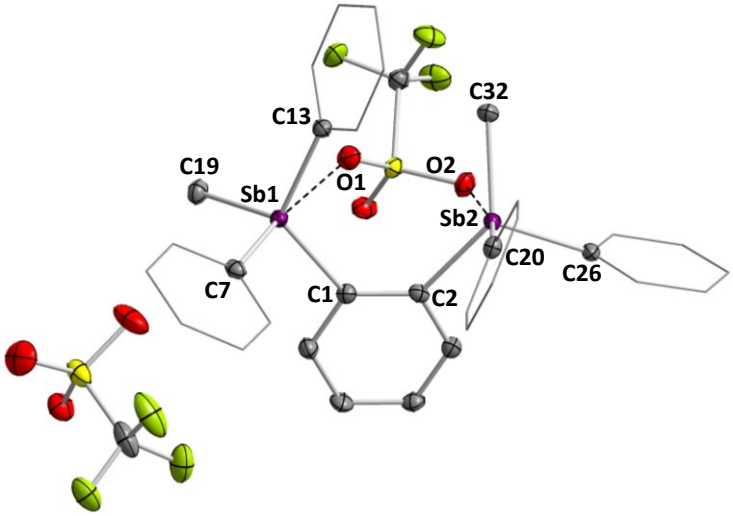

Figure 80. Solid state structure of [**42**][OTf]$_2$. Thermal ellipsoids are drawn at the 50 % probability level. The hydrogen atoms are omitted for clarity. Selected bond lengths (Å) and angles (deg): Sb1-Sb2 4.1069(3), Sb1-O1 2.8541(12), Sb2-O2 2.9838(13), O1-Sb1-C7 174.75(5), C1-Sb1-C13 118.99(6), C1-Sb1-C19 111.54(7), C13-Sb1-C19 109.47(7), O2-Sb2-C20 169.87(5), C2-Sb2-C26 106.68(6), C2-Sb2-C32 126.13(6), C26-Sb2-C32 106.80(7).

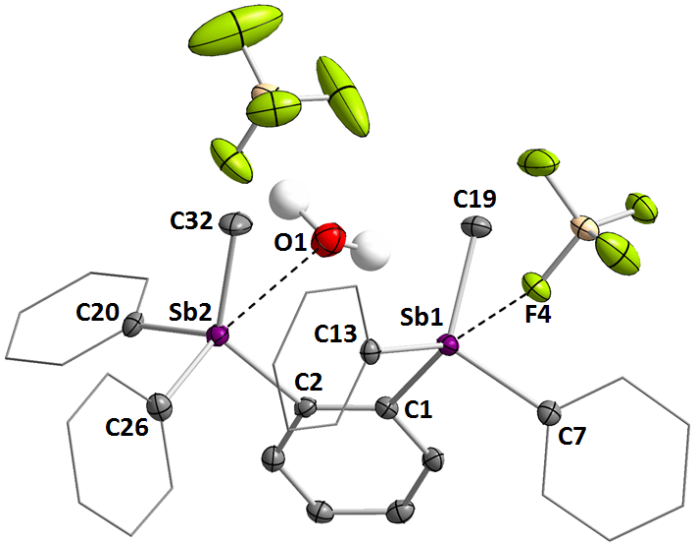

Figure 81. Solid state structure of [**42**-OH_2][BF_4]$_2$. Thermal ellipsoids are drawn at the 50 % probability level. The hydrogen atoms are omitted for clarity except for the water molecule in [**42**-OH_2][BF_4]$_2$. Selected bond lengths (Å) and angles (deg): Sb1-Sb2 4.0217(7), Sb1-F4 3.066(6), Sb2-O1 2.938(3), Sb1-O1-Sb2 74.32(7), O1-Sb1-C7 143.63(12), F4-Sb1-C1 168.01(12), C7-Sb1-C13 113.48(15), C7-Sb1-C19 111.04(16), C13-Sb1-C19 109.78(15), C13-Sb1-C31 108.98(13), O1-Sb2-C26 167.46(13), C2-Sb2-C20 104.20(14), C2-Sb2-C32 125.59(17), C20-Sb2-C32 108.55(17).

5.3 Stibonium Lewis acids as catalysts for hydrosilylation of benzaldehyde

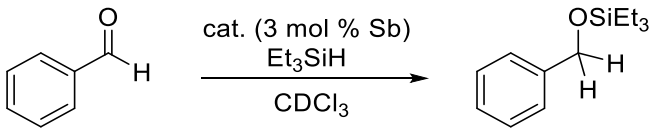

Figure 82. Hydrosilylation of benzaldehyde.

Encouraged by these results, we next investigated the catalytic properties of these stibonium compounds in the hydrosilylation of benzaldehyde using triethylsilane in $CDCl_3$ (Figure 82). While [Ph_3MeSb][OTf] and [Ph_3MeSb][BF_4] (3 mol%) did not

promote the reaction at room temperature, we observed some moderate catalytic activity in the case of [**42**][OTf]$_2$ (1.5 mol%), with 11% conversion after 8 h (Figure 96). A surprisingly contrasting behavior was observed in the case of [**42**][BF_4]$_2$ (1.5 mol%) which proves to be much more active leading to complete conversion after 8 h (Figure 97). This reaction is unaffected by addition of 3 mol% of Mes_3P as a Brønsted acid scavenger indicating that protons are not responsible for the observed catalytic activity.[279] We also note that Et_3SiH reacts with acids making the involvement of protons an even more remote possibility. These results show that: i) the distibonium catalysts are more active that their monofunctional analogs; ii) the tetrafluoroborate salt of the distibonium is significantly more active than the triflate salt. We propose that: i) the higher activity of the distibonium catalysts arises from their ability to doubly activate the carbonyl functionality of the aldehyde; ii) the higher activity of [**42**][OTf]$_2$ *vs.* [**42**][BF_4]$_2$ results from the more weakly coordinating nature of the BF_4^- anion. To support the concept of double electrophilic activation of the carbonyl substrate by [**42**]$^{2+}$ in these reactions, we failed to isolate the benzaldehyde adduct. An adduct was obtained with the more basic carbonyl substrate DMF and [**42**][OTf]$_2$.[278] Elucidation of the structure of this adduct reveals a DMF molecule bridging the two antimony centers in an unsymmetrical fashion (Figure 83). The resulting Sb1-O1 (2.555(2) Å) and Sb2-O1 (2.992(2) Å) bonds are well within the sum of the van der Waals radii of the two elements (Sb-O = 3.75 Å).[237] The DMF oxygen atom is positioned directly *trans* from a phenyl ligand (∠(O1-Sb1-C7) = 175.44(10)º, ∠(O1-Sb2-C19) = 175.49(11)º) leading to distorted trigonal bipyramidal geometries at each antimony center.[85] The solid-state IR spectrum of single crystals of [**42**-μ_2-DMF][OTf]$_2$

displays a weakening of the C-O bond as the stretching frequency was lowered to 1634 cm^{-1} from 1675 cm^{-1} in neat DMF (Figure 91). A Natural Bond Orbital analysis carried out using the crystal geometry of [**42**-μ_2-DMF]$^{2+}$ supports the concomitant interaction of the DMF oxygen atom with each antimony center as illustrated by the presence of multiple O→Sb interactions involving filled oxygen p orbitals as donor orbitals and vacant Sb-C_{Ph} σ* orbitals as acceptor orbitals (Figure 83). The energy of these O→Sb interactions was estimated to be ~12 kcal/mol using the NBO deletion protocol.[280]

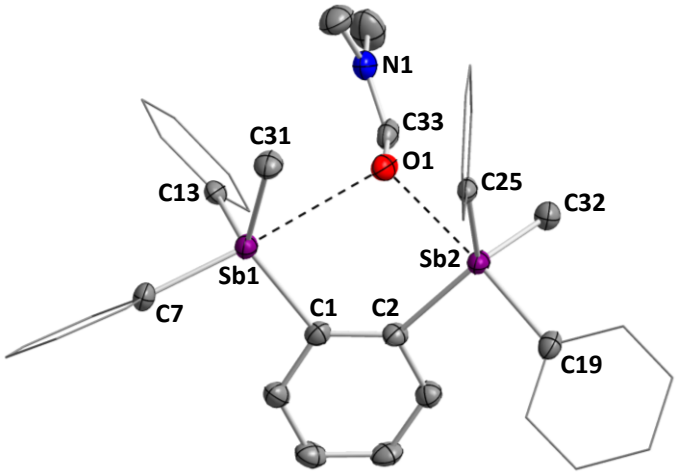

Figure 83. Solid state structure of [**42**-μ_2-DMF][OTf]$_2$. Thermal ellipsoids are drawn at the 50 % probability level. The triflate anions and the hydrogen atoms are omitted for clarity. Selected bond lengths (Å) and angles (deg): Sb1-O1 2.992(2), Sb2-O1 2.555(2), O1-C33 1.240(4), C33-N1 1.318(4), Sb1-O1-Sb2 96.92(7), O1-Sb1-C7 175.44(10), C1-Sb1-C13 103.24(12), C1-Sb1-C31 127.60(13), C13-Sb1-C31 108.98(13), O1-Sb2-C19 175.49(11), C2-Sb2-C25 126.60(12), C2-Sb2-C32 112.62(13), C25-Sb2-C32 111.86(13).

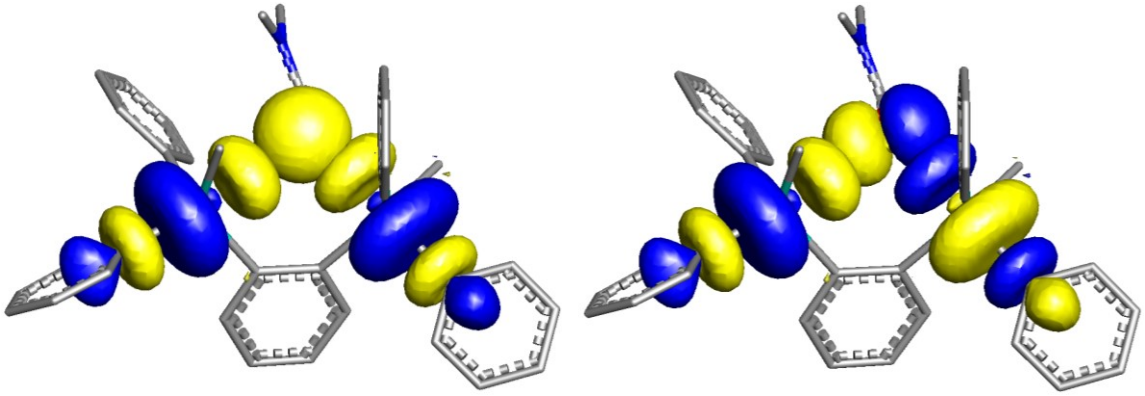

Figure 84. NBO plot (isovalue 0.05) showing two representative lp(O) → σ*(Sb-C_{Ph}) donor–acceptor interactions in [**42**-μ_2-DMF]$^{2+}$.

The four stibonium salts investigated in this study have also been evaluated for the hydrosilylation of 4-nitro-, 4-trifluoromethyl-, 4-methoxy-, and 4-dimethylaminobenzaldehyde. Hydrosilylation was not observed for these substrates. We propose that this lack of activation arises from the relatively weak Lewis acidity of the stibonium cations and their inability to activate weakly basic substrates such as 4-nitro- and 4-trifluorobenzaldehyde or overcome the stability of electron-rich substrates such as 4-methoxy- and 4-dimethylaminobenzaldehyde. To support this proposal, we have also tested the reactivity of 4-fluorobenzaldehyde and found that it undergoes clean hydrosilylation with [**42**][BF_4]$_2$ and Et_3SiH as silane. We have also tested a few other tertiary silanes and found that *i*Pr_3SiH, Ph_2MeSiH and Ph_3SiH are not reactive toward benzaldehyde in the presence of [**42**][BF_4]$_2$. We assign this lack of reactivity to the bulk of these silanes. Finally, the ^{1}H NMR spectrum of Et_3SiH remains unchanged upon mixing with [**42**][BF_4]$_2$. This observation suggests that a mechanism involving Si-H bond activation as with catalysts such $(C_6F_5)_3B$[281, 282] or $[(C_6F_5)_3FP]^+$[267] is unlikely;[283, 284]

instead, it suggests that the catalyst may be directly activating the carbonyl substrate as observed for other main group catalysts.[285-288] Collectively, these results can be reconciled by invoking the double electrophilic activation of benzaldehyde by [**42**]$^{2+}$ followed by silane reduction as depicted in Figure 85.

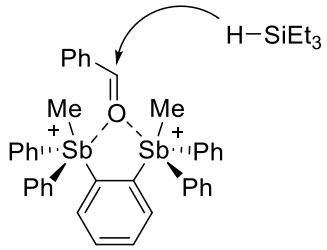

Figure 85. Double electrophilic activation of benzaldehyde by [**42**]$^{2+}$.

5.4 Conclusion

In summary, we describe the synthesis and structure of a distibonium dication which promotes the hydrosilylation of benzaldehyde under mild conditions. The unusual catalytic properties of this dication are proposed to result from its ability to doubly activate the carbonyl functionality of the substrate. This proposal is supported by the fact that simple stibonium monocations fail to promote this reaction as well as by the isolation of the DMF adduct [**42**-μ_2-DMF][OTf]$_2$ in which the DMF oxygen atom is engaged with the two antimony centers.

5.5 Experimental section

General considerations. Antimony is potentially toxic and should be handled with caution. 1,2-dibromobenzene was purchased from Oakwood Chemical and distilled from powdered CaH_2 and stored under N_2. Antimony trichloride ($SbCl_3$), triphenyl stibine (Ph_3Sb), and *n*-butyl lithium (2.2 M in hexane) were purchased from Alfa Aesar and used as received. Methyl trifluoromethanesulfonate (MeOTf) was purchased from Matrix Scientific and used as received. Trimethyloxonium tetrafluoroborate was purchased from Beantown Chemical and used as received. All preparations were carried out under an atmosphere of dry N_2 employing either a glovebox or standard Schlenk techniques. Solvents were dried by passing through an alumina column (CH_2Cl_2) or by refluxing under N_2 over Na/K (toluene, Et_2O and THF). All other solvents were ACS reagent grade and used as received. NMR spectra were recorded on a Varian Unity Inova 400 FT NMR (399.508 MHz for ^1H, 100.466 MHz for ^{13}C) or Varian Unity Inova 500 FT NMR (499.42 MHz for ^1H, 469.86 MHz for ^{19}F, 125.60 MHz for ^{13}C) spectrometer at ambient temperature. Chemical shifts are given in ppm and are referenced to residual ^1H and ^{13}C solvent signals and external $BF_3 \cdot Et_2O$ for ^{19}F. Elemental analyses were performed by Atlantic Microlab (Norcross, GA). IR spectrum was recorded by Mattson ATI Genesis FT-IR Spectrometer.

Computational details. A single point calculation was carried out on the crystal structure of [**42**-μ_2-DMF][OTf]$_2$ using Density Functional Theory (DFT) methods with the *Gaussian 09* program[208] and the following level of theory: B3LYP functional;[209, 210], mixed basis set: Sb, aug-cc-pVTZ-PP;[240] C/N/O/H, 6-31g.[213] The DFT single point

calculation output was used for the Natural Bond Orbital (NBO) analysis at the same level of theory.[289] The Natural Bond Orbitals were visualized and plotted in Jimp 2 program.[214]

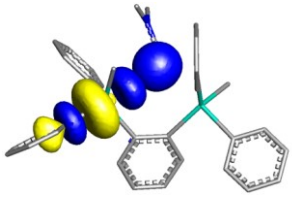

lp(O) → σ*(Sb2-C_{Ph}) 2.23 kcal/mol

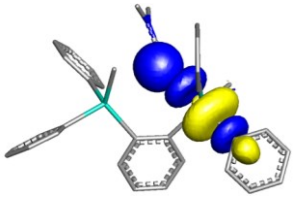

lp(O) → σ*(Sb1-C_{Ph}) 4.92 kcal/mol

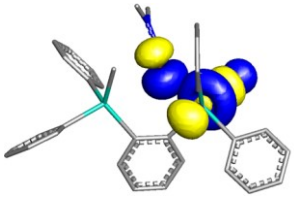

lp(O) → σ*(Sb1-C_{Ph}) 2.35 kcal/mol

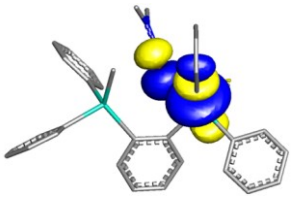

lp(O) → σ*(Sb1-C_{Ph}) 2.16 kcal/mol

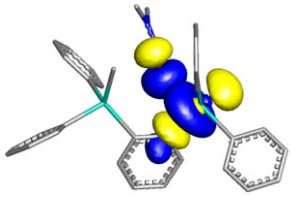

lp(O) → σ*(Sb1-C_{Ph}) 4.01 kcal/mol

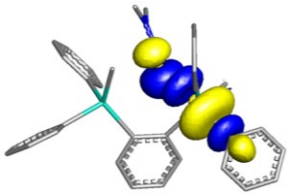

lp(O) → σ*(Sb1-C_{Ph}) 7.08 kcal/mol

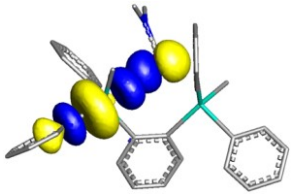

lp(O) → σ*(Sb1-C_{Ph}) 2.55 kcal/mol

Figure 86. Natural Bond Orbital (NBO) plots of the major Sb1-O and Sb2-O bonding interactions (isodensity value 0.05) with the corresponding second order energies. Only those O→Sb interactions with a second order energy > 2 kcal/mol are shown.

Crystallographic measurements. All crystallographic measurements were performed at 110(2) K using a Bruker SMART APEX II diffractometer with a CCD area detector (graphite monochromated Mo Kα radiation, λ = 0.71073 Å, ω-scans with a 0.5 step in ω) at 110 K. In each case, a specimen of suitable size and quality was selected and mounted onto a nylon loop. The semiempirical method SADABS was applied for absorption correction. The structures were solved by direct methods and refined by the full-matrix least-squares technique against F^2 with the anisotropic temperature parameters for all non-hydrogen atoms. All H-atoms were geometrically placed and refined in riding model approximation. Data reduction and further calculations were performed using the Bruker SAINT$^+$ and SHELXTL NT program packages. After numerous modeling attempts, heavily disordered solvent molecules in the structure of [**42-**μ_2-DMF][OTf]$_2$ were handled using the Squeeze program implemented in PLATON. The program calculated a solvent-accessible volume of 321 Å^3 (7.3 % of the total unit cell volume), which was then removed from subsequent structure factor calculations.

Table 12. Crystal data, data collection, and structure refinement for [**42**][OTf]$_2$ and [**42**-OH_2][BF_4]$_2$.

Crystal data	[**42**][OTf]$_2$	[**42**-OH_2][BF_4]$_2$
Empirical formula	C34 H30 F6 O6 S2 Sb2	C32 H32 B2 F8 O Sb2
Formula weight	956.20	849.69
Temperature	110(2) K	110(2) K
Wavelength	0.71073 Å	0.71073 Å
Crystal system	Monoclinic	Orthorhombic
Space group	P 21/n	Pbca
Unit cell dimensions	a = 13.4197(12) Å	a = 16.445(3) Å
	b = 13.8038(12) Å	b = 12.651(3) Å
	c = 19.1568(17) Å	c = 30.614(6) Å
	α = 90°	α = 90°
	β = 90.639(1)°	β = 90°
	γ = 90°	γ = 90°
Volume	3548.4(5) Å^3	6369(2) Å^3
Z	4	8
Density (calculated)	1.790 Mg/m^3	1.772 Mg/m^3
Absorption coefficient	1.715 mm^{-1}	1.769 mm^{-1}
F(000)	1880	3328
Crystal size	0.18 x 0.12 x 0.11 mm^3	0.297 x 0.118 x 0.096 mm^3
Theta range for data collection	2.140 to 27.103°.	1.330 to 28.286°.
Index ranges	-17<=h<=17, -18<=k<=18, -25<=l<=25	-21<=h<=21, -16<=k<=16, -40<=l<=39
Reflections collected	43579	70832
Independent reflections	8810 [R(int) = 0.0306]	7832 [R(int) = 0.0623]
Absorption correction	Semi-empirical from equivalents	Semi-empirical from equivalents
Max. and min. transmission	0.8785 and 0.6984	0.745 and 0.633
Refinement method	Full-matrix least-squares on F^2	Full-matrix least-squares on F^2
Data / restraints / parameters	8810 / 0 / 453	7832 / 0 / 410
Goodness-of-fit on F^2	1.024	1.144
Final R indices [I>2sigma(I)]	R1 = 0.0193, wR2 = 0.0447	R1 = 0.0362, wR2 = 0.0849
R indices (all data)	R1 = 0.0232, wR2 = 0.0466	R1 = 0.0565, wR2 = 0.1011
Largest diff. peak and hole	0.521 and -0.352 e.Å^{-3}	1.274 and -1.224 e.Å^{-3}

[a] $R1 = \Sigma||Fo| - |Fc||/\Sigma|Fo|$. [b] $wR2 = \{[\Sigma w(Fo^2 - Fc^2)^2]/[\Sigma w(Fo^2)^2]\}^{1/2}$.

Table 13. Crystal data, data collection, and structure refinement for [**42**-μ_2-DMF][OTf]$_2$ and [Ph_3MeSb][OTf].

Crystal data	[**42**-μ_2-DMF][OTf]$_2$	[Ph_3MeSb][OTf]
Empirical formula	C37 H37 F6 N O7 S2 Sb2	C20 H18 F3 O3 S Sb
Formula weight	1029.29	517.15
Temperature	110(2) K	110(2) K
Wavelength	0.71073 Å	0.71073 Å
Crystal system	Monoclinic	Monoclinic
Space group	P 21/c	P 21/n
Unit cell dimensions	a = 10.8430(9) Å	a = 9.0760(5) Å
	b = 15.9288(14) Å	b = 16.9976(9) Å
	c = 25.457(2) Å	c = 13.3322(7) Å
	α = 90°	α = 90°
	β = 90.5250(10)°	β = 107.437(2)°
	γ = 90°	γ = 90°
Volume	4396.7(7) Å^3	1962.25(18) Å^3
Z	4	4
Density (calculated)	1.555 Mg/m^3	1.751 Mg/m^3
Absorption coefficient	1.393 mm^{-1}	1.558 mm^{-1}
F(000)	2040	1024
Crystal size	0.18 x 0.14 x 0.14 mm^3	0.189 x 0.166 x 0.125 mm^3
Theta range for data collection	1.508 to 28.216°.	2.396 to 29.014°.
Index ranges	-14<=h<=14, -20<=k<=21, -33<=l<=33	-12<=h<=12, -23<=k<=23, -18<=l<=17
Reflections collected	51966	41869
Independent reflections	10697 [R(int) = 0.0478]	5158 [R(int) = 0.0496]
Absorption correction	Semi-empirical from equivalents	Semi-empirical from equivalents
Max. and min. transmission	0.868 and 0.796	0.933 and 0.774
Refinement method	Full-matrix least-squares on F^2	Full-matrix least-squares on F^2
Data / restraints / parameters	10697 / 0 / 500	5158 / 0 / 254
Goodness-of-fit on F^2	1.041	1.068
Final R indices [I>2sigma(I)]	R1 = 0.0361, wR2 = 0.0998	R1 = 0.0302, wR2 = 0.0482
R indices (all data)	R1 = 0.0468, wR2 = 0.1041	R1 = 0.0477, wR2 = 0.0515
Largest diff. peak and hole	0.860 and -0.612 e.Å^{-3}	0.494 and -0.551 e.Å^{-3}

[a] $R1 = \Sigma||Fo| - |Fc||/\Sigma|Fo|$. [b] $wR2 = \{[\Sigma w(Fo^2 - Fc^2)^2]/[\Sigma w(Fo^2)^2]\}^{1/2}$.

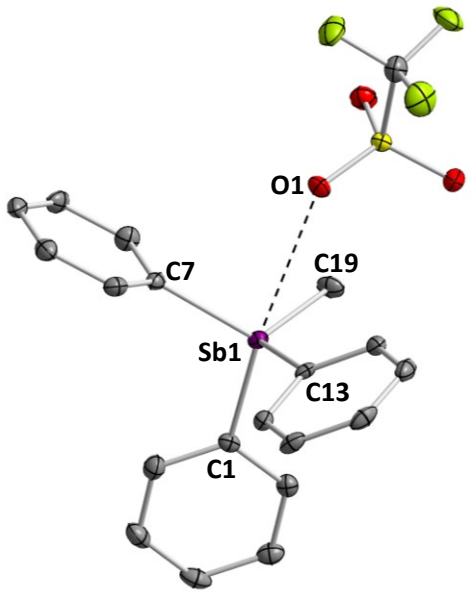

Figure 87. Crystal structure of [Ph_3MeSb][OTf]. Thermal ellipsoids are drawn at the 50 % probability level. The hydrogen atoms are omitted for clarity. Selected bond lengths (Å) and angles (deg): Sb1-O1: 3.1518(16), Sb1-C1 2.108(2), Sb1-C7 2.091(2), Sb1-C13 2.096(2), Sb1-C19 2.095(2), Sb2-C30 2.129(3), O1-Sb1-C1 173.28(7), C7-Sb1-C13 111.47(9), Cb7-Sb2-C19 112.42(9), C13-Sb1-C19 116.97(9).

Synthesis of [42][OTf]$_2$. MeOTf (0.21 mL, 1.9 × 10^{-3} mol) was added to a solution of *o*-phenylene-bis(diphenylstibine) (302 mg, 4.8 × 10^{-4} mol) in toluene (3 mL). The mixture was sealed under N_2 atmosphere in a 25 mL Schlenk tube and heated for 90 ºC for 12 h, after which a white precipitate formed. The solid was filtered, washed with Et_2O (3 × 5 mL), and dried *in vacuo* to afford [**42**][OTf]$_2$ in 62 % yield (285 mg, 3.0 × 10^{-4} mol). Single crystals of [**42**][OTf]$_2$ were obtained as colorless blocks by diffusing Et_2O into a CH_2Cl_2 solution. ^{1}H NMR (399.508 MHz, CD_3CN, 25 ºC, TMS): δ 7.88-7.84 (m; 4H; C_6H_4), 7.71 (pseudo t; ^3J (H,H) = 6.0 Hz, 4H; *p-Ph*), 7.56 (pseudo t; ^3J (H,H) = 6.4 Hz, 8H; *o-Ph*), 7.49 (pseudo d; ^3J (H,H) = 6.4 Hz, 8H; *m-Ph*), 2.14 (s; 6H; Sb-C*H3*). ^{13}C{^{1}H}NMR (125.60 MHz, CD_3CN, 25 ºC, TMS): δ 141.38 (*o*-phenylene),.136.61 (*o*-

Ph), 134.91 (*p*-Ph), 134.91 (quat. Ph), 134.81 (*o*-phenylene), 134.05 (quat. *o*-phenylene), 131.93 (*o*-Ph), 124.46 (*o*-phenylene), 120.8 (q; $CF_3SO_3^-$), 6.43 (Sb-CH_3). Elemental analysis calculated (%) for $C_{34}H_{30}F_6O_6S_2Sb_2$: C 42.71, H 3.16; found: C 42.85, H 3.20. Both ^1H and $^{13}C\{^1H\}$ NMR spectra are shown in Figure 88.

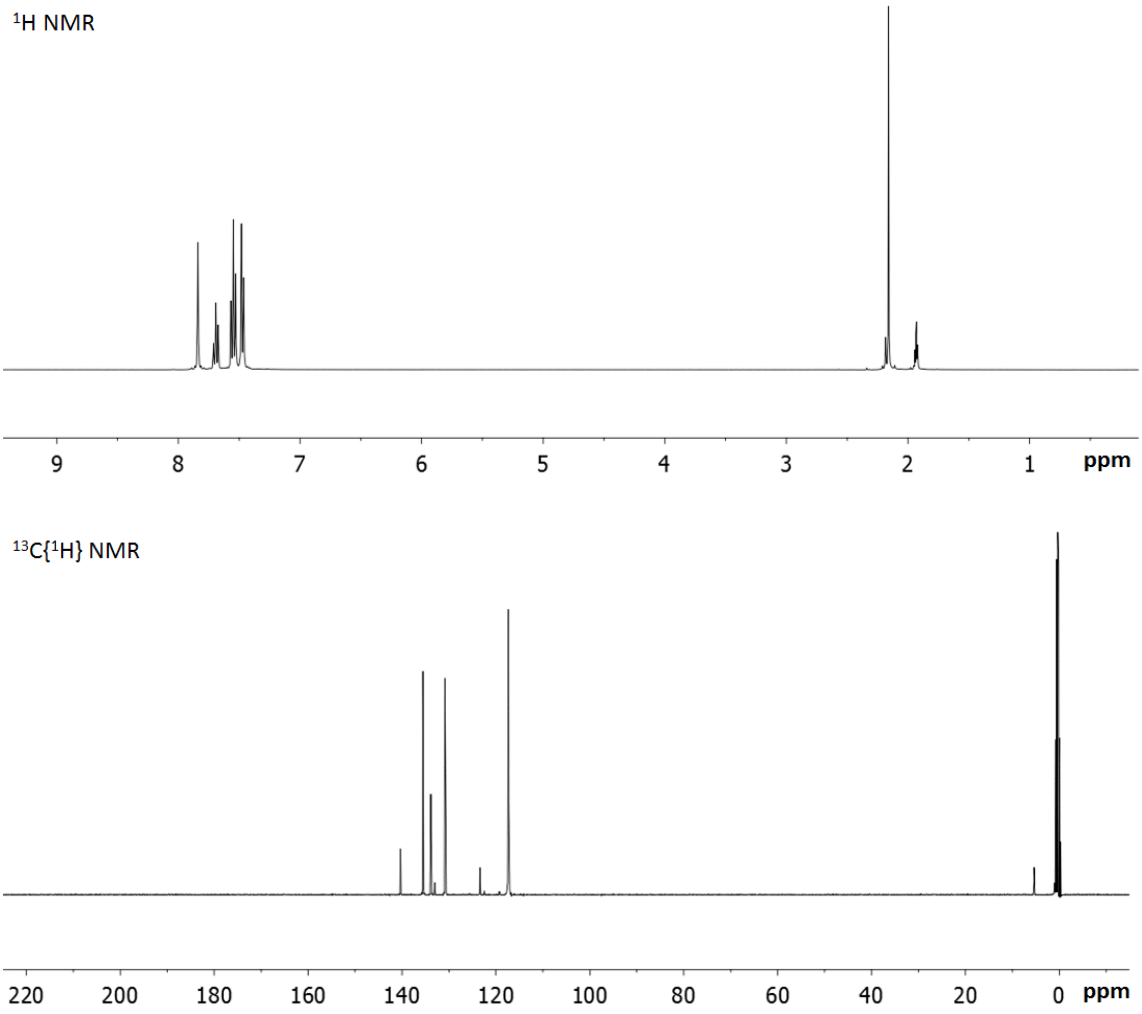

Figure 88. ^1H and $^{13}C\{^1H\}$ NMR spectra of [**42**][OTf]$_2$ in CD_3CN.

Synthesis of [42][BF_4]$_2$. [Me_3O][BF_4] (49 mg, 3.3 × 10^{-4} mol) was added to a solution of *o*-phenylene-bis(diphenylstibine) (101 mg, 1.6 × 10^{-4} mol) in a mixture of 1,2-dichloroethane (1 mL) and toluene (2 mL). The mixture was sealed in a 25 mL Schlenk tube under N_2 atmosphere and heated for 90 ºC for 12 h, after which a white precipitate formed. The solid was filtered, washed with Et_2O (3 × 5 mL), and dried *in vacuo* to afford [**42**][BF_4]$_2$ in 48 % yield (64 mg, 7.7 × 10^{-5} mol). Single crystals of [**42**-OH_2][BF_4]$_2$ were obtained in low yield as colorless blocks by layering pentane on a saturated CH_2Cl_2 solution of [**42**][BF_4]$_2$. ^{1}H NMR (399.508 MHz, CD_2Cl_2, 25 ºC, TMS): δ 7.74 (broad s; 4H), 7.66 (m; 4H), 7.55 (pseudo t; ^3J (H,H) = 6.0 Hz, 8H; *o-Ph*), 7.47 (pseudo d; ^3J (H,H) = 6.0 Hz, 8H; *m-Ph*), 2.16 (s; 6H; Sb-C*H*$_3$). ^{13}C{^{1}H} NMR (125.60 MHz, CD_2Cl_2, 25 ºC, TMS): δ 139.55 (*o*-phenylene), 134.89 (*o*-Ph), 133.21 (*o*-phenylene), 132.86 (*p*-Ph), 130.56 (*m*-Ph), 30.60 (Sb-*C*H$_3$). The Sb-bound quaternary carbon could not be detected. Elemental analysis calculated (%) for $C_{32}H_{30}B_2F_8Sb_2$: C 42.21, H 3.64; found: C 42.44, H 3.58. This elemental analysis was obtained on the bulk product. It points to the absence of water in bulk [**42**][BF4]$_2$. This elemental analysis was obtained on the bulk product. It points to the absence of water in bulk [**42**][BF_4]$_2$. Both ^{1}H and ^{13}C{^{1}H} NMR spectra are shown in Figure 89.

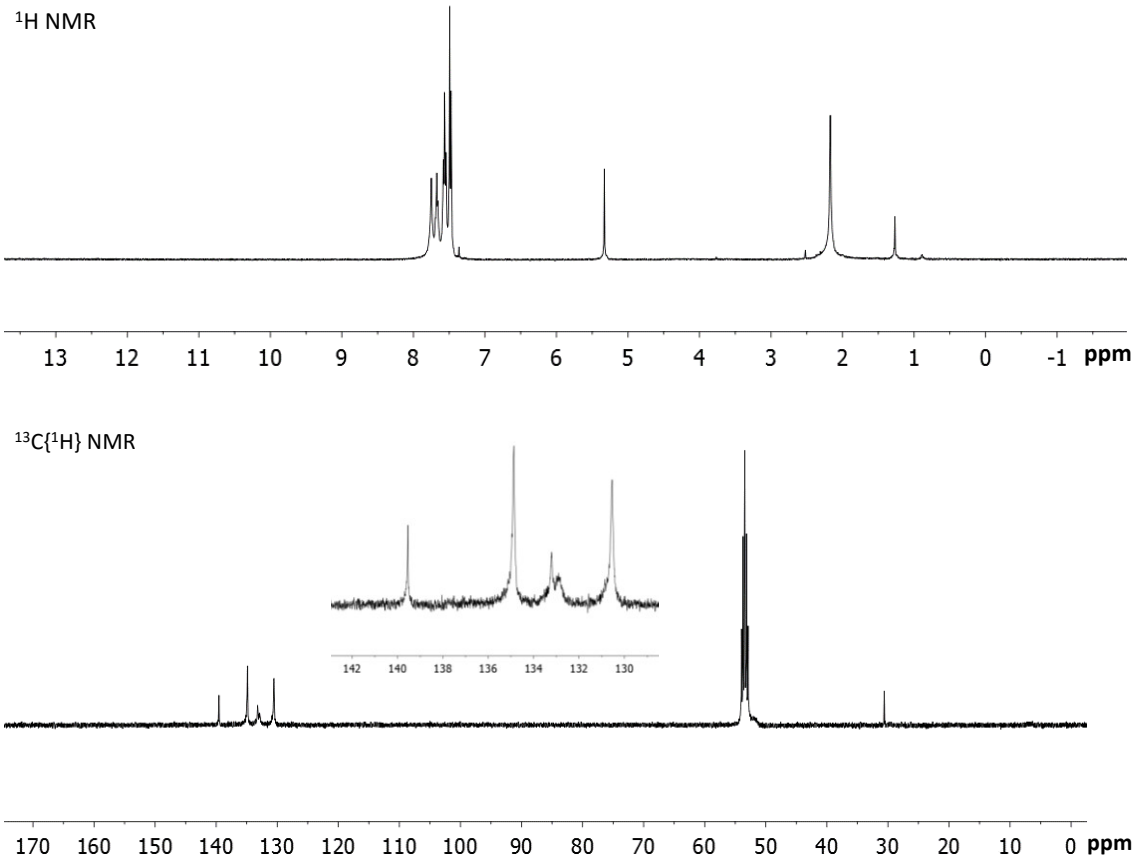

Figure 89. ^{1}H and ^{13}C{^{1}H} NMR spectra of [**42**][BF_4]$_2$ in CD_2Cl_2. The aryl region in the ^{13}C{^{1}H} NMR spectrum is magnified.

Spectrophotometric DMF titration of [42][OTf]$_2$ in CH_2Cl_2. A CH_2Cl_2 solution of DMF was added incrementally to a CH_2Cl_2 solution of [**42**][OTf]$_2$ (3.6×10^{-5} M) at room temperature and the reaction was monitored by UV-vis spectroscopy. The absorption spectrum remained unchanged upon addition of 20 equivalents of DMF, indicating that DMF does not coordinate to the Lewis acidic antimony center under these conditions. This experiment was repeated with [**42**][BF_4]$_2$, the spectrum of which was unperturbed by addition of 20 equivalents of DMF. This was also confirmed by recording

the ^{1}H NMR spectrum of [**42**-μ_2-DMF][OTf]$_2$ in CD_3CN. The ^{1}H NMR data show that the adduct is fully dissociated in solution. The resonances of free DMF are observed and the resonances of [**42**]$^{2+}$ are identical to those of [**42**][OTf]$_2$ in CD_3CN.

Synthesis of [42-μ_2-DMF][OTf]$_2$. A 32 mg sample of [**42**][OTf]$_2$ (3.3×10^{-5} mol) was placed in a vial and dissolved in 0.5 mL of DMF. Et_2O was slowly diffused into this mixture leading to the crystallization of [**42**-μ_2-DMF][OTf]$_2$ in 64 % yield (22 mg, 2.1×10^{-5} mol). ^{1}H NMR (399.508 MHz, CD_3CN, 25 ^{o}C, TMS): δ 7.89 (broad; 1H; C(O)*H*), 7.88-7.84 (m; 4H; C_6H_4), 7.71 (pseudo t; ^{3}J (H,H) = 6.0 Hz, 4H; *p-Ph*), 7.56 (pseudo t; ^{3}J (H,H) = 6.4 Hz, 8H; *o-Ph*), 7.49 (pseudo d; ^{3}J (H,H) = 6.4 Hz, 8H; *m-Ph*), 2.88 (s; 3H; DMF-CH_3), 2.76 (s; 3H; DMF-CH_3), 2.14 (s; 6H; Sb-CH_3). Elemental analysis calculated (%) for $C_{35}H_{37}F_6NO_7S_2Sb_2$: C 43.17, H 3.62, N 1.36; found: C 43.22, H 3.55, N 1.38.

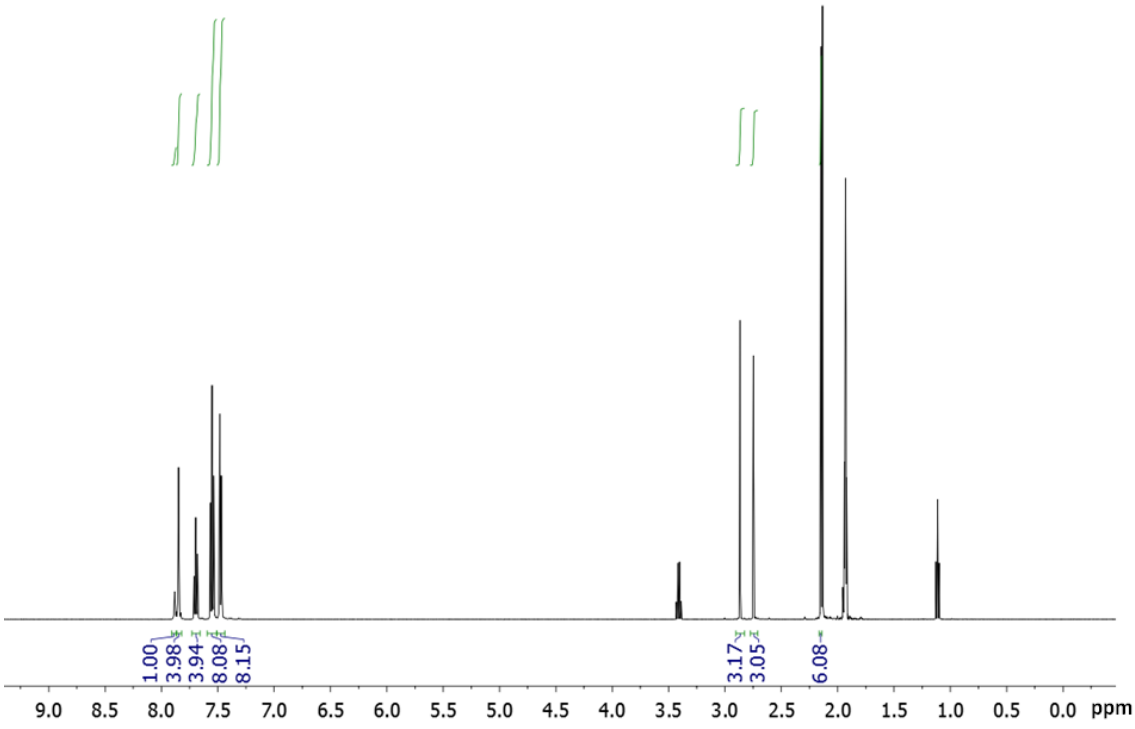

Figure 90. ^{1}H NMR spectrum of [**42**-μ_2-DMF][OTf]$_2$ in CD_3CN.

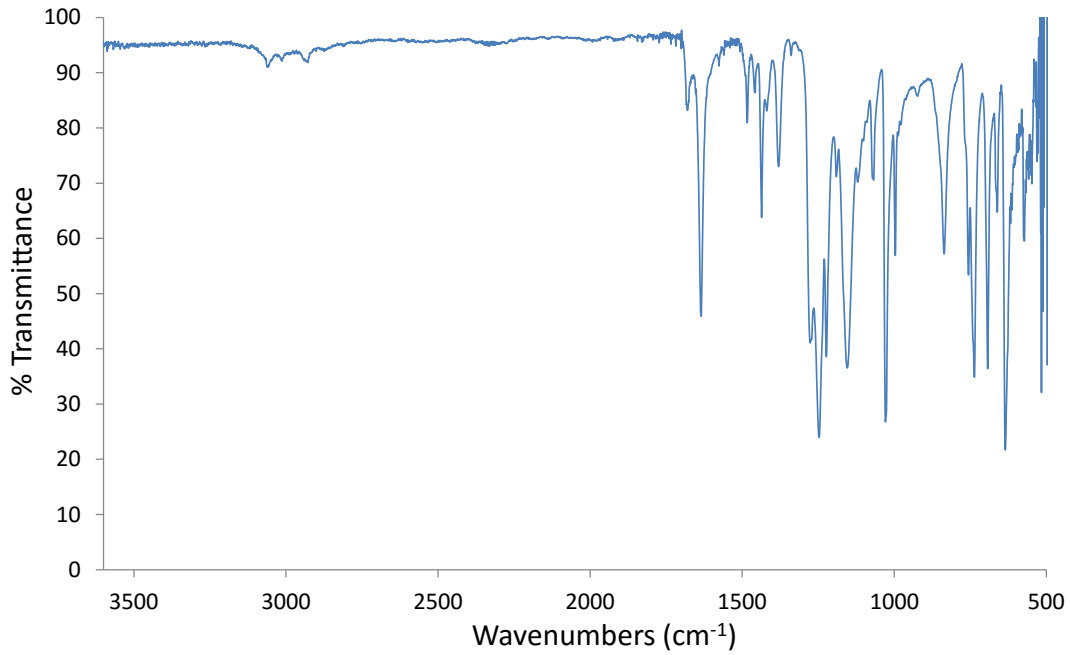

Figure 91. Solid state IR spectrum of [**42**-μ_2-DMF][OTf]$_2$.

Gutmann-Beckett method for assessing Lewis acidities of [42][OTf]$_2$, [42][BF$_4$]$_2$, [Ph$_3$MeSb][OTf], and [42][BF$_4$]. Excess Lewis acid (4 eq. of [**42**][OTf]$_2$, [**42**][BF$_4$]$_2$ or 8 eq. of [Ph$_3$MeSb][OTf], [Ph$_3$MeSb][BF$_4$]) was combined with Et$_3$PO (1 eq.) in CH_2Cl_2. All spectra were recorded at ambient temperature and referenced against free Et$_3$PO at 51.0 ppm.

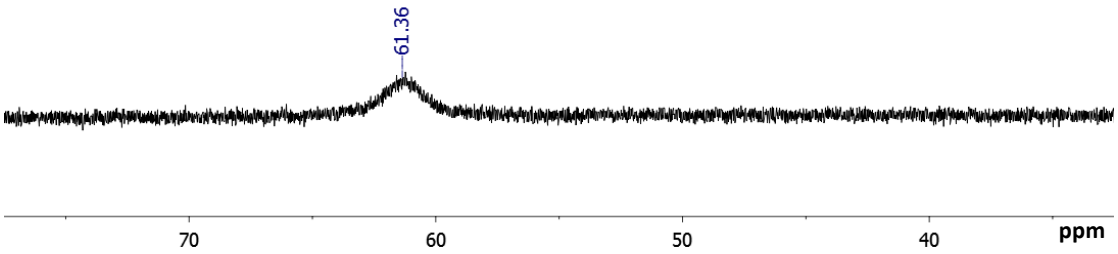

Figure 92. ^{31}P NMR spectrum of [**42**][OTf]$_2$ (28.5 mg, 3.0×10^{-5} mol, 4 eq) and Et$_3$PO (1 mg, 7.5×10^{-5} mol, 1 eq) in CH_2Cl_2 (1 mL).

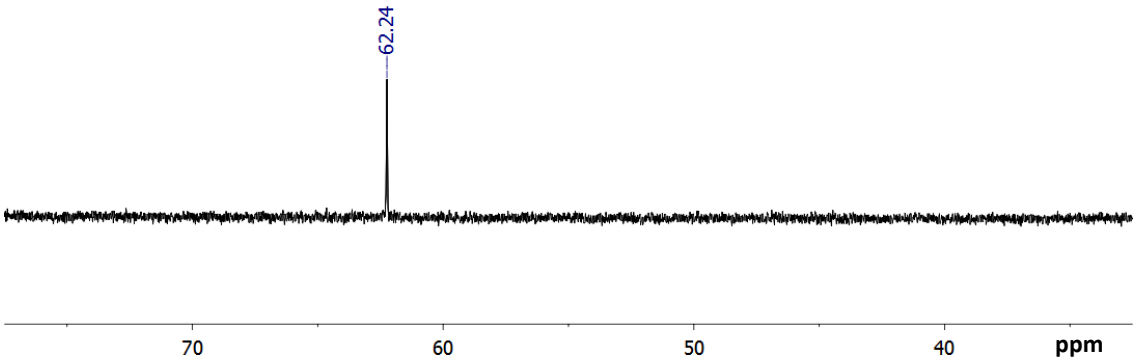

Figure 93. ^{31}P NMR spectrum of [**42**][BF$_4$]$_2$ (25.0 mg, 3.0×10^{-5} mol, 4 eq) and Et$_3$PO (1 mg, 7.5×10^{-5} mol, 1 eq) in CH_2Cl_2 (1 mL).

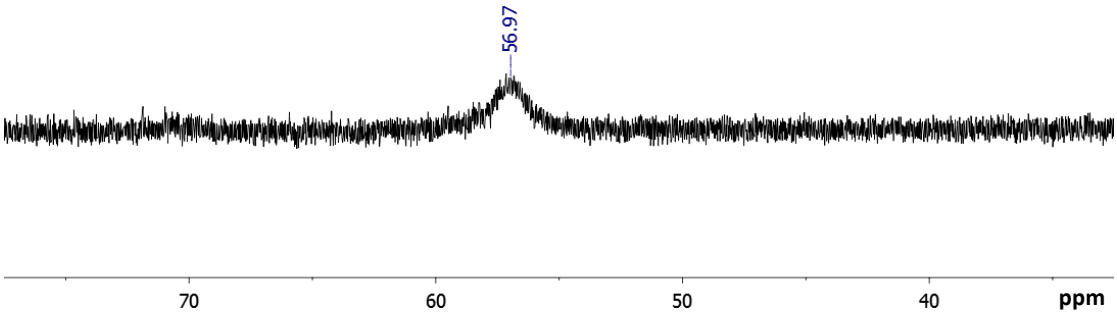

Figure 94. ^{31}P NMR spectrum of $[Ph_3MeSb][OTf]$ (30.8 mg, 6.0×10^{-5} mol, 8 eq) and Et_3PO (1 mg, 7.5×10^{-5} mol, 1 eq) in CH_2Cl_2 (1 mL).

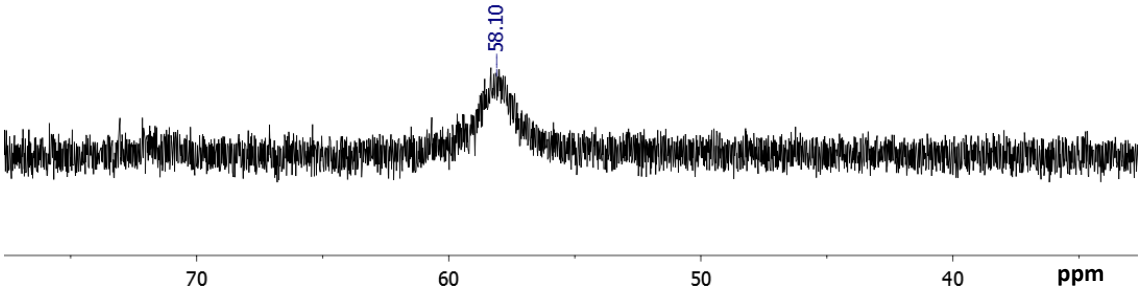

Figure 95. ^{31}P NMR spectrum of $[Ph_3MeSb][BF_4]$ (27.3 mg, 6.0×10^{-5} mol, 8 eq) and Et_3PO (1 mg, 7.5×10^{-5} mol, 1 eq) in CH_2Cl_2 (1 mL).

Hydrosilylation reactions: In a glovebox, an NMR tube was charged with benzaldehyde (0.023 mL, 2.0×10^{-4} mol), triethylsilane (0.064 mL, 4.0×10^{-4} mol), hexamethylbenzene (1.8 mg, 1.1×10^{-5} mol) and the corresponding stibonium salts (1.5 mol % [**42**][OTf]$_2$, 1.5 mol % [**42**][BF_4]$_2$, 3.0 mol % $[Ph_3MeSb][OTf]$, 3.0 mol % $[Ph_3MeSb][BF_4]$ with all concentrations based on benzaldehyde) in 1 mL of dry $CDCl_3$. After recording an initial ^1H NMR spectrum, the NMR samples were kept at room temperature and monitored periodically. For 4-fluorobenzaldehyde (21 μL, 0.2 mmol) with [**42**][BF_4]$_2$ (1.5 mol %) as a catalyst, no reaction was observed at room temperature.

Placing the NMR tube in an oil bath heated to 60 °C resulted in a conversion of 33 % after 8 h and >95% after 22 h (Figure 98 and Figure 99).

Synthesis and isolation of (benzyloxy)triethylsilane. Triethylsilane (0.319 mL, 2.0×10^{-3} mol), hexamethylbenzene (9.0 mg, 5.6×10^{-5} mol), and [**42**][BF_4]$_2$ (12.5 mg, 1.5×10^{-5} mol; 1.5 mol %) were mixed in 4 mL of dry $CHCl_3$ and the reaction mixture was stirred at ambient temperature. After 12 h, the reaction mixture was directly transferred to a short silica plug and chromatographed using 99:1 vol. hexanes/Et_3N mixture as an eluent. The solvent was removed *in vacuo* to afford the pure product as a colorless oil in 88 % isolated yield (195.7 mg, 8.8×10^{-4} mol). The ^{1}H NMR spectrum of the product agrees with that previously reported.[284] ^{1}H NMR (399.508 MHz, $CDCl_3$): δ 7.41-7.32 (m; 4H; *o*- and *m-Ph*), 7.28-7.25 (m; 1H; *p-Ph*), 4.70 (s; 2H; C*H*$_2$), 0.97 (t; ^3J (H,H) = 8.0 Hz, 9H; C*H*$_3$CH$_2$Si,), 0.68 (q; ^3J (H,H) = 8.0 Hz, 6H; CH$_3$C*H*$_2$Si).

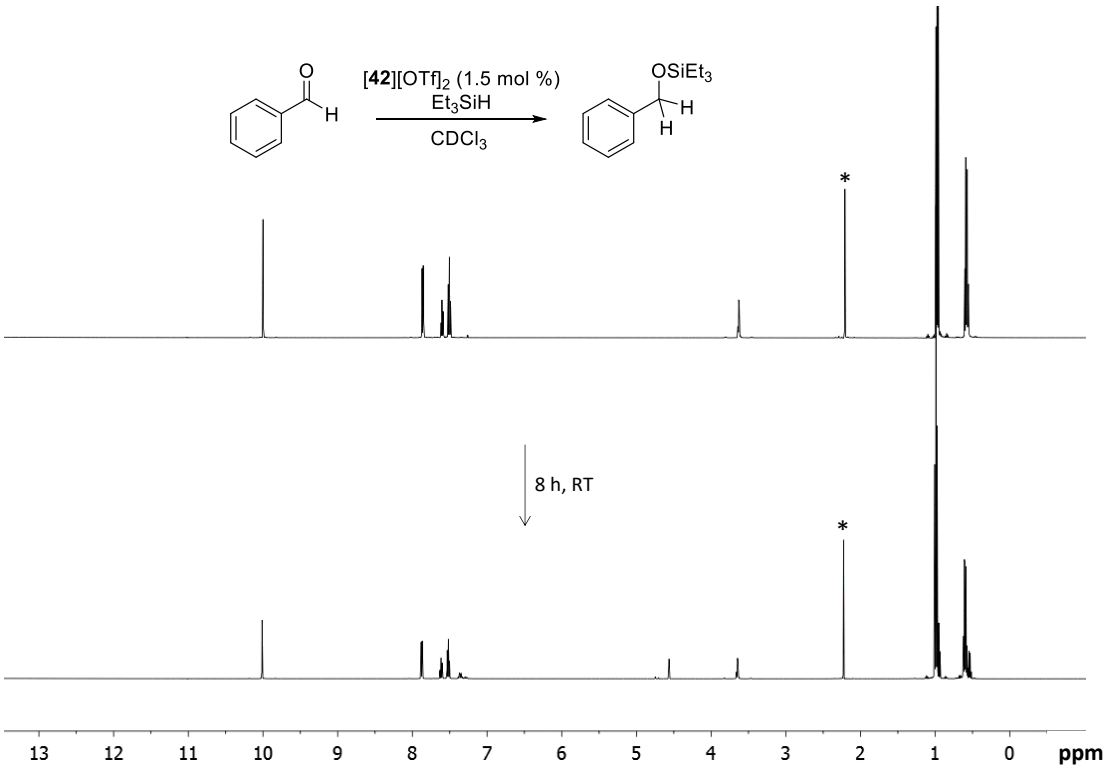

Figure 96. ^{1}H NMR spectra for the hydrosilylation of benzaldehyde with triethylsilane in the presence of 1.5 mol % of [**42**][OTf]$_2$ (2.9 mg, 3×10^{-6} mol) in $CDCl_3$. Resonance marked as "*" is hexamethylbenzene used as an internal standard.

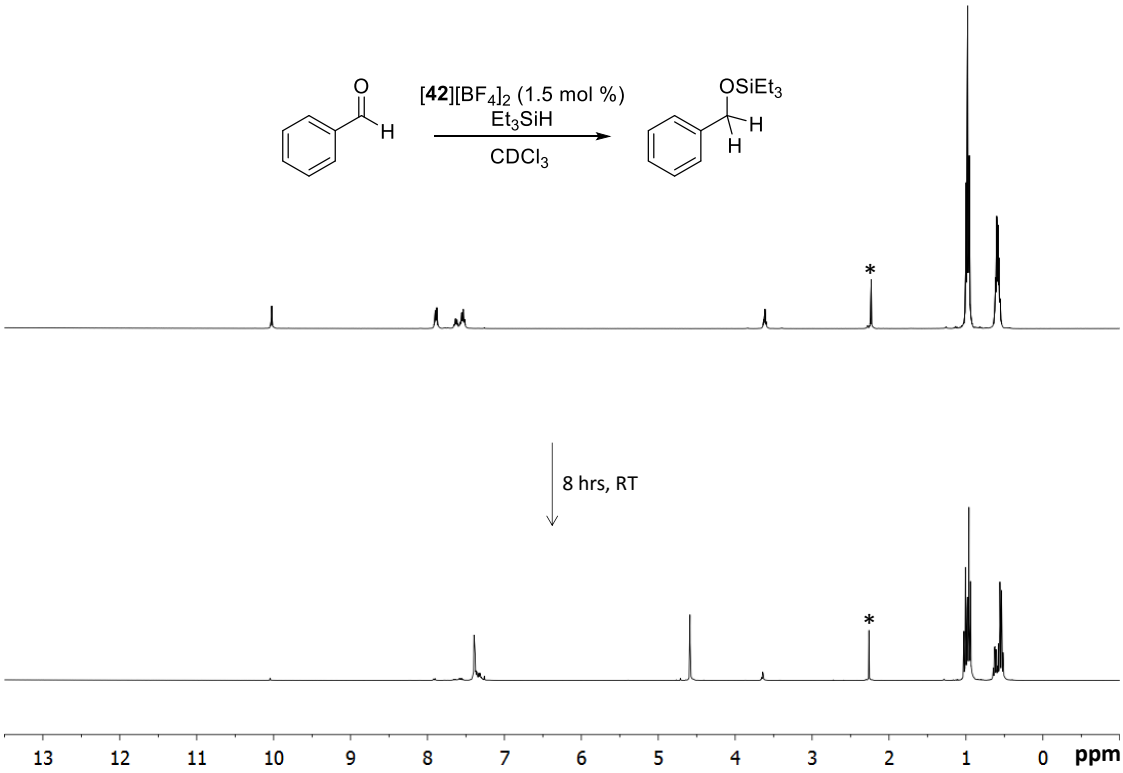

Figure 97. ^{1}H NMR spectra for the hydrosilylation of benzaldehyde with triethylsilane in the presence of 1.5 mol % of [**42**][BF_4]$_2$ (2.5 mg, 3×10^{-6} mol) in $CDCl_3$. Resonance marked as "*" is hexamethylbenzene used as an internal standard.

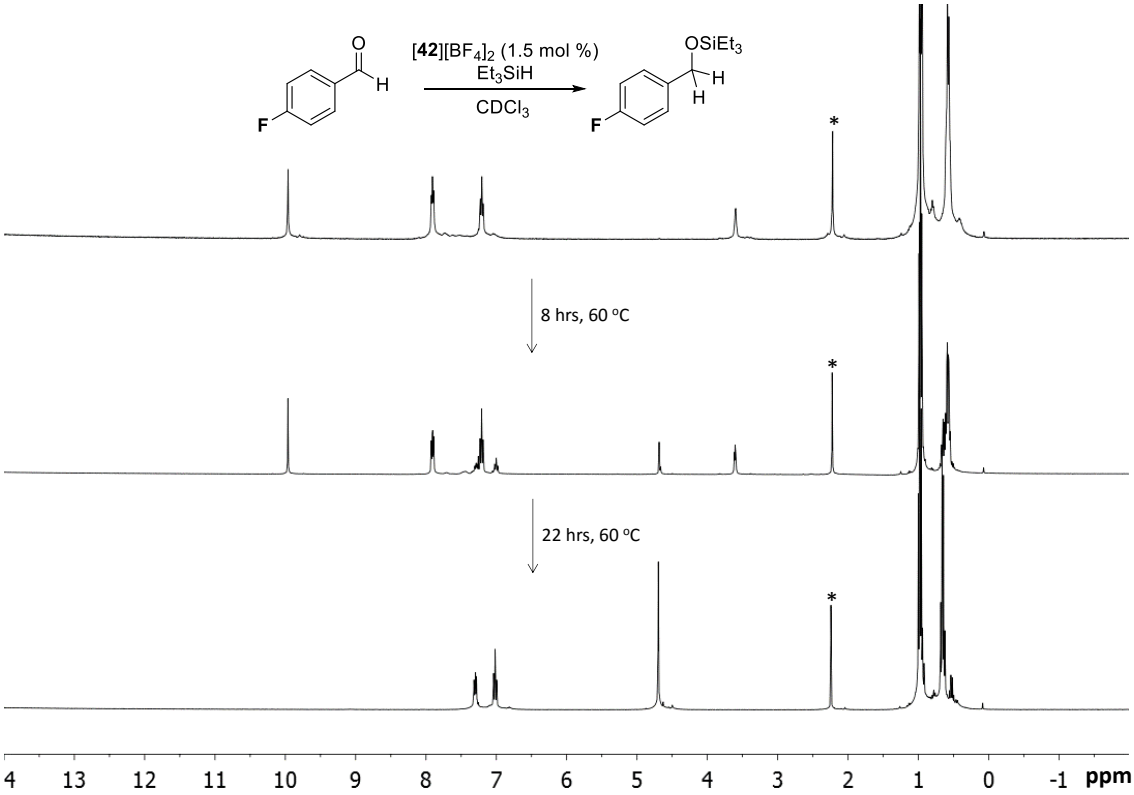

Figure 98. ^{1}H NMR spectra for the hydrosilylation of 4-fluorobenzaldehyde with triethylsilane in the presence of 1.5 mol % of [**42**][BF_4]$_2$ (2.5 mg, 3×10^{-6} mol) in $CDCl_3$ at 60 °C measured on a 400 MHz Varian NMR Spectrometer. Resonance marked as "*" is hexamethylbenzene used as an internal standard.

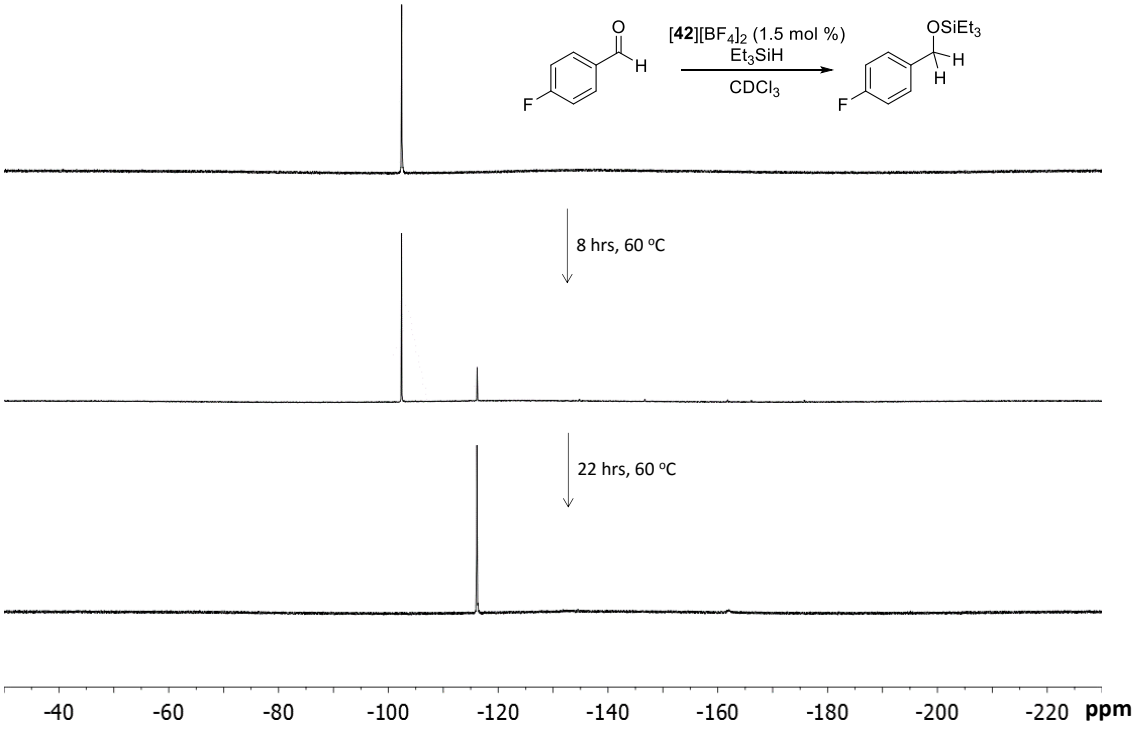

Figure 99. ^{19}F NMR spectra for the hydrosilylation of 4-fluorobenzaldehyde with triethylsilane in the presence of 1.5 mol % of [**42**][BF_4]$_2$ (2.5 mg, 3×10^{-6} mol) in $CDCl_3$ at 60 °C measured on a 400 MHz Varian NMR Spectrometer.

CHAPTER VI

SYNTHESIS AND CHARACTERIZATION OF BIFUNCTIONAL DIORGANOANTIMONY(V) COMPOUNDS WITH VARIOUS ANTIMONY-ANTIMONY SEPARATIONS

6.1 Introduction

Bifunctional Lewis acids are typically more electrophilic than their monofunctional counterparts because of the lower LUMO energy level. Depending on the proximity of the two Lewis acidic centers, the stability of Lewis adduct could also improve via chelation effect. For instance, both phosphonium boranes [*o*-**23**]$^+$ and [*p*-**23**]$^+$ react with fluoride ion to afford the corresponding phosphonium fluoroborates; however, the *ortho* isomer forms a B-F→P chelate motif, giving rise to a greater stability of the fluoride adduct than its *para* isomer (Figure 20).[113]

As part of our ongoing interest in organoantimony(V) chemistry, we decided to investigate the Lewis acidity of bifunctional distiboranes and distiboniums bearing various Sb-Sb separations. In Chapter III, we explicitly showed that 9,9-dimethylxanthenyl distiborane **36** captures and chelates fluoride in 9.5/0.5 (v/v) water/THF mixture while the monofunctional analog **10** has no affinity towards fluoride under these conditions (Figure 55). Furthermore, in chapter V, we introduced an *ortho*-phenylene-based distibonium dication [**42**]$^{2+}$ that chelates electron-rich carbonyl substrate such as DMF and effectively catalyzes hydrosilylation of benzaldehyde. Encouraged by these results, we became interested to study the electrophilic properties of other bis-organoantimony(V) species

bearing different Sb-Sb distances. In this chapter, the synthesis and characterization of bis-organoantimony compounds of naphthalene, ferrocene, dibenzofuran, and *ortho*-phenylene derivatives will be discussed.

6.2 Synthesis of naphthalenyl distibine and it oxidation products.

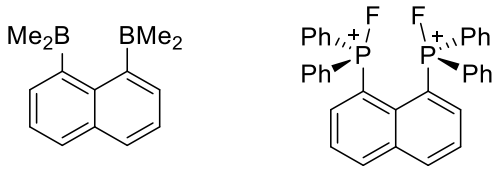

19 [**40**]$^{2+}$

Figure 100. Bifunctional Lewis acids: diborane **19** and bisfluorophosphonium [**40**]$^{2+}$.

Naphthalene is commonly used platform to prepare dinuclear compounds, especially for diborane species. One of the original naphthalene-based bidentate Lewis acids, 1,8-naphthalenyl diborane **19**, is known to chelate small anions such as hydride, fluoride, and hydroxide ions.[104] This diborane can be conveniently prepared in one-pot by reacting 2 equivalents of *n*BuLi with 1,8-dibromonaphthalene to generate the corresponding dilithium salt and subsequently quenching it dimethyl borinic acid.[105] While a variety of naphthalene-based bifunctional group 13 and group 14 acceptors have been reported, group 15 Lewis acid analogs are less common. In fact, it was not until recent when Stephan reported the synthesis and the catalytic behavior of bis(fluorophosphonium) dication.[266] Synthetically, treatment of 1,8-bis(diphosphino)naphthalene with 2 equivalents of XeF_2 affords the corresponding bis-

difluorophosphorane and subsequent addition of 2 equivalents of [Et_3Si-H-$SiEt_3$][BAr^F_4] leads to the formation of bis(fluorophosphonium) dication [**40**]$^{2+}$ as a BAr^F_4 salt. Although there is no clear evidence that the two fluorophosphonium subunits functions cooperatively, [**40**]$^{2+}$ is an excellent catalyst for organic transformations including Friedel Crafts-type dimerization, hydrosilylation, dehydrocoupling, hydrodeoxygenation, and hydrodefluorination.[266]

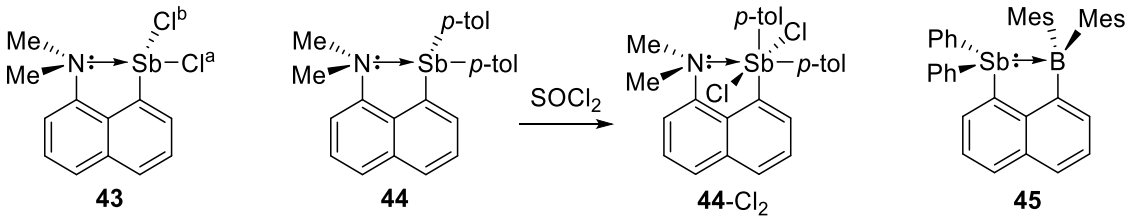

Figure 101. *Peri*-substituted antimony species **43**, **44**, **44**-Cl_2, and **45**.

There has been no report on *peri*-substituted bis-antimony(V) species up to date; however, a few examples show that antimony species in both +III and +V oxidation state can behave as electron acceptors. Norman and Cowley reported amino-stibine **43** and found that the amino group strongly interacts with the antimony(III) center *trans* to a chloride ligand (Sb-N = 2.460(4) Å).[290] It is noteworthy that the distance between the antimony center and the chloride *trans* to the amino group (Sb-Cl^a = 2.500(1) Å) is longer than that of the other Sb-Cl bond (Sb-Cl^b = 2.3821(4) Å), strongly suggesting that the presence of a donor-acceptor interaction from the lone pair of electrons of the nitrogen into the Sb-Cl^a σ* orbital (labels on Cl shown in Figure 101). Yamaguchi later reported amino-stibine **44** and showed that triarylstibine moieties are also mildly Lewis acidic. In

the crystal of **44**, the Sb-N distance is 2.831(6) Å which is well within the sum of the van der Waal's radii of the two element (Σ_{vdW}(Sb-N) = 3.8 Å). However, this separation is significantly longer than that of **43** (Sb-N = 2.460(4) Å). This illustrates that triarylstibines are weaker Lewis acceptors than arylantimony dihalides. The antimony(III) center of **44** can be oxidized with $SOCl_2$ to afford **44**-Cl_2. In the crystal of **44**-Cl_2, the Sb-N separation shortens to 2.658(4) Å, thus indicating that the N→Sb donor-acceptor interaction is also strengthened. Accordingly, the antimony center assumes an octahedral geometry as expected for a hexacoordinate antimony(V) species. Previously in our group, we reported boryl-stibino naphthalene **45** which the crystal structure revealed a Sb-B distance of 3.216 Å.[291] This separation is longer than the sum of the covalent radii (2.23 Å) but well within the sum of the van der Waal's radii of the two elements (4.0 Å). In order to better understand the nature of Sb→B interaction, the crystal structure of **45** was optimized using DFT methods and subsequently subjected to NBO analysis. The Sb-B separation of the DFT optimized structure of **45** (3.410 Å) is slightly longer than that of the crystal structure. Nonetheless, NBO analysis reveals a donor-acceptor interaction from the lone pair of electrons of antimony to the vacant p-orbital of boron which contributes to the stabilization energy of 8.65 kcal mol^{-1}. Because of this interaction, the lone pair of electrons associated with the Sb(III) center is no longer accessible and could not participate in further oxidation. With these in consideration, we becamse interested to investigate the oxidation property of 1,8-bis(diphenylstibino)naphthalene **46**.[292]

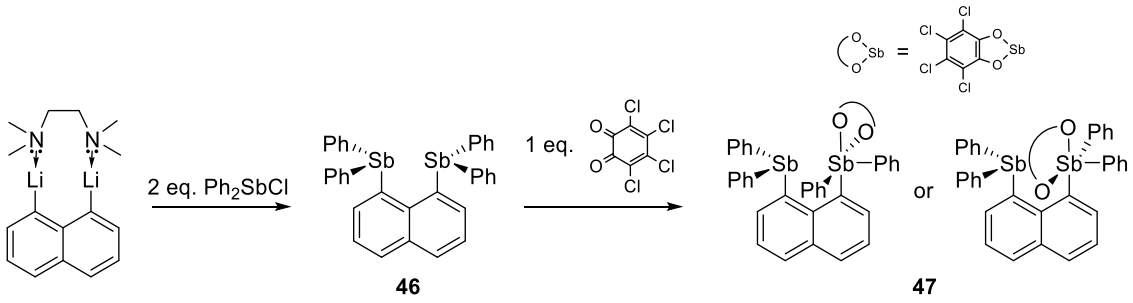

Figure 102. Synthesis of **46** and **47**.

The reported procedure for the preparation of distibine **46** uses metallic lithium for the dilithiation of 1,8-dibromonaphthalene.[292] We used a modified synthetic procedure instead by first isolating the 1,8-dilithionaphthalene tmeda salt and subsequently treating it with 2 equivalents of Ph_2SbCl at -78 ºC in THF to afford distibine **46**. The product formation was confirmed by ^1H NMR spectroscopy. With this compound in hand, we have screened the reaction of **46** with a series of oxidants including *o*-chloranil, Br_2, $CuBr_2$, and $PhICl_2$ to target the corresponding distiborane species.

Distibine **46** undergoes a clean two-electron oxidation upon reaction with 1 equivalent of *o*-chloranil to afford Sb(III)-Sb(V) compound **47** as a pale yellow solid in 92 % yield. In the ^1H NMR spectrum in $CDCl_3$, all of the resonances of the formerly symmetrical naphthalene backbone becomes inequivalent, indicating that only one of the two antimony centers has been oxidized. Single crystals of **47** were obtained as yellow blocks by diffusing pentane into a toluene solution. Elucidation of the structure by X-ray diffraction reveals a pair of enantiomers within the asymmetric unit (Figure 103). In both of the enantiomers, the Sb(III) atoms are positioned directly *trans* to a phenyl group ($\angle$(C17-Sb1-Sb2) = 172.81(5)º and $\angle$(C17-Sb1-Sb2) = 174.35(4)º), leading to distorted

octahedral geometries about the Sb(V) centers. Also, the average Sb-Sb separation of the enantiomers is 3.148 Å (Sb1-Sb2 = 3.0939(6) Å and Sb3-Sb4 = 3.2013(5) Å) which is well within the sum of the van der Waal's radii of two antimony atoms (Σ_{vdW}(Sb-Sb) = 4.4 Å).[237] These observations designate the presence of a donor-acceptor interaction involving the lone pair of electrons of Sb(III) as a donor and the Sb(V)-C_{Ph} σ* orbital as an acceptor. In order to further examine the Sb(III)→Sb(V) interaction, **47** has been computationally optimized using DFT methods (Gaussian 09 program, functional B3LYP, mixed basis set Sb cc-pVTZ-pp; Cl 6-311+g(d); C/H/O 6-31g(d)) and analyzed using the NBO methods (Figure 104). The Sb-Sb distance in the DFT optimized structure is 3.168 Å which is close to the average Sb-Sb separation found in the crystal structure. The NBO calculation confirms a donor-acceptor interaction from the lone pair of electrons of Sb(III) to the Sb(V)-C_{Ph} σ* orbital, contributing to a stabilization energy of 15.42 kcal mol^{-1}. Successive addition of another equivalent of *o*-chloranil to **47** did not lead to a formation of the corresponding distiborane species, thus indicating that the donor-acceptor interaction strongly engages the two antimony centers and prevents further oxidation.

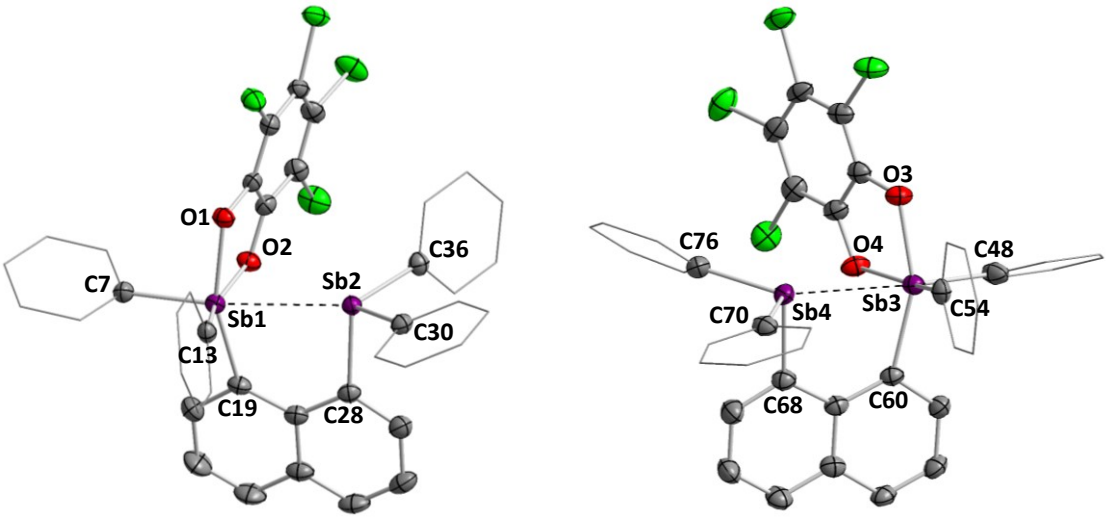

Figure 103. The crystal structures of both enantiomers of **47** found in the asymmetric unit. Thermal ellipsoids are drawn at the 50 % probability level. The hydrogen atoms and toluene molecules are omitted for clarity. Selected bond lengths (Å) and angles (deg): Sb1-Sb2 3.0939(6), Sb3-Sb4 3.2013(5), O1-Sb1-O2 78.76(7), C13-Sb1-O1 88.49(8), C13-Sb1-C19 102.20(10), C19-Sb1-O2 85.39(8), Sb2-Sb1-C7 172.81(7), O3-Sb3-O4 78.60(7), C54-Sb1-O3 89.32(9), C54-Sb3-C60 99.90(10), C60-Sb1-O4 85.01(8), Sb4-Sb3-C48 174.36(9).

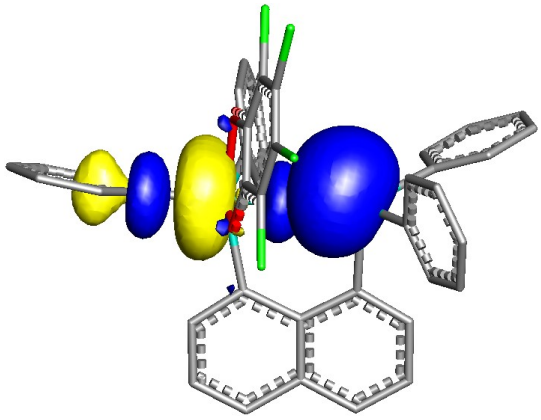

Figure 104. NBO plot (isovalue 0.05) showing representative lp(Sb) → σ*(Sb-C_{Ph}) donor–acceptor interaction in **47**.

Oxidation of **46** with halogen equivalents have also been studied. For these reactions, we initially proposed the formation of two possible products by 1) homolytic addition of halogens across the two antimony centers or 2) oxidative addition of halogens on one of the antimony centers, similar to that of **47** (Figure 105). The reaction of **46** with Br_2 leads to decomposition to an unknown product even at low temperature. This could be prevented by using a milder brominating agent such as $CuBr_2$. Indeed, the reaction of **46** with 2 equivalents of $CuBr_2$ proceeds cleanly to afford **48** in 88 % yield. Although single crystals suitable for X-ray diffraction analysis could not be obtained, the ^{1}H NMR spectrum features resemblance to that of **47**, hence indicating that only one of the antimony(III) centers has been oxidized. Likewise, **49** has been cleanly synthesized by the reaction of **46** with 1 equivalent of $PhICl_2$ at ambient temperature in 90 % yield. Again, the ^{1}H NMR spectrum displays analogous splitting pattern to those of **47** and **48**, thereby verifying that the oxidation only occurs on one of the two antimony centers. Stibino-stiborane **49** has also been subjected to X-ray diffraction analysis (Figure 106, left). The crystal structure of **49** reveals a Sb-Sb separation of 3.426(6) Å which is significantly longer compared to that of **49** (average Sb-Sb = 3.148 Å). The two chloride ligands are oriented *trans* to each other, analogous to triphenylantimony dihalide species. Furthermore, the τ-value of Sb1 is 0.32 (∠(Cl1-Sb1-Cl2) = 170.37(4)^o and ∠(C1-Sb1-C11) = 151.05(13)^o), indicating that Sb1 adopts a distorted square pyramidal geometry.

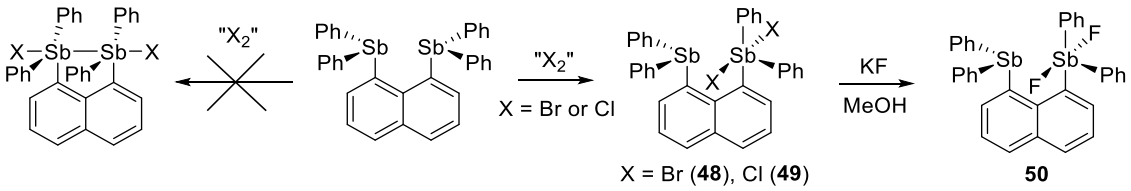

Figure 105. Synthesis of **48**, **49**, and **50**.

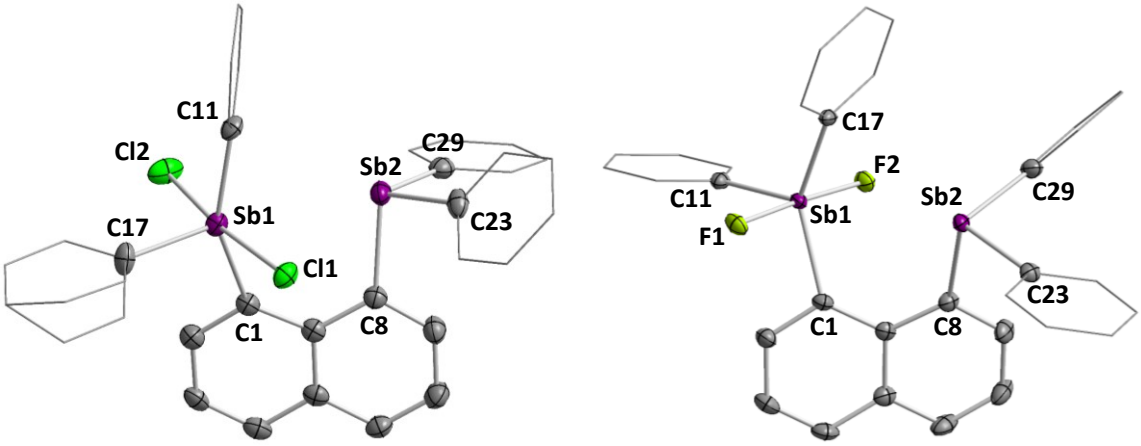

Figure 106. Crystal structures of **49** (left) and **50** (right). Thermal ellipsoids are drawn at the 50 % probability level. The hydrogen atoms are omitted for clarity. One of the phenyl rings of **49** is disordered and is depicted in the figure. Selected bond lengths (Å) and angles (deg) for **49**: Sb1-Sb2 3.426(6), Sb1-Cl1 2.4676(9), Sb1-Cl2 2.4701(9), Cl1-Sb1-Cl2 170.37(4), C1-Sb1-C11 151.05(13), Cl1-Sb1-C1 87.84(9), Cl1-Sb1-C11 90.04(10), Cl2-Sb1-C1 87.52(9), Cl2-Sb1-C11 89.94(10). Selected bond lengths (Å) and angles (deg) for **50**: Sb1-Sb2 3.542(9), Sb1-F1 1.9760(11), Sb1-F2 1.9776(11), F1-Sb1-F2 176.54(5), F1-Sb1-C1 88.92(6), F1-Sb1-C11 88.92(6), F2-Sb1-C1 88.41(6), F2-Sb1-C11 92.02(6), C1-Sb1-C11 107.90(7), C1-Sb1-C17 139.82(7), C11-Sb1-C17 112.28(7).

The chloride ligands of **49** can be easily exchanged with fluorides by the reaction of KF in MeOH/CH_2Cl_2 mixture to afford **50** in 91 % yield (Figure 105). The ^{19}F NMR resonance appears as a singlet at -136.2 ppm in $CDCl_3$, slightly more downfield from that of triphenylantimony difluoride (-153.2 ppm). Single crystals of **50** were obtained as colorless blocks by slowly diffusing pentane into a THF solution and have been subjected

to X-ray diffraction analysis (Figure 106, right). Interestingly, the Sb-Sb separation of **50** is 3.542(9) Å which is slightly longer than that of **49** (3.426(6) Å). The τ-value of Sb1 is 0.61 and the C1-Sb1-C7 angle is 139.82(7)°, thus indicating that the triarylantimony difluoride moiety is closer to a trigonal bipyramidal than a square pyramidal geometry.

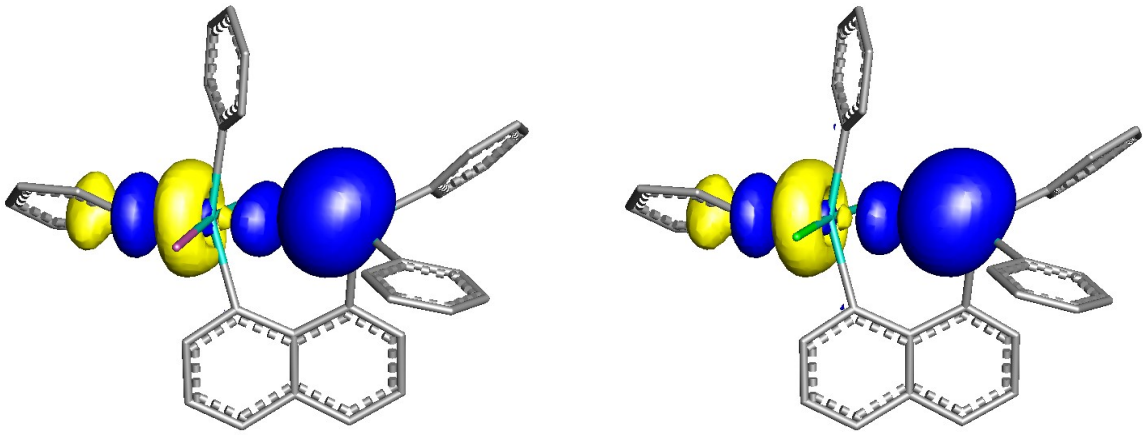

Figure 107. NBO plots (isovalue 0.05) showing representative lp(Sb) → σ*(Sb-C_{Ph}) donor–acceptor interactions in **48** (left) and **49** (right).

To confirm the presence of possible donor-acceptor interactions between the two antimony centers, the structures of **48**, **49** and **50** were optimized using DFT methods (Gaussian 09 program, functional B3LYP, mixed basis set Sb cc-pVTZ-pp; Br cc-pVTZ; Cl 6-311+g(d); F 6-31g(d'); C/H 6-31g(d)) and subsequently subjected to NBO analysis (Figure 107). In the optimized structures, the Sb-Sb distances of **48**, **49** and **50** are 3.420, 3.451, and 3.717 Å, respectively. Compared to the Sb-Sb separations measured in the crystal structures, these values are slightly shorter for **49** (3.426(6) Å in the crystal) and elongated for **50** (3.542(9) Å in the crystal). Nonetheless, the geometries about the

antimony(V) centers in the optimized structures are analogous to those of the crystal structures. NBO analysis reveals donor-acceptor interactions from the lone pair of electrons of Sb(III) to the empty Sb(V)-C_{Ph} σ* orbitals for both **48** and **49**. The estimated deletion energies corresponding to these interactions are 14.8 kcal mol^{-1} for **48** and 12.2 kcal mol^{-1} for **49**. In **50**, however, no significant donor-acceptor interaction between Sb(III) and Sb(V) centers was found.

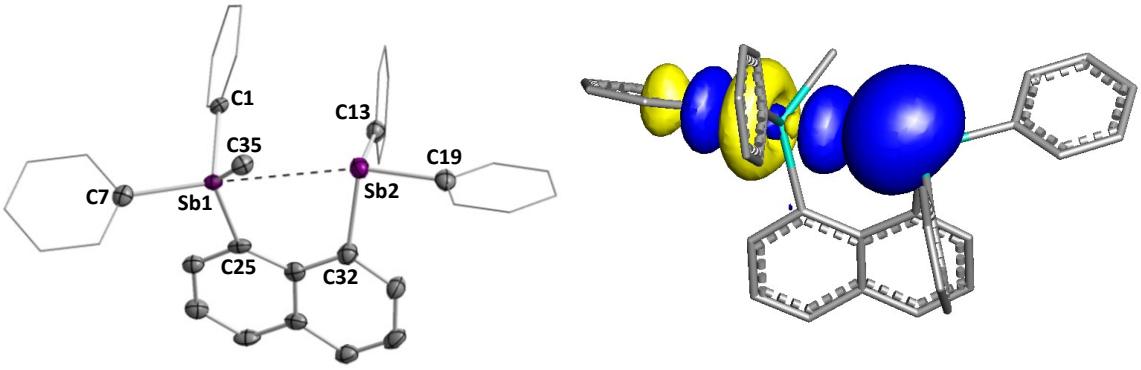

Figure 108. Left: crystal structure of [**51**][OTf]. Thermal ellipsoids are drawn at the 50 % probability level. The hydrogen atoms and toluene molecules are omitted for clarity. Selected bond lengths (Å) and angles (deg): Sb1-Sb2 3.4429(8), C7-Sb1-Sb2 176.55(13), C1-Sb1-C7 102.6(2), C1-Sb1-C35 107.4(2), C7-Sb1-C35 107.8(2), C13-Sb2-C19 100.2(2), C13-Sb2-C32 94.6(2), C19-Sb2-C32 96.3(2). Right: NBO plot (isovalue 0.05) showing representative lp(Sb) → σ*(Sb-C_{Ph}) donor–acceptor interaction.

Following a similar procedure to generate *ortho*-phenylene distibonium dication [**42**][$OTf]_2$, distibine **46** has been treated with 4 equivalents of MeOTf in 3 mL of toluene at 90 ºC for 24 h. Unlike [**42**][$OTf]_2$, no precipitation formed over time under these conditions or upon standing at ambient temperature. Instead, a white solid precipitated out of solution after the addition of 15 mL of Et_2O. The ^{1}H NMR spectrum of the white

powder showed a mixture of products which none of them could be identified. After numerous attempts, one of the many products crystallized and have been subjected to single crystal X-ray diffraction analysis. These crystals have been identified as a triflate salt of monostibonium cation [**51**][OTf] (Figure 108, left). In the solid state structure, Sb(III) and Sb(V) centers adopt a distorted trigonal pyramidal geometry and a tetrahedral geometry, respectively, with a Sb-Sb separation of 3.4429(8) Å. The C7-Sb1-Sb2 angle is 176.55(13)^{o} suggesting that the lone pair of electrons of the Sb(III) moiety is donating electron density to the vacant Sb(V)-C_{Ph} σ* orbital. To better understand the electronic structure, the crystal structure of [**51**]$^{+}$ was subjected to DFT calculations in the absence of a triflate anion (Gaussian 09 program, functional B3LYP, mixed basis set Sb cc-pVTZ-pp; C/H 6-31g(d)), followed by NBO analysis (Figure 108, right). As expected, theoretical calculations found a Sb(III)→Sb(V) interaction similar to those of **47**-**49**, associated with a deletion energy of 8.76 kcal mol^{-1}.

6.3 Ferrocene as a platform for bifunctional organoantimony(V) Lewis acids

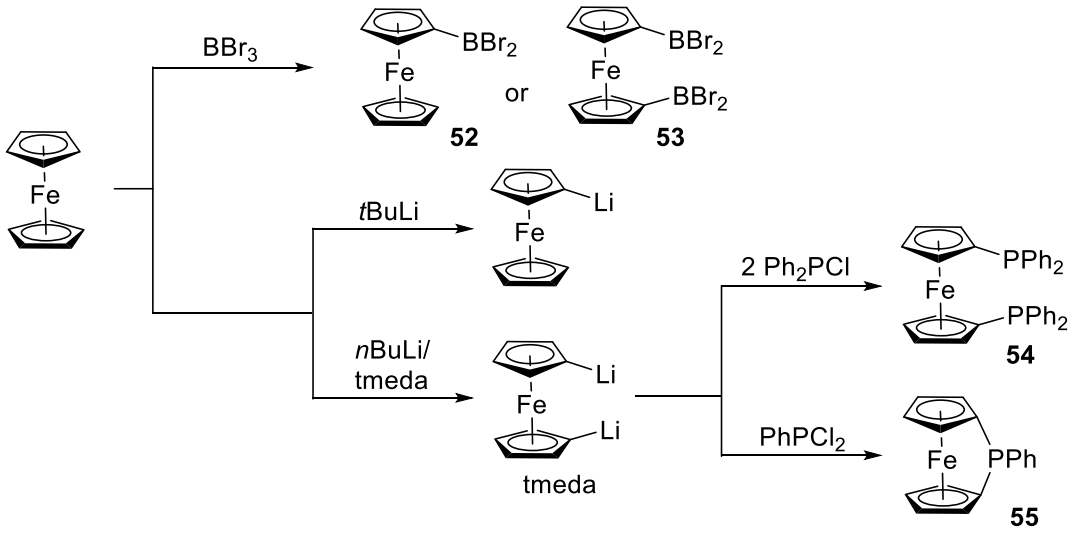

Figure 109. Synthesis of **52**, **53**, **54**, and **55**.

Ferrocene is one of the most popular organometallic compounds because of its remarkable air-stability and unique redox property. The cyclopentadienyl (Cp) rings freely rotate in solution with a low energy barrier along the $Cp_{centroid}$-Fe-$Cp_{centroid}$ axis. Ferrocene can be easily functionalized at the Cp rings and numerous related compounds have been reported in literature. For example, the ferrocene Cp rings can undergo electrophilic substitution of BBr_3 in CS_2 to give 1-dibromoborylferrocene (**52**) or 1,1'-bis(dibromoboryl)ferrocene (**53**) in a controlled manner.[293, 294] These species are precursors for the synthesis of ferrocenylboranes bearing diverse substituents such as pinacolates, catecholates, and amines.[293, 295, 296] Lithium salts of ferrocene can also be synthesized as nucleophiles for transmetallation reactions. The reaction of ferrocene with

*t*BuLi selectively affords the monolithioferrocene while *n*BuLi in addition of tmeda can promote a second lithiation to form 1,1'-dilithioferrocene.[297] The latter species has been readily employed for the preparation of dinuclear compounds such as 1,1'-bis(diphenylphosphino)ferrocene (**54**)[298-300] or bridging compounds such as PPh-bridged 1,1'-ferrocenophane (**55**).[301, 302]

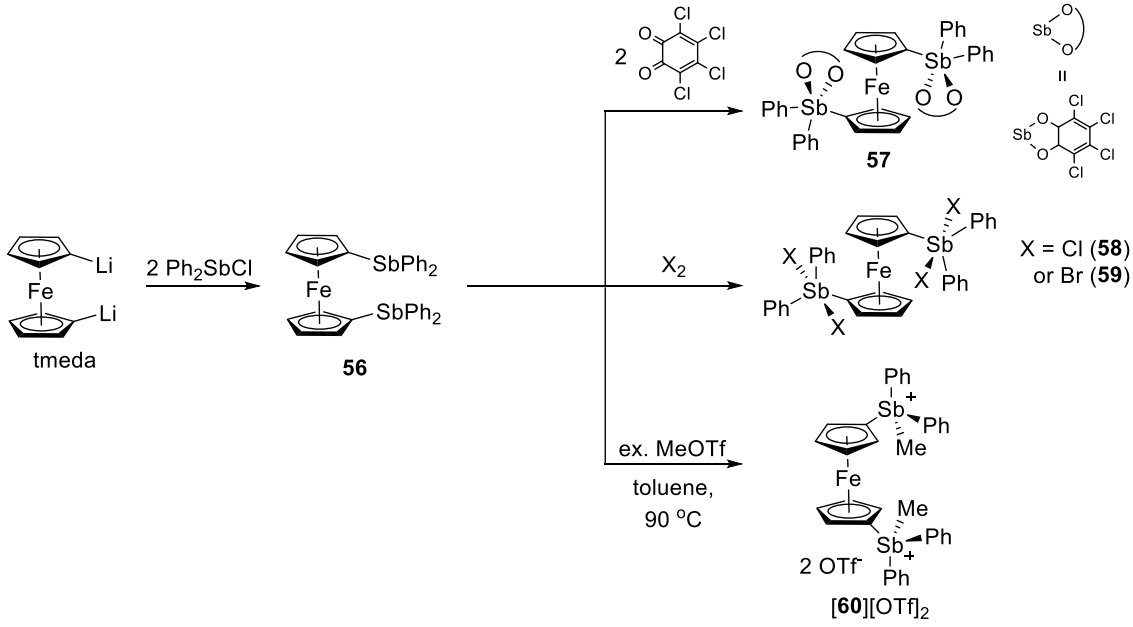

Figure 110. Synthesis of **56**, **57**, **58**, **59**, and [**60**][OTf]$_2$.

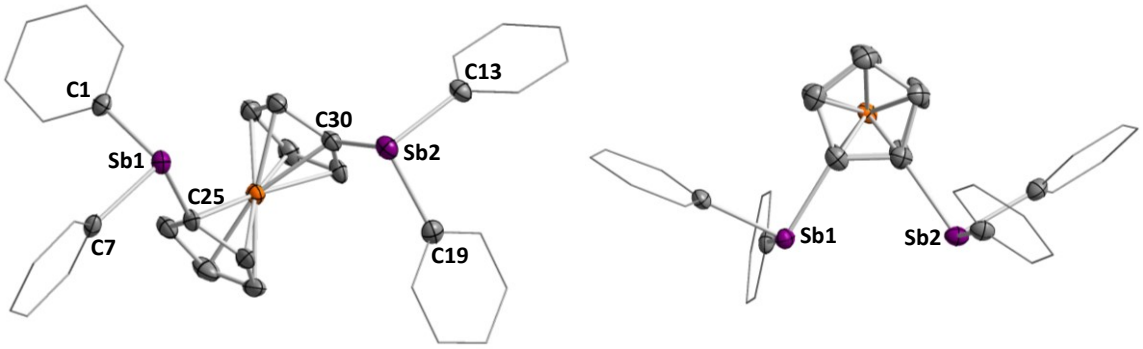

Figure 111. Left: crystal structure of **56**. Thermal ellipsoids are drawn at the 50 % probability level. The hydrogen atoms are omitted for clarity. Selected bond lengths (Å) and angles (deg): Sb1-Sb2 4.9758(12), C1-Sb1-C7 92.80(7), C1-Sb1-C25 95.46(7), C7-Sb1-C25 95.09(7), C13-Sb2-C19 98.53(7), C13-Sb2-C30 95.15(7), C19-Sb2-C30 96.81(7). Right: top view of the crystal structure of **56**.

Utilizing the synthetic strategy to access diphosphine **54**, we similarly prepared the distibine analog **56** as an air-stable orange solid. The ^{1}H NMR spectrum of **56** features cyclopentadienyl resonances as a pair of pseudo triplets at 4.21 and 4.00 ppm ($^{3}J_{H\text{-}H}$ = 4.0 Hz), comparable to those found in the diphosphine analog **54**.[298] Distibine **56** has also been characterized by single crystal X-ray diffraction analysis. In the crystal structure, the Cp ligands are oriented in an eclipsed conformation and the two antimony centers are separated by 4.9758(12) Å (Figure 111). With this compound in hand, we decided to exploit its reactivity with various oxidants. The reactions of two equivalents of *o*-chloranil, Br_2, and $PhICl_2$ with **56** in CH_2Cl_2 cleanly oxidizes the Sb(III) centers to afford **57**, **58**, and **59**, respectively, without affecting the Fe(II) core. Excess addition of oxidants, however, induced a color change of the solution from orange to green, indicatory of oxidation of Fe(II) to Fe(III). These corresponding Fe(III) species could not be isolated nor identified.

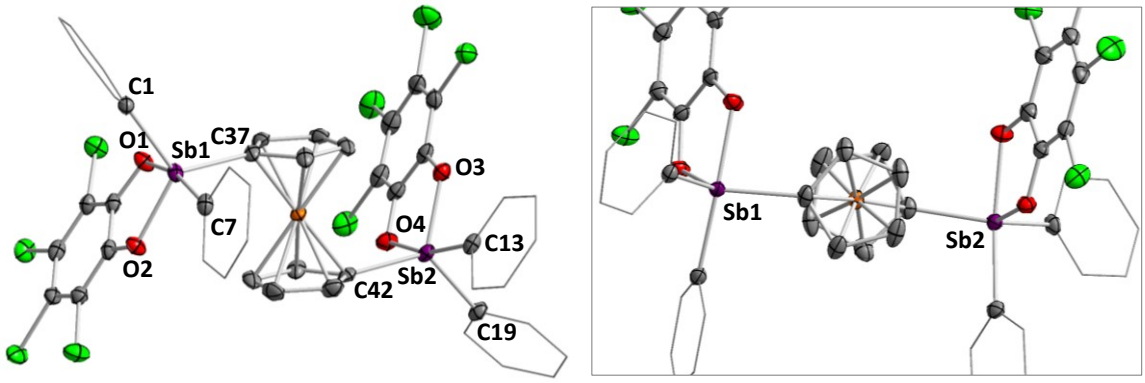

Figure 112. Left: crystal structure of **57**. Thermal ellipsoids are drawn at the 50 % probability level. The hydrogen atoms are omitted for clarity. Selected bond lengths (Å) and angles (deg): Sb1-Sb2 7.125, O1-Sb1-C7 166.39(10), O2-Sb1-C1 117.06(10), O2-Sb1-C37 122.70(10), C1-Sb1-C37 116.56(11), O4-Sb2-C19 165.69(10), O3-Sb2-C19 116.89(10), O3-Sb2-C42 117.91(10), C13-Sb2-C42 121.59(11). Right: top view of the crystal structure of **57**.

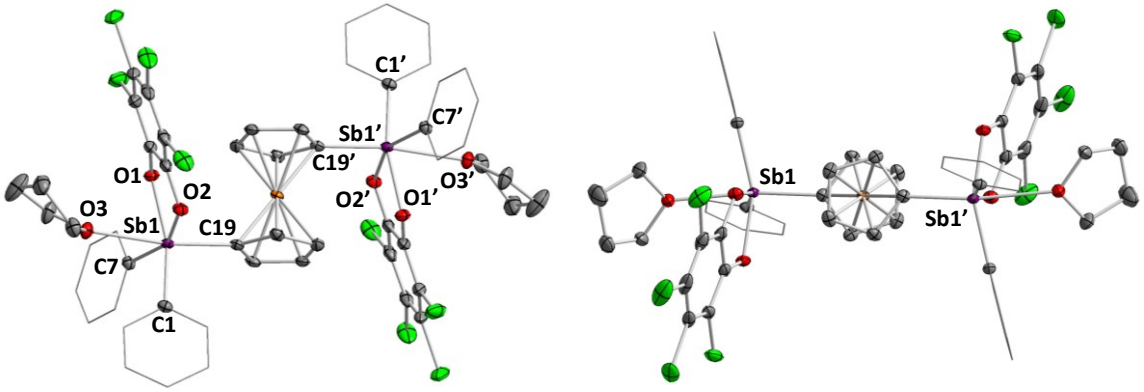

Figure 113. Left: crystal structure of **57**-$(THF)_2$. Thermal ellipsoids are drawn at the 50 % probability level. The hydrogen atoms are omitted for clarity. Selected bond lengths (Å) and angles (deg): Sb1-O3 2.5381(13), O1-Sb1-O2 78.09(5), O1-Sb1-C7 86.47(6), O2-Sb1-C1 86.90(5), C1-Sb1-C7 101.59(6), O3-Sb1-C19 170.85(5). Right: top view of the crystal structure of **57**-$(THF)_2$.

Distiboranes **57**, **58**, and **59** were isolated as air-stable solids and have been fully characterized. In the ^1H NMR spectra of **57** and **58**, the Cp signals appear as singlets as

opposed to pseudo triplets in **56**, and the chemical shifts are also more downfield. The ^{1}H NMR spectrum of **59** features similar patterns to that of **56** apart from the chemical shifts being more downfield. For all **57**, **58**, and **59**, only one set of phenyl resonances have been found, indicating that they are all equivalent in solution. Distiboranes **57**, **58**, and **59** have also been structurally characterized by single crystal X-ray diffraction analyses. Single crystals of base-free **57** have been obtained by layering hexanes onto a solution of CH_2Cl_2 at ambient temperature. The crystal structure of **57** reveals that the ferrocene backbone takes that of a staggered conformation (Figure 112). Also, the two antimony moieties are oriented facing opposite directions, possibly due to steric effects. The antimony centers adopt a trigonal bipyramidal geometry as expected for base-free stiborane moieties. Upon crystallization of **57** in the presence of THF, each antimony center separately coordinates a solvent molecule to form a hexacoordinate species with a Sb-O separation of 2.5381(13) Å (Figure 113). This demonstrates that the two electrophilic sites may not function cooperatively and behave as a pair of monofunctional Lewis acids. In the crystals of **58** and **59**, a pair of independent distiborane molecules have been found in the asymmetric unit. The structures of both **58** and **59** are analogous in the solid state and the ferrocene backbones are oriented in both staggered and eclipsed conformations (Figure 114 and Figure 115). All antimony centers adopt a distorted trigonal bipyramidal geometry with the halide ligands aligned *trans* from each other, similar to those of triphenylantimony dihalide species.

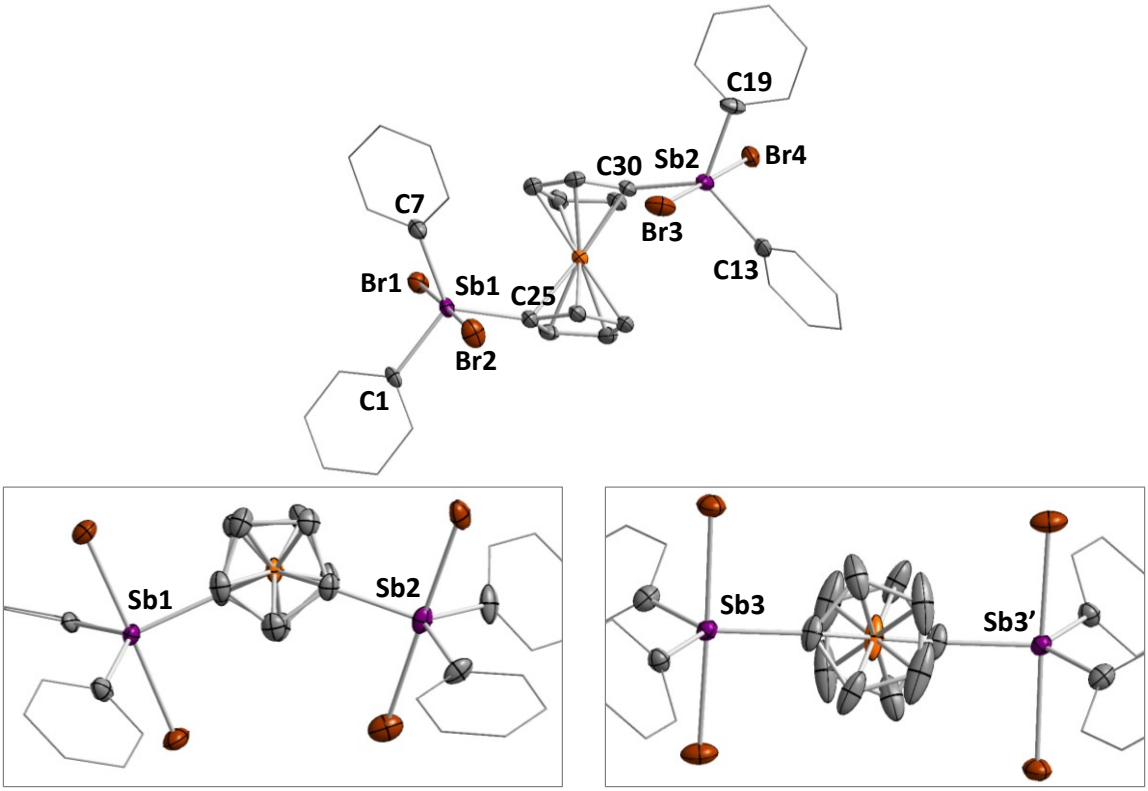

Figure 114. Top: one of the two crystal structure of **58**. Thermal ellipsoids are drawn at the 50 % probability level. The hydrogen atoms are omitted for clarity. Selected bond lengths (Å) and angles (deg) (the metrical parameters of the second independent salt are given in brackets): Sb1-Br1 2.6233(16) [2.6311(12)], Sb1-Br2 2.6530(17) [2.6249(12)], Sb2-Br3 2.6196(13), Sb2-Br4 2.6465(13), Br1-Sb1-Br2 178.550(13) [177.687(14)], C1-Sb1-C7 120.57(11) [118.46(13)], C1-Sb1-C25 117.84(12) [117.60(12)], C7-Sb1-C25 121.57(12) [123.94(12)], Br3-Sb2-Br4 178.626(14), C13-Sb2-C19 114.25(14), C13-Sb2-C30 125.37(13), C19-Sb2-C30 125.37(13). Bottom: top view of the crystal structures of **58**.

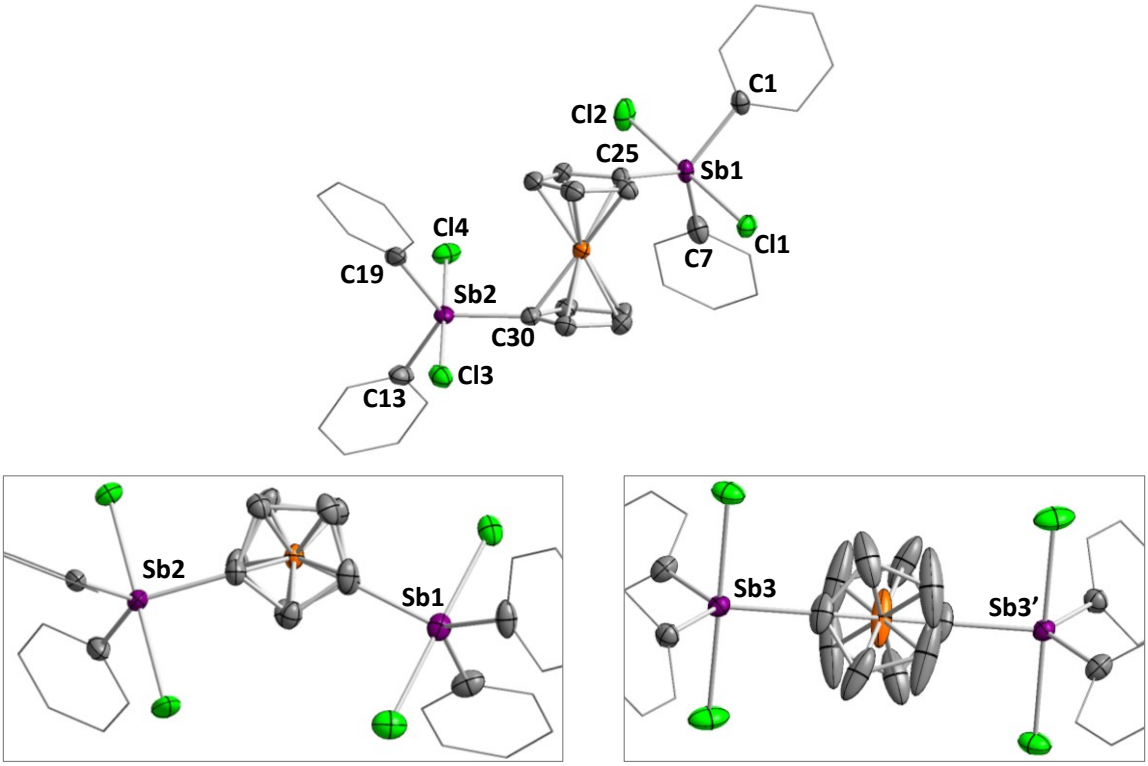

Figure 115. Top: one of the two crystal structure of **59**. Thermal ellipsoids are drawn at the 50 % probability level. The hydrogen atoms are omitted for clarity. Selected bond lengths (Å) and angles (deg) (the metrical parameters of the second independent salt are given in brackets): Sb1-Cl1 2.4662(16) [2.4644(13)], Sb1-Cl2 2.4867(17) [2.4575(13)], Sb2-Cl3 2.4652(14), Sb2-Cl4 2.4775(15), Cl1-Sb1-Cl2 179.37(3) [178.61(3)], C1-Sb1-C7 119.10(11) [118.36(12)], C1-Sb1-C25 118.10(11) [119.46(12)], C7-Sb1-C25 122.79(11) [122.18(13)], Cl3-Sb2-Cl4 179.29(3), C13-Sb2-C19 117.02(13), C13-Sb2-C30 119.52(12), C19-Sb2-C30 123.45(12). Bottom: top view of the crystal structures of **59**.

In efforts to synthesize a distibonium catalyst, **56** was reacted with excess MeOTf in toluene at 90 °C. After 6 h, an orange solid precipitated out of solution which has been identified as distibonium species [**60**][OTf]$_2$. The ^{1}H NMR spectrum displays a diagnostic antimony-bound methyl resonance at 2.56 ppm and two cyclopentadienyl resonances at 4.74 and 4.44 ppm as singlets. Single crystals of [**60**][OTf]$_2$ were obtained as orange

blocks and have been characterized by X-ray diffraction analysis (Figure 116). In the crystal, two sets of distibonium salt [**60**][OTf]$_2$ have been found in the asymmetric unit in addition to a CH_2Cl_2 molecule. Each antimony center bears a tightly-bound methyl group and consequently adopts a tetrahedral geometry with the triflate counter anions weakly associated via long Sb-O interactions ranging 2.759(3)-2.986(3) Å. The two antimony centers of [**60**]$^{2+}$ are oriented in staggered conformation, leading to a long average Sb-Sb separation of 6.03 Å. With this compound in hand, we first examined its Lewis acidity by applying the Gutmann-Beckett method. In a solution of CH_2Cl_2, broad ^{31}P NMR signal of the bound Et_3PO has been found at 58.1 ppm which is downfield by 7.1 ppm from free Et_3PO (δ = 51.0 ppm). We also examined the catalytic property of [**60**][OTf]$_2$ by monitoring the hydrosilylation reaction of benzaldehyde. The experimental protocol is the same as described in Chapter V of this dissertation (1.5 mol % [**60**][OTf]$_2$, 0.2 mmol benzaldehyde, and 0.4 mmol Et_3SiH in $CDCl_3$). This distibonium dication, however, has been found to be a lousy catalyst for such reaction and no sign of product formation has been observed even at 60 ºC for 24 h in $CDCl_3$. We speculate that this lack of catalytic behavior arises from the ability of the functionalized Cp rings to freely rotate along the $Cp_{centroid}$-Fe-$Cp_{centroid}$, which voids the possibility of chelation to activate the carbonyl substrates as in the *ortho*-phenylene analog [**42**]$^{2+}$.

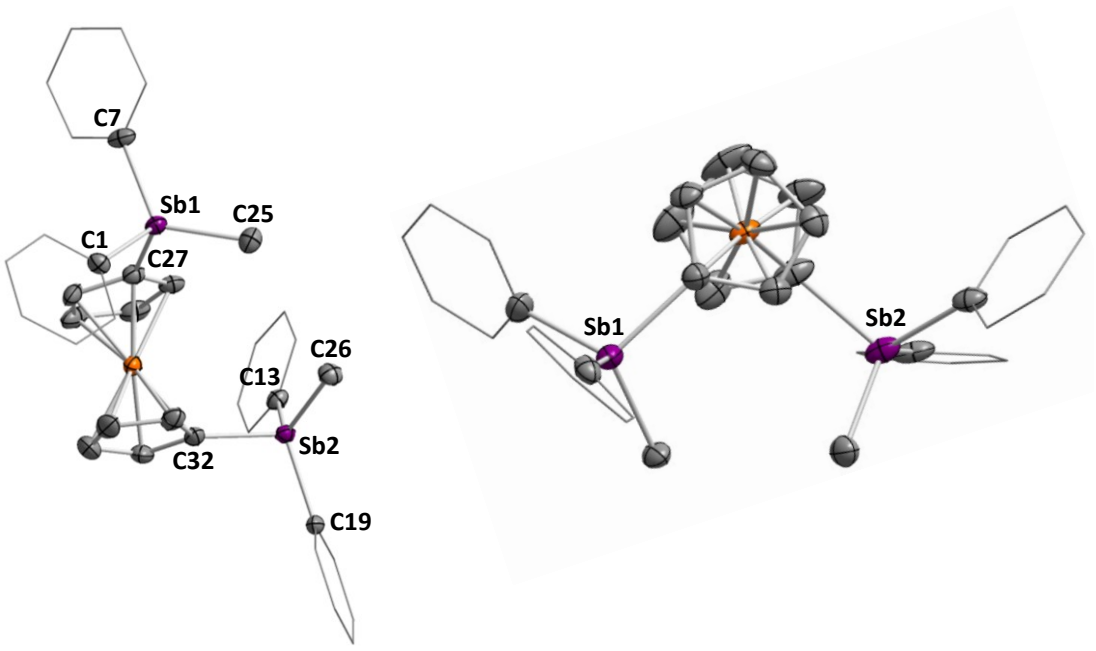

Figure 116. Left: one of the two crystal structure of [**60**]$^{2+}$. Thermal ellipsoids are drawn at the 50 % probability level. The hydrogen atoms, solvent molecule, and triflate anions are omitted for clarity. Selected bond lengths (Å) and angles (deg) (the metrical parameters of the second independent salt are given in brackets): Sb1-Sb2 6.032(3) [6.031(2)], C1-Sb1-C7 109.14(14) [117.03(13)], C1-Sb1-C25 112.87(15) [113.47(13)], C7-Sb1-C25 117.53(14) [103.81(12)], C13-Sb2-C19 112.65(15) [109.28(13)], C13-Sb2-C26 117.26(15) [115.27(13)], C19-Sb2-C26 111.53(14) [121.24(14)]. Right: top view of the crystal structure of [**60**]$^{2+}$.

6.4 Dibenzofuran-based distibine and distiborane compounds

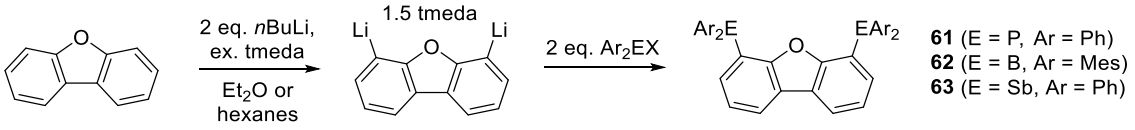

Figure 117. Synthesis of **61**, **62**, and **63**. (Ar_2EX is Ph_2PCl for **61**, Mes_2BF for **62**, and Ph_2SbCl for **63**)

Dibenzofuran is also easily functionalized especially in the 4 and 6 positions. For instance, Schroth reported the synthesis and the characterization of 4,6-bis(diphenylphosphino)dibenzofuran (**61**).[303] Because of its large separation between the two phosphorus centers (average P-P = 5.529 Å)[304] and the central oxygen donor, diphosphine **61** can behave as either a mono-, bi-, or tridentate ligand towards transition metals.[305-314] Our group later described the synthesis and the characterizartion of dimesitylboryl analog (**62**), which has a large B-B separation of 5.79 Å.[230] Both compounds **61** and **62** can be conveniently prepared by the reaction of dibenzofuran with 2 equivalents of *n*BuLi or *sec*-BuLi in the presence of tmeda to afford 4,6-dilithiodibenzofuran, followed by the addition of 2 equivalents of Ph_2PCl and Mes_2BF, respectively. In this section, we will report the synthesis and the characterization of the distibine analog and its oxidation product.

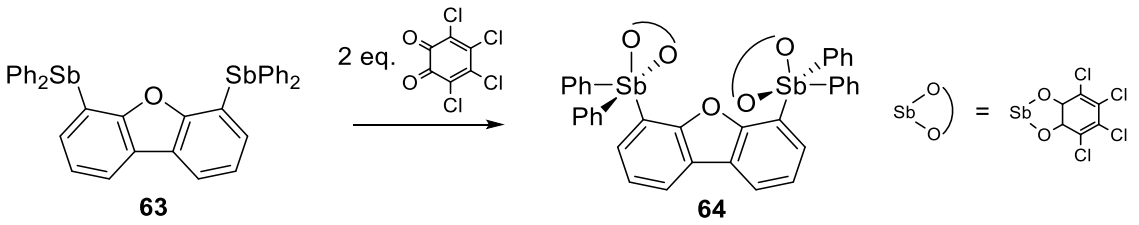

Figure 118. Synthesis of **64**.

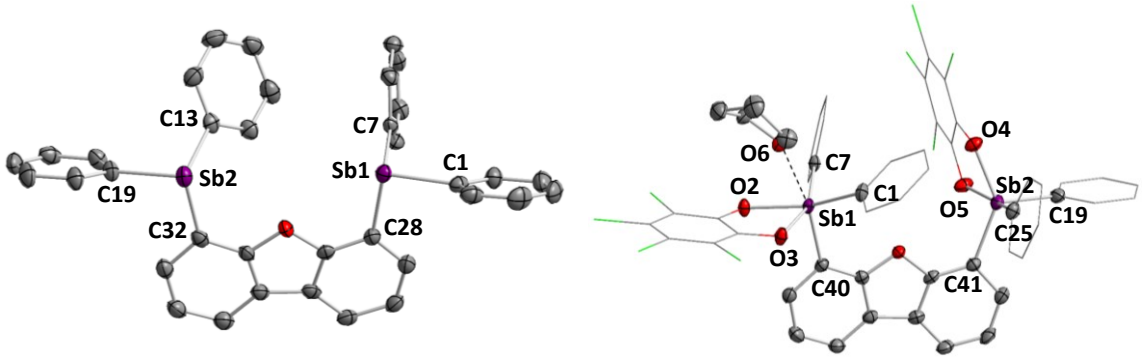

Figure 119. Crystal structures of **63** (left) and **64** (right). Thermal ellipsoids are drawn at the 50 % probability level. The hydrogen atoms and a free THF molecule (in **64**) are omitted for clarity. Selected bond lengths (Å) and angles (deg) of **63**: Sb1-Sb2 5.5786(12), C1-Sb1-C7 97.7(2), C1-Sb1-C28 97.3(2), C7-Sb1-C28 95.6(2), C13-Sb2-C19 95.7(2), C13-Sb2-C32 98.2(2), C19-Sb2-C32 95.2(2). Selected bond lengths (Å) and angles (deg) of **64**: Sb1-O6 2.4837(19), O2-Sb1-C1 155.83(9), O3-Sb1-C7 158.92(9), O6-Sb1-C40 169.75(9), O4-Sb2-C41 138.43(10), O5-Sb2-C25 160.61(9).

Following the abovementioned synthetic strategy, distibine **63** has been prepared as an air-stable solid in 54 % yield. The ^{1}H NMR spectrum of **63** shows that the dibenzofuran backbone is symmetrical and all four phenyl rings are equivalent in solution. Single crystals of **63** have been obtained as colorless blocks by diffusing pentane into a THF solution at ambient temperature and the structure has been revealed by X-ray diffraction analysis (Figure 119, left). The solid state structure shows that the Sb-Sb

separation is 5.5786(12) Å, comparable to the separation between the two phosphorus centers in the diphosphine analog **61** (5.529 Å). The two antimony centers adopt a distorted trigonal pyramidal geometry, as expected for triarylstibine moieties.

Both antimony centers of distibine **63** undergoes clean two-electron oxidation with *o*-chloranil to afford **64** as a pale yellow solid in 95 % yield. In the ^{1}H NMR spectrum, the resonances of the dibenzofuran backbone appear as sharp doublets at 8.24 and 7.68 ppm and a sharp triplet at 7.54 ppm. Moreover, all four phenyl rings in this compound are also found to be equivalent. While we failed to crystallize **64** without coordination of a base, single crystals of a THF adduct have been obtained by diffusing pentane into a THF solution (Figure 119, right). In the crystal, one of the two antimony centers weakly interacts with a THF molecule (Sb1-O6 = 2.4837(19) Å) and therefore takes that of a distorted octahedral geometry. The other antimony center remains base free and adopts a distorted square pyramidal geometry, possibly due to steric hindrance which prevents the coordination of a second solvent molecule.

6.5 *Ortho*-phenylene-based distiborane compounds

In chapter V, we described an *ortho*-phenylene-based distibonium dication [**42**]$^{2+}$ as an efficient catalyst for the hydrosilylation of benzaldehyde. In this section, we will introduce the synthesis, characterization, and applications of the neutral distiborane analogs. In particular, we will focus on the fluoride anion binding properties of these species.

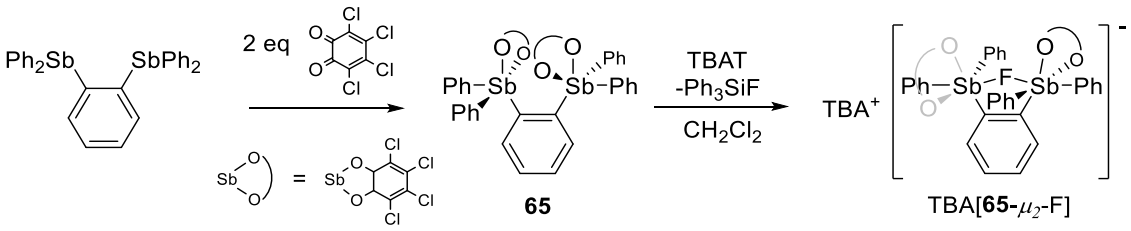

Figure 120. Synthesis of **65** and TBA[**65**-μ_2-F].

The oxidation of bis(diphenylstibino)benzene with 2 equivalents of *o*-chloranil cleanly affords the corresponding distiborane **65** as a pale yellow solid in 92 % yield. This compound is soluble in THF and toluene but only scarcely soluble in $CHCl_3$, CH_2Cl_2, and Et_2O. The ^1H NMR spectrum in $CDCl_3$ features a broad resonance centered at 7.72 ppm and a multiplet ranging from 7.57 to 7.46 ppm, which integrates to 1:2 ratio. Yellow single crystals of **65** were successfully grown by diffusing pentane into a toluene solution and the structure was determined by X-ray diffraction analysis (Figure 121, left). The crystal structure of **65** reveals that the compound has C_2 symmetry and the two antimony centers are separated by 3.7773(5) Å. Both antimony centers adopt a distorted square pyramidal geometry with $\tau = 0.12$ for Sb1 and $\tau = 0.11$ for Sb2, possibly due to steric effects. Also, the antimony atoms and the oxygen atoms of the neighboring catecholate ligands are separated by 2.796(2) Å for Sb1-O4 and 2.863(2) Å for Sb2-O2, thus indicating a possible donor-acceptor interaction between the two atoms. Compound **65** has also been investigated computationally using DFT methods (B3LYP functional with the mixed basis sets: aug-cc-pVTZ-pp for Sb, 6-311g(d) for Cl, 6-31g for C, O and H). These calculations show that the LUMO is concentrated on the two antimony atoms which can be envisioned

as the linear combination of the two Sb-O and the two Sb-C σ* orbitals occupying the equatorial plane (Figure 121, right).

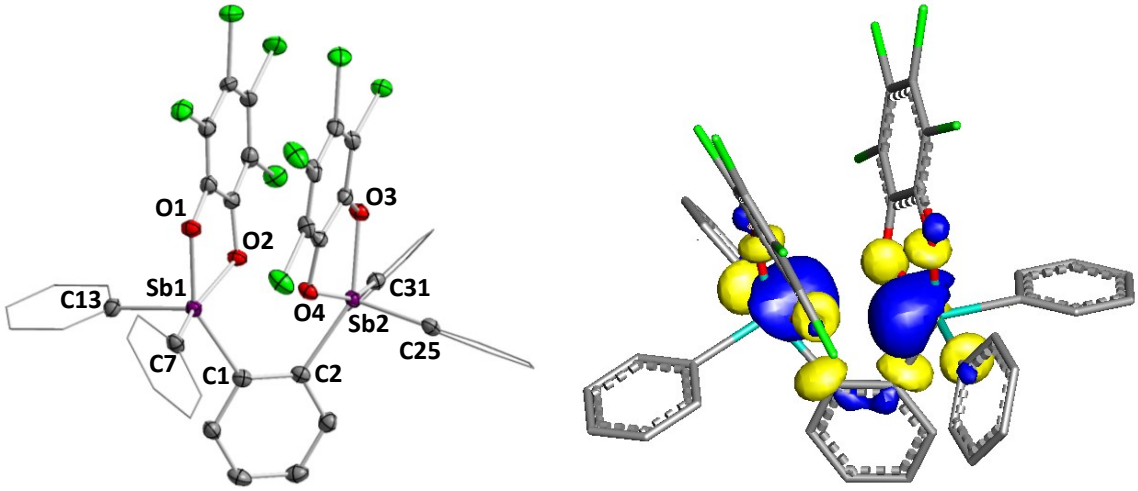

Figure 121. Left: crystal structure of **65**. Thermal ellipsoids are drawn at the 50 % probability level. The hydrogen atoms and toluene molecules are omitted for clarity. Selected bond lengths (Å) and angles (deg): Sb1-Sb2 3.7773(5), Sb1-O4 2.796(2), Sb2-O2 2.863(2), O1-Sb1-O2 78.77(8), O1-Sb1-C7 87.21(10), O2-Sb1-C1 84.22(9), C1-Sb1-C7 100.11(11), O3-Sb2-O4 78.73(7), O3-Sb2-C31 87.20(9), O4-Sb2-C2 84.55(9), C2-Sb2-C31 100.22(11). Right: contour plot of the LUMO of **65** (isovalue = 0.05).

With this compound in hand, we decided to explore its reaction towards small anions such as fluoride ions. To this end, distiborane **65** has been treated with TBAT in CH_2Cl_2 and stirred for 15 min (Figure 120). After removing the solvent *in vacuo* and successively washing the residue with Et_2O, pure TBA[**65**-μ_2-F] has been isolated as a white solid in 76 % yield. This TBA antimonate salt has been fully characterized by multi-nuclear NMR and ESI-MS spectroscopies as well as single crystal X-ray diffraction, and its composition has been revealed by elemental analysis. In the ^{1}H NMR spectrum of TBA[**65**-μ_2-F] in CD_3CN, the signals are sigfinicatnly sharpened from **65** and only one set

of phenyl resonances has been found. The ^{19}F NMR signal of the fluoride ion appears as a singlet at -73.3 ppm, which significantly differs to the resonance of the bridging fluoride in the 9,9-dimethylxanthene analog TBA[**36**-μ_2-F]. ESI-MS spectrum of this salt shows the molecular peak of [**65**-μ_2-F]$^-$ at 1136.7223 amu. Colorless single crystals of TBA[**65**-μ_2-F] were obtained by diffusing pentane into a THF solution and the solid state structure has been characterized by X-ray diffraction analysis (Figure 122). The crystal structure displays that [**65**-μ_2-F]$^-$ takes that of a C_2 symmetry and the fluoride ion is bridging between the two antimony centers in a bent fashion with a Sb1-F1-Sb2 angle of 124.54(7)°. The Sb-F bond lengths are 2.1213(14) Å for Sb1-F1 and 2.2356(14) Å for Sb2-F1 which are comparable to those in the 9,9-dimethylxanthene analog TBA[**36**-μ_2-F] (Sb1-F1 = 2.1684(17) Å and Sb2-F1 = 2.1621(18) Å). Also, the separation between the two antimony centers has slightly elongated from 3.7773(5) Å in **65** to 3.8569(5) Å in [**65**-μ_2-F]$^-$.

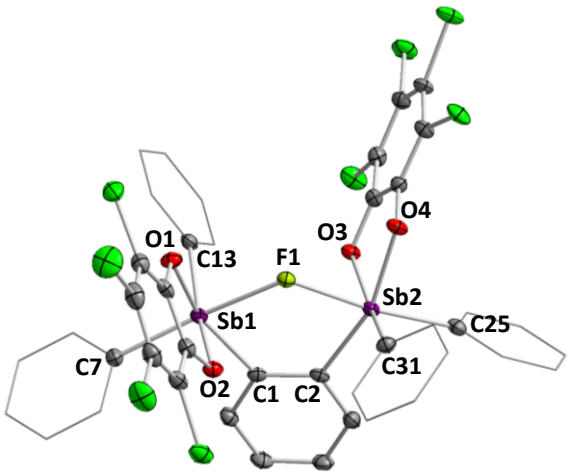

Figure 122. Crystal structure of [TBA][**65**-μ_2-F]. Thermal ellipsoids are drawn at the 50 % probability level. The hydrogen atoms and toluene molecules are omitted for clarity. Selected bond lengths (Å) and angles (deg): Sb1-Sb2 3.8569(5), Sb1-F1 2.1213(14), Sb2-F1 2.2356(14) Å, Sb1-F1-Sb2 124.54(7), F1-Sb1-C7 170.78(8), F1-Sb2-C25 169.25(8), O1-Sb1-O2 78.44(7), O1-Sb1-C13 86.85(8), O2-Sb1-C1 87.56(8), C1-Sb1-C13 104.66(10), O3-Sb2-O4 78.76(7), O3-Sb2-C2 86.93(8), O4-Sb2-C31 87.16(9), C2-Sb2-C31 103.90(10).

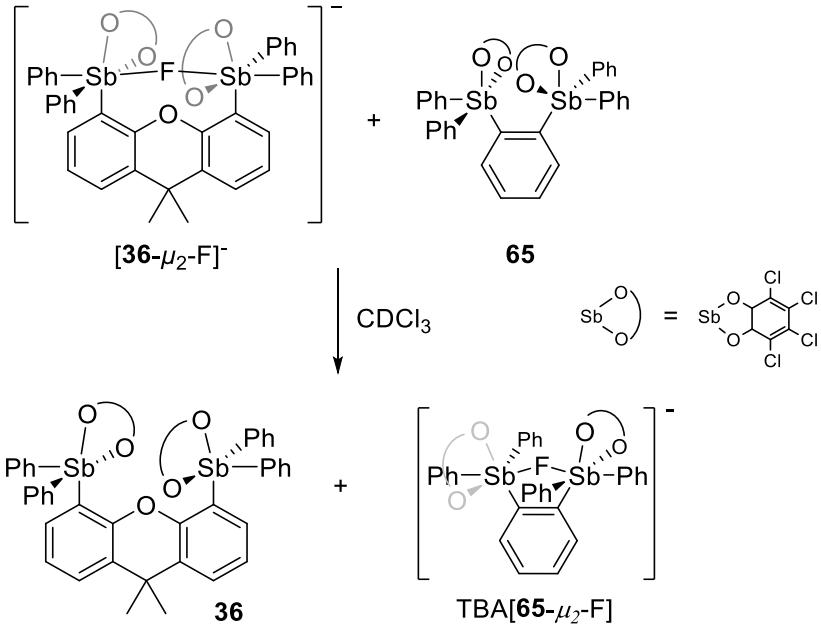

Figure 123. The competition experiment of [**36**-μ_2-F]$^-$ and **65** in $CDCl_3$.

To get a better insight of the fluoride ion affinity of **65**, gas phase fluoride ion affinity (FIA) has been estimated using computational methods. These calculations show that [**65**-μ_2-F]$^-$ is stabilized by approximately 20 kJ mol^{-1} more than that of the 9,9-dimethylxanthene analog [**36**-μ_2-F]$^-$ (FIA = 378.4 kJ mol^{-1} for **65** and 359.88 kJ mol^{-1} for **36**). Indeed, NMR studies reveal that the reaction of **65** with equimolar amount of [**36**-μ_2-F]$^-$ in $CDCl_3$ results in a quantitative formation of [**65**-μ_2-F]$^-$ and **36**, thus indicating that **65** is more fluorophilic than **36** (Figure 123). With this in mind, we became eager to examine the fluoride binding property of **65** in aqueous solution; however, **65** immediately hydrolyzes upon exposure to a solution containing high concentration of water, which limited the use of **65** in aqueous media.

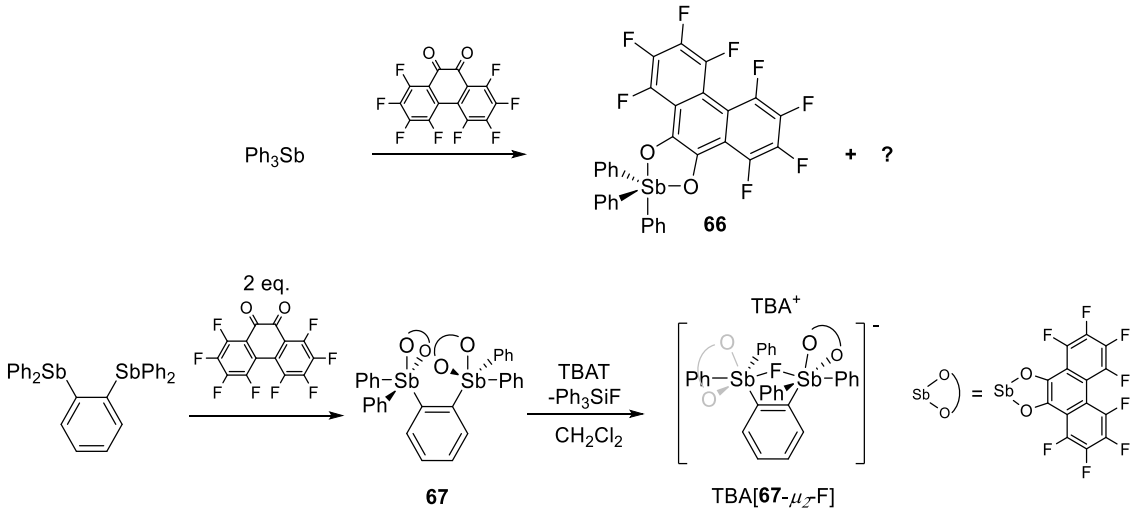

Figure 124. Synthesis of **66**, **67**, and TBA[**67**-μ_2-F].

We also investigated the oxidation of triarylstibine species with a more electron-deficient quinone, octafluorophenthra-9,10-quinone, which was synthesized by a modified procedure described in the literature.[315, 316] To initiate our study, we first monitored the reaction of octafluorophenthra-9,10-quinone with Ph_3Sb in Et_2O under N_2 atmosphere. Upon standing at ambient temperature, X-ray diffraction quality single crystals were obtained as yellow blocks which the structure has been identified as triphenylstiborane **66** (Figure 125). The crystal structure of **66** features similar characteristics to those of triphenylstiborane **10** in which the antimony center takes that of a trigonal bipyramidal geometry ($\Sigma(C_{Ph}\text{-}Sb\text{-}C_{Ph})$ = 356.88º) and the oxygen atoms of the perfluorophenanthrenediyl-9,10-dioxy ligand occupy the axial and the apical positions.[46] Both ^1H and ^{19}F NMR spectra, however, indicate that the bulk crystal sample consists unknown impurities that could not be separated from the desired product. Furthermore, exposure of these crystals to air leads to further decomposition of **66** and formation of unknown impurities.

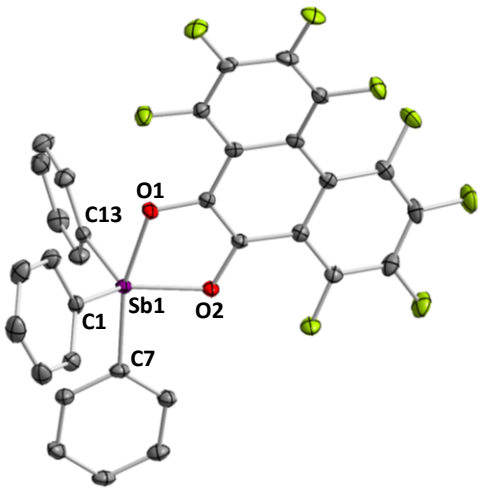

Figure 125. Crystal structure of **66**. Thermal ellipsoids are drawn at the 50 % probability level. The hydrogen atoms and toluene molecules are omitted for clarity. Selected angles (deg): O1-Sb1-O2 78.40(5), O1-Sb1-C7 165.09(6), O2-Sb1-C1 128.16(6), O2-Sb1-C13 110.84(6), C1-Sb1-C13 117.88(7).

The reaction of bis(diphenylstibino)benzene with 2 equivalents of octafluorophenthra-9,10-quinone in Et_2O or CH_2Cl_2 affords distiborane **67** as yellow single crystals upon standing at room temperature (Figure 124, bottom). The crystal structure of distiborane **67** has been determined by single crystal X-ray diffraction analysis (Figure 126, left). Gratifyingly, this reaction can be carried out in air as opposed to the synthesis of **66**, thereby demonstrating that **67** is stable in the presence of molecular oxygen. We speculate that this remarkable air-stability arises from the short Sb1-O3 and Sb2-O1 contacts (2.557(2) and 2.525(2) Å, respectively) which blocks the sixth coordination site of the antimony centers. Also in the crystal, the two antimony centers are separated by 3.568(3) Å, marginally shorter than that of **65** (3.7773(5) Å). Multi-nuclear NMR studies in $CDCl_3$ indicate that the bulk crystal sample is made of only distiborane **67**. The ^1H NMR spectrum shows the *ortho*-phenylene resonances as a

multiplet at 7.67 ppm and a broad phenyl signal centered at 7.39 ppm. The ^{19}F NMR spectrum features 5 broad signals corresponding to the perfluorophenanthrenediyl-9,10-dioxy ligand, indicating that the fluorine atoms in the 4 and 5 positions are inequivalent in solution (Figure 133). Distiborane **67** has also been investigated computationally using DFT methods (B3LYP functional with the mixed basis sets: aug-cc-pVTZ-pp for Sb, 6-31g(d') for F, 6-31g for C, O and H). The DFT optimized structure of **67** is in good agreement with that experimentally determined. As expected, the LUMO is concentrated on the two antimony atoms which both contribute via σ* orbitals of the two Sb-O and the Sb-C_{Ar} characters, similar to that of **65** (Figure 126, right).

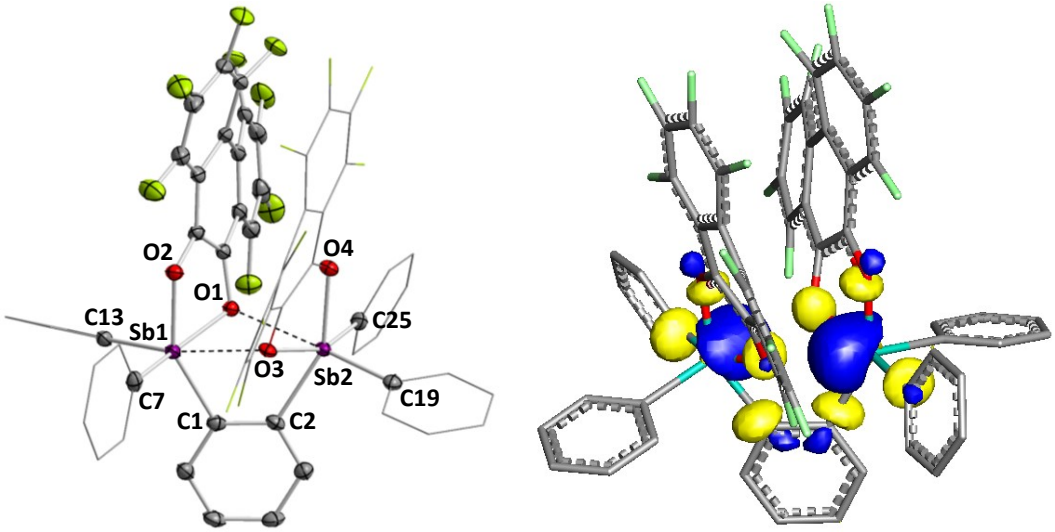

Figure 126. Left: crystal structure of **67**. Thermal ellipsoids are drawn at the 50 % probability level. The hydrogen atoms and CH_2Cl_2 molecules are omitted for clarity. Selected bond lengths (Å) and angles (deg): Sb1-Sb2 3.568(3), Sb1-O3 2.557(2), Sb2-O1 2.525(2), O1-Sb1-O2 78.06(8), O1-Sb1-C1 80.69(9), O2-Sb1-C7 88.73(10), C1-Sb1-C7 105.26(11), O3-Sb2-O4 77.41(9), O3-Sb2-C2 81.66(11), O4-Sb2-C25 88.87(10), C2-Sb2-C25 104.59(11), O3-Sb1-C13 166.30(8), O1-Sb2-C19 168.49(9). Right: contour plot of the LUMO of **67** (isovalue = 0.05).

Following these observations, we sought to exploit the fluoride binding property of **67**. To this end, **67** has been reacted with TBAT in CH_2Cl_2 at ambient temperature (Figure 124, bottom). After removing the solvent *in vacuo* and carefully washing the residue with Et_2O, pure [TBA][**67**-μ_2-F] has been isolated as a yellow solid in 66 % yield. The ^{1}H NMR spectrum shows that the aryl signals significantly sharpens from the free distiborane **67** and that all four phenyl rings are equivalent in solution. In the ^{19}F NMR spectrum of [**67**-μ_2-F]$^-$, 8 distinct resonances are found between -130 and -170 ppm, corresponding to the perfluorophenanthrenediyl-9,10-dioxy ligand (Figure 134). The ^{19}F NMR signal of the bridging fluoride appears at -76.8 ppm, which is close to that of [**65**-μ_2-F]$^-$ (-73.3 ppm). The crystal structure of [TBA][**67**-μ_2-F] has been characterized by X-ray diffraction analysis (Figure 127). The solid state structure of [**67**-μ_2-F]$^-$ confirms that the fluoride anion is indeed tightly bound to both antimony centers Sb1-F100 and Sb2-F100 distances of 2.130(3) and 2.139(3) Å, respectively, which are comparable to those of [**65**-μ_2-F]$^-$ (2.1213(14) Å for Sb1-F1 and 2.2356(14) Å for Sb2-F1). Furthermore, the bridging fluoride adopts a bent geometry with a Sb1-F100-Sb2 angle of 126.27(16)^o. We have also estimated the FIA of **67** using DFT methods. The optimization and frequency calculation have been carried out at the B3LYP functional with the mixed basis sets: aug-cc-pVTZ-pp for Sb, 6-31g(d') for F, 6-31g for C, O and H. Subsequently, enthalpies have been determined by a single point calculation at the DFT optimized structure applying the B3LYP functional and aug-cc-pVTZ-pp level of theory on Sb and 6-311+g(2d,p) level of theory on C, H, O, and F.[227] The results of these theoretical studies show that the FIA of **67** is 388.1 kJ mol^{-1}, which is marginally higher than that of **65**

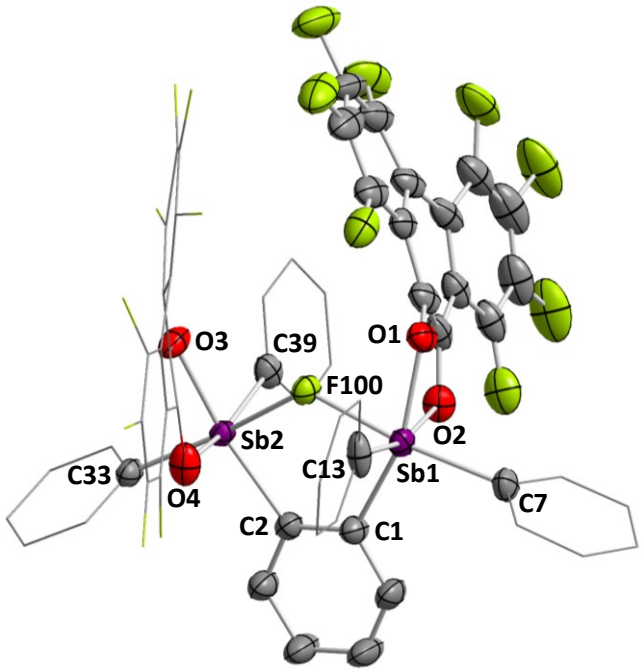

Figure 127. Crystal structure of one of the three parts of [TBA][**67**-μ_2-F]. Thermal ellipsoids are drawn at the 50 % probability level. The hydrogen atoms and the TBA cation are omitted for clarity. Selected bond lengths (Å) and angles (deg): Sb1-C1 2.115(3), Sb1-C7 2.103(3), Sb1-C19 2.129(3), Sb1-O1 2.0551(18), Sb1-O2 2.0360(18), Sb2-C32 2.134(3), Sb2-C40 2.093(3), Sb2-C46 2.110(3), Sb2-O4 2.0389(18), Sb2-O5 2.0554(18), Sb1-F100-Sb2 126.27(16), O1-Sb1-O2 78.46(7), C1-Sb1-C7 102.92(10), C1-Sb1-C19 101.51(10), C7-Sb1-C19 101.51(10), O4-Sb2-O5 78.60(7), C32-Sb2-C40 103.43(10), C32-Sb2-C46 101.35(10), C40-Sb2-C46 107.67(10).

6.6 Conclusion

In summary, we have prepared a series of distibine compounds bearing different Sb-Sb proximities and studied their reaction towards oxidants such as *o*-chloranil, Br_2, $CuBr_2$, and $PhICl_2$. We found that Sb-Sb separations is crucial for the two-electron oxidation of both antimony centers. In the case of naphthalenyl derivative **46**, only one of the two antimony(III) moieties was able to oxidize due to a strong Sb(III)→Sb(V) interaction which prevents further reactivity. By contrast, both antimony(III) centers of

distibine bearing a larger Sb-Sb distance can be successfully oxidized to afford new types of bis-organoantimony(V) bifunctional Lewis acids. In particular, we have been able to isolate bis-organoantimony(V) species incorporated to ferrocene, dibenzofuran, and *ortho*-phenylene backbones. We have also shown that the proximity of the two antimony centers are crucial for the binding mode of Lewis bases. For example, distiborane and distibonium species bearing ferrocene or dibenzofuran backbones contain largely separated Sb-Sb moieties which were not found to chelate Lewis bases such as THF. By contrast, the more rigid *ortho*-phenylene distiboranes **65** and **67** are excellent chelators toward fluoride ion, which the affinities exceed that of the 9,9-dimethylxanthene analog **36** that was previously reported to bind fluoride in 9.5/0.5 (v/v) THF/H_2O mixture.[249]

6.7 Experimental section

General considerations. *Antimony is potentially toxic and should be handled with caution.* Perfluoro(tetradecahydrophenanthrene) was purchased from Beantown Chemical and used as received. Aluminum powder and $HgCl_2$, and *n*BuLi (2.65 M in hexane) were purchased from Alfa Aesar and used as received. Tetrachloro-*o*-benzoquinone (*o*-chloranil) was purchased from Acros Organics. Br_2, I_2, and Cp_2TiCl_2 were purchased from Sigma Aldrich and used as received. Methyl trifluoromethanesulfonate (MeOTf) was purchased from Matrix Scientific and used as received. $CuBr_2$ was purchased from Alfa Aesar. TBAT was purchased from TCI and used as received. Ph_2SbCl,[317] $PhICl_2$,[318] 1,8-dilithionaphthalene·tmeda salt,[319], 1,8-bis(diphenylstibino)naphthalene,[292] *ortho*-bis(diphenylstibino)benzene,[114, 274], 1,1'-

dilithioferrocene·tmeda,[297] 4,6-dilithiobenzofuran[230] were prepared by following or modifying previously reported procedure from literature. All preparations were carried out under an atmosphere of dry N_2 employing either a glovebox or standard Schlenk techniques unless specified. Solvents were dried by passing through an alumina column (pentane and CH_2Cl_2) or by refluxing under N_2 over Na/K (hexanes, Et_2O, and THF). All other solvents were ACS reagent grade and used as received. NMR spectra were recorded on a Varian Unity Inova 400 FT NMR (399.508 MHz for ^1H, 100.466 MHz for ^{13}C) or Varian Unity Inova 500 FT NMR (499.42 MHz for ^1H, 469.86 MHz for ^{19}F, 125.60 MHz for ^{13}C) spectrometer at ambient temperature. Chemical shifts are given in ppm and are referenced to residual ^1H and ^{13}C solvent signals and external $BF_3·Et_2O$ for ^{19}F. Elemental analyses were performed by Atlantic Microlab (Norcross, GA). Electronic absoption spectra were recorded at ambient temperature using an Ocean Optics USB4000 spectrometer with an Ocean Optics ISS light source. Electrospray ionization mass spectra were recorded on Applied Biosystems PE SCIEX QSTAR.

Computational details. Density functional theory (DFT) structural optimizations with the *Gaussian 09* program.[208] In all cases, the structures were optimized using the B3LYP functional;[209, 210], and the following mixed basis set: Sb, aug-cc-pVTZ-PP;[240] Cl, 6-311+g(d); F, 6-31g(d');[212] C/O/H, 6-31g).[213] For all optimized structures, frequency calculations were carried out to confirm the absence of imaginary frequencies. The molecular orbitals were visualized and plotted in Jimp 2 program.[214]

Crystallographic measurements. The crystallographic measurements were performed at 110(2) K using a Bruker APEX-II CCD area detector diffractometer, with a graphite-monochromated Mo-K_α radiation (λ = 0.71069 A). A specimen of suitable size and quality was selected and mounted onto a nylon loop. The semi-empirical method SADABS was applied for absorption correction. The structure was solved by direct methods, which successfully located most of the non-hydrogen atoms. Subsequent refinement on F^2 using the SHELXTL/PC package (version 6.1) allowed location of the remaining non-hydrogen atoms. All H-atoms were geometrically placed and refined using a standard riding model.[262, 263]

Table 14. Crystal data, data collection, and structure refinement for **47** and **49**.

Crystal data	**47**	**49**
Empirical formula	C80 H52 Cl8 O4 Sb4	C34 H26 Cl2 Sb2
Formula weight	1847.81	748.95
Temperature	110(2) K	110(2) K
Wavelength	0.71073 Å	0.71073 Å
Crystal system	Triclinic	Triclinic
Space group	P -1	P -1
Unit cell dimensions	a = 10.321(2) Å	a = 9.1560(17) Å
	b = 17.490(4) Å	b = 12.528(2) Å
	c = 20.157(4) Å	c = 12.854(2) Å
	α = 85.848(2)°.	α = 104.756(2)°.
	β = 86.832(2)°.	β = 90.200(2)°.
	γ = 82.071(2)°.	γ = 92.321(2)°.
Volume	3590.6(13) $Å^3$	1424.5(5) $Å^3$
Z	2	2
Density (calculated)	1.709 Mg/m^3	1.746 Mg/m^3
Absorption coefficient	1.837 mm^{-1}	2.106 mm^{-1}
F(000)	1808	732
Crystal size	0.19 x 0.17 x 0.12 mm^3	0.286 x 0.223 x 0.151 mm^3
Theta range for data collection	2.028 to 28.175°	1.638 to 28.338°
Index ranges	-13<=h<=13, -22<=k<=23, -26<=l<=26	-11<=h<=12, -16<=k<=16, -16<=l<=17
Reflections collected	42708	16888
Independent reflections	17191 [R(int) = 0.0300]	6763 [R(int) = 0.0228]
Absorption correction	Semi-empirical from equivalents	Semi-empirical from equivalents
Max. and min. transmission	0.808 and 0.654	0.854 and 0.634
Refinement method	Full-matrix least-squares on F^2	Full-matrix least-squares on F^2
Data / restraints / parameters	17191 / 0 / 865	6763 / 0 / 366
Goodness-of-fit on F^2	1.019	1.038
Final R indices [I>2sigma(I)]	R1 = 0.0276, wR2 = 0.0639	R1 = 0.0354, wR2 = 0.0964
R indices (all data)	R1 = 0.0353, wR2 = 0.0673	R1 = 0.0392, wR2 = 0.0995
Largest diff. peak and hole	1.765 and -0.519 e.$Å^{-3}$	2.613 and -0.825 e.$Å^{-3}$

[a] $R1 = \Sigma||Fo| - |Fc||/\Sigma|Fo|$. [b] $wR2 = \{[\Sigma w(Fo^2 - Fc^2)^2]/[\Sigma w(Fo^2)^2]\}^{1/2}$.

Table 15. Crystal data, data collection, and structure refinement for **50** and [**51**][OTf]$_2$.

Crystal data	**50**	[**51**][OTf]
Empirical formula	C34 H26 F2 Sb2	C36 H29 F3 O3 S Sb2
Formula weight	716.05	842.15
Temperature	110(2) K	110(2) K
Wavelength	0.71073 Å	0.71073 Å
Crystal system	Triclinic	Monoclinic
Space group	P -1	C 2/c
Unit cell dimensions	a = 9.6741(13) Å	a = 21.673(5) Å
	b = 11.7296(16) Å	b = 12.751(3) Å
	c = 12.4558(17) Å	c = 24.308(5) Å
	α = 86.822(2)°	α = 90°
	β = 86.6780(10)°	β = 103.901(2)°
	γ = 81.176(2)°	γ = 90°
Volume	1392.8(3) Å^3	6521(2) Å^3
Z	2	8
Density (calculated)	1.707 Mg/m^3	1.716 Mg/m^3
Absorption coefficient	1.975 mm^{-1}	1.774 mm^{-1}
F(000)	700	3312
Crystal size	0.617 x 0.414 x 0.124 mm^3	0.33 x 0.28 x 0.18 mm^3
Theta range for data collection	1.639 to 28.271°	1.726 to 28.715°
Index ranges	-12<=h<=12, -15<=k<=15, -16<=l<=16	-28<=h<=29, -16<=k<=16, -31<=l<=31
Reflections collected	16383	35947
Independent reflections	6571 [R(int) = 0.0199]	7882 [R(int) = 0.0474]
Absorption correction	Semi-empirical from equivalents	Semi-empirical from equivalents
Max. and min. transmission	0.764 and 0.605	0.724 and 0.536
Refinement method	Full-matrix least-squares on F^2	Full-matrix least-squares on F^2
Data / restraints / parameters	6571 / 0 / 344	7882 / 0 / 407
Goodness-of-fit on F^2	1.027	1.179
Final R indices [I>2sigma(I)]	R1 = 0.0189, wR2 = 0.0455	R1 = 0.0528, wR2 = 0.1060
R indices (all data)	R1 = 0.0218, wR2 = 0.0474	R1 = 0.0709, wR2 = 0.1123
Largest diff. peak and hole	0.639 and -0.431 e.Å^{-3}	1.588 and -1.399 e.Å^{-3}

[a] $R1 = \Sigma||Fo| - |Fc||/\Sigma|Fo|$. [b] $wR2 = \{[\Sigma w(Fo^2 - Fc^2)^2]/[\Sigma w(Fo^2)^2]\}^{1/2}$.

Table 16. Crystal data, data collection, and structure refinement for **56** and **57**.

Crystal data	**56**	**57**
Empirical formula	C34 H28 Fe Sb2	C46 H28 Cl8 Fe O4 Sb2
Formula weight	735.91	1227.63
Temperature	110(2) K	110(2) K
Wavelength	0.71073 Å	0.71073 Å
Crystal system	Monoclinic	Triclinic
Space group	P 21/c	P -1
Unit cell dimensions	a = 14.181(5) Å	a = 10.276(2) Å
	b = 13.034(5) Å	b = 12.604(3) Å
	c = 20.892(6) Å	c = 17.700(4) Å
	α = 90°	α = 105.487(3)°.
	β = 132.748(15)°	β = 93.743(3)°.
	γ = 90°	γ = 97.742(3)°.
Volume	2835.7(18) $Å^3$	2176.8(9) $Å^3$
Z	4	2
Density (calculated)	1.724 Mg/m^3	1.873 Mg/m^3
Absorption coefficient	2.418 mm^{-1}	2.098 mm^{-1}
F(000)	1440	1200
Crystal size	0.28 x 0.24 x 0.14 mm^3	0.39 x 0.18 x 0.10 mm^3
Theta range for data collection	1.956 to 29.729°	1.201 to 28.252°
Index ranges	-18<=h<=19, -18<=k<=18, -27<=l<=28	-13<=h<=13, -16<=k<=16, -22<=l<=23
Reflections collected	18202	25766
Independent reflections	4229 [R(int) = 0.0371]	10277 [R(int) = 0.0309]
Absorption correction	Semi-empirical from equivalents	Semi-empirical from equivalents
Max. and min. transmission	0.729 and 0.402	0.706 and 0.578
Refinement method	Full-matrix least-squares on F^2	Full-matrix least-squares on F^2
Data / restraints / parameters	4229 / 0 / 334	10277 / 0 / 550
Goodness-of-fit on F^2	1.008	1.039
Final R indices [I>2sigma(I)]	R1 = 0.0234, wR2 = 0.0527	R1 = 0.0324, wR2 = 0.0714
R indices (all data)	R1 = 0.0299, wR2 = 0.0544	R1 = 0.0422, wR2 = 0.0756
Largest diff. peak and hole	0.402 and -0.329 e.$Å^{-3}$	1.408 and -0.534 e.$Å^{-3}$

[a] $R1 = \Sigma||Fo| - |Fc||/\Sigma|Fo|$. [b] $wR2 = \{[\Sigma w(Fo^2 - Fc^2)^2]/[\Sigma w(Fo^2)^2]\}^{1/2}$.

Table 17. Crystal data, data collection, and structure refinement for **57**-$(THF)_2$ and **58**.

Crystal data	**57**-$(THF)_2$	**58**
Empirical formula	C54 H44 Cl8 Fe O6 Sb2	C34 H28 Br4 Fe Sb2
Formula weight	1371.84	1055.55
Temperature	110(2) K	110(2) K
Wavelength	0.71073 Å	0.71073 Å
Crystal system	Triclinic	Triclinic
Space group	P -1	P -1
Unit cell dimensions	a = 9.5187(16) Å b = 9.8837(17) Å c = 14.432(3) Å α = 93.543(2)° β = 106.168(2)° γ = 93.034(2)°	a = 11.721(7) Å b = 14.674(9) Å c = 15.716(10) Å α = 87.740(7)° β = 87.135(7)° γ = 70.935(7)°
Volume	1298.1(4) $Å^3$	2551(3) $Å^3$
Z	1	3
Density (calculated)	1.755 Mg/m^3	2.061 Mg/m^3
Absorption coefficient	1.772 mm^{-1}	6.720 mm^{-1}
F(000)	680	1500
Crystal size	0.38 x 0.36 x 0.24 mm^3	0.29 x 0.21 x 0.16 mm^3
Theta range for data collection	2.070 to 29.785°	1.840 to 29.697°
Index ranges	-12<=h<=12, -13<=k<=13, -20<=l<=20	-16<=h<=15, -20<=k<=19, -21<=l<=21
Reflections collected	16616	32759
Independent reflections	6760 [R(int) = 0.0167]	13223 [R(int) = 0.0376]
Absorption correction	Semi-empirical from equivalents	Semi-empirical from equivalents
Max. and min. transmission	0.816 and 0.551	0.515 and 0.213
Refinement method	Full-matrix least-squares on F^2	Full-matrix least-squares on F^2
Data / restraints / parameters	6760 / 0 / 322	13223 / 0 / 556
Goodness-of-fit on F^2	1.038	1.016
Final R indices [I>2sigma(I)]	R1 = 0.0211, wR2 = 0.0508	R1 = 0.0288, wR2 = 0.0651
R indices (all data)	R1 = 0.0229, wR2 = 0.0518	R1 = 0.0391, wR2 = 0.0687
Largest diff. peak and hole	0.957 and -0.928 e.$Å^{-3}$	0.960 and -1.131 e.$Å^{-3}$

[a] $R1 = \Sigma||Fo| - |Fc||/\Sigma|Fo|$. [b] $wR2 = \{[\Sigma w(Fo^2 - Fc^2)^2]/[\Sigma w(Fo^2)^2]\}^{1/2}$.

Table 18. Crystal data, data collection, and structure refinement for **59** and [**60**][OTf]$_2$.

Crystal data	**59**	[**60**][OTf]$_2$
Empirical formula	C34 H28 Cl4 Fe Sb2	C77 H69 Cl3 F12 Fe2 O12 S4 Sb4
Formula weight	877.71	2247.61
Temperature	110(2) K	110(2) K
Wavelength	0.71073 Å	0.71073 Å
Crystal system	Triclinic	Triclinic
Space group	P -1	P -1
Unit cell dimensions	a = 11.674(7) Å	a = 13.911(8) Å
	b = 14.311(8) Å	b = 15.393(9) Å
	c = 15.519(9) Å	c = 21.888(13) Å
	α = 88.368(7)°.	α = 82.866(7)°.
	β = 85.703(6)°.	β = 86.352(7)°.
	γ = 71.736(6)°.	γ = 65.030(6)°.
Volume	2455(2) Å^3	4215(4) Å^3
Z	3	2
Density (calculated)	1.781 Mg/m^3	1.771 Mg/m^3
Absorption coefficient	2.426 mm^{-1}	1.877 mm^{-1}
F(000)	1284	2212
Crystal size	0.36 x 0.26 x 0.18 mm^3	0.23 x 0.12 x 0.07 mm^3
Theta range for data collection	1.841 to 29.709°	1.615 to 25.917°
Index ranges	-15<=h<=16, -19<=k<=19, -21<=l<=20	-17<=h<=16, -18<=k<=18, -26<=l<=26
Reflections collected	31376	44297
Independent reflections	12686 [R(int) = 0.0272]	16278 [R(int) = 0.0331]
Absorption correction	Semi-empirical from equivalents	Semi-empirical from equivalents
Max. and min. transmission	0.786 and 0.526	0.8798 and 0.6721
Refinement method	Full-matrix least-squares on F^2	Full-matrix least-squares on F^2
Data / restraints / parameters	12686 / 0 / 556	16278 / 0 / 1050
Goodness-of-fit on F^2	1.029	1.018
Final R indices [I>2sigma(I)]	R1 = 0.0295, wR2 = 0.0685	R1 = 0.0306, wR2 = 0.0672
R indices (all data)	R1 = 0.0347, wR2 = 0.0712	R1 = 0.0402, wR2 = 0.0718
Largest diff. peak and hole	1.529 and -1.491 e.Å^{-3}	2.034 and -1.149 e.Å^{-3}

[a] $R1 = \Sigma||Fo| - |Fc||/\Sigma|Fo|$. [b] $wR2 = \{[\Sigma w(Fo^2 - Fc^2)^2]/[\Sigma w(Fo^2)^2]\}^{1/2}$.

Table 19. Crystal data, data collection, and structure refinement for **63** and **64**-THF.

Crystal data	**63**	**64**-THF
Empirical formula	C36 H26 O Sb2	C56 H42 Cl8 O7 Sb2
Formula weight	718.07	1353.99
Temperature	110(2) K	110(2) K
Wavelength	0.71073 Å	0.71073 Å
Crystal system	Orthorhombic	Triclinic
Space group	P 21 21 21	P -1
Unit cell dimensions	a = 6.152(2) Å	a = 12.637(2) Å
	b = 13.174(5) Å	b = 12.657(2) Å
	c = 34.918(13) Å	c = 18.640(3) Å
	α = 90°	α = 86.058(2)°
	β = 90°	β = 77.413(2)°
	γ = 90°	γ = 74.725(2)°
Volume	2829.9(18) $Å^3$	2806.7(8) $Å^3$
Z	4	2
Density (calculated)	1.685 Mg/m^3	1.602 Mg/m^3
Absorption coefficient	1.937 mm^{-1}	1.394 mm^{-1}
F(000)	1408	1344
Crystal size	0.221 x 0.169 x 0.120 mm^3	0.192 x 0.165 x 0.114 mm^3
Theta range for data collection	1.936 to 28.358°	1.837 to 25.495°
Index ranges	-8<=h<=8, -17<=k<=17, -46<=l<=46	-15<=h<=15, -14<=k<=15, -22<=l<=22
Reflections collected	34858	18627
Independent reflections	7021 [R(int) = 0.0642]	10404 [R(int) = 0.0285]
Absorption correction	Semi-empirical from equivalents	Semi-empirical from equivalents
Max. and min. transmission	0.842 and 0.675	0.747 and 0.641
Refinement method	Full-matrix least-squares on F^2	Full-matrix least-squares on F^2
Data / restraints / parameters	7021 / 0 / 352	10404 / 0 / 658
Goodness-of-fit on F^2	1.033	1.05
Final R indices [I>2sigma(I)]	R1 = 0.0364, wR2 = 0.0821	R1 = 0.0303, wR2 = 0.0732
R indices (all data)	R1 = 0.0430, wR2 = 0.0857	R1 = 0.0359, wR2 = 0.0756
Largest diff. peak and hole	0.725 and -0.623 e.$Å^{-3}$	0.789 and -0.714 e.$Å^{-3}$

[a] $R1 = \Sigma||Fo| - |Fc||/\Sigma|Fo|$. [b] $wR2 = \{[\Sigma w(Fo^2 - Fc^2)^2]/[\Sigma w(Fo^2)^2]\}^{1/2}$.

Table 20. Crystal data, data collection, and structure refinement for **65** and TBA[**65**-μ_2-F].

Crystal data	**65**	TBA[**65**-μ_2-F]
Empirical formula	C42 H24 Cl8 O4 Sb2	C62 H70 Cl8 F N O5 Sb2
Formula weight	1119.71	1455.29
Temperature	110(2) K	110(2) K
Wavelength	0.71073 Å	0.71073 Å
Crystal system	Monoclinic	Triclinic
Space group	P 21/n	P -1
Unit cell dimensions	a = 11.2471(19) Å	a = 11.3958(18) Å
	b = 19.236(3) Å	b = 12.849(2) Å
	c = 18.633(3) Å	c = 21.497(3) Å
	α = 90°	α = 95.435(2)°
	β = 92.575(2)°	β = 90.868(2)°
	γ = 90°	γ = 91.812(2)°
Volume	4027.2(11) $Å^3$	3131.5(8) $Å^3$
Z	4	2
Density (calculated)	1.847 Mg/m^3	1.543 Mg/m^3
Absorption coefficient	1.916 mm^{-1}	1.255 mm^{-1}
F(000)	2184	1472
Crystal size	0.21 x 0.18 x 0.13 mm^3	0.24 x 0.22 x 0.16 mm^3
Theta range for data collection	2.075 to 28.394°	1.593 to 28.214°
Index ranges	-15<=h<=15, -25<=k<=25, -24<=l<=24	-15<=h<=15, -16<=k<=17, -28<=l<=27
Reflections collected	48182	37055
Independent reflections	10017 [R(int) = 0.0502]	14742 [R(int) = 0.0261]
Absorption correction	Semi-empirical from equivalents	Semi-empirical from equivalents
Max. and min. transmission	0.857 and 0.676	0.921 and 0.759
Refinement method	Full-matrix least-squares on F^2	Full-matrix least-squares on F^2
Data / restraints / parameters	10017 / 0 / 505	14742 / 0 / 717
Goodness-of-fit on F^2	1.05	1.047
Final R indices [I>2sigma(I)]	R1 = 0.0321, wR2 = 0.0663	R1 = 0.0327, wR2 = 0.0677
R indices (all data)	R1 = 0.0414, wR2 = 0.0693	R1 = 0.0441, wR2 = 0.0732
Largest diff. peak and hole	0.828 and -0.469 e.$Å^{-3}$	2.218 and -1.203 e.$Å^{-3}$

[a] $R1 = \Sigma||Fo| - |Fc||/\Sigma|Fo|$. [b] $wR2 = \{[\Sigma w(Fo^2 - Fc^2)^2]/[\Sigma w(Fo^2)^2]\}^{1/2}$.

Table 21. Crystal data, data collection, and structure refinement for **66** and **67**.

Crystal data	**66**	**67**
Empirical formula	C32 H15 F8 O2 Sb	C60.50 H29.03 Cl6 F16 O4 Sb2
Formula weight	705.19	1580.07
Temperature	110(2) K	110(2) K
Wavelength	0.71073 Å	0.71073 Å
Crystal system	Triclinic	Triclinic
Space group	P -1	P -1
Unit cell dimensions	a = 8.8626(12) Å	a = 10.646(10) Å
	b = 11.4164(15) Å	b = 12.039(12) Å
	c = 12.8227(17) Å	c = 22.80(2) Å
	a= 96.740(2)°	α = 88.953(12)°
	b= 92.201(2)°	β = 89.387(11)°
	g = 91.203(2)°	γ = 81.840(11)°
Volume	1287.0(3) $Å^3$	2892(5) $Å^3$
Z	2	2
Density (calculated)	1.820 Mg/m^3	1.815 Mg/m^3
Absorption coefficient	1.161 mm^{-1}	1.312 mm^{-1}
F(000)	692	1544
Crystal size	0.196 x 0.168 x 0.128 mm^3	0.254 x 0.133 x 0.032 mm^3
Theta range for data collection	1.600 to 28.500°	1.709 to 28.384°
Index ranges	-11<=h<=11, -15<=k<=15, -17<=l<=17	-14<=h<=13, -15<=k<=16, -29<=l<=30
Reflections collected	15233	34288
Independent reflections	6382 [R(int) = 0.0195]	13683 [R(int) = 0.0348]
Absorption correction	Semi-empirical from equivalents	Semi-empirical from equivalents
Max. and min. transmission	0.836 and 0.724	0.852 and 0.817
Refinement method	Full-matrix least-squares on F^2	Full-matrix least-squares on F^2
Data / restraints / parameters	6382 / 0 / 388	13683 / 0 / 840
Goodness-of-fit on F^2	1.057	1.029
Final R indices [I>2sigma(I)]	R1 = 0.0228, wR2 = 0.0558	R1 = 0.0331, wR2 = 0.0722
R indices (all data)	R1 = 0.0253, wR2 = 0.0571	R1 = 0.0445, wR2 = 0.0784
Largest diff. peak and hole	0.924 and -0.854 e.$Å^{-3}$	1.561 and -0.642 e.$Å^{-3}$

[a] $R1 = \Sigma||Fo| - |Fc||/\Sigma|Fo|$. [b] $wR2 = \{[\Sigma w(Fo^2 - Fc^2)^2]/[\Sigma w(Fo^2)^2]\}^{1/2}$.

Table 22. Crystal data, data collection, and structure refinement for TBA[**67**-μ_2-F].

Crystal data	TBA[**67**-μ_2-F]
Empirical formula	C74 H60 F17 N O4 Sb2
Formula weight	1593.73
Temperature	110(2) K
Wavelength	0.71073 Å
Crystal system	Monoclinic
Space group	C 2/c
Unit cell dimensions	a = 43.782(13) Å
	b = 12.384(3) Å
	c = 24.941(7) Å
	α = 90°
	β = 96.702(6)°
	γ = 90°
Volume	13431(6) Å^3
Z	8
Density (calculated)	1.576 Mg/m^3
Absorption coefficient	0.903 mm^{-1}
F(000)	6384
Crystal size	0.183 x 0.164 x 0.126 mm^3
Theta range for data collection	1.644 to 26.394°
Index ranges	-54<=h<=53, -15<=k<=15, -30<=l<=31
Reflections collected	64060
Independent reflections	13691 [R(int) = 0.0557]
Max. and min. transmission	Semi-empirical from equivalents
Refinement method	0.872 and 0.780
Data / restraints / parameters	Full-matrix least-squares on F^2
Goodness-of-fit on F^2	13691 / 4988 / 1421
Final R indices [I>2sigma(I)]	1.049
R indices (all data)	R1 = 0.0580, wR2 = 0.1713
Absolute structure parameter	R1 = 0.0857, wR2 = 0.1940
Largest diff. peak and hole	2.421 and -0.723 e.Å^{-3}

[a] $R1 = \Sigma||Fo| - |Fc||/\Sigma|Fo|$. [b] $wR2 = \{[\Sigma w(Fo^2 - Fc^2)^2]/[\Sigma w(Fo^2)^2]\}^{1/2}$.

Synthesis of 47. A CH_2Cl_2 solution (3 mL) of *o*-chloranil (30 mg, 1.2×10^{-4} mol) was added to a stirred CH_2Cl_2 solution (5 mL) of **46** (84 mg, 1.2×10^{-4} mol) dropwise at ambient temperature. After 30 min, the solvent was removed *in vacuo* and the residue was washed with two portions of MeOH (5 mL each) to afford **47** as a yellow solid in 92 % yield. Pale yellow single crystals of **47** suitable for X-ray diffraction analysis were obtained by diffusing pentane into a saturated toluene solution at ambient temperature. ^{1}H NMR (399.508 MHz, $CDCl_3$): δ 8.00-7.96 (m, naphthalene, 2H), 7.85 (pseudo d, 2H, *o-Ph*, $^3J_{H\text{-}H}$ = 8.0 Hz), 7.63-7.55 (m, 4H, naphthalene), 7.47-7.30 (m, 10H, naphthalene + *Ph*), 7.23-7.16 (m, 4H, *Ph*), 7.03 (pseudo t, 2H, *p-Ph*, $^3J_{H\text{-}H}$ = 8.0 Hz), 6.94 (pseudo d, 2H, *o-Ph*, $^3J_{H\text{-}H}$ = 8.0 Hz), 6.59 (pseudo d, 2H, *o-Ph*, $^3J_{H\text{-}H}$ = 8.0 Hz). Aryl region of ^{1}H NMR spectrum of **47** is shown in Figure 128.

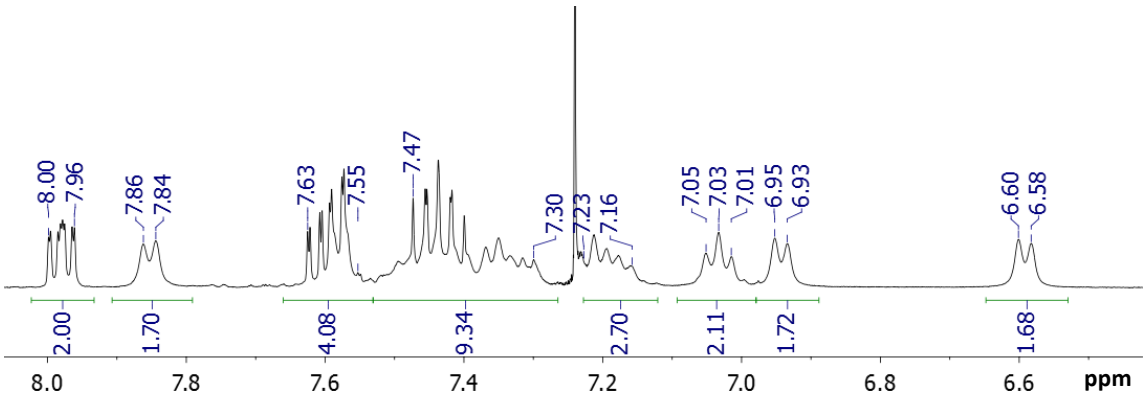

Figure 128. Aryl region of ^{1}H NMR spectrum of **47**.

Synthesis of 48. A MeOH solution (3 mL) of $CuBr_2$ (34 mg, 1.5×10^{-4} mol) was added to a stirred CH_2Cl_2 solution (5 mL) of **46** (104 mg, 1.5×10^{-4} mol) dropwise at

-78 °C. After 30 min, the mixture was gradually warmed up to ambient temperature and additionally stirred for an hour. The solvent was then removed *in vacuo* and 10 mL of CH_2Cl_2 was added to the residue to afford a white suspension. The suspension was over Celite and the remaining solid was washed with two portions of CH_2Cl_2 (3 mL each). After removing the solvent under vacuum and washing the residue with two portions of pentane (3 mL each), **48** was isolated as an off-white solid in 88 % yield. ^{1}H NMR (399.508 MHz, $CDCl_3$): δ 8.38 (d, 2H, *o*-Sb*Ph*, $^3J_{H\text{-}H}$ = 6.4 Hz), 8.34-8.31 (m, 2H, naphthalene), 7.94-7.85 (m, 4H, naphthalene), 7.78 (d, 4H, *o*-Sb*Ph*, $^3J_{H\text{-}H}$ = 6.4 Hz), 7.56-7.53 (m, 3H, naphthalene + *m*-Sb*Ph*), 7.49-7.42 (m, 6H, naphthalene + *p*-Sb*Ph*), 7.32 (t, 2H, *p*-Sb*Ph*, $^3J_{H\text{-}H}$ = 6.0 Hz), 7.26 (t, 4H, *m*-Sb*Ph*, $^3J_{H\text{-}H}$ = 6.0 Hz).

Synthesis of 49. Compound **49** was prepared using a similar method to synthesize **48**. A CH_2Cl_2 solution (3 mL) of $PhICl_2$ (36 mg, 1.3×10^{-4} mol) was added to a stirred CH_2Cl_2 solution (5 mL) of **46** (88 mg, 1.3×10^{-4} mol) dropwise at ambient temperature. After 30 min, the solvent was removed *in vacuo* and the residue was washed with two portions of pentane (5 mL each) to afford **49** as an off-white solid in 90 % yield (87 mg, 1.2×10^{-4} mol). Colorless single crystals of **49** suitable for X-ray diffraction analysis were obtained by layering pentane into a saturated CH_2Cl_2 solution at ambient temperature. ^{1}H NMR (399.508 MHz, $CDCl_3$): δ 8.40 (d, 2H, *o*-Sb*Ph*, $^3J_{H\text{-}H}$ = 7.2 Hz), 8.10-8.07 (m, 2H, naphthalene), 7.90-7.87 (m, 4H, naphthalene), 7.83 (t, 2H, *p*-Sb*Ph*, $^3J_{H\text{-}H}$ = 7.2 Hz), 7.70 (d, 1H, naphthalene, $^3J_{H\text{-}H}$ = 7.2 Hz), 7.49-7.20 (m, 13H, overlap with $CDCl_3$ signal). $^{13}C\{^1H\}$ NMR (125.60 MHz, $CDCl_3$): δ 157.53 (*Ph* quaternary), 156.99 (*Ph* quaternary), 141.30 (*Ph* quaternary), 140.52, 139.82 (naphthalene quaternary),

138.01, 137.89 (*o*-Sb(III)*Ph*), 136.26 (*o*-Sb(V)*Ph*^{a}), 135.98, 135.81 (naphthalene quaternary), 135.49 (*o*-Sb(V)*Ph*^{b}), 135.21, 132.90 (*p*-Sb(III)*Ph*), 132.59, 132.54, 131.16, 131.01, 130.93, 130.27, 129.20 (*p*-Sb(V)*Ph*^{a}), 129.16 (*p*-Sb(V)*Ph*^{b}), 129.00 (*m*-Sb(III)*Ph*), 129.98 (*m*-Sb(V)*Ph*^{a}), 128.81 (*m*-Sb(V)*Ph*^{b}), 128.33, 126.74, 125.08. Elemental analysis calculated (%) for $C_{26}H_{28}Cl_4Sb_2$: C, 49.81; H, 3.20; found C, 50.43; H, 3.25.

Synthesis of 50. A MeOH solution (3 mL) of KF (16 mg, 2.8×10^{-4} mol) was added to a stirred CH_2Cl_2 solution (5 mL) of **49** (53 mg, 7.1×10^{-5} mol) dropwise at ambient temperature. After 30 min, the solvent was removed *in vacuo* and 10 mL of CH_2Cl_2 was added to the residue to afford a white suspension. The suspension was over Celite and the remaining solid was washed with two portions of CH_2Cl_2 (3 mL each). After removing the solvent under vacuum and washing the residue with two portions of pentane (3 mL each), **50** was isolated as an off-white solid in 88 % yield. Single crystals of **50** suitable for X-ray diffraction analysis were obtained by slowly diffusing pentane into a THF solution at ambient temperature. ^{1}H NMR (399.508 MHz, $CDCl_3$): δ 8.22 (d, 1H, naphthalene, $^{3}J_{H\text{-}H}$ = 7.2 Hz), 8.05-8.02 (m, 4H, naphthalene), 7.92 (d, 1H, naphthalene, $^{3}J_{H\text{-}H}$ = 8.0 Hz), 7.85 (d, 1H, naphthalene, $^{3}J_{H\text{-}H}$ = 7.6 Hz), 7.77 (d, 1H, naphthalene, $^{3}J_{H\text{-}H}$ = 8.0 Hz), 7.47-7.33 (m, 8H, naphthalene + Sb*Ph*), 7.28-7.18 (m, 8H; overlap with $CDCl_3$ signal). $^{13}C\{^{1}H\}$ NMR (125.60 MHz, $CDCl_3$): δ 140.20 (naphthalene), 139.89 (Sb(III)*Ph* quaternary), 139.11 (quaternary), 137.54 (t, Sb(V)*Ph* quaternary, $^{2}J_{C\text{-}F}$ = 3.8 Hz), 136.26, 135.84 (*o*-Sb(III)*Ph*), 135.76 (naphthalene), 134.40 (t, *o*-Sb(V)*Ph*, $^{2}J_{C\text{-}F}$ = 5.4 Hz), 133.53 (naphthalene), 131.31 (*p*-Sb(III)*Ph*), 130.79

(naphthalene), 129.51 (*m*-Sb(V)*Ph*), 128.80 (naphthalene), 128.71 (*m*-Sb(III)*Ph*), 128.38 (*p*-Sb(V)*Ph*), 126.64 (naphthalene), 125.03 (naphthalene). ^{19}F NMR (375.84 MHz, $CDCl_3$): δ -136.2. Elemental analysis calculated (%) for $C_{26}H_{28}F_4Sb_2$: C, 57.03; H, 3.66; found C, 57.24; H, 3.69.

Synthesis of 56. A solution of Ph_2SbCl (1.991 g, 6.4×10^{-3} mol) in THF (10 mL) was added to a solution of 1,1'-dilithioferrocene·tmeda (1.0040 g, 3.2×10^{-3} mol) in Et_2O (5 mL)/THF (5 mL) at -78 °C. After stirring at this temperature for 30 min, the cooling bath was removed and the solution was gradually warmed up to ambient temperature. After stirring for another 12 h, the solvent was removed *in vacuo* and 20 mL of CH_2Cl_2 was added to the residue. The resulting mixture was filtered over Celite and the filtrate was concentrated *in vacuo* to obtain an orange oil. The residue was washed with MeOH (10 mL) to obtain pure **56** as an orange solid in 64 % yield (1.5055 g, 2.0×10^{-3} mol). Orange single crystals of **56** sufficient for X-ray crystallography were obtained by layering MeOH to a $CDCl_3$ solution at ambient temperature. ^{1}H NMR (399.508 MHz, $CDCl_3$): δ 7.47-7.45 (m, 8H, *o*-C_6H_5), 7.32-7.28 (m, 12H, *m*- and *p*-C_6H_5), 4.22 (pseudo t, 4H, Cp-*H*, $^3J_{H\text{-}H}$ = 1.5 Hz), 4.00 (pseudo t, 4H, Cp-*H*, $^3J_{H\text{-}H}$ = 1.5 Hz). $^{13}C\{^1H\}$ NMR (125.60 MHz, $CDCl_3$): δ 138.76 (Sb*Ph* quaternary), 136.35 (*o*-Sb*Ph*), 128.79 (*m*-Sb*Ph*), 128.62 (*p*-Sb*Ph*), 75.11 (Cp), 71.98 (Cp), 69.45 (Cp quaternary). Elemental analysis calculated (%) for $C_{34}H_{28}FeSb_2$: C, 55.49; H, 3.83; found C, 55.56; H, 3.88.

Synthesis of 57. A CH_2Cl_2 solution (5 mL) of *o*-chloranil (246 mg, 5.3×10^{-4} mol) was added dropwise to a stirred CH_2Cl_2 solution of **56** (196 mg, 2.7×10^{-4} mol) in a vial at ambient temperature. After stirring with 3 h, the solvent was removed under

vacuum and MeOH (10 mL) was added to the residue. The orange solid was collected by filtration and washed with two portions of MeOH (5 mL) to afford pure **57** in 82 % yield (267 mg, 2.2×10^{-4} mol). Single crystals of base-free **57** were obtained as orange blocks by layering hexanes onto a CH_2Cl_2 solution at ambient temperature. Single crystals of THF-coordinated **57** (**57**-$(THF)_2$) were obtained as orange blocks by layering hexanes onto a THF solution at ambient temperature. ^{1}H NMR (399.508 MHz, $CDCl_3$): δ 7.76 (pseudo d, 8H, *o*-C_6H_5, $^3J_{H\text{-}H}$ = 8.0), 7.58-7.49 (m, 12H, *m*- and *p*-C_6H_5), 4.41 (s, 4H, Cp-*H*), 4.33 (s, 4H, Cp-*H*). $^{13}C\{^1H\}$ NMR (125.60 MHz, $CDCl_3$): δ 144.25 (*o*-chloranil), 136.00 (*Ph* quaternary), 134.64 (*o*-Sb*Ph*), 132.06 (*p*-Sb*Ph*), 129.61 (*m*-Sb*Ph*), 120.55 (*o*-chloranil), 116.36 (*o*-chloranil), 75.56 (Cp), 73.76 (Cp), 72.20 (quaternary Cp). Elemental analysis calculated (%) for $C_{46}H_{28}Cl_8FeO_4Sb_2$: C, 45.00; H, 2.30; found C, 45.43; H, 2.33.

Synthesis of 58. A hexanes solution (3 mL) of Br_2 (40 mg, 5.0×10^{-4} mol) was added dropwise to a stirred hexanes suspension of **56** (184 mg, 2.5×10^{-4} mol) in a vial at ambient temperature. After 30 min, the orange solid was collected by filtration and washed with two portions of pentane (5 mL) to afford pure **58** in 98 % yield (259 mg, 2.4×10^{-4} mol). Single crystals of **58** were obtained as orange blocks by diffusing hexanes into a toluene solution at ambient temperature. ^{1}H NMR (399.508 MHz, $CDCl_3$): δ 8.20-8.17 (m, 8H, *o*-C_6H_5), 7.57-7.52 (m, 12H, *m*- and *p*-C_6H_5), 5.34 (s, 4H, Cp-*H*), 4.54 (s, 4H, Cp-*H*). $^{13}C\{^1H\}$ NMR (125.60 MHz, $CDCl_3$): δ142.62 (*Ph* quaternary), 133.39 (*o*-Sb*Ph*), 131.59 (*p*-Sb*Ph*), 129.49 (*m*-Sb*Ph*), 80.89 (*Ph* quaternary), 76.91 (Cp), 74.91 (Cp). Elemental analysis calculated (%) for $C_{34}H_{28}Br_4FeSb_2$: C, 38.69; H, 2.67; found C, 39.02; H, 2.71.

Synthesis of 59. A CH_2Cl_2 solution (5 mL) of $PhICl_2$ (82 mg, 3.0×10^{-4} mol) was added dropwise to a stirred CH_2Cl_2 solution of **56** (110 mg, 1.5×10^{-4} mol) in a vial at ambient temperature. After 30 min, the solvent was removed *in vacuo* and the residue was washed with pentane (5 mL). The orange solid was collected by filtration and washed with two portions of pentane (5 mL) to afford pure **59** in 96 % yield (116 mg, 1.3×10^{-4} mol). Single crystals of **59** were obtained as orange blocks by diffusing hexanes into a toluene solution at ambient temperature. ^{1}H NMR (399.508 MHz, $CDCl_3$): δ 8.28-8.20 (m, 8H, *o*-C_6H_5), 7.59-7.51 (m, 12H, *m*- and *p*-C_6H_5), 5.17 (pseudo t, 4H, Cp-*H*, $^3J_{H\text{-}H}$ = 4.0 Hz), 4.44 (pseudo t, 4H, Cp-*H*, $^3J_{H\text{-}H}$ = 4.0 Hz). $^{13}C\{^1H\}$ NMR (125.60 MHz, $CDCl_3$): δ 140.70 (*Ph* quaternary), 131.75 (*o*-Sb*Ph*), 131.52 (*p*-Sb*Ph*), 129.35 (*m*-Sb*Ph*), 80.23 (Cp quaternary), 76.28 (Cp), 74.61 (Cp).

Synthesis of [60][OTf]$_2$. MeOTf (0.15 mL, 1.3×10^{-3} mol) was added to a solution of 3 in toluene (3 mL). The mixture was sealed under N_2 atmosphere in a 25 mL Schlenk tube and heated to 90 ºC for 12 hours, after which an orange precipitate formed. The solid was filtered, washed with Et_2O (3 × 5 mL), and dried *in vacuo* to afford [**60**][OTf]$_2$ in 48 % yield (172 mg, 1.6×10^{-4} mol). Single crystals of [**60**][OTf]$_2$ were obtained as orange blocks by slow diffusion of Et_2O to a $CDCl_3$ solution at ambient temperature. ^{1}H NMR (399.508 MHz, $CDCl_3$): δ 7.67-7.56 (m, 20H, Sb-C_6H_5), 4.74 (s, 4H, Cp-*H*), 4.44 (s, 4H, Cp-*H*), 2.56 (s, 6H, Sb-CH_3). $^{13}C\{^1H\}$ NMR (125.60 MHz, $CDCl_3$): δ 134.81 (*o*-Sb*Ph*), 133.18 (*p*-Sb*Ph*), 130.74 (*m*-Sb*Ph*), 125.10 (*Ph* quaternary), 120.8 (q; $CF_3SO_3^-$), 75.15 (Cp), 74.52 (Cp), 63.50 (Cp quaternary), 3.91 (Sb-CH_3). $^{19}F\{^1H\}$ NMR (375.86 MHz, $CDCl_3$): δ -78.5 ($CF_3SO_3^-$). Elemental analysis calculated

(%) for $C_{38}H_{34}F_6FeO_6S_2Sb_2$: C, 42.89; H, 3.22; found C, 42.72; H, 3.29. The purity of [**60**][OTf]$_2$ was confirmed by NMR spectroscopy. Both ^{1}H and ^{13}C{^{1}H} NMR spectra are shown in Figure 129 as a measure of purity prior to catalysis studies.

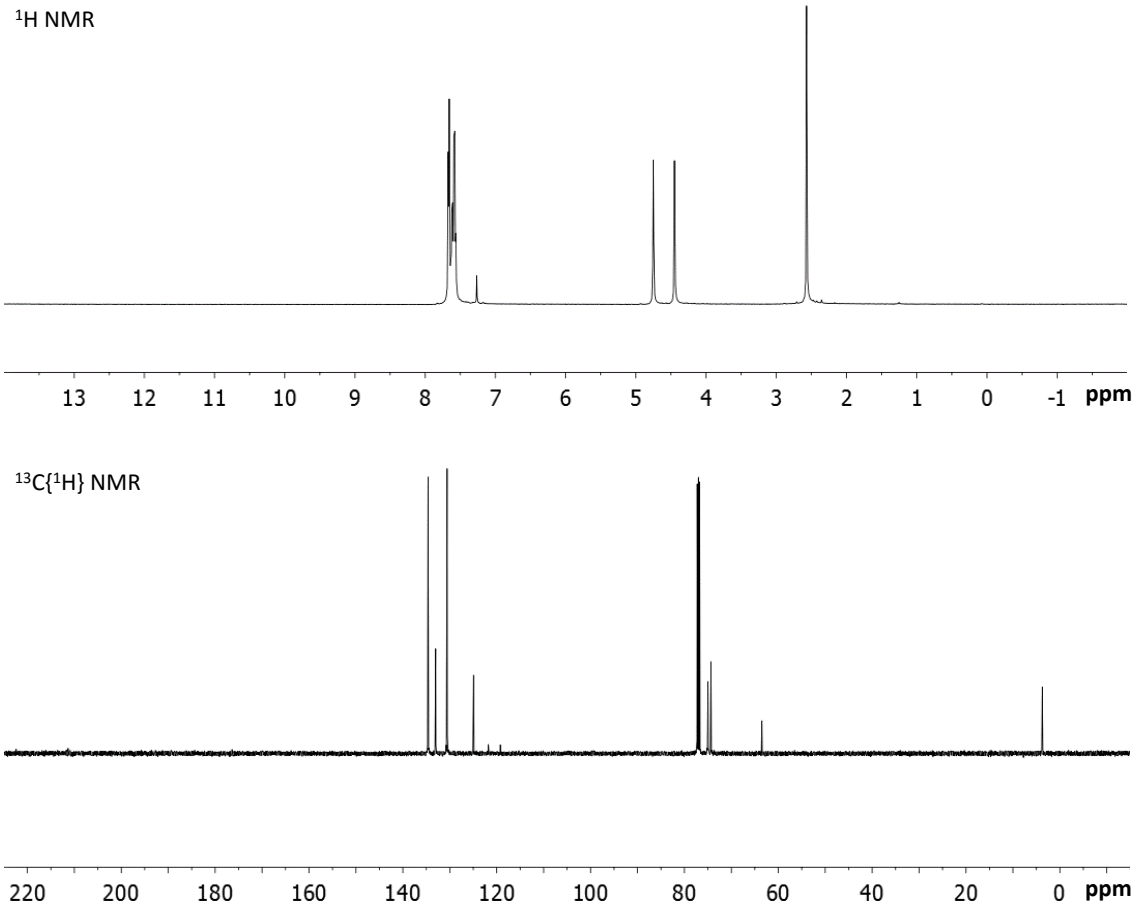

Figure 129. ^{1}H and ^{13}C{^{1}H} NMR spectra of [**60**][OTf]$_2$ in $CDCl_3$.

Synthesis of **63**. In a glovebox, a 50 mL Schlenk flask was charged with 4,6-dilithiodibenzofuran·1.5 tmeda (200 mg, 5.6×10^{-4} mol). The flask was transferred to a Schlenk line and Et_2O (5 mL) was added. The resulting suspension was cooled down to -

78 ºC and a Et_2O (5 mL) suspension of Ph_2SbCl (352 mg, 1.1×10^{-3} mol) was slowly added via cannula. After stirring at -78 ºC for 30 min, the cooling bath was removed and the reaction mixture was gradually warmed up to ambient temperature and stirred for another 6 h. The solvent was removed *in vacuo*, CH_2Cl_2 (10 mL) was added to the residue, and the suspension was filtered through Celite to remove LiCl. The solvent was once again removed under vacuum and MeOH (5 mL) was added to afford a white solid which was collected via filtration. After drying under vacuum, pure **63** was isolated as a white solid. Single crystals of **63** were obtained as colorless blocks by diffusing pentane into a saturated THF solution. ^{1}H NMR (399.508 MHz, $CDCl_3$): δ 7.91 (dd, 2H, dibenzofuran, $^3J_{H\text{-}H}$ = 4.0 Hz and 3.2 Hz), 7.47-7.40 (m, 8H, *m*-Sb*Ph*), 7.32-7.17 (m, 14H, dibenzofuran + *o*- and *p*-Sb*Ph*). ^{13}C{^{1}H} NMR (125.60 MHz, $CDCl_3$): δ 160.15 (*Ph* quaternary), 137.30 (dibenzofuran), 136.42 (*o*-Sb*Ph*), 134.17 (dibenzofuran), 128.79 (*m*-Sb*Ph*), 128.57 (*p*-Sb*Ph*), 123.61 (dibenzofuran), 123.06 quaternary dibenzofuran), 121.42 (dibenzofuran), 120.30 (quaternary dibenzofuran). Elemental analysis calculated (%) for $C_{36}H_{26}OSb_2$: C, 60.21; H, 3.65; found C, 60.72; H, 3.68.

Synthesis of 64. A CH_2Cl_2 (3 mL) solution of *o*-chloranil (68 mg, 2.8×10^{-4} mol) was slowly added to a stirred CH_2Cl_2 (5 mL) solution of **63** (101 mg, 1.4×10^{-4} mol) in a vial at ambient temperature. After stirring for 2 h, the solvent was removed *in vacuo* and MeOH (5 mL) was added to afford a pale yellow suspension. The solvent was filtered off and the residue was washed with two portions of MeOH (3 mL each) and dried under vacuum to afford pure **64** as a yellow solid in 95 % yield (160 mg, 1.3×10^{-4} mol). Single crystals of **64** coordinating a THF molecule (**64**-THF) has been obtained as pale yellow

crystals by diffusing pentane into a THF solution at ambient temperature. ^{1}H NMR (399.508 MHz, $CDCl_3$): δ 8.24 (d, 2H, dibenzofuran, $^{3}J_{H\text{-}H}$ = 8.0 Hz), 7.68 (d, 2H, dibenzofuran, $^{3}J_{H\text{-}H}$ = 4.0 Hz), 7.54 (t, 2H, dibenzofuran, $^{3}J_{H\text{-}H}$ = 4.0 Hz), 7.47-7.44 (m, 8H), 7.29-7.21 (m, 10H; overlap with $CDCl_3$ signal). $^{13}C\{^{1}H\}$ NMR (125.60 MHz, $CDCl_3$): δ 157.90 (*o*-chloranil), 144.17 (*o*-chloranil), 134.36 (*o*-Sb*Ph*), 133.90 (*Ph* quaternary), 133.51 (*o*-chloranil), 132.22 (*p*-Sb*Ph*), 129.57 (*m*-Sb*Ph*), 124.47 (dibenzofuran), 124.25 (dibenzofuran), 124.12 (dibenzofuran), 120.57 (dibenzofuran), 120.21 (dibenzofuran), 116.42 (dibenzofuran). Elemental analysis calculated (%) for $C_{48}H_{26}Cl_8O_5Sb_2$: C, 47.65; H, 2.17; found C, 48.02; H, 2.21.

Synthesis of *ortho*-bis(diphenylstibino)benzene. This distibine compound was prepared by a modified procedure reported by our group[114] and Murray.[274] A 50 mL Schlenk flask was charged with (2-bromophenyl)diphenylstibine (1.1145 g, 2.6 mmol) and Et_2O (15 mL). The solution was cooled down to -78 ºC and 1.5 M tBuLi in pentane (3.4 mL, 5.2 mmol) was added dropwise in the course of 10 min. After an hour, a white solid precipitated out of solution which corresponds to the Li salt. The solvent was decanted via filter cannulation and the Li salt was washed with Et_2O (5 mL each) at -78 ºC. The residue was suspended in Et_2O (10 mL) and cooled down to -78 ºC. A THF solution (10 mL) of Ph_2SbCl (0.8035 g, 2.6 mmol) was added dropwise to this suspension using a plastic syringe in which the solid fully dissolved in solution. After stirring at -78 ºC for an hour, the reaction mixture was removed from the cooling bath and gradually warmed up to ambient temperature and stirred overnight. After adding a drop of water, the solvent was removed *in vacuo* and CH_2Cl_2 (10 mL) was added and dried with

anhydrous $MgSO_4$. The suspension was filter over Celite to remove LiCl and $MgSO_4$ and the residue was successively washed with two portions of CH_2Cl_2 (5 mL each). The filtrate was collected and the solvent was removed *in vacuo* to afford a pale yellow oil. After washing the oil with MeOH (10 mL), *ortho*-bis(diphenylstibino)benzene was isolated as a white powder in 48 % yield (0.7838 g, 1.2 mmol). The product was confirmed by ^{1}H NMR spectroscopy.

Synthesis of **65**. A CH_2Cl_2 solution (5 mL) of *o*-chloranil (118 mg, 4.8×10^{-4} mol) was added dropwise to a stirred CH_2Cl_2 solution of *ortho*-bis(diphenylstibino)benzene (151 mg, 2.4×10^{-4} mol) in a vial. After 3 h, a pale yellow suspension formed. The solvent was removed under vacuum and MeOH (10 mL) was added to the residue. The pale yellow solid was collected by filtration and washed with two portions of MeOH (5 mL) to afford pure **65** in 90 % yield (242 mg, 2.2×10^{-4} mol). Single crystals of **65** were obtained as yellow blocks by slowly diffusing pentane into a THF solution at ambient temperature. ^{1}H NMR (399.508 MHz, $CDCl_3$): δ 7.72 (broad s, 8H, Sb*Ph*), 7.57-7.46 (m, 16H). $^{13}C\{^1H\}$ NMR (125.60 MHz, $CDCl_3$): δ 145.06 (*o*-chloranil), 143.52 (*o*-chloranil), 135.29 (*o*-phenylene), 134.95 (broad, *o*-Sb*Ph*), 133.74 (*Ph* quaternary), 132.35 (broad, *p*-Sb*Ph*), 131.74 (*o*-chloranil), 130.46 (*o*-phenylene), 129.58 (*m*-Sb*Ph*), 129.18 (*o*-phenylene quaternary). Elemental analysis calculated (%) for $C_{42}H_{24}Cl_8O_4Sb_2$: C, 45.05; H, 2.16; found C, 44.78; H, 2.13. The ^{1}H and $^{13}C\{^1H\}$ NMR spectra of 65 are shown in Figure 130 as a measure of purity.

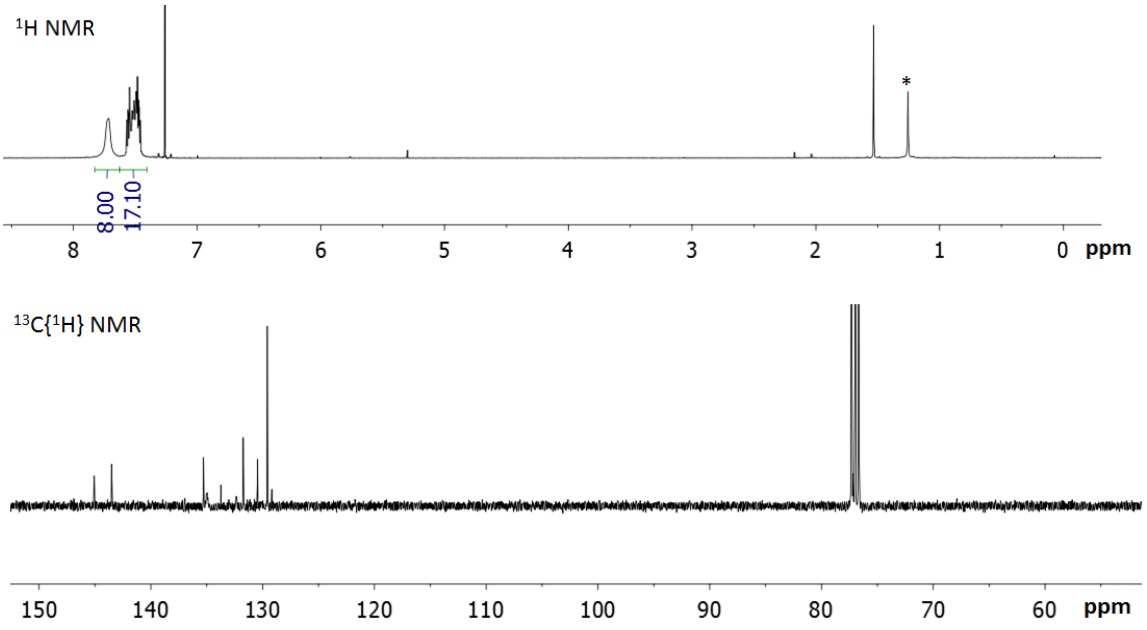

Figure 130. ^{1}H and ^{13}C{^{1}H} NMR spectra of **65**. The resonance marked as "*" is solvent impurity from $CDCl_3$.

Synthesis of TBA[65-μ_2-F]. In a glovebox, a vial was charged with **65** (64.4 mg, 5.8× 10^{-5} mol) and CH_2Cl_2 solution (3 mL). A CH_2Cl_2 solution of TBAT was added to this mixture and stirred for 10 min. After removing the solvent *in vacuo*, the residue was washed with Et_2O (3 mL) and the white solid was collected by filtration. The white solid was dried under vacuum to afford pure TBA[**65**-μ_2-F] in 78 % yield (62.0 mg, 4.5 × 10^{-5} mol). Single crystals of TBA[**65**-μ_2-F] were obtained as colorless blocks by slowly diffusing pentane into a THF solution at ambient temperature. ^{1}H NMR (399.508 MHz, CD_3CN): δ 7.66 (pseudo d, 4H, m-Sb*Ph*), 7.52-7.25 (broad m, 20H), 3.05 (m, 8H, TBA-C*H*$_2$), 1.58 (broad, 8H, TBA-C*H*$_2$), 1.33 (m, 8H, TBA-C*H*$_2$), 0.95 (t, 12H, TBA-C*H*$_3$, $^{3}J_{H-H}$ = 7.5 Hz). ^{13}C{^{1}H} NMR (125.60 MHz, CD_3CN): δ 150.08 (d, SbPh quaternary, $^{2}J_{C-F}$ = 20.1 Hz), 146.11 (*o*-chloranil), 143.17 (d, *o*-chloranil, $^{3}J_{C-F}$ = 10.1 Hz), 141.49 (d, Sb-

bound *o*-phenylene quaternary, $^{2}J_{C\text{-}F}$ = 18.5 Hz), 135.22 (*o*-phenylene), 134.57 (*o*-Sb*Ph*^{a}), 134.02 (*o*-Sb*Ph*^{b}), 133.45 (*o*-chloranil), 129.99 (*p*-Sb*Ph*^{a}), 129.87 (*p*-Sb*Ph*^{b}), 129.59 (*o*-phenylene), 128.75 (*m*-Sb*Ph*^{a}), 128.34 (*m*-Sb*Ph*^{b}), 128.08 (*o*-phenylene), 58.33 (TBA), 23.29 (TBA), 19.24 (TBA), 12.70 (TBA). ^{19}F NMR (375.84 MHz, $CDCl_3$): δ -73.3. Elemental analysis calculated (%) for $C_{58}H_{60}Cl_8FNO_4Sb_2$: C, 45.05; H, 2.16; found C, 44.78; H, 2.13.

Synthesis of 1,2,3,4,5,6,7,8,9,10-decafluorophenanthrene. *The procedure written in the original manuscript is unclear with numerous typos in the text.*[315] *We developed an optimal condition that produce consistent results. This procedure uses $HgCl_2$ and needs to be treated with care.* A 100 mL Schlenk flask was charged with Cp_2TiCl_2 (0.312 g, 1.3 mmol), $HgCl_2$ (1.72 g, 6.4 mmol) and aluminum powder (1.74g, 64.5 mmol) and 30 mL of THF was added. A crystal of I_2 was subsequently added quickly and the mixture was degassed. The solution color turns from red to dark yellow within 15 min, an indication of the formation of activated low-valent "Cp_2Ti" complex. The flask was refilled with N_2 and neat perfluoro(tetradecahydrophenanthrene) (4.06 g, 6.5 mmol) was added via syringe over 5 min in which the temperature gradually raised. After stirring the mixture for 30 min and cooling it down to ambient temperature, the reaction mixture was degassed once again and the flask was refilled with fresh N_2. The resulting dark yellow slurry was periodically degassed (every 12 h) and refilled with N_2. After stirring for 3 days, the solution color turned to dark purple and the solvent was removed *in vacuo*. The residue was washed with three portions of Et_2O (20 mL each) and the solid was removed via filtration over Celite. The red filtrate was concentrated and was purified by

silica gel column chromatography using hexanes as an eluent to afford 1,2,3,4,5,6,7,8,9,10-decafluorophenanthrene as a colorless solid in 28 % yield (644 mg, 1.8 mmol). The product formation was confirmed by ^{19}F NMR spectroscopy. ^{19}F NMR (375.84 MHz, $CDCl_3$): δ -125.58 (m; 2F), -144.00 (m; 2F), -144.88 (m; 2F), -151.08 (m; 2F), -152.55 (m; 2F). The ^{19}F NMR spectrum is shown in Figure 131.

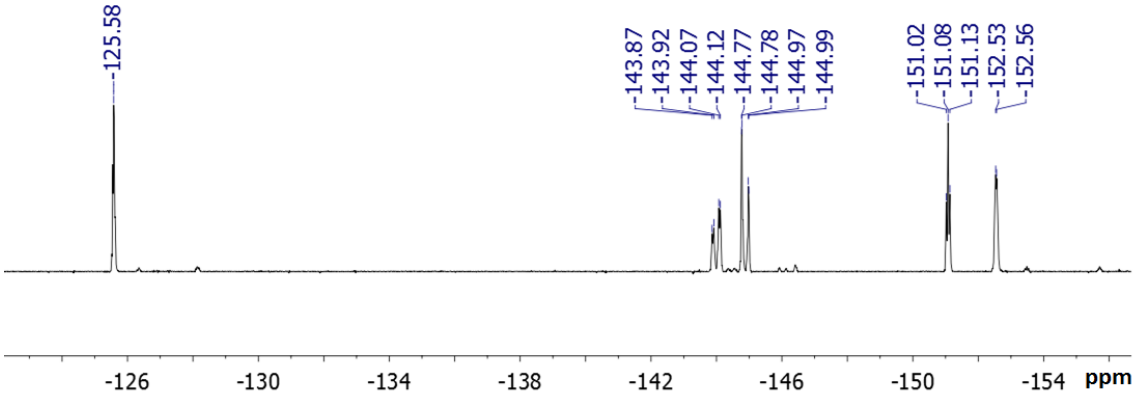

Figure 131. ^{19}F NMR spectrum of perfluorophenanthrene in $CDCl_3$.

Synthesis of octafluorophenthra-9,10-quinone. This compound was prepared by modifying the procedure reported in literature.[316] A 25 mL Schlenk tube was charged with 1,2,3,4,5,6,7,8,9,10-decafluorophenanthrene (500 mg, 1.4 mmol) and oleum (20-24 % SO_3; 10 mL) under N_2 atmosphere. The color immediately turned brown. The reaction was heated up to 100 °C and stirred for 3 h. The brown mixture was poured onto ice and transferred to a separation funnel. After adding Et_2O (50 mL), the biphasic mixture was shaken and the two layers were separated. The aqueous layer was extracted twice with of Et_2O (30 mL each). The organic solutions were combined, dried over anhydrous $MgSO_4$,

and filtered through Celite. The filtrate was concentrated and was purified by silica gel (40 g) column chromatography initially using 100 % hexanes for 10 min as the eluent and gradually changing the hexanes:CH_2Cl_2 ratio to 6:4 (by volume) across 20 min to afford octafluorophenthra-9,10-quinone as an intense yellow crystalline solid in 33 % yield (162 mg, 4.6×10^{-4} mol). The product formation was confirmed by ^{19}F NMR spectroscopy. ^{19}F NMR (375.84 MHz, $CDCl_3$): δ -125.40 (m; 2F), -133.26 (m; 2F), -139.61 (m; 2F), -148.03 (m; 2F). Note: this compound is air stable and insensitive to light and could be stored on the bench. The ^{19}F NMR spectrum is shown in Figure 132.

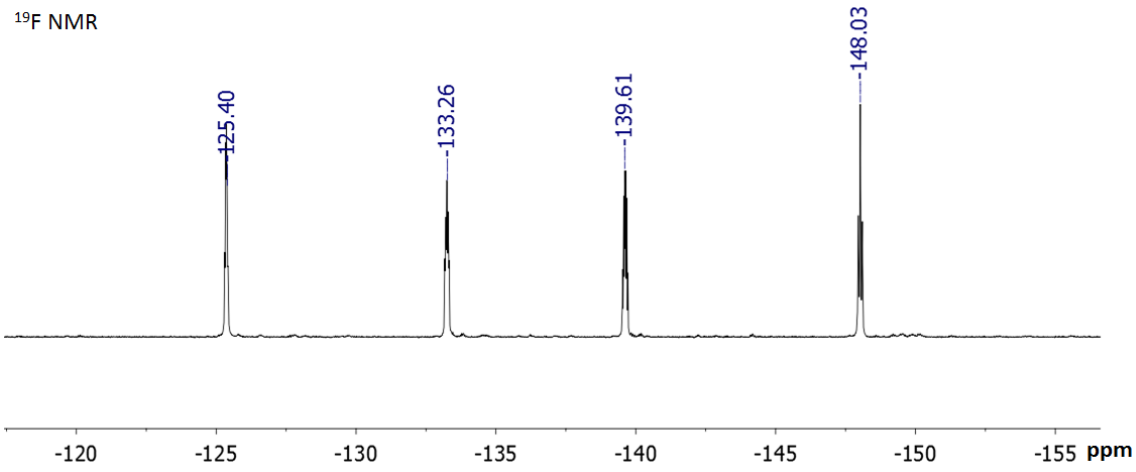

Figure 132. ^{19}F NMR spectrum of octafluorophenthra-9,10-quinone in $CDCl_3$.

Synthesis of 67. A Et_2O (3 mL) solution of *ortho*-bis(diphenylstibino)benzene (95 mg, 2.7×10^{-4} mol) was added to a CH_2Cl_2 (0.5 mL) solution of octafluorophenthra-9,10-quinone (83 mg, 1.3×10^{-4} mol) in a vial. After letting the mixture stand for 3 h at ambient temperature, yellow crystals formed, collected by filtration and dried *in vacuo* to obtain pure **67** in 81 % yield (143 mg, 2.7×10^{-4} mol). Single crystals of **67** were obtained as yellow blocks by letting a CH_2Cl_2 solution stand at 0 °C. ^{1}H NMR (399.508 MHz, $CDCl_3$): δ 7.67 (m, phenylene), 7.39 (broad s). $^{13}C\{^{1}H\}$ NMR (125.60 MHz, $CDCl_3$): δ 145.88 (Sb*Ph* quaternary), 135.86 (*o*-phenylene), 134.52 (*o*-Sb*Ph*), 131.54 (*o*-phenylene), 130.13 (*p*-Sb*Ph*), 129,29 (*m*-Sb*Ph*). The perfluorophenanthrenediyl-9,10-dioxy $^{13}C\{^{1}H\}$ NMR resonances could not be observed possibly due to broadening. ^{19}F NMR (375.84 MHz, $CDCl_3$): δ -129.3 (broad d, 4F, $^{3}J_{F\text{-}F}$ = 108.8 Hz), -142.90 (broad s, 2F), -146.41 (broad s, 2F), -156.91 (s, 4F), 160.74 (broad s). Elemental analysis calculated (%) for $C_{58}H_{24}F_{16}O_4Sb_2$: C, 52.29; H, 1.82; found C, 52.59; H, 1.86. ^{1}H, $^{13}C\{^{1}H\}$ and ^{19}F NMR spectra are shown in Figure 133.

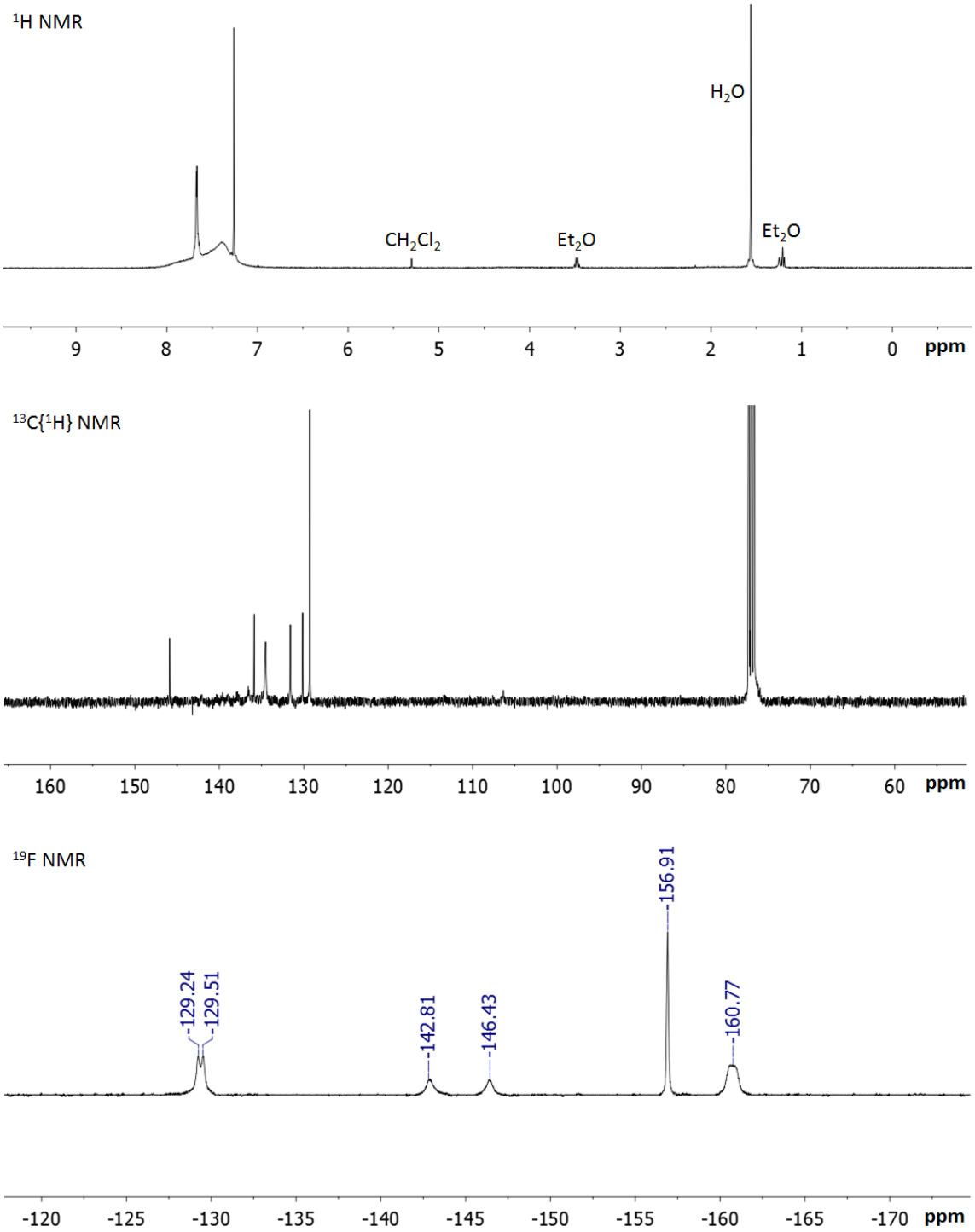

Figure 133. ^{1}H, $^{13}C\{^{1}H\}$ and ^{19}F NMR spectra of **67** in $CDCl_3$ at room temperature.

Synthesis of TBA[67-μ_2-F]. In a glovebox, a CH_2Cl_2 (2 mL) solution of TBAT (40 mg, 6.8×10^{-5} mol) was added to a CH_2Cl_2 (2 mL) solution of **67** (90 mg, 6.8×10^{-5} mol) in a vial. The reaction mixture was stirred for 15 min and the solvent was removed in vacuo. After successive washing of the residue with two portions of Et_2O (3 mL) each, pure TBA[**67**-μ_2-F] was isolated as a yellow solid in 66 % yield (78 mg, 4.9×10^{-5} mol). Single crystals of TBA[**67**-μ_2-F] suitable for X-ray diffraction analysis was obtained as yellow blocks by diffusing pentane into a saturated toluene solution at ambient temperature. ^{1}H NMR (399.508 MHz, $CDCl_3$): δ 7.66 (pseudo d, 4H, m-Sb*Ph*), 7.52-7.25 (broad m, 20H), 3.05 (m, 8H, TBA-C*H*$_2$), 1.58 (broad, 8H, TBA-C*H*$_2$), 1.33 (m, 8H, TBA-C*H*$_2$), 0.95 (t, 12H, TBA-C*H*$_3$, $^3J_{H\text{-}H}$ = 7.5 Hz,). $^{13}C\{^1H\}$ NMR (125.60 MHz, CD_3CN): δ 150.16, 150.00, 146.11, 143.31, 143.04, 141.56, 141.37, 135.22 (Sb*Ph* quaternary), 134.57 (*o*-Sb*Ph*), 134.02 (*o*-phenylene), 133.45, 129.99, 129.87 (*p*-Sb*Ph*), 129.59 (*o*-phenylene), 128.75 (*o*-phenylene), 128.34 (*m*-Sb*Ph*), 128.08 (*o*-phenylene), 58.33 (TBA), 23.29 (TBA), 19.24 (TBA), 12.70 (TBA). ^{19}F NMR (375.84 MHz, $CDCl_3$): δ -76.8 (s, 1F, bridging fluoride), -130.5 (pseudo t, 1F, $^3J_{F\text{-}F}$ = 15 Hz), -130.9 (pseudo t, 1F, $^3J_{F\text{-}F}$ = 15 Hz), -131.8 (pseudo t, 1F, $^3J_{F\text{-}F}$ = 15 Hz), -132.3 (pseudo t, 1F, $^3J_{F\text{-}F}$ = 15 Hz), -143.7 (pseudo q, 2F, $^3J_{F\text{-}F}$ = 23 Hz, $^3J_{F\text{-}F}$ = 11 Hz), -147.8 (pseudo q, 2F, $^3J_{F\text{-}F}$ = 23 Hz, $^3J_{F\text{-}F}$ = 11 Hz), -159.4 (t, 2F, $^3J_{F\text{-}F}$ = 23 Hz), -159.7 (t, 2F, $^3J_{F\text{-}F}$ = 23 Hz), -164.7 (t, 2F, $^3J_{F\text{-}F}$ = 23 Hz), -165.2 (t, 2F, $^3J_{F\text{-}F}$ = 23 Hz). Elemental analysis calculated (%) for $C_{74}H_{60}F_{17}NO_4Sb_2$: C, 55.77; H, 3.79; N, 0.88; found C, 56.03; H, 3.84; N, 0.90. ^{1}H, $^{13}C\{^1H\}$ and ^{19}F NMR spectra are shown in Figure 134.

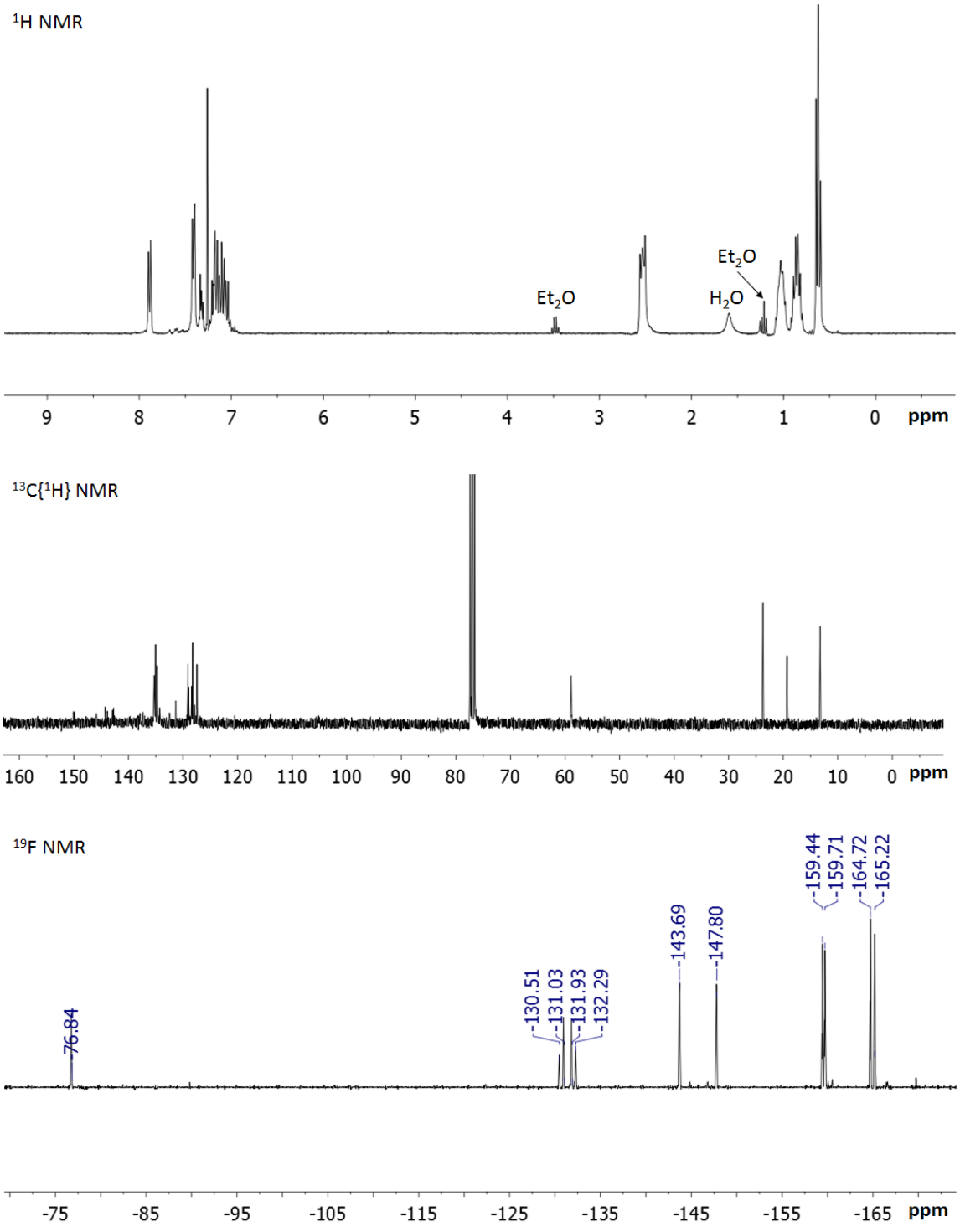

Figure 134. ^{1}H, $^{13}C\{^{1}H\}$ and ^{19}F NMR spectra of TBA[**67**-μ_2-F] in $CDCl_3$.

6.8 Future work

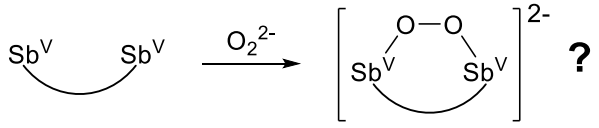

Figure 135. Proposed binding of peroxide by distiboranes

The application of bidentate Lewis acid is not limited to chelation of fluoride ions but also to stabilize larger anions as well as heteroatomic organic compounds. In particular, we are interested to bind and store peroxide because of the application in energy storage in fuel cells and Li-O_2 batteries.[320] Peroxides are also powerful oxidants that exhibit synthetically interesting reactivity derived from its inherently weak O-O bond.[321] While a number of group 13[322-332] and group 14[333, 334] Lewis acids have reported to form stable peroxide adducts, the use of group 15 acceptors, especially organoantimony(V) species,[335, 336] are significantly underdeveloped. Based on our early work, organoantimony(V) compounds are stable in the presence of peroxides which make them viable candidates to store such species. With this in mind, we propose to investigate the peroxide binding affinity of distiborane compounds. Peroxide dianions can be generated *in situ* by comproportionation of superoxide in DMF. Alternatively, reduction of dioxygen with decamethylferrocene can be accelerated in the presence of Lewis acids to generate peroxide dianions as reported by Agapie.[332]

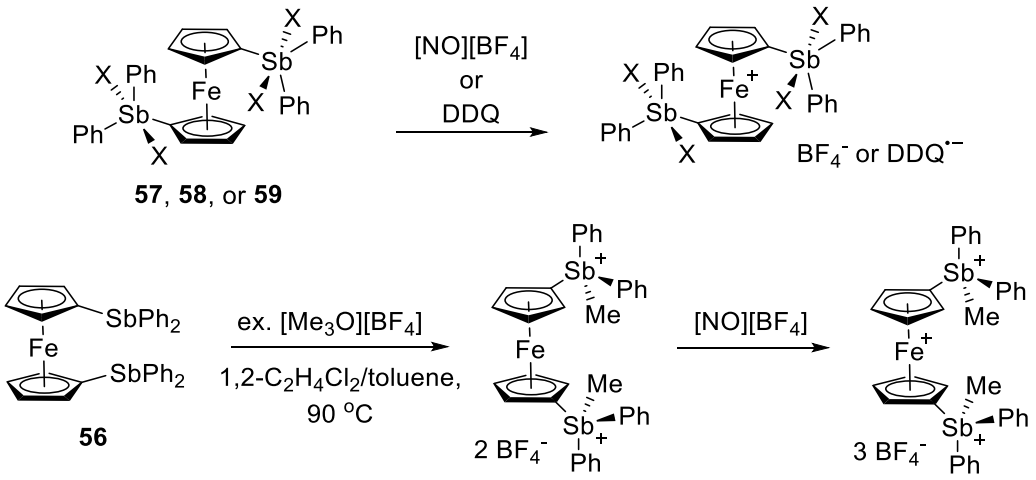

Figure 136. Proposed synthesis of ferrocenium distiborane species.

Previous studies showed that the Lewis acidity can greatly increase by positioning the main-group acceptor in the vicinity of a cationic transition metal moiety.[337-341] For instance, Shinkai along with our group showed that ferrocenium boranes are significantly more fluorophilic than their neutral counterparts.[109, 342] We propose to apply this strategy to prepare ferrocenium distiborane cations by a single-electron oxidation of distiboranes **57-59** with $[NO][BF_4]$ or DDQ (2,3-dichloro-5,6-dicyanobenzoquinone) (Figure 136, top). We will also attempt to synthesize ferrocenium distibonium trication by first treating distibine **56** with excess $[Me_3O][BF_4]$ to afford the corresponding distibonium tetrafluoroborate salt and subsequently oxidizing the iron(II) core with $[NO][BF_4]$ (Figure 136, bottom). These ferrocenium compounds will be tested as anion receptors and catalysts, and te behavior will be compared to the ferrocenyl distiborane and distibonium precursors.

CHAPTER VII

SYNTHESIS AND CHARACTERIZATION OF INTRAMOLECULAR NITROGEN- AND PHOSPHORUS-ANTIMONY HETERONUCLEAR COMPOUNDS

7.1 Introduction

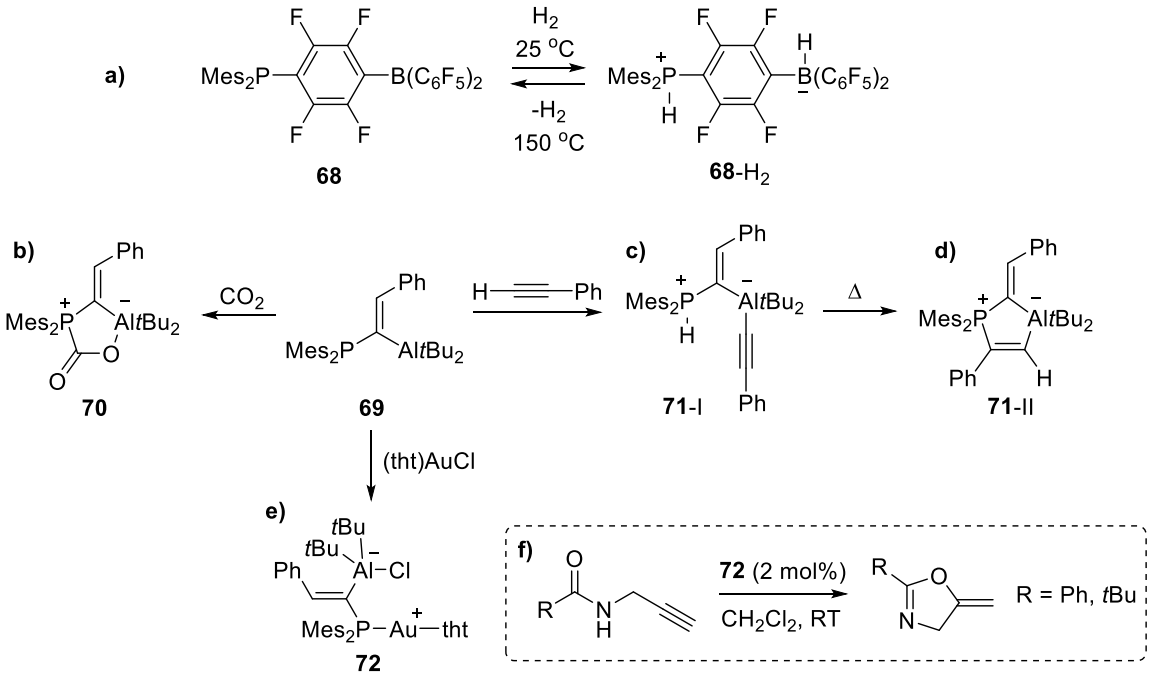

Figure 137. Reactivity and applications of ambiphilic compounds **68** and **69**. The scheme drawn within the dotted box is the cyclization of propargylamides catalyzed by **72**.

Compounds bearing both Lewis acidic- and basic-moieties, also known as ambiphilic compounds, have gathered a great deal of attention because of their applications in Frustrated Lewis Pair (FLP) chemistry,[141, 343-346] bifunctional

organocatalysis,[347, 348] and transition metal chemistry.[349] Most classical cases feature compounds incorporating B- or Al-based Lewis acceptors. For example, Stephan reported that phosphino-borane **68**, which bears a sterically demanding dimesitylphosphino donor as well as a bis(pentafluorophenyl)boryl acceptor, can heterolytically cleave H_2 gas at room temperature to afford **68**-H_2 (Figure 137 **a**).[350] Phosphonium-borate **68**-H_2 is remarkable stable at ambient temperature but heating to 150 °C prompts the elimination and regeneration of H_2. The authors address that this is the first example of metal-free, reversible activation of diatomic hydrogen. In 2011, Uhl described a geminal P/Al-based FLP **69** that irreversibly activates terminal acetylenes and CO_2 to form **70**-I and **71**, respectively (Figure 137 **b** and **c**).[351] Heating of the acetylene adduct **70**-I promotes a rearrangement of the compound to form **70-**II which is the more thermodynamically stable product (Figure 137 **d**). Bourissou later investigated the coordination chemistry of compound **69** with Rh-, Pd-, and Au-fragments.[352] For instance, treatment of **69** with (tht)AuCl (tht: tetrahydrothiophene) in CH_2Cl_2 cleanly afforded the zwitterionic gold(I) complex **72** (Figure 137 **e**). Crystallographic analysis verified that the Lewis acidic alane moiety abstracts the chloride ligand from the gold(I) center, which the authors addressed as a silver-free activation of a gold(I) precatalyst. Indeed, complex **72** (2 mol%) is an active catalyst for the cyclization of propargylamides in CH_2Cl_2 at ambient temperature to afford the corresponding alkyldiene oxazolines in high yields within hours (Figure 137 **f**).

In recent years, our group has been investigating and developing bimetallic complexes coupled with antimony Lewis acids for the application of anion sensing,[192, 193, 223, 250] organic transformation catalysis,[353] and halogen storage.[354] Despite these

contributions, antimony-based ambiphilic compounds are still considerably underdeveloped. In this chapter, we will propose the synthesis and the characterization of new types of antimony-based ambiphilic compounds.

7.2 Intramolecular amino-organoantimony(V) species: platform for the synthesis of amidostiboranes

Earlier in this dissertation (Chapter I, 1.1.1), we provided a background on amidophosphoranes species (compounds **2** and **3**) that activate CO_2 and CS_2 under mild conditions. Both of these compounds feature a Lewis basic amido group and a Lewis acidic phosphorus(V) center that only weakly interact with each other, thus leaving the nucleophilicity and the electrophilicity unquenched for further reactivity. With this in mind, we decided to target and synthesize ambiphilic compounds bearing amido donors as well as organoantimony(V) acceptors, which are potentially stronger Lewis acids than their phosphorus counterparts.

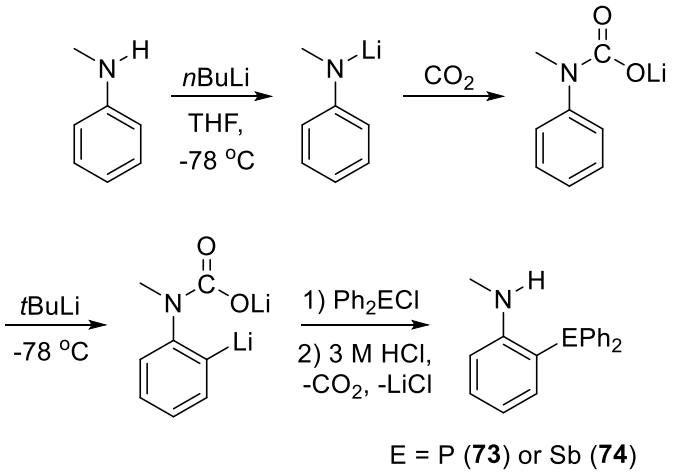

Figure 138. Synthesis of aminophosphine **73** and aminostibine **74**.

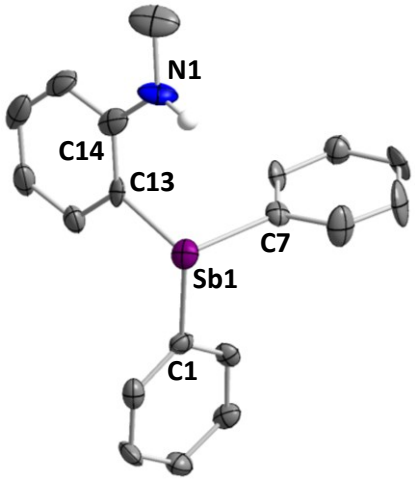

Figure 139. Crystal structure of **74**. Thermal ellipsoids are drawn at the 50 % probability level. The hydrogen atoms are omitted for clarity. Selected bond lengths (Å) and angles (deg) (the metrical parameters of the second independent salt are given in brackets): Sb1-N1 3.180 [3.194], C1-Sb1-C7 95.9(4) [95.2(4)], C1-Sb1-C13 97.4(4) [96.6(4)], C7-Sb1-C13 95.8(4) [96.9(4)], N1-C14-C13 120.1(10) [123.2(12)].

To initiate our study, we first synthesized aminostibine **74** as a colorless crystalline solid by following the procedure to prepare aminophosphine **73** (Figure 138).[355] This compound has been characterized by NMR spectroscopy and single crystal X-ray diffraction analysis. In the ^{1}H NMR spectrum of **74**, the methyl group appears as a doublet at 2.73 ppm and the nitrogen-bound proton is found as a broad singlet at 3.87 ppm. Moreover, the benzyl-CH_2 resonance is observed as a multiplet ranging from 6.71-6.67 ppm. Single crystals of **74** have been obtained as colorless blocks upon standing in a saturated EtOH solution at 0 ºC (Figure 139). Crystallagraphic analysis finds a pair of **74** molecules within the asymmetric unit, in which one of the compounds is disordered at the benzylamino arm. The average separation between Sb and N atoms is 3.254 Å and the

average ∠(N1-C14-C13) is 119.2°, thus indicating that neither the nitrogen atom nor the nitrogen-bound proton is interacting with the antimony center.

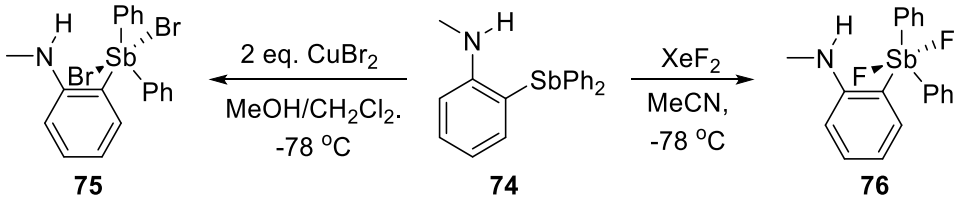

Figure 140. Synthesis of amino(dihalostiborane) **75** and **76**.

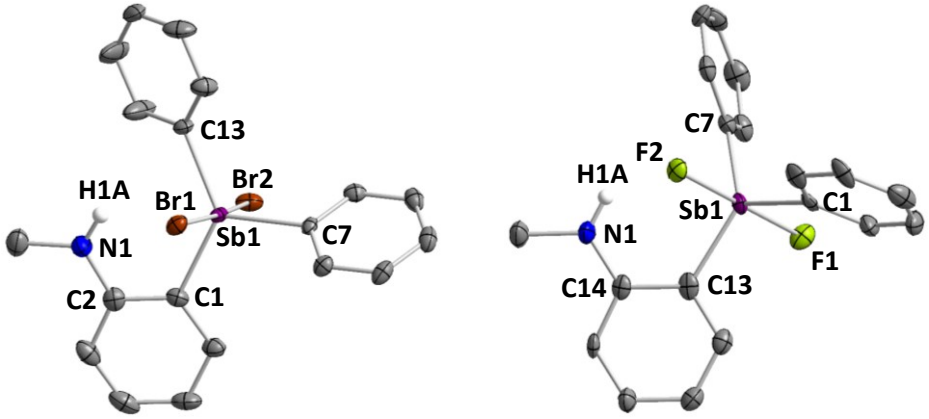

Figure 141. Crystal structures of **75** (left) and **76** (right). Thermal ellipsoids are drawn at the 50 % probability level. All hydrogen atoms except the nitrogen-bound protons are omitted for clarity. Selected bond lengths (Å) and angles (deg) for **75** (the metrical parameters of the second independent salt are given in brackets): Sb1-Br1 2.6498(5) [2.6304(5)], Sb1-Br2 2.6411(5) [2.6555(6)], Br1-Sb1-Br2 174.243(14)° [173.975(15)°], C1-Sb1-C7 112.41(13) [113.79(14)], C1-Sb1-C13 130.07(14) [129.67(14)], C7-Sb1-C13 117.51(13) [116.49(12)], N1-C2-C1 117.9(3) [120.2(3)]. Selected bond lengths (Å) and angles (deg) for **76** (the metrical parameters of the second independent salt are given in brackets): Sb1-F1 1.985(6) [1.981(6)], Sb1-F2 1.982(5) [2.045(6)], F1-Sb1-F2 179.8(2) [178.4(2)], C1-Sb1-C7 119.2(3) [120.6(4)], C1-Sb1-C13 116.6(3) [118.7(3)], C7-Sb1-C13 124.2(4) [120.7(3)], N1-C14-C13 121.3(9) [119.9(6)].

With this compound in hand, we decided to oxidize the antimony(III) center via halogenation. The reactions of **74** with Br_2 and $PhICl_2$ proceeded uncleanly even at cold temperature and none of the products could be identified nor isolated. By contrast, **74** undergoes clean two electron oxidation with 2 equivalents of $CuBr_2$ in $MeOH/CH_2Cl_2$ mixture at -78 °C to afford amino(dibromostiborane) **75** in quantitative yield (Figure 140). This compound has been fully characterized. The ^1H NMR resonances of **75** are all more downfield from those of the stibine counterpart **74**, and the diagnostic methyl and nitrogen-bound proton signals appear at 2.88 and 4.76 ppm, respectively. The colorless single crystals of **75** have been obtained by diffusing pentane into a toluene solution at ambient temperature and the structure has been determined by X-ray diffraction analysis (Figure 141, left). In the crystal, two independent molecules of **75** have been found in the asymmetric unit. Both antimony(V) centers adopt a distorted trigonal bipyramidal geometry defined by average $\Sigma\angle(C_{Ph}\text{-}Sb1\text{-}C_{Ph}) = 359.9^o$ and average $Br_{axial}\text{-}Sb\text{-}Br_{axial} = 174.109^o$. Furthermore, the average Sb-N separation is 3.164 Å and the average ∠(N1-C2-C1) is 119.1°, which suggest that the donor-acceptor interaction from the nitrogen lone pair of electrons to the $Sb\text{-}C_{Ph}$ σ* orbital is insignificant.

Next, we decided to synthesize the difluoride analog of **75**. Exchanging the bromide ligands of **75** with fluoride using KF, TBAT, or AgF afforded multiple undesired products which could not be separated. Instead, amino(difluorostiborane) **76** has been cleanly isolated by the reaction of **74** with xenon difluoride (XeF_2) in MeCN at -78 °C as an off-white solid (Figure 140). This compound has been characterized by multi-nuclear NMR as well as single crystal X-ray crystallography. The ^{19}F NMR spectrum of **76**

reveals a doublet at -137.4 ppm while the ^{1}H NMR spectrum depicts the nitrogen-bound proton signal as a broad multiplet centered at 6.03 ppm that couples to both methyl protons and antimony-bound fluoride ligands ($^{3}J_{H\text{-}H}$ = 4.8 Hz and $J_{H\text{-}F}$ = 10.1 Hz). Single crystals of **76** were successfully grown as colorless blocks by slow evaporation of a pentane into a THF solution at 0 ºC (Figure 141, right). In the crystal, two **76** molecules were found in the asymmetric unit, similar to that of the dibromide analog **75**. The antimony centers adopt a trigonal bipyramidal geometry as defined by average $\Sigma\angle(C_{Ph}\text{-Sb1-}C_{Ph})$ = 360.0º and average F-Sb1-F = 179.1(1)º. Furthermore, one of the two fluoride ligands is leaning towards the nitrogen atom with an average N-F separation of 2.856 Å, thus suggesting the presence of a hydrogen bond between the two atoms. This explains the NH-F coupling observed in both ^{1}H and ^{19}F NMR spectra. Similar to that of **75**, no obvious N→Sb interaction could be determined by the crystal structure (average Sb-N separation = 3.304 Å and average ∠(N1-C14-C13) = 120.6º). Further modifications of aminodihalostiboranes **75** and **76** using MeOTf, TMSOTf, or *t*BuLi to afford the corresponding amidohalostiboranes were not successful.

7.3 Synthesis and characterization of *ortho*-phenylene phosphino-stibonium cations and their reactivity

Because the electronic and the steric properties are easily controlled, phosphines are one of the most commonly utilized donor groups incorporated to ambiphilic compounds. Subsequently, a number of studies related to such compounds have been reported in the applications of both transition-metal- and FLP-chemistry. In this section, we will introduce the synthesis and the characterization of tetraarylstibonium cation acceptor bearing a pendant triarylphosphine donor. We will also cover the preliminary results on its reactivity as well as its coordination chemistry.

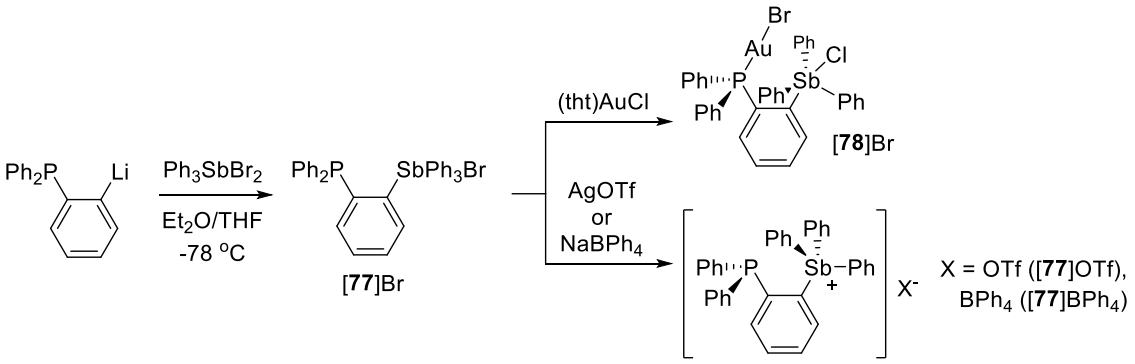

Figure 142. Synthesis of [**77**]Br, [**78**]Br, [**77**]OTf, and [**77**]BPh_4.

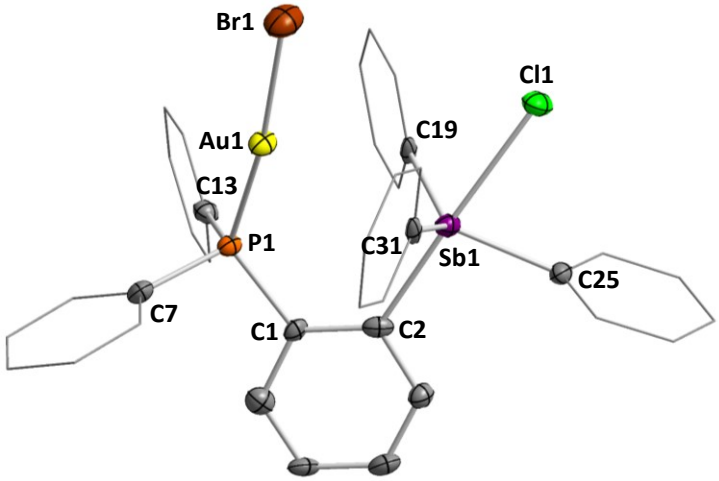

Figure 143. Crystal structure of [**78**]Br. Thermal ellipsoids are drawn at the 50 % probability level. The hydrogen atoms are omitted for clarity. Selected bond lengths (Å) and angles (deg): Au1-Br1 2.420(2), Sb1-Cl1 2.659(3), Au1-Sb1 3.543(3), Br1-Au1-P1 170.56(4), Cl-P1-C7 102.1(3), C1-P1-C13 106.1(3), C7-P1-C13 105.5(3), Cl1-Sb1-C2 175.79(15), C19-Sb1-C25 113.6(2), C19-Sb1-C31 129.6(2), C25-Sb1-C31 113.1(2).

First, we synthesized phosphino-stibonium bromide [**77**]Br by the reaction of 2-lithio(diphenylphosphino)benzene with Ph_3SbBr_2 in Et_2O/THF mixture at -78 ºC (Figure 142). This air- and moisture-stable compound is highly soluble in $CHCl_3$, CH_2Cl_2, THF, MeOH, and MeCN and insoluble in Et_2O, pentane, and hexanes. The ^{31}P NMR spectrum in $CDCl_3$ shows a sharp singlet at 19.0 ppm, which is considerably more downfield compared to triphenylphosphine (-6.0 ppm). This suggests the possibility of a donor-acceptor interaction between the lone pair of electrons of the phosphine moiety to the empty Sb-C_{Ph} σ* orbital. Despite of this interaction, the treatment of [**77**]Br with (tht)AuCl in CH_2Cl_2 afforded the corresponding gold(I) complex [**78**]Br as a pale yellow solid in 92 % yield. This complex is stable in air for at least a week but is sensitive to light. The ^{31}P NMR resonance could not be obtained for this complex and only ^{1}H and

$^{13}C\{^{1}H\}$ NMR spectroscopy could be utilized to determine the solution phase structure. Complex [**78**]Br has also been structurally characterized by single crystal X-ray diffraction analysis (Figure 143). The crystal structure of [**78**]Br verifies the coordination of a gold(I) fragment to the phosphine donor (Au1-P1 = 2.246(2) Å). Also in the solid state, we find that the halide ions have exchanged upon complexation, and the chloride and bromide ions are paired with the hard antimony(V) and soft gold(I) centers, respectively, with Sb-Cl bond length of 2.659(3) Å and Au-Br bond length of 2.420(2) Å. These observations indicate that the tetraarylstibonium subunit is an active Lewis acid and [**77**]Br indeed behaves as an ambiphilic ligand. Furthermore, the gold and the antimony centers adopt a slightly bent (∠(Br1-Au1-P1) = 170.56(4)°) and a distorted trigonal biyramidal geometry (∠(Cl1-Sb1-C2) = 175.79(15)° and Σ(∠(C_{Ph}-Sb1-C_{Ph}) = 356.3°), respectively, thus suggesting the presence of a donor-acceptor interaction from the gold to the animony. However, the gold and antimony atoms are largely separated by 3.543(3) Å (Σ_{cov}(Au-Sb) = 2.75 Å)[254] which signifies that this interaction is insignificant.

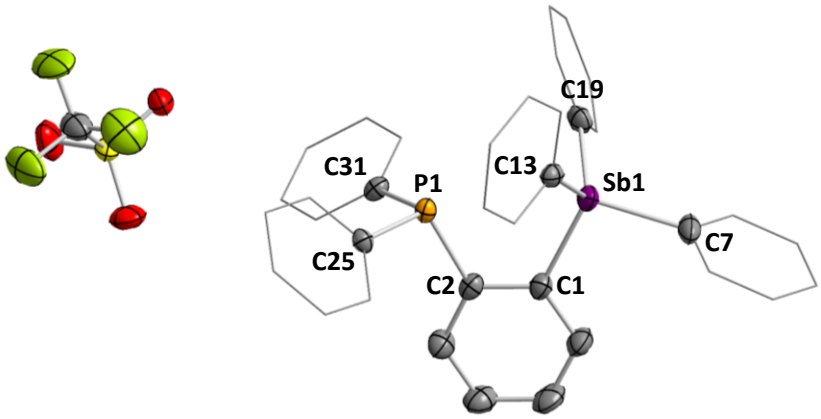

Figure 144. Crystal structure of [**77**][OTf]. Thermal ellipsoids are drawn at the 50 % probability level. The hydrogen atoms are omitted for clarity. Selected bond lengths (Å) and angles (deg) (the metrical parameters of the second independent salt are given in brackets): P1-Sb1 3.2594(8) [3.3035(8)], P1-Sb1-C7 158.04(7) [160.64(7)], C1-Sb1-C13 110.73(9) [110.31(9)], C1-Sb1-C19 110.66(10) [115.48(9)], C13-Sb1-C19 114.37(9) [115.29(9)], P1-C2-C1 116.75(18) [117.34(17)].

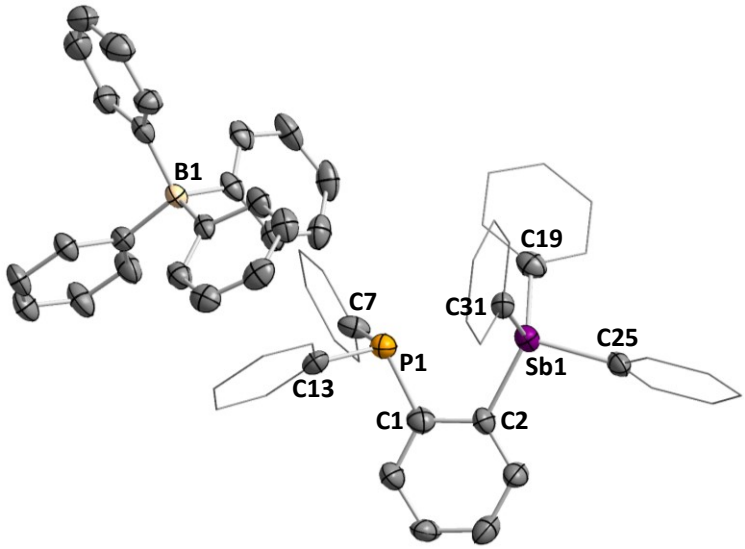

Figure 145. Crystal structure of [**77**][BPh_4]. Thermal ellipsoids are drawn at the 50 % probability level. The hydrogen atoms are omitted for clarity. Selected bond lengths (Å) and angles (deg): P1-Sb1 3.2082(19), P1-Sb1-C25 160.59(16), C19-Sb1-C25 102.9(3), C19-S1-C31 108.2(2), C25-Sb1-C31 104.9(2), C1-P1-C7 107.0(3), C1-P1-C13 103.3(3), C7-Sb1-C13 103.7(3), P1-C1-C2 115.7(5).

Analogous to that of Ph_4SbBr, the bromide ion can be conveniently abstracted and exchanged with more weakly coordinating anions by the reaction of the corresponding silver or sodium salts. The treatment of [**77**]Br with AgOTf and $NaBPh_4$ proceeded cleanly to afford [**77**][OTf] and [**77**][BPh_4], respectively, in quantitative yields. Both of these stibonium salts have been fully characterized. In the ^1H NMR spectra, the resonances of salt [**77**][OTf] are sharp and finely resolved whereas the signals of salt [**77**][BPh_4] are significantly more broadened. The ^{31}P NMR signals of [**77**][OTf] and [**77**][BPh_4] appear at 11.3 and 11.2 ppm, respectively, surprisingly more upfield than that of [**77**]Br (^{31}P δ = 19.0 ppm). Colorless single crystals of both [**77**][OTf] and [**77**][BPh_4] were successively grown and the solid state structures have been determined by X-ray diffraction analyses. In the crystal of [**77**][OTf], two ionic pairs have been found in the asymmetric unit, and the cations and the anions are well separated (Figure 144). The P-Sb distances are 3.2594(8) and 3.3035(8) Å, which are well within the sum of the van der Waal's radii of the two elements ($\sum_{vdW}$(P-Sb) = 4.15 Å).[237] Furthermore, the P1-C2-C1 angles are 116.75(18)^o and 117.34(17)^o, indicating that the phosphine moiety is slightly tilting towards the antimony center. These parameters are even smaller for the crystal structure of [**77**][BPh_4] with the P-Sb distance of 3.2082(19) Å and P1-C1-C2 angle of 115.7(5)^o (Figure 145). These crystallographic observations made for [**77**][OTf] and [**77**][BPh_4] suggest the presence of donor-acceptor interactions from the phosphine moieties to the Lewis acidic antimony(V) centers.

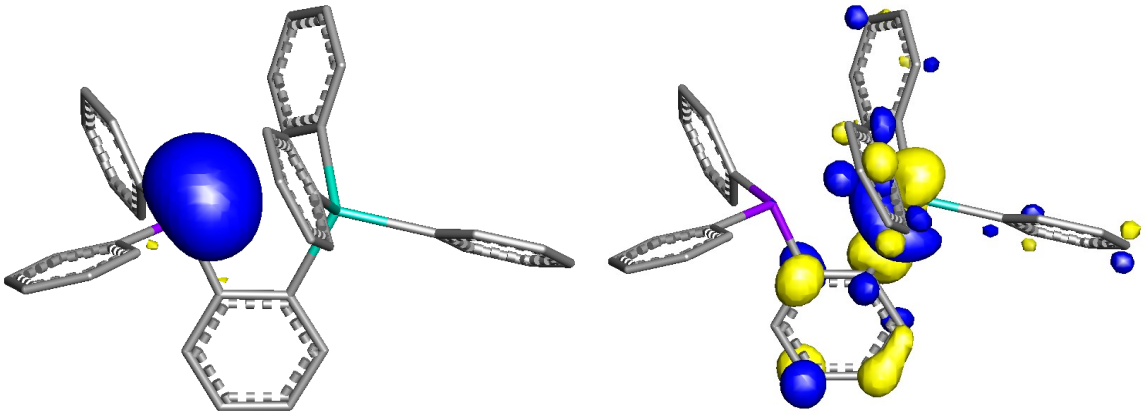

Figure 146. Contour plots of the HOMO (left) and the LUMO (right) of [**77**]$^{+}$ (isovalue = 0.05).

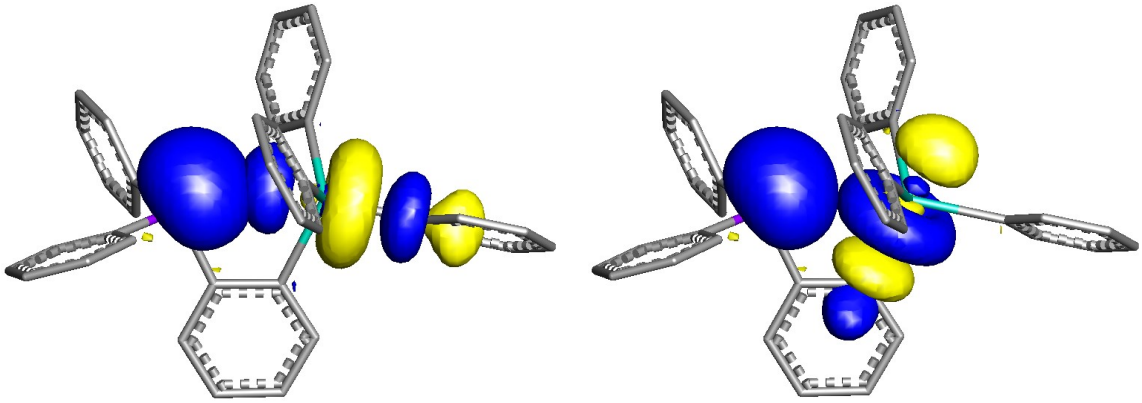

Figure 147. NBO plots (isovalue 0.05) showing two representative lp(P) → σ* (Sb-C_{Ph}) donor‑acceptor interactions in [**77**]$^{+}$.

To better understand the nature of these interactions, the structure of [**77**]$^{+}$ has been optimized using DFT methods (B3LYP functional with the mixed basis sets: aug-cc-pVTZ-pp for Sb, 6-311g(d) for P, 6-31g for C and H) in the absence of the counterions. The DFT optimized structure is similar to that of the crystal structure of [**77**]$^{+}$ with P-Sb distance of 3.152 Å and P1-C1-C2 angle of 115.58°. While the HOMO represents the lone

pair of electrons localized on the phosphorus atom as expected, the LUMO is distributed throughout the tetraarylstibonium moiety with only partial contribution by the antimony center (Figure 146). Analysis of the optimized structure using NBO methods suggest that the LUMO is interacting with two of the σ* Sb-C_{Ph} orbitals, which are associated with a modest stabilization energy of 14.16 kcal mol^{-1} (Figure 147).

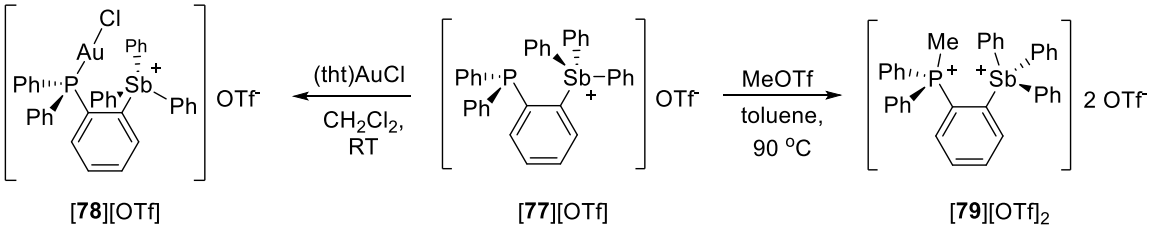

Figure 148. Synthesis of gold complex [**78**][OTf] and dication [**79**][$OTf]_2$.

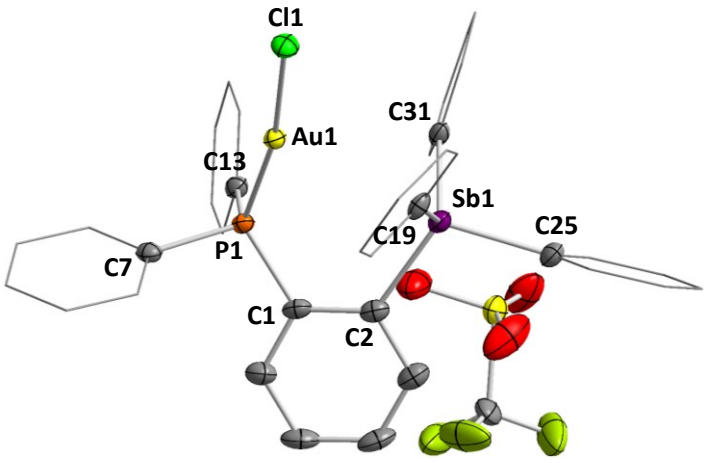

Figure 149. Crystal structure of [**78**][OTf]. Thermal ellipsoids are drawn at the 50 % probability level. The hydrogen atoms are omitted for clarity. Selected bond lengths (Å) and angles (deg): Au1-Sb1 3.4083(4), Au1-Cl1 2.2905(9), Cl1-Au1-P1 169.62(3), Au1-Sb1-C25 165.16(11), C2-Sb1-C19 109.06(14), C2-Sb1-C31 110.69(14), C19-Sb1-C31 122.87(14).

With these compounds in hand, we first decided to investigate the coordination chemistry of salts [**77**][OTf] and [**77**][BPh_4] with late transition metals. The treatment of [**77**][BPh_4] with (tht)AuCl resulted in a decomposition of the gold complex, similar to the phenomenon reported by Echavarren.[356] By contrast, complexation of [**77**][OTf] with (tht)AuCl cleanly affords the corresponding gold complex [**78**][OTf] as a colorless solid (Figure 148). This complex gradually decomposes in air but can be stored in a glove box at -35 ^{o}C for weeks in absence of light. Gold complex [**78**][OTf] has been characterized by multi-nuclear NMR spectroscopy and single crystal X-ray analysis. In the ^{1}H NMR spectrum, the antimony- and phosphorus-bound phenyl resonances are observed in 3:2 ratio. The ^{31}P NMR signal is observed at 34.3 ppm, confirming the coordination of a gold(I) fragment to the phosphine ligand. Crystallographic analysis of [**78**][OTf] reveals that the phosphino-stibonium cation and the triflate anion are well separated, and the chloride remains strongly intact to the gold atom (Au1-Cl1 = 2.2905(9) Å) (Figure 149). Moreover, the gold center assumes a bent geometry with a Cl1-Au1-P1 angle of 169.62(3)^{o}, which is comparable to that of [**78**]Br (170.56(4)^{o}). On the other hand, the Au-Sb separation is slightly contracted from 3.543(3) Å in [**78**]Br to 3.4083(4) Å in [**78**][OTf], thereby demonstrating that the Lewis acidity of tetraarylstibonium moiety is enhanced in the presence of a non-coordinating triflate anion as opposed to a more nucleophilic chloride anion.

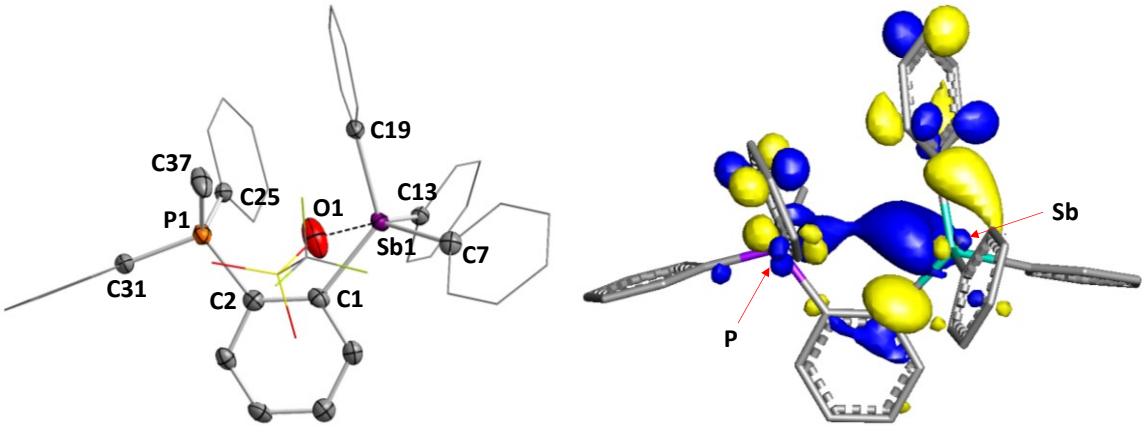

Figure 150. Left: crystal structure of [**79**][OTf]. Thermal ellipsoids are drawn at the 50 % probability level. The hydrogen atoms, MeOH molecule, and one of the triflate anions are omitted for clarity. Selected bond lengths (Å) and angles (deg): Sb1-P1 3.8738(11), Sb1-O1 2.871(7) Å, C1-Sb1-C7 109.56(10), C1-Sb1-C19 126.67(10), C7-Sb1-C13 102.70(11), C2-P1-C25 108.43(12), C2-P1-C31 107.59(13), C25-P1-C31 109.15(16). Right: contour plot of the LUMO+1 of [**79**]$^{+}$ (isovalue = 0.045).

Lastly, we examined the reactivity of [**77**][OTf] towards electrophilic alkylating agents to access dicationic phosphonium-stibonium species. Treatment of phosphino-stibonium [**77**][OTf] with excess MeOTf in toluene at 90 ºC successfully afforded the corresponding phosphonium-stibonium dication [**79**][OTf]$_2$ as a white solid in 51 % yield (Figure 148). This dicationic salt has been characterized by multi-nuclear NMR spectroscopy as well as single crystal X-ray diffraction. The ^{1}H NMR spectrum in CD_3CN displays the phosphorus-bound methyl group as a doublet at 2.51 ppm ($^{3}J_{H\text{-}P}$ = 13.6 Hz). The ^{31}P NMR resonance appears at 25.2 ppm, consistent with other reported methylated triarylphosphonium species.[110, 113] In the crystal, both phosphorus and antimony centers of [**79**]$^{2+}$ adopt a distorted tetrahedral geometry and the two atoms are separated by 3.8738(11) Å, marginally shorter than the Sb-Sb distance in [**42**][OTf]$_2$ (4.1069(3) Å)

(Figure 150, left). Also, while one of the triflate anions is well separated from the dication complex, the other triflate anion weakly interacts with the antimony center resulting in a Sb-O separation of 2.871(7) Å. The electronic structure of [**79**]$^{2+}$ has been analyzed by DFT methods (B3LYP functional with the mixed basis sets: aug-cc-pVTZ-pp for Sb, 6-311g(d) for P, 6-31g for C and H) in the absence of triflate anions. In the optimized structure, the HOMO and the LUMO are predominantly localized on the aryl rings and the LUMO+1 landscapes the combination of P-C_{Ph} and Sb-C_{Ar} σ* orbitals (Figure 150, right). Encouraged by these results, we sought to crystallize [**79**][OTf]$_2$ in the presence of an electron-rich substrate such as DMF to examine whether [**79**]$^{2+}$ can sufficiently function as a bifunctional bidentate Lewis acid, reminiscent to that of *o*-distibonium [**42**]$^{2+}$. However, this attempt failed and only free dications were isolated from the crystals. We suspect that the steric hindrance about the binding pocket prevents the chelation of a large organic nucleophile.

7.4 Conclusion

In this chapter, we introduced the synthesis and the characterization of potential ambiphilic compounds. We successively generated aminodifluorostiborane **76** following the same procedure reported to prepare that of the phosphorene equivalent; however, further alteration to afford the corresponding amidofluorostiborane failed due to rapid decomposition upon addition of TMSOTf, *n*BuLi or *t*BuLi. We also investigated the synthesis and the application of phosphino-stibonium cation [**77**]$^{+}$. Despite the modest donor-acceptor interactions between the phosphorus and the antimony centers, both

nucleophilicity and electrophilicity of [**77**]Br and [**77**][OTf] remain unquenched, allowing the coordination of a gold(I) fragment. Within the gold complexes [**78**]Br and [**78**][OTf], the donor-acceptor interaction of gold(I) to antimony was stronger for the latter species due to the enhanced Lewis acidity of the tetraarylstibonium moiety. Finally, treatment of [**77**][OTf] with MeOTf led to the formation of phosphinum-stibonium dicationic species [**79**][OTf]$_2$. While theoretical study suggests that [**79**]$^{2+}$ is indeed a bifunctional Lewis acid, the binding site is sterically hindered and precludes access of large organic nucleophiles.

Overall, our recent work established synthetic strategies to design new types of ambiphilic compounds bearing organoantimony(V) acceptors. We seek to utilize and investigate these compounds and their derivatives as potential candidates for applications including coordination chemistry of transition metals and their reactivity and FLP-induced small molecule activations, which have not been well-developed with compounds bearing organoantimony(V) acceptors.

7.5 Experimental section

General considerations. *Antimony is potentially toxic and should be handled with caution*. *N*-methylaniline was purchased from Sigma Aldrich and dried over CaH_2 and distilled prior to use. *t*BuLi (1.6 M in pentane) was purchased from Sigma Aldrich and used as received. *n*BuLi (2.65 M in hexane) was purchased from Alfa Aesar and used as received. MeOTf and xenon difluoride (XeF_2) were purchased from Matrix Scientific and used as received. 2-bromo(diphenylphosphino)benzene[357] and $PhICl_2$[318] were prepared by previously reported procedures. All preparations were carried out under an atmosphere of dry N_2 employing either a glovebox or standard Schlenk techniques. Solvents were dried by passing through an alumina column (pentane and CH_2Cl_2), by refluxing under N_2 over Na/K (toluene, Et_2O and THF), or by refluxing under N_2 over CaH_2 (MeCN). All other solvents were ACS reagent grade and used as received. NMR spectra were recorded on a Varian Unity Inova 400 FT NMR (399.508 MHz for ^1H, 100.466 MHz for ^{13}C, 375.84 MHz for ^{19}F, 161.720 MHz for ^{31}P) spectrometer at ambient temperature. Chemical shifts are given in ppm and are referenced to residual ^1H and ^{13}C solvent signals, external $BF_3{\cdot}Et_2O$ for ^{11}B and ^{19}F, and external H_3PO_4 (85 %) for ^{31}P. Elemental analyses were performed by Atlantic Microlab (Norcross, GA). IR spectrum was recorded by Mattson ATI Genesis FT-IR Spectrometer.

Computational details. Density functional theory (DFT) structural optimizations with the *Gaussian 09* program.[208] In all cases, the structures were optimized using the B3LYP functional;[209, 210], and the following mixed basis set: Sb, aug-cc-pVTZ-PP;[240] P, 6-311g(d); F, 6-31g(d');[212] C/O/H, 6-31g.[213] For all optimized structures, frequency

calculations were carried out to confirm the absence of imaginary frequencies. The molecular orbitals were visualized and plotted in Jimp 2 program.[214]

Crystallographic measurements. All crystallographic measurements were performed at 110(2) K using a Bruker SMART APEX II diffractometer with a CCD area detector (graphite monochromated Mo Kα radiation, ω-scans with a 0.5 step in ω) at 110 K. In each case, a specimen of suitable size and quality was selected and mounted onto a nylon loop. The semiempirical method SADABS was applied for absorption correction. The structures were solved by direct methods and refined by the full-matrix least-squares technique against F^2 with the anisotropic temperature parameters for all non-hydrogen atoms. All H-atoms were geometrically placed and refined in riding model approximation. Data reduction and further calculations were performed using the Bruker SAINT$^+$ and SHELXTL NT program packages.

Table 23. Crystal data, data collection, and structure refinement for **74** and **75**.

Crystal data	**74**	**75**
Empirical formula	C76 H70 N4 Sb4	C38 H36 Br4 N2 Sb2
Formula weight	1526.36	1083.83
Temperature	110(2) K	110(2) K
Wavelength	0.71073 Å	0.71073 Å
Crystal system	Monoclinic	Triclinic
Space group	C 2/c	P -1
Unit cell dimensions	a = 32.492(16) Å	a = 8.3710(16) Å
	b = 6.694(3) Å	b = 9.0182(17) Å
	c = 30.074(15) Å	c = 27.625(5) Å
	α = 90°	α = 92.846(2)°
	β = 90.632(5)°	β = 92.306(2)°
	γ = 90°	γ = 115.895(2)°
Volume	6541(5) $Å^3$	1869.3(6) $Å^3$
Z	4	2
Density (calculated)	1.550 Mg/m^3	1.926 Mg/m^3
Absorption coefficient	1.680 mm^{-1}	5.750 mm^{-1}
F(000)	3032	1040
Crystal size	0.180 x 0.068 x 0.032 mm^3	0.244 x 0.182 x 0.088 mm^3
Theta range for data collection	1.253 to 26.520°	2.220 to 28.304°
Index ranges	-40<=h<=40, -8<=k<=7, -37<=l<=37	-11<=h<=10, -12<=k<=11, -36<=l<=36
Reflections collected	24958	22207
Independent reflections	6549 [R(int) = 0.0677]	8831 [R(int) = 0.0208]
Absorption correction	Semi-empirical from equivalents	Semi-empirical from equivalents
Max. and min. transmission	0.770 and 0.730	0.738 and 0.466
Refinement method	Full-matrix least-squares on F^2	Full-matrix least-squares on F^2
Data / restraints / parameters	6549 / 6 / 398	8831 / 0 / 417
Goodness-of-fit on F^2	1.281	1.092
Final R indices [I>2sigma(I)]	R1 = 0.0925, wR2 = 0.1600	R1 = 0.0295, wR2 = 0.0644
R indices (all data)	R1 = 0.1250, wR2 = 0.1711	R1 = 0.0365, wR2 = 0.0667
Largest diff. peak and hole	1.143 and -2.843 e.$Å^{-3}$	1.263 and -0.710 e.$Å^{-3}$

[a] $R1 = \Sigma||Fo| - |Fc||/\Sigma|Fo|$. [b] $wR2 = \{[\Sigma w(Fo^2 - Fc^2)^2]/[\Sigma w(Fo^2)^2]\}^{1/2}$.

Table 24. Crystal data, data collection, and structure refinement for **76** and [**78**]Br.

Crystal data	**76**	[**78**]Br
Empirical formula	C38 H36 F4 N2 Sb2	C36 H29 Au Br Cl P Sb
Formula weight	840.19	926.64
Temperature	293(2) K	110(2) K
Wavelength	0.71073 Å	0.71073 Å
Crystal system	Triclinic	Monoclinic
Space group	P -1	P 21/c
Unit cell dimensions	a = 6.6564(11) Å	a = 13.342(12) Å
	b = 8.8593(14) Å	b = 10.636(10) Å
	c = 30.037(5) Å	c = 22.58(2) Å
	α = 86.665(2)°	α = 90°
	β = 84.013(2)°	β = 99.373(11)°
	γ = 72.683(2)°	γ = 90°
Volume	1681.1(5) $Å^3$	3161(5) $Å^3$
Z	2	4
Density (calculated)	1.660 Mg/m^3	1.947 Mg/m^3
Absorption coefficient	1.659 mm^{-1}	6.913 mm^{-1}
F(000)	832	1768
Crystal size	0.128 x 0.098 x 0.076 mm^3	0.120 x 0.080 x 0.070 mm^3
Theta range for data collection	1.364 to 28.274°	1.828 to 26.332°.
Index ranges	-8<=h<=8, -11<=k<=11, -39<=l<=39	-16<=h<=16, -13<=k<=13, -28<=l<=28
Reflections collected	17974	30866
Independent reflections	7642 [R(int) = 0.0335]	6415 [R(int) = 0.0737]
Absorption correction	Semi-empirical from equivalents	Semi-empirical from equivalents
Max. and min. transmission	0.803 and 0.707	0.6347 and 0.4081
Refinement method	Full-matrix least-squares on F^2	Full-matrix least-squares on F^2
Data / restraints / parameters	7642 / 36 / 397	6415 / 0 / 364
Goodness-of-fit on F^2	1.369	1.036
Final R indices [I>2sigma(I)]	R1 = 0.0882, wR2 = 0.1768	R1 = 0.0362, wR2 = 0.0761
R indices (all data)	R1 = 0.0962, wR2 = 0.1798	R1 = 0.0534, wR2 = 0.0836
Largest diff. peak and hole	2.328 and -3.070 e.$Å^{-3}$	1.525 and -1.339 e.$Å^{-3}$

[a] $R1 = \Sigma||Fo| - |Fc||/\Sigma|Fo|$. [b] $wR2 = \{[\Sigma w(Fo^2 - Fc^2)^2]/[\Sigma w(Fo^2)^2]\}^{1/2}$.

Table 25. Crystal data, data collection, and structure refinement for [**77**][OTf] and [**77**]BPh_4.

Crystal data	[**77**][OTf]	[**77**][BPh_4]
Empirical formula	C74 H58 F6 O6 P2 S2 Sb2	C60 H49 B P Sb
Formula weight	1526.76	933.52
Temperature	110(2) K	110(2) K
Wavelength	0.71073 Å	0.71073 Å
Crystal system	Monoclinic	Monoclinic
Space group	P 21/c	P 21/n
Unit cell dimensions	a = 20.107(4) Å	a = 11.393(3) Å
	b = 9.665(2) Å	b = 23.149(6) Å
	c = 34.059(7) Å	c = 18.003(5) Å
	α = 90°	α = 90°
	β = 91.888(2)°	β = 98.971(4)°
	γ = 90°	γ = 90°
Volume	6615(2) $Å^3$	4690(2) $Å^3$
Z	4	4
Density (calculated)	1.533 Mg/m^3	1.322 Mg/m^3
Absorption coefficient	0.999 mm^{-1}	0.662 mm^{-1}
F(000)	3072	1920
Crystal size	0.430 x 0.260 x 0.220 mm^3	0.110 x 0.080 x 0.080 mm^3
Theta range for data collection	2.027 to 28.313°	1.759 to 26.575°
Index ranges	-26<=h<=26, -12<=k<=12, -45<=l<=45	-14<=h<=14, -28<=k<=28, -22<=l<=22
Reflections collected	79141	50475
Independent reflections	16313 [R(int) = 0.0464]	9676 [R(int) = 0.1465]
Absorption correction	Semi-empirical from equivalents	Semi-empirical from equivalents
Max. and min. transmission	0.8944 and 0.7245	0.7856 and 0.7456
Refinement method	Full-matrix least-squares on F^2	Full-matrix least-squares on F^2
Data / restraints / parameters	16313 / 0 / 866	9676 / 0 / 568
Goodness-of-fit on F^2	1.02	1.03
Final R indices [I>2sigma(I)]	R1 = 0.0328, wR2 = 0.0683	R1 = 0.0687, wR2 = 0.1558
R indices (all data)	R1 = 0.0451, wR2 = 0.0731	R1 = 0.1296, wR2 = 0.1832
Largest diff. peak and hole	1.049 and -0.662 e.$Å^{-3}$	1.935 and -1.547 e.$Å^{-3}$

[a] $R1 = \Sigma||Fo| - |Fc||/\Sigma|Fo|$. [b] $wR2 = \{[\Sigma w(Fo^2 - Fc^2)^2]/[\Sigma w(Fo^2)^2]\}^{1/2}$.

Table 26. Crystal data, data collection, and structure refinement for [**78**][OTf] and [**79**][OTf]$_2$.

Crystal data	[**78**]OTf	[**79**][OTf]$_2$
Empirical formula	C37 H29 Au Cl F3 O3 P S Sb	C40 H35 F6 O7 P S2 Sb
Formula weight	995.8	958.52
Temperature	110(2) K	110(2) K
Wavelength	0.71073 Å	0.71073 Å
Crystal system	Monoclinic	Monoclinic
Space group	C 2/c	P 21/n
Unit cell dimensions	a = 17.152(2) Å	a = 14.776(4) Å
	b = 11.4989(16) Å	b = 15.222(4) Å
	c = 36.250(5) Å	c = 19.126(4) Å
	α = 90°	a= 90°
	β = 102.441(2)°	b= 112.723(15)°
	γ = 90°	g = 90°
Volume	6981.9(16) Å^3	3967.9(18) Å^3
Z	8	4
Density (calculated)	1.895 Mg/m^3	1.605 Mg/m^3
Absorption coefficient	5.206 mm^{-1}	0.919 mm^{-1}
F(000)	3840	1932
Crystal size	0.240 x 0.140 x 0.140 mm^3	0.180 x 0.140 x 0.110 mm^3
Theta range for data collection	2.148 to 28.342°	1.767 to 28.406°
Index ranges	-22<=h<=22, -15<=k<=15, -48<=l<=48	-19<=h<=19, -20<=k<=20, -25<=l<=25
Reflections collected	42771	29825
Independent reflections	8700 [R(int) = 0.0456]	6705 [R(int) = 0.0600]
Absorption correction	Semi-empirical from equivalents	Semi-empirical from equivalents
Max. and min. transmission	0.8844 and 0.4678	0.854 and 0.773
Refinement method	Full-matrix least-squares on F^2	Full-matrix least-squares on F^2
Data / restraints / parameters	8700 / 0 / 479	6705 / 0 / 580
Goodness-of-fit on F^2	1.084	0.793
Final R indices [I>2sigma(I)]	R1 = 0.0288, wR2 = 0.0619	R1 = 0.0341, wR2 = 0.0554
R indices (all data)	R1 = 0.0336, wR2 = 0.0635	R1 = 0.0523, wR2 = 0.0590
Largest diff. peak and hole	1.303 and -0.986 e.Å^{-3}	0.317 and -0.308 e.Å^{-3}

[a] $R1 = \Sigma||Fo| - |Fc||/\Sigma|Fo|$. [b] $wR2 = \{[\Sigma w(Fo^2 - Fc^2)^2]/[\Sigma w(Fo^2)^2]\}^{1/2}$.

Synthesis of 74. This compound was synthesized by following a modified procedure to prepare its phosphine analog **73**. A 100 mL Schlenk flask was charged with *N*-methylaniline (1.0322 g, 9.6×10^{-3} mol) and THF (30 mL) and the mixture was cooled down to -78 ºC. A hexane solution of *n*BuLi (2.65 M; 3.6 mL, 9.6×10^{-3} mol) was added dropwise and stirred for 30 min at which time a white precipitate formed. The suspension was warmed up to 0 ºC and CO_2 gas was bubbled through. Upon stirring, the solid completely dissolved resulting in a pale yellow solution. The mixture was cooled down to -78 ºC and *t*BuLi (1.7 M in pentane; 5.7 mL, 9.6×10^{-3} mol) was added dropwise in which the color changed to intense yellow. The reaction mixture was warmed up to -20 ºC and stirred for another 30 min. The mixture was brought down to -78 ºC again and a THF solution (10 mL) of Ph_2SbCl (3.000 g, 9.6×10^{-3} mol) was added slowly via cannula. The cooling bath was removed after 30 min and the orange reaction mixture was stirred overnight. An aqueous solution of HCl (1 M, 50 mL) was added to the reaction mixture in which CO_2 gas gradually bubbled out and some black precipitate formed. The pH of the reaction mixture was then raised to 14 using a NaOH solution (6 M). After stirring for 15 min, the reaction mixture was extracted with three portions of EtOAc (30 mL), the organic layers were combined, dried over $MgSO_4$, filtered through a Celite plug, and the solvent was removed *in vacuo*. To this residue, EtOH (40 mL) was added and the resulting cloudy suspension was heated up to boil and quickly passed through Celite. Upon cooling down to -30 ºC, single crystals of **74** was isolated as colorless plates in 58 % yield (2.1350 g, 5.6×10^{-3} mol). ^{1}H NMR (399.508 MHz, $CDCl_3$): δ 7.49-7.46 (m, 4H, *o*-Sb*Ph*), 7.37-7.27 (m, 7H, *p*- and *m*-Sb*Ph* + *o*-phenylene), 7.09 (dd, 1H, *o*-phenylene, $^3J_{H\text{-}H} = 7.6$ Hz,

$^{5}J_{H\text{-}H}$ = 1.6 Hz), 6.71-6.67 (m, 2H, *o*-phenylene), 2.72 (s, 3H, N-C*H*$_3$). $^{13}C\{^{1}H\}$NMR (100.466 MHz, $CDCl_3$): δ 153.27 (N-bound quaternary), 137.43 (Sb-bound *o*-phenylene quaternary), 136.42 (*o*-phenylene), 136.38 (*o*-Sb*Ph*), 130.52 (*o*-phenylene), 129.00 (*m*-Sb*Ph*), 128.75 (*p*-Sb*Ph*), 123.36 (Sb*Ph* quaternary), 118.57 (*o*-phenylene), 110.31 (*o*-phenylene), 31.18 (Sb-*C*H_3). Elemental analysis calculated (%) for $C_{19}H_{18}NSb$: C, 59.72; H, 4.75; found C, 60.16; H, 4.76.

Synthesis of 75. A MeOH solution (5 mL) of $CuBr_2$ (0.413 g, 1.8×10^{-3} mol) was added to a CH_2Cl_2 solution (10 mL) of **74** (0.353 g, 9.2×10^{-4} mol) at -78 ºC. After stirring for 30 min, the solvent was removed *in vacuo* and CH_2Cl_2 (10 mL) and a small amount of activated carbon were added. The resulting mixture was filtered through Celite to remove CuBr and the solvent was again removed under vacuum. The residue was triturated with two portions of pentane (3 mL each) to afford **75** as an off-white solid in 86 % yield (0.431 g, 7.9×10^{-4} mol). Single crystals of **75** were obtained by pentane into a THF solution. ^{1}H NMR (399.508 MHz, $CDCl_3$): δ 7.49-7.46 (m, 4H, *o*-Sb*Ph*), 7.37-7.27 (m, 7H, *p*- and *m*-Sb*Ph* + *o*-phenylene), 7.09 (dd, 1H, *o*-phenylene, $^{3}J_{H\text{-}H}$ = 7.6 Hz, $^{5}J_{H\text{-}H}$ = 1.6 Hz), 6.71-6.67 (m, 2H, *o*-phenylene), 3.88 (broad s, 1H, N*H*), 2.72 (s, 3H, N-C*H*$_3$). $^{13}C\{^{1}H\}$NMR (100.466 MHz, $CDCl_3$): δ 147.96 (*o*-phenylene), 140.10 (Sb-bound *o*-phenylene quaternary), 138.71 (N-bound quaternary), 134.09 (*o*-Sb*Ph*), 132.52 (*o*-phenylene), 131.53 (*p*-Sb*Ph*), 130.69 (*o*-phenylene), 129.47 (*m*-Sb*Ph*), 121.26 (*o*-phenylene), 116.40 (*o*-phenylene), 31.68 (Sb-*C*H_3). Elemental analysis calculated (%) for $C_{19}H_{18}Br_2NSb$: C, 42.11; H, 3.35; found C, 41.98; H, 3.30.

Synthesis of 76. A 25 mL Schlenk tube was charged with **74** (0.226 g, 5.9×10^{-4} mol) and CH_2Cl_2 (5 mL), and was cooled down to -40 ºC using a dry ice/MeCN bath. To this solution, XeF_2 (0.100 g, 5.9×10^{-4} mol) in CH_2Cl_2 (5 mL) was added dropwise across 10 min in which the color changed from colorless to pale orange. After stirring for 30 min, the cooling bath was removed and the reaction mixture was warmed up to ambient temperature to stir for another 30 min. The solvent was removed *in vacuo* and the residue was washed with two portions of cold pentane (3 mL each). After drying under vacuum, pure **76** was isolated as a white solid in 72 % yield (0.179 g, 4.3×10^{-4} mol). ^{1}H NMR (399.508 MHz, $CDCl_3$): δ 8.17-8.15 (m, 4H, *o*-Sb*Ph*), 7.70 (d, 1H, *o*-phenylene, $^{3}J_{H\text{-}H}$ = 7.6 Hz), 7.55 (pseudo t, 6H, *p*- and *m*-Sb*Ph*), 7.40 (t, 1H, *o*-phenylene, $^{3}J_{H\text{-}H}$ = 8.4 Hz), 6.80 (t, 1H, *o*-phenylene, $^{3}J_{H\text{-}H}$ = 7.6 Hz), 6.72 (d, 1H, *o*-phenylene, $^{3}J_{H\text{-}H}$ = 8.4 Hz), 6.03 (broad m, 1H, N*H*, $^{3}J_{H\text{-}H}$ = 4.8 Hz, $J_{H\text{-}F}$ = 10.1 Hz), 2.78 (d, 3H, N-C*H*$_3$, $J_{H\text{-}F}$ = 10.1 Hz). ^{13}C{^{1}H}NMR (100.466 MHz, $CDCl_3$): δ 153.61 (N-bound quaternary), 135.78 (t, Sb-bound *o*-phenylene quaternary, $^{1}J_{C\text{-}F}$ = 4.3 Hz), 135.35 (t, *o*-Sb*Ph*, $^{3}J_{C\text{-}F}$ = 5.0 Hz), 135.28 (merged with *o*-SbPh signals; *o*-phenylene), 134.02 (t, Sb*Ph* quaternary, $^{3}J_{C\text{-}F}$ = 15.0 Hz), 133.22 (*o*-phenylene), 132.11 (*p*-Sb*Ph*), 129.56 (t, *m*-Sb*Ph*, $^{3}J_{C\text{-}F}$ = 1.3 Hz), 123.36 (Sb*Ph* quaternary), 118.57 (*o*-phenylene), 110.31 (*o*-phenylene), 30.50 (Sb-*C*H$_3$). ^{19}F NMR (375.84 MHz, $CDCl_3$): δ -137.4 (d, $J_{H\text{-}F}$ = 10.1 Hz). Elemental analysis calculated (%) for $C_{19}H_{18}NF_2Sb$: C, 54.32; H, 4.32; found C, 54.58; H, 4.37.

Synthesis of [77]Br. In a 50 mL Schlenk flask, *n*-Butyllithium (2.2 M) in hexanes (0.8 mL, 1.8 mmol) was slowly added to a Et_2O solution (10 mL) of (2-bromophenyl)diphenylphosphine (0.613 g, 1.8 mmol) at -78 ºC. After stirring for 1 h, the

corresponding lithium salt formed as a white precipitate. The solvent was decanted off using a cannula fitted with a filter tip and the residue was washed with two portions of Et_2O (5 mL each). The lithium salt was then suspended in Et_2O (20 mL) and cooled down to -78 °C. This mixture was slowly transferred to a solution of Ph_3SbBr_2 in THF (5 mL) via cannula. After stirring at room temperature for 3 h, an off-white solid precipitated out of solution. The solid was collected by filtration and washed with two portions of Et_2O (5 mL each) to obtain [**77**]Br in 68 % yield (0.848 g, 1.2 mmol). ^{1}H NMR (399.508 MHz, $CDCl_3$): δ 7.82 (d, 6H, *o*-Sb*Ph*), 7.68-7.65 (m, 1H, *o*-phenylene), 7.56-7.33 (m, 11H), 7.27-7.11 (m, 10H). $^{13}C\{^1H\}$NMR (100.466 MHz, $CDCl_3$): δ 136.92 (d, P-bound *o*-phenylene quaternary, $^1J_{C\text{-}P} = 7.6$ Hz), 135.85 (Sb-bound *o*-phenylene quaternary), 135.35 (*o*-Sb*Ph*), 135.04 (broad, P*Ph* quaternary), 134.05 (*m*-P*Ph*), 133.03 (*p*-P*Ph*), 132.85 (*o*-phenylene), 131.08 (*o*-phenylene), 131.37 (*o*-phenylene), 130.84 (*p*-Sb*Ph*), 129.43 (*m*-Sb*Ph*), 129.13 (*o*-phenylene), 128.54 (d, *o*-P*Ph*, $^2J_{C\text{-}P} = 6.8$ Hz). ^{31}P NMR (161.720 MHz, $CDCl_3$): δ 18.9. Elemental analysis calculated (%) for $C_{36}H_{29}BrPSb$: C, 62.28; H, 4.21; found C, 62.39; H, 4.24.

Synthesis of [78]Br. A CH_2Cl_2 solution (5 mL) of [77]Br (0.105 g, 1.5×10^{-4} mol) was added dropwise to a stirred CH_2Cl_2 solution (5 mL) of (tht)AuCl (0.0485 g, 1.5×10^{-4} mol). After stirring for 15 min, the solvent was removed *in vacuo* and the residue was washed with two portions of Et_2O (3 mL each) to afford [**78**]Br as a pale yellow solid in 82 % yield (0.115 g, 1.2×10^{-4} mol). Single crystals of [**78**]Br were obtained as yellow blocks by diffusing Et_2O into a saturated CH_2Cl_2 solution at ambient temperature. ^{1}H NMR (399.508 MHz, $CDCl_3$): δ 7.82 (d, 6H, *o*-Sb*Ph*), 7.60-7.50 (m, 3H, *o*-phenylene),

7.47-7.28 (m, 15H), 7.22 (pseudo t, 4H, *o*-P*Ph*). $^{13}C\{^{1}H\}$NMR (100.466 MHz, $CDCl_3$): δ 141.21 (Sb*Ph* quaternary), 136.32 (Sb-bound *o*-phenylene quaternary), 136.72 (*o*-phenylene), 136.13 (*o*-Sb*Ph*), 135.16 (d, P-bound *o*-phenylene quaternary, $^{1}J_{C\text{-}P}$ = 19.1 Hz), 135.16 (d, P*Ph* quaternary, $^{1}J_{C\text{-}P}$ = 9.6 Hz), 134.51 (*o*-phenylene), 134.42 (*m*-Sb*Ph*), 133.81 (*p*-Sb*Ph*), 133.63 (*o*-phenylene), 132.96 (d, *o*-P*Ph*, $^{2}J_{C\text{-}P}$ = 2.0 Hz), 132.04 (d, *o*-P*Ph*, $^{2}J_{C\text{-}P}$ = 10.2 Hz), 131.86 (broad). ^{31}P NMR signal could not be obtained. Elemental analysis calculated (%) for $C_{36}H_{29}AuBrClPSb$: C, 46.66; H, 3.15; found C, 46.78; H, 3.16.

Synthesis of [77][OTf]. In a glove box, AgOTf (0.072 g, 2.8×10^{-4} mol) was added to a stirred CH_2Cl_2 solution of [**77**]Br (0.194g, 2.8×10^{-4} mol). The reaction was stirred in the absence of light for 4 h, at which time it was filtered over a Celite plug. All volatiles were removed from the filtrate to give a sticky, colorless oil, which was triturated with two portions of Et_2O (3 mL each) to afford [**77**][OTf]. Single crystals of [**77**][OTf] were obtained as colorless blocks by diffusing pentane into a $CDCl_3$ solution. ^{1}H NMR (399.508 MHz, $CDCl_3$): δ 7.78-7.75 (m, 2H, *o*-phenylene), 7.70-7.68 (pseudo d, 7H, *o*-Sb*Ph* + *o*-phenylene, $^{3}J_{H\text{-}H}$ = 7.2 Hz), 7.65-7.59 (m, 4H., *o*-phenylene), 7.55 (pseudo t, 6H, *m*-Sb*Ph*), 7.33 (t, 2H, *p*-P*Ph*, $^{3}J_{H\text{-}H}$ = 8.0 Hz), 7.24 (merged with $CDCl_3$ signal; dt, 3H, *p*-Sb*Ph*, $^{3}J_{H\text{-}H}$ = 7.4 Hz, $^{5}J_{H\text{-}H}$ = 2.0 Hz), 6.97 (t, 4H, *m*-P*Ph*, $^{3}J_{H\text{-}H}$ = 8.4 Hz). $^{13}C\{^{1}H\}$NMR (100.466 MHz, $CDCl_3$): δ 142.00 (Sb-bound *o*-phenylene quaternary), 136.92 (Sb*Ph* quaternary), 136.64 (d, P-bound *o*-phenylene quaternary, $^{1}J_{C\text{-}P}$ = 32.3 Hz), 135.21 (d, *m*-P*Ph*, $^{3}J_{C\text{-}P}$ = 3.0 Hz), 134.24 (*o*-phenylene), 133.30 (*o*-phenylene), 133.09 (*o*-Sb*Ph*), 132.78 (*o*-Sb*Ph*), 132.77 (*o*-phenylene), 132.62 (*p*-Sb*Ph*), 130.91 (*m*-SbPh), 129.76 (*p*-P*Ph*), 128.98 (d, *o*-P*Ph*, $^{2}J_{C\text{-}P}$ = 8.0 Hz), 125.32 (d, P*Ph* quaternary, $^{1}J_{C\text{-}P}$ = 12.1 Hz) 120.8

(q, *C*$F_3SO_3^-$). ^{31}P NMR (161.720 MHz, $CDCl_3$): δ 11.3 (s). Elemental analysis calculated (%) for $C_{37}H_{29}F_3O_3PSSb$: C, 58.21; H, 3.83; found C, 58.11; H, 3.85.

Synthesis of [77][BPh$_4$]. An EtOH solution (3 mL) of $NaBPh_4$ (0,051 g, 1.5×10^{-4} mol) was added to a stirring CH_2Cl_2 solution (1 mL) [**77**]Br (0.104 g, 1.5×10^{-4} mol). A white precipitate began to form immediately and the reaction mixture was stirred at ambient temperature for 1 h. The solid was collected by filtration and washed with two portions of EtOH (2 mL each) followed by two portions of Et_2O (2 mL each) to afford [**77**][BPh_4] (0.129 g, 1.4×10^{-4} mol). Colorless single crystals of [**77**][BPh_4] suitable for X-ray diffraction were obtained by diffusing pentane into a THF solution at ambient temperature. ^{1}H NMR (399.508 MHz, $CDCl_3$): δ 7.72-7.68 (m, 1H, *o*-phenylene), 7.60 (t, 4H, *o*-P*Ph*, $^3J_{H\text{-}H}$ = 7.2 Hz), 7.49-7.43 (m, 15H, *o*-Sb*Ph* + *m*-Sb*Ph* + *o*-phenylene), 7.38 (broad, 11H, *o*-B*Ph*$_4^-$ + *o*-phenylene), 7.33 (t, 2H, *p*-P*Ph*, $^3J_{H\text{-}H}$ = 8.0 Hz), 7.24 (merged with $CDCl_3$ signal; t, 3H, *p*-Sb*Ph*, $^3J_{H\text{-}H}$ = 8.0 Hz), 6.95-6.89 (m, 12H, *m*-B*Ph*$_4^-$ + *m*-*P*Ph), 6.78 (t, 4H, *p*-B*Ph*$_4^-$, $^3J_{H\text{-}H}$ = 7.2 Hz). ^{13}C{^{1}H}NMR (100.466 MHz, $CDCl_3$): δ 164.25 (q, BPh_4^- quaternary, $^1J_{C\text{-}B}$ = 49.6 Hz), 142.53 (Sb-bound *o*-phenylene), 137.25 (*o*-phenylene), 136.58 (*o*-phenylene), 136.54 (*o*-phenylene), 136.34 (B*Ph*$_4^-$), 134.88 (B*Ph*$_4^-$), 134.86, 134.77 (*o*-Sb*Ph*), 132.60 (*o*-P*Ph*, $^2J_{C\text{-}P}$ = 11.0 Hz), 132.35 (*o*-phenylene), 131.24 (*m*-Sb*Ph*), 130.40 (Sb*Ph* quaternary), 130.05 (o-phenylene), 129.12 (*m*-P*Ph*, $^3J_{C\text{-}P}$ = 7.7 Hz), 124.14 (d, P*Ph* quaternary, $^1J_{C\text{-}P}$ = 16.7 Hz), 125.40 (*o*-B*Ph*$_4^-$, $^2J_{C\text{-}B}$ = 5.8 Hz), 121.51 (*p*-Sb*Ph*). ^{31}P NMR (161.720 MHz, $CDCl_3$): δ 11.2 (s). Elemental analysis calculated (%) for $C_{60}H_{49}BPSb$: C, 77.19; H, 5.29; found C, 77.41; H, 5.33.

Synthesis of [78][OTf]. This salt was prepared by the similar procedure to prepare [**78**]Br. A CH_2Cl_2 solution (5 mL) of [**77**][OTf] (0.077 g, 1.0×10^{-4} mol) was added dropwise to a stirred CH_2Cl_2 solution (5 mL) of (tht)AuCl (0.032 g, 1.0×10^{-4} mol). After stirring for 15 min, the solvent was removed *in vacuo* and the residue was washed with two portions of Et_2O (3 mL each) to afford [**78**][OTf] as a colorless yellow solid in 88 % yield (0.087 g, 8.8×10^{-5} mol). Single crystals of [**78**][OTf] were obtained as colorless blocks by diffusing Et_2O into a saturated THF solution at ambient temperature. ^{1}H NMR (399.508 MHz, $CDCl_3$): δ 7.86-7.78 (m, 3H, *o*-phenylene), 7.71 (d, 6H, *o*-Sb*Ph*, $^{3}J_{H\text{-}H}$ = 9.2 Hz), 7.66-7.60 (m, 3H, *p*-P*Ph* + *o*-phenylene), 7.56-7.51 (m, 9H, *p*- and *m*-P*Ph*), 7.47-7.41 (m, 4H, *m*-P*Ph*), 7.24-7.18 (m, 4H, *o*-PPh + *o*-phenylene). ^{13}C{^{1}H}NMR (100.466 MHz, $CDCl_3$): δ 164.99 (Sb*Ph* quaternary), 139.88 (d, P-bound *o*-phenylene quaternary, $^{1}J_{C\text{-}P}$ = 16.5 Hz), 137.64 (*o*-phenylene), 137.55 (*o*-phenylene), 135.60 (*o*-Sb*Ph*), 134.35 (d, *m*-P*Ph*, $^{3}J_{C\text{-}P}$ = 12.0 Hz), 134.29 (Sb-bound quaternary), 133.58 (*p*-Sb*Ph*), 132.76 (d, *p*-P*Ph*, $^{4}J_{C\text{-}P}$ = 1.6 Hz), 131.28 (*m*-Sb*Ph*), 129.99 (d, *o*-P*Ph*, $^{2}J_{C\text{-}P}$ = 14.2 Hz), 126.90 (*o*-phenylene), 126.00 (*o*-phenylene), 124.93 (*o*-phenylene), 120.8 (q, *C*$F_3SO_3^-$). ^{31}P NMR (161.720 MHz, $CDCl_3$): δ 34.3 (s). Elemental analysis calculated (%) for $C_{37}H_{29}AuClF_3O_3PSSb$: C, 44.63; H, 2.94; found C, 44.71; H, 2.97.

Synthesis of [79][OTf]$_2$. In a 25 mL Schlenk tube, MeOTf (0.15 mL, 1.3×10^{-3} mol) was added to a solution of [**77**][OTf] (0.100 g, 1.3×10^{-4} mol) in toluene (3 mL). The mixture was sealed under N_2 atmosphere in a 25 mL Schlenk tube and heated for 90 ^{o}C for 12 h, after which a white precipitate formed. The solid was filtered, washed with three portions of Et_2O (5 mL each), and dried *in vacuo* to afford [**79**][OTf]$_2$ in 51 % yield

(172 mg, 1.6×10^{-4} mol). Single crystals of [**79**][OTf]$_2$ were obtained as colorless blocks by diffusing Et_2O into a MeOH solution. ^{1}H NMR (399.508 MHz, CD_3CN): δ 8.12-7.97 (m, 3H, *o*-phenylene), 7.81-7.76 (m, 6H, *o*-Sb*Ph*), 7.62 (t, 3H, *m*-Sb*Ph*, $^3J_{H\text{-}H}$ = 7.6 Hz), 7.51-7.44 (m, 14H, *p*-Sb*Ph* + P*Ph*). $^{13}C\{^1H\}$NMR (100.466 MHz, $CDCl_3$): δ 141.77 (d, P-bound *o*-phenylene quaternary, $^1J_{C\text{-}P}$ = 13.0 Hz), 141.23 (d, P*Ph* quaternary, $^1J_{C\text{-}P}$ = 11.9 Hz), 136.13 (d, *m*-PPh, $^3J_{C\text{-}P}$ = 8.0 Hz), 135.77 (*o*-Sb*Ph*), 134.39 (*o*-phenylene), 134.30 (m-Sb*Ph*), 133.63 (d, *p*-P*Ph*, $^4J_{C\text{-}P}$ = 3.0 Hz), 131.35 (*p*-Sb*Ph*), 130.82 (d, *o*-P*Ph*, $^2J_{C\text{-}P}$ = 9.9 Hz), 128.55 (d, *o*-phenylene, $^2J_{C\text{-}P}$ = 6.3 Hz), 126.03 (*o*-phenylene), 125.13 (*o*-phenylene), 129.43 (*m*-Sb*Ph*), 129.13 (*o*-phenylene), 128.54 (d, *o*-P*Ph*, $^3J_{C\text{-}P}$ = 6.8 Hz), 120.8 (q, *C*$F_3SO_3^-$), 118.33 (*o*-phenylene), 10.01 (d, P*C*H_3, $^1J_{C\text{-}P}$ = 50.5 Hz). ^{31}P NMR (161.720 MHz, $CDCl_3$): δ 25.2 (broad s). Elemental analysis calculated (%) for $C_{39}H_{32}F_6O_6PS_2Sb$: C, 50.50; H, 3.48; found C, 50.71; H, 3.51.

7.6 Future work

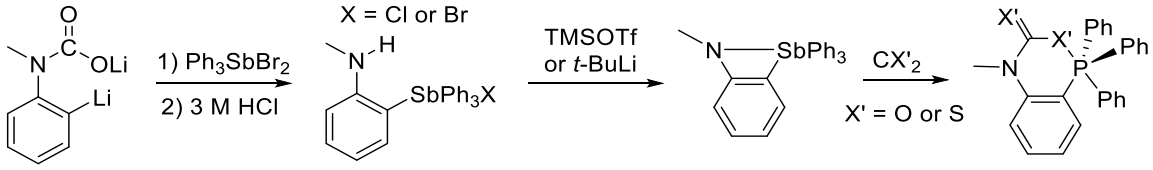

Figure 151. Proposed synthesis of amido-tetraarylstiborane for the activation of CO_2 or CS_2.

With the growing interest of metal-free activation of small molecules such as CO_2, we will continue to prepare and investigate ambiphilic compounds bearing antimony(V) moieties. Because of the instability of triarylhalostibonium moieties, the isolation of an antimony analog of amidophosphorane **3** was not successful. Tetraarylstibonium species, however, are significantly more stable yet exhibit strong Lewis acidity.[78, 118] With this in mind, we plan to seek whether tetraarylstibonium acceptors can be employed as an alternative of triarylhalostibonium cations for the preparation of amidotetraarylstiborane (Figure 151). Once we verify the stability of this amidotetraarylstiborane, we plan to examine its reactivity towards CO_2 and CS_2 to afford the corresponding adducts.

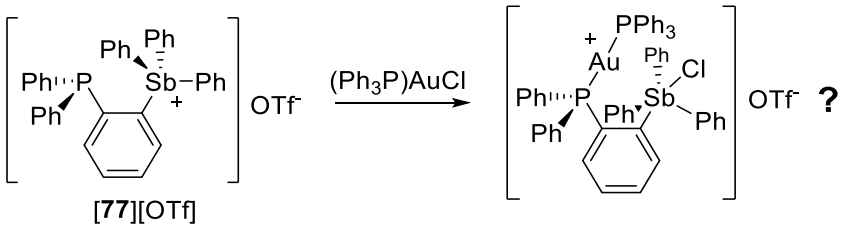

Figure 152. Proposed application of [**77**][OTf] for the silver-free activation of gold(I) pre-catalyst.

In this chapter, we reported the synthesis and the reactivity of *ortho*-phenylene-based phosphino-stibonium cation [**77**]$^+$. The reaction of [77][OTf] with (tht)AuCl resulted in the displacement of the labile tht ligand with the phosphine donor of [77]$^+$ while the chloride ligand remaining strongly bound to the gold(I) center ([78][OTf]). With this in mind, we propose to investigate the coordination of [77][OTf] with a gold(I) complex containing a stronger phosphine donor, (Ph_3P)AuCl, to generate a cationic gold(I) complex in the absence of silver salts. We will also monitor the catalytic behavior of this cationic gold(I) complex along with [78][OTf] towards simple organic transformations such as cyclization of propargylamides (reaction described in

Figure 137 f).

CHAPTER VIII

SUMMARY

8.1 Lewis acidic stiborafluorenes for fluoride sensing

In search of an effective fluoride sensor compatible in aqueous solution, we investigated the Lewis acidity of organoantimony(V) compounds as potential alternatives to previously reported triarylborane species. In particular, we focused on the study of stiborafluorene compounds because of their large steric opening to access the antimony(V) center for anion coordination. We prepared a series of organostiboranes containing (2,2'-biphenylene)phenylantimony subunit and catecholate (**32**), tetrachlorocatecholate (**11**), or 1,2-dihydroxyanthraquinone, also known as alizarin (**33**). DFT calculations reveal that the Lewis acidiy of these species arise from the precedence of a low lying Sb-C_{Ph} σ* orbital which resembles that of the LUMO of highly electrophilic fluorence cations. While **32** exhibit no measureable fluoride affinity in a 7/3 (v/v) THF/H_2O mixture, both **11** and **33** sufficiently bind fluorde ions under the same conditions with corresponding K_F values of 13,500 (± 1400) and 16,100 (± 1100) M^{-1}, respectively. The formation of the fluoride adducts [**11**-F]$^-$ and [**33**-F]$^-$ were verified by the two as tris(dimethylamino)sulfonium salts, which were fully characertized. While the conversion of **11** to [**11**-F]$^-$ showed no obvious colorimetric response, the fluoride complexation of **33** led to an immediate color change from yellow to dark red. This fluoride binding event is also accompanied by a drastic increase in fluorescence (at 616 nm) from Φ = 0.2% for **33** to 3.0% for [**33**-F]$^-$. With this dual colorimetric and fluorescent properties, **33** was applied to quantitatively

examine fluoride concentrations of tap or bottle water in biphasic H_2O/CH_2Cl_2 mixture which were in good agreement with the water quality reports generated for each water sample.

8.2 Bifunctional distiboranes for fluoride anion chelation

Previous studies show that polyfunctional or polydentate Lewis acids can greatly stabilize the Lewis base adducts via chelation effect. With this in mind, we synthesized the 9,9-dimethylxanthene-based distiborane **36** which the crystal structure reveals that the two square pyramidal stiborane subunits are oriented in a face-to-face fashion and the two antimony centers are separated by 4.7805(7) Å. The electronic structure of distiborane **36** was examined using computational methods. In the optimized structure, the LUMO of **36** is concentrated on both of the antimony centers via the combination of the two Sb-C_{Ph} σ* orbitals. Furthermore, the electrostatic potential surface map of **36** shows a large accumulation of positive character on the two antimony centers.

The reaction of **36** with fluoride ions in CH_2Cl_2 resulted in the formation of a bridging fluoroantimonate complex [**36**-μ_2-F]$^-$ which resembles to that of a highly stable $[Sb_2F_{11}]^-$ anion. We subsequently continued to investigate the fluoride binding property of **36** in aqueous media. Spectrophotometric fluoride titration was carried out in 9.5/0.5 (v/v) H_2O/THF mixture at pH of 4.34 and found that **36** is indeed an excellent chelator and readily binds fluoride with an associated K_F of 700 (± 30) M^{-1}. By contrast, the monofunctional analog **10** showed no signs of measurable fluoride affinity under the same conditions. Indeed, spectrophotometric acid-base titrations reveal that **36** is more acidic

by two orders of magnitude compared to its monofunctional analog **10**. To our knowledge, this is one of the first examples of neutral main-group compound that can competitively complexes fluoride ions in 95 % water solution.

8.3 Stibonium cations bearing polycyclic aromatic fluorophores for sensing fluoride in water

In 2012, our lab reported that (9-anthryl)triphenylstibonium cation ([**28**]$^+$) is a competent Lewis acid that can readily bind and detect fluoride ions in 9/1 (v/v) water/DMSO mixture at sub-ppm concentrations. This fluoride binding event is also accompanied by a marked increase of the 9-anthryl-based fluorescence. Despite this photophysical response, the excitation of this fluorostiborane requires radiation below the visible region (λ_{ex} = 375 nm) and the resulting fluorescence quantum yield is only modest (Φ_{FL} = 14.1 %).

To improve this system, we synthesized and exploited the photophysical properties of tetraarylstibonium cations bearing other polycyclic aromatic fluorophores including 1-phenanthryl, 1-pyrenyl and 3-peryelenyl substituents ([**37**]$^+$, [**38**]$^+$ and [**39**]$^+$, respectively). While the phenanthryl analog [**37**]$^+$ decomposed in a mixture of 9/1 (v/v) water/DMSO at acidic pH, the pyrenyl analog [**38**]$^+$ and the perylenyl analog [**39**]$^+$ effectively bound fluoride ions under these conditions yielding K_F of 10,000 (± 800) M^{-1} and 10,000 (± 500) M^{-1}, respectively. The conversion of [**38**]$^+$ into **38**-F induced an increase of fluorescence quantum yield from Φ_{FL} = 0.5 % to 5.2 %. This surge of fluorescence, however, occurs within the UV light region which makes it difficult to observe by a naked eye. By contrast,

the conversion of [**39**]$^+$ into **39**-F resulted in a marked increase of fluorescence from Φ_{FL} = 7.3 % to 59.2 %. Most importantly, the excitation of **39**-F occurs at the visible region (λ_{ex} = 423 nm) as opposed to the UV region for both **28**-F and **38**-F. Finally, [**39**]$^+$ selectively binds fluoride at pH = 4.8 and was applied to quantitatively measure sub-ppm concentrations of fluoride anions in drinking water samples.

8.4 Distibonium catalyst for hydrosilylation of benzaldehyde

Lewis acids are commonly used in the activation of electron-rich heteroatomic substrates such as carbonyls. As part of our ongoing interest in organoantimony(V) acceptors, we sought to exploit the inherent Lewis acidity of stibonium cations as catalysts for organic transformations. In particular, we investigated the catalytic behaviors of triflate (OTf^-) and tetrafluoroborate (BF_4^-) salts of *o*-phenylene-based distibonium dication [**42**]$^{2+}$ as well as salts of its monofunctional analog, [Ph_3MeSb]$^+$ toward hydrosilylation of benzaldehyde. Although both salts of [Ph_3MeSb]$^+$ are catalytically inactive at ambient temperature, [**42**][OTf]$_2$ moderately promotes the reaction with conversion of 11 % after 8 h at room temperature. Strikingly, [**42**][BF_4]$_2$ is a significantly more robust catalyst, leading to near complete conversion after 8 h under the same conditions. These observations indicate that 1) distibonium [**42**]$^{2+}$ is more catalytically active than its monofunctional analog and 2) the Lewis acidity of [**42**]$^{2+}$ with BF_4^- anions is greater than its OTf^- analog. We hypothesized that these findings are due to 1) the ability of [**42**]$^{2+}$ to chelate and activate the carbonyl substrate and 2) the weakly coordinating nature of BF_4^- anions. To rationalize this proposal, we crystallized [**42**]$^{2+}$ in the presence of DMF, an

electron-rich amide substrate. In the crystal, a DMF molecule is indeed chelating between the two antimony centers from its terminal oxygen atom which the NBO analysis reveals that the total stabilization energy of the Sb-O interactions is approximately 12 kcal mol^{-1}. Similar crystallization failed for $[Ph_3MeSb]^+$, exemplifying the significance of chelation effect to stabilize the corresponding Lewis base adduct.

8.5 Synthesis and characterization of bis-organoantimony(V) compounds with various Sb-Sb separations

From previous reports on bifunctional Lewis acids, the proximity of the two Lewis acidic sites greatly impacts the reactivity of bifunctional acceptors. With this in minds, we prepared a series of distibine species and converted them into the corresponding organotantimony(V) compounds via oxidation or alkylation.

First, we attempted to access the distiborane species incorporated into a naphthalene backbone. The reaction of distibine **46** with one equivalent of oxidants *o*-chloranil, $CuBr_2$, and $PhICl_2$ afforded the corresponding mixed valent Sb(III)-Sb(V) species **47**, **48**, and **49**, respectively. NBO analysis reveals that the Sb(III)→Sb(V) interactions in all of these compounds are approximately 10 kcal mol^{-1}. Because of these interactions, the antimony(III) centers of **47**, **48**, and **49** cannot participate in further oxidation. Similar conclusions were drawn for monocationic derivative $[\mathbf{51}]^+$.

Ferrocenyl distibine **56**, on the other hand, cleanly undergoes two-electron oxidation on both antimony centers using *o*-chloranil, Br_2, and $PhICl_2$ to afford the corresponding distiboranes **57**, **58**, and **59**, respectively. We found that the two antimony

centers of **57** can independently coordinate donor solvent molecules such as THF. This is an attribute to the ability of **57** to rotate along the $Cp_{centroid}$-Fe-$Cp_{centroid}$ axis. Also, the crystal structures of **58** and **59** demonstrated that the two distiboranes can adopt either staggered or eclipsed conformation in the solid state, indicating that the thermodynamical stability are similar between the two orientations. The two antimony centers of **56** were also alkylated with MeOTf to afford the corresponding dicationic [**60**][OTf]$_2$. This compound was tested as a catalyst for hydrosilylation of benzaldehyde in $CDCl_3$. Unlike the ortho-phenylene derivative [**42**]$^{2+}$, [**60**]$^{2+}$ showed no measurable catalytic behavior even at elevated temperature. This lack of reactivity arises from the freely rotating ferrocene backbone which prevents the two antimony centers to strongly chelate the carbonyl substrate for electrophilic activation.

Dibenzofuran-based distiborane **64** was also synthesized by the reaction of disitbine **63** with 2 equivalents of *o*-chloranil. Single crystals of this distiborane compound was crystalized in the presence of THF. Although the two antimony centers are largely separated (~6 Å), only one of two coordinated a THF molecule as a consequence of steric effects.

Finally, we prepared *ortho*-distiboranes bearing tetrachlorocatecholate ligand (**65**) and perfluorophenanthrenediyl-9,10-dioxy ligand (**67**). Both of these distiboranes bind fluoride ions to afford the corresponding bridging antimonate species [**65**-μ_2-F]$^-$ and [**67**-μ_2-F]$^-$. Computational studies reveal that the fluoride ion affinities are 378.4 kJ mol^{-1} for **65** and 388.1 kJ mol^{-1} for **67**. These values exceed that of 9,9-dimethylxanthene-based distiborane **36** (FIA = 359.88 kJ mol^{-1}), thus indicating that **65** and **67** are more

fluorophilic than **36**. Indeed, competition experiment between [**65**-μ_2-F]$^-$ and equimolar amounts of **36** quantitatively affords **65** and [**36**-μ_2-F]$^-$ in $CDCl_3$.

8.6 Designing antimony(V)-based ambiphilic compounds

Compounds bearing both Lewis acidic- and basic-sites, also known as ambiphilic compounds, have become widely utilized as ligands toward transition metals and for FLP chemistry. Most common ambiphilic compounds contain boron- or aluminum-based moieties or more recently phosphonium subunits as the Lewis acceptors. By contrast, organoantimony(V) Lewis acids are less frequently employed despite their strong electrophilic nature.

We first attempted to synthesize an antimony analog of amidofluorophosphorane **3** which activates and strongly coordinates CO_2 under mild conditions. Although the synthetic approach proceeded smoothly up to the preparation of aminodifluorostiborane **76**, further modification failed due to the instability of the triarylhalostibonium moiety. We are currently pursuing to develop a method to stabilize such intermediate species for further reactivity.

We also synthesized a tetraarylstibonium compound bearing a pendant phosphine donor ([**77**]Br). We found that the nuclephilicity of the phosphine moiety in this compound is unquenched and the treatment of [**77**]Br with (tht)AuCl afforded the corresponding gold(I) complex [**78**]Br. The crystal structure of [**78**]Br reveals that the chloride and the bromide anions exchange upon complexation, leading to the formation of Sb-Cl and Au-Br bonds. Next, we decided to exchange the bromide ligand of [**77**]Br to a

more weakly coordinating anion to enhance the Lewis acidity of the antimony(V) center. The reaction of [**77**]Br with AgOTf and $NaPh_4$ cleanly afforded phosphino-stibonium salts [**77**][OTf] and [**77**][BPh_4]. The crystal structures of both salts suggest the possibility of donor-acceptor interactions between the phosphine donors and the tetraarylstibonium acceptors. The precedence of these interactions in [**77**]$^+$ were confirmed by NBO analysis which estimated the associated deletion energy (E_{del}) of approximately 14 kcal mol^{-1}. While the reaction of [**77**][BPh_4] with (tht)AuCl resulted in a decomposition product, [**77**][OTf] cleanly coordinated a Au(I)Cl fragment to afford [**78**]OTf in quantitative yield. The solid state structure of [**78**]OTf reveals that the proximity of Au-Sb is shorter than that of [**78**]Br, thereby indicating that the tetraarylstibonium moiety is more Lewis acidic with a weakly coordinating triflate anion as opposed to a chloride anion.

Lastly, [**77**][OTf] was treated with MeOTf to afford the corresponding phosphonium-stibonium dication [**79**][$OTf]_2$. Computational studies reveal that the LUMO+1 is composed by the combination of both P-C_{Ph} and Sb-C_{Ph} σ* orbitals, thus suggesting that [**79**][$OTf]_2$ is potentially a bifunctional Lewis acid. However, unlike [**42**]$^{2+}$, isolation of a DMF adduct failed because of the steric hindrance about the binding site.

REFERENCES

(1) Babbini, D. C.; Mulligan, F. L.; Schulhauser, H. R.; Sweigart, T. C.; Nichol, G. S.; Hurst, S. K., *Inorg. Chem.* **2010,** *49* (9), 4307-4312.

(2) Wittig, G.; Schöllkopf, U., *Chem. Ber.* **1954,** *87* (9), 1318-1330.

(3) Wong, C. Y.; Kennepohl, D. K.; Cavell, R. G., *Chem. Rev.* **1996,** *96* (6), 1917-1952.

(4) Well, M.; Jones, P. G.; Schmutzler, R., *J. Fluorine Chem.* **1991,** *53* (2), 261-275.

(5) The, K. I.; Vande Griend, L.; Whitla, W. A.; Cavell, R. G., *J. Am. Chem. Soc.* **1977,** *99* (22), 7379-7380.

(6) Hounjet, L. J.; Caputo, C. B.; Stephan, D. W., *Angew. Chem. Int. Ed.* **2012,** *51* (19), 4714-4717.

(7) Gutmann, V.; Hubacek, H.; Steininger, A., *Monatsh. Chem.* **1964,** *95* (3), 678-86.

(8) Gutmann, V.; Mairinger, F., *Z. Anorg. Allg. Chem.* **1957,** *289* (5-6), 279-287.

(9) Baaz, M.; Gutmann, V.; Masaguer, J. R., *Monatsh. Chem. Verw. Tl. 92* (3), 590-599.

(10) Mallouk, T. E.; Rosenthal, G. L.; Mueller, G.; Brusasco, R.; Bartlett, N., *Inorg. Chem.* **1984,** *23* (20), 3167-3173.

(11) Krossing, I.; Raabe, I., *Chem. Eur. J.* **2004,** *10* (20), 5017-5030.

(12) Bohrer, H.; Trapp, N.; Himmel, D.; Schleep, M.; Krossing, I., *Dalton Trans.* **2015,** *44* (16), 7489-7499.

(13) Olah, G. A.; Tolgyesi, W. S.; Kuhn, S. J.; Moffatt, M. E.; Bastien, I. J.; Baker, E. B., *J. Am. Chem. Soc.* **1963,** *85*, 1328-34.

(14) Olah, G. A.; Baker, E. B.; Evans, J. C.; Tolgyesi, W. S.; McIntyre, J. S.; Bastien, I. J., *J. Am. Chem. Soc.* **1964,** *86* (7), 1360-73.

(15) Olah, G. A.; Lukas, J., *J. Am. Chem. Soc.* **1967,** *89* (9), 2227-2228.

(16) Olah, G. A.; Schlosberg, R. H., *J. Am. Chem. Soc.* **1968,** *90* (10), 2726-2727.

(17) Commeyras, A.; Olah, G. A., *J. Am. Chem. Soc.* **1969,** *91* (11), 2929-2942.

(18) Olah, G. A.; Klopman, G.; Schlosberg, R. H., *J. Am. Chem. Soc.* **1969,** *91* (12), 3261-3268.

(19) Hammett, L. P.; Deyrup, A. J., *J. Am. Chem. Soc.* **1932,** *54* (7), 2721-2739.

(20) Reed, C. A., *Chem. Commun.* **2005,** (13), 1669-1677.

(21) Olah, G. A.; Comisarow, M. B.; Cupas, C. A.; Pittman, C. U., *J. Am. Chem. Soc.* **1965,** *87* (13), 2997-2998.

(22) Olah, G.; Lukas, J., *J. Am. Chem. Soc.* **1968,** *90* (4), 933-938.

(23) Olah, G. A.; Parker, D. G.; Yoneda, N.; Pelizza, F., *J. Am. Chem. Soc.* **1976,** *98* (8), 2245-2250.

(24) Mootz, D.; Bartmann, K., *Angew. Chem.* **1988,** *100* (3), 424-5.

(25) Bickel, A. F.; Gaasbeek, C. J.; Hogeveen, H.; Oelderik, J. M.; Platteeuw, J. C., *Chem. Comm.* **1967,** (13), 634-635.

(26) Hogeveen, H.; Bickel, A. F., *Chem. Comm.* **1967,** (13), 635-636.

(27) Askew, H. F.; Gates, P. N.; Muir, A. S., *Journal of Raman Spectroscopy* **1991,** *22* (5), 265-274.

(28) Snyder, S. A.; Treitler, D. S., *Angew. Chem. Int. Ed.* **2009,** *48* (42), 7899-7903.

(29) Snyder, S. A.; Treitler, D. S.; Brucks, A. P., *J. Am. Chem. Soc.* **2010,** *132* (40), 14303-14314.

(30) Snyder, S. A.; Treitler, D. S.; Schall, A., *Tetrahedron* **2010,** *66* (26), 4796-4804.

(31) Wittig, G.; Clauß, K., *Liebigs Ann. Chem.* **1952,** *577* (1), 26-39.

(32) Wheatley, P. J., *J. Chem. Soc.* **1964,** (0), 3718-3723.

(33) Beauchamp, A. L.; Bennett, M. J.; Cotton, F. A., *J. Am. Chem. Soc.* **1968,** *90* (24), 6675-6680.

(34) Brabant, C.; Hubert, J.; Beauchamp, A. L., *Can. J. Chem.* **1973,** *51* (17), 2952-2957.

(35) García-Monforte, M. A.; Alonso, P. J.; Ara, I.; Menjón, B.; Romero, P., *Angew. Chem. Int. Ed.* **2012,** *51* (11), 2754-2757.

(36) Breunig, H. J.; Koehne, T.; Moldovan, O.; Preda, A. M.; Silvestru, A.; Silvestru, C.; Varga, R. A.; Piedra-Garza, L. F.; Kortz, U., *J. Organomet. Chem.* **2010,** *695* (9), 1307-1313.

(37) Lim, Y. Y.; Drago, R. S., *Inorg. Chem.* **1972,** *11* (1), 202-204.

(38) Nishii, N.; Matsumura, Y.; Okawara, R., *J. Organomet. Chem.* **1971,** *30* (1), 59-65.

(39) Nishii, N.; Hashimoto, K.; Okawara, R., *J. Organomet. Chem.* **1973,** *55* (1), 133-137.

(40) Tunde Bamgboye, T.; Begley, M. J.; Bryan Sowerby, D., *J. Organomet. Chem.* **1989,** *362* (1–2), 77-85.

(41) Bordner, J.; Doak, G. O.; Peters, J. R., *J. Am. Chem. Soc.* **1974,** *96* (21), 6763-6765.

(42) Hall, M.; Sowerby, D. B., *J. Am. Chem. Soc.* **1980,** *102* (2), 628-632.

(43) Dodonov, V. A.; Fedorov, A. Y.; Fukin, G. K.; Zaburdyaeva, S. N.; Zakharov, L. N.; Ignatenko, A. V., *Main Group Chem.* **1999,** *3*, 15-22.

(44) Holmes, R. R.; Day, R. O.; Chandrasekhar, V.; Holmes, J. M., *Inorg. Chem.* **1987,** *26* (1), 163-168.

(45) Biros, S. M.; Bridgewater, B. M.; Villeges-Estrada, A.; Tanski, J. M.; Parkin, G., *Inorg. Chem.* **2002,** *41* (15), 4051-4057.

(46) Holmes, R. R.; Day, R. O.; Chandrasekhar, V.; Holmes, J. M., *Inorg. Chem.* **1987,** *26* (1), 157-163.

(47) Cherkasov, V. K.; Grunova, E. V.; Poddel'sky, A. I.; Fukin, G. K.; Kurskii, Y. A.; Abakumova, L. G.; Abakumov, G. A., *J. Organomet. Chem.* **2005,** *690* (5), 1273-1281.

(48) Cherkasov, V. K.; Abakumov, G. A.; Grunova, E. V.; Poddel'sky, A. I.; Fukin, G. K.; Baranov, E. V.; Kurskii, Y. V.; Abakumova, L. G., *Chem. Eur. J.* **2006,** *12*, 3916-3927.

(49) Abakumov, G. A.; Vavilina, N. N.; Kurskii, Y. A.; Abakumova, L. G.; Fukin, G. K.; Cherkasov, V. K.; Shavyrin, A. S.; Baranov, E. V., *Russ. Chem. Bull.* **2007,** *56* (9), 1813-1820.

(50) Arsenyev, M. V.; Shurygina, M. P.; Poddel'sky, A. I.; Druzhkov, N. O.; Chesnokov, S. A.; Fukin, G. K.; Cherkasov, V. K.; Abakumov, G. A., *J. Polym. Res.* **2013,** *20* (3), 1-9.

(51) Smolyaninov, I. V.; Poddel'skii, A. I.; Antonova, N. A.; Smolyaninova, S. A.; Berberova, N. T., *Russ. J. Coord. Chem.* **2013,** *39* (2), 165-174.

(52) Poddel'sky, A. I.; Baranov, E. V.; Fukin, G. K.; Cherkasov, V. K.; Abakumov, G. A., *J. Organomet. Chem.* **2013,** *733*, 44-48.

(53) Poddel'sky, A. I.; Smolyaninov, I. V.; Berberova, N. T.; Fukin, G. K.; Cherkasov, V. K.; Abakumov, G. A., *J. Organomet. Chem.* **2015,** *789–790*, 8-13.

(54) Shen, K.-W.; McEwen, W. E.; La Placa, S. J.; Hamilton, W. C.; Wolf, A. P., *J. Am. Chem. Soc.* **1968,** *90* (7), 1718-1723.

(55) Rüther, R.; Huber, F.; Preut, H., *J. Organomet. Chem.* **1985,** *295* (1), 21-28.

(56) Sharutin, V. V.; Sharutina, O. K.; Pakusina, A. P.; Smirnova, S. A.; Pushilin, M. A., *Russ. J. Coord. Chem.* **2005,** *31* (2), 108-114.

(57) Sharutin, V. V.; Sharutina, O. K.; Pakusina, A. P.; Platonova, T. P.; Zadachina, O. P.; Gerasimenko, A. V., *Russ. J. Coord. Chem.* **2003,** *29* (2), 89-92.

(58) Wang, G.-C.; Xiao, J.; Yu, L.; Li, J.-S.; Cui, J.-R.; Wang, R.-Q.; Ran, F.-X., *J. Organomet. Chem.* **2004,** *689* (9), 1631-1638.

(59) Sharutin, V. V.; Pakusina, A. P.; Zadachina, O. P.; Sharutina, O. K.; Gerasimenko, A. V.; Pushilin, M. A., *Russ. J. Coord. Chem.* **2004,** *30* (6), 397-402.

(60) Sharutin, V. V.; Molokova, O. V.; Sharutina, O. K.; Akimova, T. I.; Gerasimenko, A. V.; Pushilin, M. A., *Russ. J. Coord. Chem.* **2004,** *30* (8), 559-565.

(61) Egorova, I. V.; Zhidkov, V. V.; Grinishak, I. P.; Rakhanskii, A. A., *Russ. J. Gen. Chem.* **2014,** *84* (7), 1371-1373.

(62) Sharutin, V. V.; Sharutina, O. K.; Molokova, O. V.; Ettenko, E. N.; Krivolapov, D. B.; Gubaidullin, A. T.; Litvinov, I. A., *Russ. J. Gen. Chem.* **2004,** *71* (8), 1243-1247.

(63) Knop, O.; Vincent, B. R.; Cameron, T. S., *Can. J. Chem.* **1989,** *67* (1), 63-70.

(64) Baker, L.-J.; Rickard, C. E. F.; Taylor, M. J., *J. Chem. Soc., Dalton Trans.* **1995,** (17), 2895-2899.

(65) Sharutin, V. V.; Pakusina, A. P.; Egorova, I. V.; Platonova, T. P.; Bukvetskii, B. V.; Popov, D. Y., *Russ. J. Coord. Chem.* **2001,** *28* (12), 827-830.

(66) Sharutin, V. V.; Sharutina, O. K.; Bondar', E. A.; Pakusina, A. P.; Adonin, N. Y.; Starichenko, V. F.; Fukin, G. K.; Zakharov, L. N., *Russ. J. Coord. Chem.* **2001,** *27* (6), 393-397.

(67) Sharutin, V. V.; Sharutina, O. K.; Osipov, P. E.; Platonova, T. P.; Pakusina, A. P.; Fukin, G. K.; Zakharov, L. N., *Russ. J. Coord. Chem.* **2001,** *27* (7), 483-485.

(68) Sharutin, V. V.; Sharutina, O. K.; Bondar', E. A.; Pakusina, A. P.; Gatilov, Y. V.; Adonin, N. Y.; Starichenko, V. F., *Russ. J. Coord. Chem.* **2002,** *28* (5), 333-340.

(69) Sharutin, V. V.; Pakusina, A. P.; Smirnova, S. A.; Fukin, G. K., *Russ. J. Coord. Chem.* **2004,** *30* (6), 392-396.

(70) Sharutin, V. V.; Pakusina, A. P.; Senchurin, V. S.; Gerasimenko, A. V.; Gerasimenko, E. A., *Russ. J. Coord. Chem.* **2002,** *28* (8), 540-543.

(71) Ivanov, M. A.; Sharutin, V. V.; Ivanov, A. V.; Gerasimenko, A. V.; Antsutkin, O. N., *Russ. J. Coord. Chem.* **2008,** *34* (7), 527-535.

(72) Sharutin, V. V.; Molokova, O. V.; Sharutina, O. K., *Russ. J. Inorg. Chem.* **2013,** *58* (4), 400-405.

(73) Sharutin, V. V.; Sharutina, O. K.; Senchurin, S. V., *Russ. J. Inorg. Chem.* **2014,** *59* (9), 951-955.

(74) Ferguson, G.; Hawley, D. M., *Acta Crystallogr. B* **1974,** *30* (1), 103-111.

(75) Liu, R.-C.; Ma, Y.-Q.; Yu, L.; Li, J.-S.; Cui, J.-R.; Wang, R.-Q., *Appl. Organomet. Chem.* **2003,** *17* (9), 662-668.

(76) Sharutin, V. V.; Sharutina, O. K.; Platonova, T. P.; Pakusina, A. P.; Gerasimenko, A. V.; Gerasimenko, E. A.; Bukvetskii, B. V.; Popov, D. Y., *Russ. J. Coord. Chem.* **2003,** *29* (1), 11-15.

(77) Sharutin, V. V.; Sharutina, O. K.; Zadachina, O. P.; Litvinova, S. A.; Reutov, V. A.; Gerasimenko, A. V.; Gerasimenko, E. A.; Bukvetskii, B. V.; Popov, D. Y., *Russ. J. Coord. Chem.* **2003,** *29* (1), 6-10.

(78) Robertson, A. P. M.; Chitnis, S. S.; Jenkins, H. A.; McDonald, R.; Ferguson, M. J.; Burford, N., *Chem. Eur. J.* **2015,** *21* (21), 7902-7913.

(79) Low, J. N.; Ferguson, G.; Wardell, J. L., *Acta Crystallogr. C* **2000,** *56* (8), e317.

(80) Lloyd, M. A.; Brock, C. P., *Acta Crystallogr. B* **1997,** *53* (5), 773-779.

(81) Ferguson, G.; Glidewell, C.; Lloyd, D.; Metcalfe, S., *J. Chem. Soc., Perkin Trans. 2* **1988,** (5), 731-735.

(82) Sharutin, V. V.; Senchurin, V. S.; Fastovets, O. A.; Pakusina, A. P.; Sharutina, O. K., *Russ. J. Inorg. Chem.* **2009,** *54* (3), 389-395.

(83) Sharutin, V. V.; Pakusina, A. P.; Sharutina, O. K.; Kovaleva, O. A.; Gerasimenko, A. V.; Pushilin, M. A., *Russ. J. Coord. Chem.* **2004,** *30* (8), 541-549.

(84) Robertson, A. P. M.; Burford, N.; McDonald, R.; Ferguson, M. J., *Angew. Chem. Int. Ed.* **2014,** *53* (13), 3480-3483.

(85) Chitnis, S. S.; Robertson, A. P. M.; Burford, N.; Patrick, B. O.; McDonald, R.; Ferguson, M. J., *Chem. Sci.* **2015,** *6* (11), 6545-6555.

(86) Aaseth, J.; Shimshi, M.; Gabrilove, J. L.; Birketvedt, G. S., *J. Trace Elem. Exp. Med.* **2004,** *17* (2), 83-92.

(87) Briancon, D., *Rev. Rhum.* **1997,** *64* (2), 78-81.

(88) Vallejos-Sanchez, A. A.; Medina-Solis, C. E.; Casanova-Rosado, J. F.; Maupome, G.; Minaya-Sanchez, M.; Perez-Olivares, S., *Acta Odontol Scand.* **2006** *64* (4), 209-213.

(89) Kalia, L. V.; Lee, L.; Kalia, S. K.; Pirouzmand, F.; Rapoport, M. J.; Aviv, R. I.; Mozeg, D.; Symons, S. P., *Can. J. Neurol. Sci.* **2010,** *37* (02), 276-278.

(90) Kakumanu, N.; Rao, S. D., *New Engl. J. Med.* **2013,** *368* (12), 1140-1140.

(91) Carton, R. J., *Fluoride* **2006,** *39* (3), 163-172.

(92) Sebelius, K., *Federal Register* **2011,** *76*, 2383-2388.

(93) Chaniotakis, N.; Jurkschat, K.; Mueller, D.; Perdikaki, K.; Reeske, G., *Eur. J. Inorg. Chem.* **2004,** (11), 2283-2288.

(94) Badr, I. H. A.; Meyerhoff, M. E., *J. Am. Chem. Soc.* **2005,** *127* (15), 5318-5319.

(95) Marcus, Y., *J. Chem. Soc., Faraday Trans.* **1991,** *87* (18), 2995-2999.

(96) Schmidtchen, F. P.; Berger, M., *Chem. Rev.* **1997,** *97* (5), 1609-1646.

(97) Gerken, M.; Boatz, J. A.; Kornath, A.; Haiges, R.; Schneider, S.; Schroer, T.; Christe, K. O., *J. Fluorine Chem.* **2002,** *116* (1), 49-58.

(98) Light, T. S.; Cappuccino, C. C., *J. Chem. Educ.* **1975,** *52* (4), 247.

(99) Mitchell-Koch, J. T.; Malinowska, E.; Meyerhoff, M. E., *Electroanalysis* **2005,** *17* (15-16), 1347-1353.

(100) Mitchell-Koch, J. T.; Pietrzak, M.; Malinowska, E.; Meyerhoff, M. E., *Electroanalysis* **2006,** *18* (6), 551-557.

(101) Arancibia, J. A.; Rullo, A.; Olivieri, A. C.; Di Nezio, S.; Pistonesi, M.; Lista, A.; Fernandez Band, B. S., *Anal. Chim. Acta* **2004,** *512* (1), 157-163.

(102) Solé, S.; Gabbaï, F. P., *Chem. Commun.* **2004,** (11), 1284-1285.

(103) Yamaguchi, S.; Akiyama, S.; Tamao, K., *J. Am. Chem. Soc.* **2001,** *123* (46), 11372-11375.

(104) Katz, H. E., *J. Org. Chem.* **1985,** *50* (25), 5027-5032.

(105) Katz, H. E., *J. Am. Chem. Soc.* **1985,** *107* (5), 1420-1421.

(106) Williams, V. C.; Piers, W. E.; Clegg, W.; Elsegood, M. R. J.; Collins, S.; Marder, T. B., *J. Am. Chem. Soc.* **1999,** *121* (13), 3244-3245.

(107) Lewis, S. P.; Taylor, N. J.; Piers, W. E.; Collins, S., *J. Am. Chem. Soc.* **2003,** *125* (48), 14686-14687.

(108) Chase, P. A.; Henderson, L. D.; Piers, W. E.; Parvez, M.; Clegg, W.; Elsegood, M. R. J., *Organometallics* **2006,** *25* (2), 349-357.

(109) Dusemund, C.; Sandanayake, K. R. A. S.; Shinkai, S., *Chem. Commun.* **1995,** (3), 333-334.

(110) Lee, M. H.; Agou, T.; Kobayashi, J.; Kawashima, T.; Gabbaï, F. P., *Chem. Commun.* **2007,** (11), 1133-1135.

(111) Kim, Y.; Gabbaï, F. P., *J. Am. Chem. Soc.* **2009,** *131* (9), 3363-3369.

(112) Hudnall, T. W.; Gabbaï, F. P., *J. Am. Chem. Soc.* **2007,** *129* (39), 11978-11986.

(113) Hudnall, T. W.; Kim, Y.-M.; Bebbington, M. W. P.; Bourissou, D.; Gabbaï, F. P., *J. Am. Chem. Soc.* **2008,** *130* (33), 10890-10891.

(114) Wade, C. R.; Gabbaï, F. P., *Organometallics* **2011,** *30*, 4479-4481.

(115) Kojima, S.; Doi, Y.; Okuda, M.; Akiba, K.-y., *Organometallics* **1995,** *14* (4), 1928-1937.

(116) Moffett, K. D.; Simmler, J. R.; Potratz, H. A., *Anal. Chem.* **1956,** *28* (8), 1356-1356.

(117) Bowen, L. H.; Rood, R. T., *J. Inorg. Nucl. Chem.* **1966,** *28* (9), 1985-1990.

(118) Ke, I.-S.; Myahkostupov, M.; Castellano, F. N.; Gabbaï, F. P., *J. Am. Chem. Soc.* **2012,** *134* (37), 15309-15311.

(119) Corma, A.; García, H., *Chem. Rev.* **2003,** *103* (11), 4307-4366.

(120) Naidu, V. R.; Ni, S.; Franzén, J., *ChemCatChem* **2015,** *7* (13), 1896-1905.

(121) Klare, H. F. T.; Oestreich, M., *Dalton Trans.* **2010,** *39* (39), 9176-9184.

(122) Massey, A. G.; Park, A. J., *J. Organomet. Chem.* **1964,** *2* (3), 245-250.

(123) Erker, G., *Dalton Trans.* **2005,** (11), 1883-1890.

(124) Döring, S.; Erker, G.; Fröhlich, R.; Meyer, O.; Bergander, K., *Organometallics* **1998,** *17* (11), 2183-2187.

(125) Beckett, M. A.; Brassington, D. S.; Coles, S. J.; Hursthouse, M. B., *Inorg. Chem. Commun.* **2000,** *3* (10), 530-533.

(126) Jia, L.; Yang, X.; Stern, C.; Marks, T. J., *Organometallics* **1994,** *13* (10), 3755-7.

(127) Mu, Y.; Piers, W. E.; MacQuarrie, D. C.; Zaworotko, M. J.; Young, V. G., Jr., *Organometallics* **1996,** *15* (12), 2720-2726.

(128) Welch, G. C.; Stephan, D. W., *J. Am. Chem. Soc.* **2007,** *129* (7), 1880-1881.

(129) Chase, P. A.; Welch, G. C.; Jurca, T.; Stephan, D. W., *Angew. Chem. Int. Ed.* **2007,** *46* (42), 8050-8053.

(130) Chase, P. A.; Jurca, T.; Stephan, D. W., *Chem. Commun.* **2008,** (14), 1701-1703.

(131) Wang, H.; Frohlich, R.; Kehr, G.; Erker, G., *Chem. Commun.* **2008,** (45), 5966-5968.

(132) Hounjet, L. J.; Bannwarth, C.; Garon, C. N.; Caputo, C. B.; Grimme, S.; Stephan, D. W., *Angew. Chem. Int. Ed.* **2013,** *52* (29), 7492-7495.

(133) Greb, L.; Oña-Burgos, P.; Schirmer, B.; Grimme, S.; Stephan, D. W.; Paradies, J., *Angew. Chem. Int. Ed.* **2012,** *51* (40), 10164-10168.

(134) Greb, L.; Daniliuc, C.-G.; Bergander, K.; Paradies, J., *Angew. Chem. Int. Ed.* **2013,** *52* (22), 5876-5879.

(135) Segawa, Y.; Stephan, D. W., *Chem. Commun.* **2012,** *48* (98), 11963-11965.

(136) Tamke, S.; Daniliuc, C.-G.; Paradies, J., *Org. Biomol. Chem.* **2014,** *12* (45), 9139-9144.

(137) Chernichenko, K.; Madarász, Á.; Pápai, I.; Nieger, M.; Leskelä, M.; Repo, T., *Nat Chem* **2013,** *5* (8), 718-723.

(138) Mahdi, T.; Stephan, D. W., *Angew. Chem. Int. Ed.* **2015,** *54* (29), 8511-8514.

(139) Scott, D. J.; Simmons, T. R.; Lawrence, E. J.; Wildgoose, G. G.; Fuchter, M. J.; Ashley, A. E., *ACS Catal.* **2015,** *5* (9), 5540-5544.

(140) Werner, T., *Adv. Synth. Catal.* **2009,** *351* (10), 1469-1481.

(141) Bayne, J. M.; Stephan, D. W., *Chem. Soc. Rev.* **2016**.

(142) Mukaiyama, T.; Kashiwagi, K.; Matsui, S., *Chem. Lett.* **1989,** *18* (8), 1397-1400.

(143) Mukaiyama, T.; Matsui, S.; Kashiwagi, K., *Chem. Lett.* **1989,** *18* (6), 993-996.

(144) Terada, M.; Kouchi, M., *Tetrahedron* **2006,** *62* (2–3), 401-409.

(145) Caputo, C. B.; Hounjet, L. J.; Dobrovetsky, R.; Stephan, D. W., *Science* **2013,** *341*, 1374-1377.

(146) Nava, M.; Reed, C. A., *Organometallics* **2011,** *30* (17), 4798-4800.

(147) Pérez, M.; Hounjet, L. J.; Caputo, C. B.; Dobrovetsky, R.; Stephan, D. W., *J. Am. Chem. Soc.* **2013,** *135* (49), 18308-18310.

(148) Perez, M.; Qu, Z.-W.; Caputo, C. B.; Podgorny, V.; Hounjet, L. J.; Hansen, A.; Dobrovetsky, R.; Grimme, S.; Stephan, D. W., *Chem-Eur J* **2015,** *21* (17), 6491-6500.

(149) Perez, M.; Caputo, C. B.; Dobrovetsky, R.; Stephan, D. W., *Proc. Natl. Acad. Sci. U.S.A.* **2014,** *111* (30), 10917-10921.

(150) Mehta, M.; Holthausen, M. H.; Mallov, I.; Pérez, M.; Qu, Z.-W.; Grimme, S.; Stephan, D. W., *Angew. Chem.* **2015,** *127* (28), 8368-8372.

(151) Baba, A.; Kashiwagi, H.; Matsuda, H., *Tetrahedron Lett.* **1985,** *26* (10), 1323-1324.

(152) Baba, A.; Fujiwara, M.; Matsuda, H., *Tetrahedron Lett.* **1986,** *27* (1), 77-80.

(153) Fujiwara, M.; Baba, A.; Matsuda, H., *J. Heterocycl. Chem.* **1988,** *25* (5), 1351-1357.

(154) Fujiwara, M.; Baba, A.; Matsuda, H., *Bull. Chem. Soc. Jpn.* **1990,** *63* (4), 1069-1073.

(155) Fujiwara, M.; Imada, M.; Baba, A.; Matsuda, H., *Tetrahedron Lett.* **1989,** *30* (6), 739-742.

(156) Li, N.; Qiu, R.; Zhang, X.; Chen, Y.; Yin, S.-F.; Xu, X., *Tetrahedron* **2015,** *71* (25), 4275-4281.

(157) Pan, B.; Gabbaï, F. P., *J. Am. Chem. Soc.* **2014,** *136* (27), 9564-9567.

(158) Douvris, C.; Ozerov, O. V., *Science* **2008,** *321*, 1188-1190.

(159) Erickson, B. E., *Chem. Eng. News*, DOI:10.1021/CEN010611145659.

(160) Smith, T. A. D., *J. Labelled Compd. Radiopharm.* **2012,** *55* (8), 281-288.

(161) Wenzel, M.; Hiscock, J. R.; Gale, P. A., *Chem. Soc. Rev.* **2012,** *41*, 480-520.

(162) Bowman-James, K.; Bianchi, A.; Garcia-Espana, *Anion Coordination Chemistry*. Wiley-VCH Verlag GmbH & Co. KGaA: 2012; pp 559.

(163) Gale, P. A., *Chem. Commun.* **2011,** *47*, 82-6.

(164) Kim, S.-K.; Sessler, J. L., *Chem. Soc. Rev.* **2010,** *39*, 3784-3809.

(165) Kang, S.-O.; Llinares, J. M.; Day, V. W.; Bowman-James, K., *Chem. Soc. Rev.* **2010,** *39*, 3980-4003.

(166) Anzenbacher, P., Jr., *Top. Heterocycl. Chem.* **2010,** *24*, 205-235.

(167) Amendola, V.; Fabbrizzi, L.; Mosca, L., *Chem. Soc. Rev.* **2010,** *39*, 3889-3915.

(168) Cametti, M.; Rissanen, K., *Chem. Commun.* **2009**, 2809-2829.

(169) Yoon, J.; Kim, S. K.; Singh, N. J.; Kim, K. S., *Chem. Soc. Rev.* **2006,** *35*, 355-360.

(170) Sessler, J. L.; Camiolo, S.; Gale, P. A., *Coord. Chem. Rev.* **2003,** *240* (1-2), 17-55.

(171) Beer, P. D.; Gale, P. A., *Angew. Chem. Int. Ed.* **2001,** *40* (3), 486-516.

(172) Cametti, M.; Dalla Cort, A.; Mandolini, L.; Nissinen, M.; Rissanen, K., *New J. Chem.* **2008,** *32* (7), 1113-1116.

(173) D'Souza, C. A.; McBride, W. J.; Sharkey, R. M.; Todaro, L. J.; Goldenberg, D. M., *Bioconjugate Chem.* **2011,** *22* (9), 1793-1803.

(174) Liu, Z.; Li, Y.; Lozada, J.; Schaffer, P.; Adam, M. J.; Ruth, T. J.; Perrin, D. M., *Angew. Chem. Int. Ed.* **2013,** *52* (8), 2303-2307.

(175) Bhalla, R.; Darby, C.; Levason, W.; Luthra, S. K.; McRobbie, G.; Reid, G.; Sanderson, G.; Zhang, W., *Chem. Sci.* **2014,** *5* (1), 381-391.

(176) Cheng, F.; Bonder, E. M.; Jäkle, F., *J. Am. Chem. Soc.* **2013,** *135* (46), 17286-17289.

(177) Zhao, H.; Leamer, L. A.; Gabbaï, F. P., *Dalton Trans.* **2013,** *42* (23), 8164-8178.

(178) De Vries, T. S.; Prokofjevs, A.; Vedejs, E., *Chem. Rev.* **2012,** *112* (7), 4246-4282.

(179) Wade, C. R.; Broomsgrove, A. E. J.; Aldridge, S.; Gabbaï, F. P., *Chem. Rev.* **2010,** *110* (7), 3958-3984.

(180) Hudnall, T. W.; Chiu, C.-W.; Gabbaï, F. P., *Acc. Chem. Res.* **2009,** *42* (2), 388-397.

(181) Hudson, Z. M.; Wang, S., *Acc. Chem. Res.* **2009,** *42*, 1584-1596.

(182) Agou, T.; Sekine, M.; Kobayashi, J.; Kawashima, T., *Chem. Eur. J.* **2009,** *15* (20), 5056-5062.

(183) Dielmann, F.; Moore, C. E.; Rheingold, A. L.; Bertrand, G., *J. Am. Chem. Soc.* **2013,** *135* (38), 14071-14073.

(184) Conrad, E.; Burford, N.; McDonald, R.; Ferguson, M. J., *J. Am. Chem. Soc.* **2009,** *131*, 17000-17008.

(185) Kim, Y.; Hudnall, T. W.; Bouhadir, G.; Bourissou, D.; Gabbaï, F. P., *Chem. Commun.* **2009**, 3729-3731.

(186) Ren, Y.; Kan, W. H.; Thangadurai, V.; Baumgartner, T., *Angew. Chem. Int. Ed.* **2012,** *51* (16), 3964-3968.

(187) Ohshita, J.; Matsui, S.; Yamamoto, R.; Mizumo, T.; Ooyama, Y.; Harima, Y.; Murafuji, T.; Tao, K.; Kuramochi, Y.; Kaikoh, T.; Higashimura, H., *Organometallics* **2010,** *29* (15), 3239-3241.

(188) Baumgartner, T.; Réau, R., *Chem. Rev.* **2006,** *106* (11), 4681-4727.

(189) Matano, Y.; Imahori, H., *Org. Biomol. Chem.* **2009,** *7* (7), 1258-1271.

(190) Hissler, M.; Dyer, P. W.; Réau, R., *Coord. Chem. Rev.* **2003,** *244* (1–2), 1-44.

(191) Jean, M., *Anal. Chim. Acta* **1971,** *57* (2), 438-439.

(192) Wade, C. R.; Ke, I.-S.; Gabbaï, F. P., *Angew. Chem. Int. Ed.* **2012,** *51* (2), 478-481.

(193) Lin, T.-P.; Nelson, R. C.; Wu, T.; Miller, J. T.; Gabbaï, F. P., *Chem. Sci.* **2012,** *3*, 1128-1136.

(194) Wade, C. R.; Lin, T.-P.; Nelson, R. C.; Mader, E. A.; Miller, J. T.; Gabbaï, F. P., *J. Am. Chem. Soc.* **2011,** *133*, 8948-8955.

(195) Zhao, H.; Gabbaï, F. P., *Nat. Chem.* **2010,** *2*, 984-990.

(196) Shindo, M.; Okawara, R., *Inorg. Nucl. Chem. Lett.* **1969,** *5*, 77-80.

(197) Fukin, G. K.; Zakharov, L. N.; Domrachev, G. A.; Fedorov, A. Y.; Zaburdyaeva, S. N.; Dodonov, V. A., *Russ. Chem. Bull.* **1999,** *48*, 1722-1732.

(198) Melaïmi, M.; Gabbaï, F. P., *J. Am. Chem. Soc.* **2005,** *127* (27), 9680-9681.

(199) Krüger, G. J.; Pistorius, C. W. F. T.; Heyns, A. M., *Acta Crystallogr. B* **1976,** *32* (10), 2916-2918.

(200) Martinez-Vargas, S.; Gomez-Tagle, P.; Yatsimirsky, A. K., *Inorg. Chim. Acta* **2011,** *373*, 226-232.

(201) Shoda, S.-i.; Shintate, K.; Ishihara, M.; Noguchi, M.; Kobayashi, A., *Chem. Lett.* **2007,** *36*, 16-17.

(202) Sathish, R. S.; Kumar, M. R.; Rao, G. N.; Kumar, K. A.; Janardhana, C., *Spectrochim. Acta A-M* **2007,** *66* (2), 457-461.

(203) Kubo, Y.; Ishida, T.; Minami, T.; James, T. D., *Chem. Lett.* **2006,** *35* (9), 996-997.

(204) Kubo, Y.; Kobayashi, A.; Ishida, T.; Misawa, Y.; James, T. D., *Chem. Commun.* **2005,** (22), 2846-2848.

(205) Kubo, Y.; Ishida, T.; Kobayashi, A.; James, T. D., *J. Mater. Chem.* **2005,** *15* (27-28), 2889-2895.

(206) Wade, C. R.; Gabbaï, F. P., *Dalton Trans.* **2009**, 9169-9175.

(207) DiCesare, N.; Lakowicz, J. R., *Anal. Biochem.* **2002,** *301* (1), 111-116.

(208) Frisch, M. J.; Trucks, G. W.; Schlegel, H. B.; Scuseria, G. E.; Robb, M. A.; Cheeseman, J. R.; Scalmani, G.; Barone, V.; Mennucci, B.; Petersson, G. A.; Nakatsuji, H.; Caricato, M.; Li, X.; Hratchian, H. P.; Izmaylov, A. F.; Bloino, J.; Zheng, G.; Sonnenberg, J. L.; Hada, M.; Ehara, M.; Toyota, K.; Fukuda, R.; Hasegawa, J.; Ishida, M.; Nakajima, T.; Honda, Y.; Kitao, O.; Nakai, H.; Vreven, T.; Montgomery, J., J. A.; ; Peralta, J. E.; Ogliaro, F.; Bearpark, M.; Heyd, J. J.; Brothers, E.; Kudin, K. N.; Staroverov, V. N.; Kobayashi, R.; Normand, J.; Raghavachari, K.; Rendell, A.; Burant, J. C.; Iyengar, S. S.; Tomasi, J.; Cossi, M.; Rega, N.; Millam, J. M.; Klene, M.; Knox, J. E.; Cross, J. B.; Bakken, V.; Adamo, C.; Jaramillo, J.; Gomperts, R.; Stratmann, R. E.; Yazyev, O.; Austin, A. J.; Cammi, R.; Pomelli, C.; Ochterski, J. W.; Martin, R. L.; Morokuma, K.; Zakrzewski, V. G.; Voth, G. A.; Salvador, P.; Dannenberg, J. J.; Dapprich, S.; Daniels, A. D.; Farkas, Ö.; Foresman, J. B.; Ortiz, J. V.; Cioslowski, J.; Fox, D. J., *Gaussian 09*, Revision B.01, Gaussian, Inc.: Wallingford, CT: 2009.

(209) Miehlich, B.; Savin, A.; Stoll, H.; Preuss, H., *Chem. Phys. Lett.* **1989,** *157* (3), 200-206.

(210) Lee, C. T.; Yang, W. T.; Parr, R. G., *Phys. Rev. B* **1988,** *37* (2), 785-789.

(211) Peterson, K. A., *J. Chem. Phys.* **2003,** *119* (21), 11099-11112.

(212) Hariharan, P. C.; Pople, J. A., *Theor. Chim. Acta* **1973,** *28* (3), 213-22.

(213) Hehre, W. J.; Ditchfield, R.; Pople, J. A., *J. Chem. Phys.* **1972,** *56* (5), 2257-2261.

(214) Manson, J.; Webster, C. E.; Pérez, L. M.; Hall, M. B., http://www.chem.tamu.edu/jimp2/index.html.

(215) Yee, E. L.; Gansow, O. A.; Weaver, M. J., *J. Am. Chem. Soc.* **1980,** *102* (7), 2278-2285.

(216) Tripier, R.; Platas-Iglesias, C.; Boos, A.; Morfin, J.-F.; Charbonnière, L., *Eur. J. Inorg. Chem.* **2010,** *2010* (18), 2735-2745.

(217) Lima, L. M. P.; Lecointre, A.; Morfin, J.-F.; de Blas, A.; Visvikis, D.; Charbonnière, L. J.; Platas-Iglesias, C.; Tripier, R., *Inorg. Chem.* **2011,** *50* (24), 12508-12521.

(218) Brugnara, A.; Topic, F.; Rissanen, K.; Lande, A. d. l.; Colasson, B.; Reinaud, O., *Chem. Sci.* **2014,** *5* (10), 3897-3904.

(219) Song, K. C.; Lee, K. M.; Kim, H.; Lee, Y. S.; Lee, M. H.; Do, Y., *J. Organomet. Chem.* **2012,** *713* (0), 89-95.

(220) Kubo, Y.; Yamamoto, M.; Ikeda, M.; Takeuchi, M.; Shinkai, S.; Yamaguchi, S.; Tamao, K., *Angew. Chem. Int. Ed.* **2003,** *42* (18), 2036-2040.

(221) Yamaguchi, S.; Shirasaka, T.; Akiyama, S.; Tamao, K., *J. Am. Chem. Soc.* **2002,** *124* (30), 8816-8817.

(222) Benjamin, S. L.; Levason, W.; Reid, G.; Warr, R. P., *Organometallics* **2012,** *31* (3), 1025-1034.

(223) Ke, I.-S.; Jones, J. S.; Gabbaï, F. P., *Angew. Chem. Int. Ed.* **2014,** *53* (10), 2633-2637.

(224) Hirai, M.; Gabbaï, F. P., *Chem. Sci.* **2014,** *5* (5), 1886-1893.

(225) Baker, L.-J.; Rickard, C. E. F.; Taylor, M. J., *Acta Crystallogr. C* **1999,** *55* (3), 335-337.

(226) Katz, H. E., *Inclusion Compd.* **1991,** *4*, 391-405.

(227) Melaïmi, M.; Sole, S.; Chiu, C.-W.; Wang, H.; Gabbaï, F. P., *Inorg. Chem.* **2006,** *45* (20), 8136-8143.

(228) Jiang, C.; Blacque, O.; Berke, H., *Chem. Commun.* **2009,** (37), 5518-5520.

(229) Zhao, H.; Gabbaï, F. P., *Organometallics* **2012,** *31* (6), 2327-2335.

(230) Wang, H.; Gabbaï, F. P., *Organometallics* **2005,** *24* (12), 2898-2902.

(231) CCDC 1027319 (**34**), 1027320 (**36**), 1027321 (TBA[**36**-μ_2-F]) and 1027322 (TBA[**10**-F]) contain the supplementary crystallographic data for this paper. These data can be obtained free of charge from The Cambridge Crystallographic Data Centre via www.ccdc.cam.ac.uk/data_request/cif.

(232) Lichtenberg, D.; Ahyayauch, H.; Alonso, A.; Goñi, F. M., *Trends Biochem. Sci.* **2013,** *38* (2), 85-93.

(233) Deno, N. C.; Jaruzelski, J. J.; Schriesheim, A., *J. Am. Chem. Soc.* **1955,** *77*, 3044-51.

(234) Lee, M. H.; Gabbaï, F. P., *Inorg. Chem.* **2007,** *46* (20), 8132-8138.

(235) Zhang, D.; Rettig, S. J.; Trotter, J.; Aubke, F., *Inorg. Chem.* **1996,** *35* (21), 6113-6130.

(236) Gillespie, R. J.; Moss, K. C., *J. Chem. Soc. A* **1966,** (0), 1170-1175.

(237) Batsanov, S. S., *Inorg. Mater.* **2001,** *37* (9), 871-885.

(238) Timoshkin, A. Y.; Frenking, G., *Organometallics* **2008,** *27* (3), 371-380.

(239) Zhao, H.; Reibenspies, J. H.; Gabbaï, F. P., *Dalton Trans.* **2013,** *42* (3), 608-610.

(240) Peterson, K. A.; Figgen, D.; Goll, E.; Stoll, H.; Dolg, M., *J. Chem. Phys.* **2003,** *119* (21), 11113-11123.

(241) Matsuo, S.; Kiyomiya, K.-i.; Kurebe, M., *Arch. Toxicol.* **1998,** *72* (12), 798-806.

(242) Zhou, Y.; Zhang, J. F.; Yoon, J., *Chemical Reviews* **2014,** *114* (10), 5511-5571.

(243) Xu, Z.; Kim, S. K.; Yoon, J., *Chem. Soc. Rev.* **2010,** *39*, 457-1466.

(244) Ribeiro, C.; Brogueira, P.; Lavareda, G.; Carvalho, C. N.; Amaral, A.; Santos, L.; Morgado, J.; Scherf, U.; Bonifácio, V. D. B., *Biosens. Bioelectron.* **2010,** *26* (4), 1662-1665.

(245) Wu, X.; Chen, X.-X.; Song, B.-N.; Huang, Y.-J.; Ouyang, W.-J.; Li, Z.; James, T. D.; Jiang, Y.-B., *Chem. Commun.* **2014,** *50* (90), 13987-13989.

(246) Lin, T.-P.; Ke, I.-S.; Gabbaï, F. P., *Angew. Chem. Int. Ed.* **2012,** *51*, 4985–4988.

(247) Jones, J. S.; Wade, C. R.; Gabbaï, F. P., *Angew. Chem. Int. Ed.* **2014,** *53*, 8876-8879.

(248) Wade, C. R.; Gabbai, F. P., *Z Naturforsch B* **2014,** *69* (11-12), 1199-1205.

(249) Hirai, M.; Gabbaï, F. P., *Angew. Chem. Int. Ed.* **2015,** *54* (4), 1205-1209.

(250) Jones, J. S.; Wade, C. R.; Gabbaï, F. P., *Organometallics* **2015,** *34* (11), 2647-2654.

(251) Yamaguchi, S.; Akiyama, S.; Tamao, K., *J. Am. Chem. Soc.* **2000,** *122* (28), 6793-6794.

(252) Yamaguchi, S.; Akiyama, S.; Tamao, K., *J. Organomet. Chem.* **2002,** *646* (1–2), 277-281.

(253) Dawson, W. R.; Windsor, M. W., *J. Phys. Chem.* **1968,** *72* (9), 3251-3260.

(254) Cordero, B.; Gomez, V.; Platero-Prats, A. E.; Reves, M.; Echeverria, J.; Cremades, E.; Barragan, F.; Alvarez, S., *Dalton Trans.* **2008,** (21), 2832-2838.

(255) Ferguson, G.; Glidewell, C.; Lloyd, D.; Metcalfe, S., *J. Chem. Soc. Perk. Trans. 2* **1988,** (5), 731-735.

(256) Knop, O.; Vincent, B. R.; Cameron, T. S., *Can. J. Chem.* **1989,** *67* (1), 63-70.

(257) Goel, R. G., *Can. J. Chem.* **1969,** *47* (24), 4607-4612.

(258) CCDC 1450667 (**37**-Br), 1450668 (**38**-F), 1450669 (**39**-Br), 1450670 (**39**-F) contain the supplementary crystallographic data for this paper. These data can be obtained free of charge from The Cambridge Crystallographic Data Centre via www.ccdc.cam.ac.uk/data_request/cif.

(259) Kimura, M.; Iwata, A.; Itoh, M.; Yamada, K.; Kimura, T.; Sugiura, N.; Ishida, M.; Kato, S., *Helv. Chim. Acta* **2006,** *89* (4), 747-783.

(260) Kathayat, R. S.; Finney, N. S., *J. Am. Chem. Soc.* **2013,** *135* (34), 12612-12614.

(261) Raphael Karikachery, A.; Lee, H. B.; Masjedi, M.; Ross, A.; Moody, M. A.; Cai, X.; Chui, M.; Hoff, C. D.; Sharp, P. R., *Inorg. Chem.* **2013,** *52* (7), 4113-4119.

(262) Bruker, SAINTPlus. *Data Reduction and Correction Program v. 6.2*, Bruker AXS, Madison, Wisconsin, USA, 2001.

(263) Sheldrick, G. M., SHELXTL-2008/4, *Structure Determination Software Suite*, Bruker AXS, Madison, Wisconsin, USA, 2008.

(264) Hounjet, L. J.; Caputo, C. B.; Stephan, D. W., *Dalton Trans.* **2013,** *42* (7), 2629-2635.

(265) Holthausen, M. H.; Mehta, M.; Stephan, D. W., *Angew. Chem. Int. Ed.* **2014,** *53* (25), 6538-6541.

(266) Holthausen, M. H.; Hiranandani, R. R.; Stephan, D. W., *Chem. Sci.* **2015,** *6* (3), 2016-2021.

(267) Holthausen, M. H.; Bayne, J. M.; Mallov, I.; Dobrovetsky, R.; Stephan, D. W., *J. Am. Chem. Soc.* **2015,** *137* (23), 7298-7301.

(268) Vaugeois, J.; Wuest, J. D., *J. Am. Chem. Soc.* **1998,** *120* (50), 13016-13022.

(269) Tschinkl, M.; Schier, A.; Riede, J.; Gabbaï, F. P., *Organometallics* **1999,** *18* (9), 1747-1753.

(270) Kostas, I. D.; Gruter, G.-J. M.; Akkerman, O. S.; Bickelhaupt, F.; Kooijman, H.; Smeets, W. J. J.; Spek, A. L., *Organometallics* **1996,** *15* (21), 4450-4458.

(271) Wuest, J. D., *Acc. Chem. Res.* **1999,** *32* (1), 81-89.

(272) King, J. B.; Gabbaï, F. P., *Organometallics* **2003,** *22* (6), 1275-1280.

(273) Ooi, T.; Takahashi, M.; Yamada, M.; Tayama, E.; Omoto, K.; Maruoka, K., *J. Am. Chem. Soc.* **2004,** *126* (4), 1150-1160.

(274) Levason, W.; McAuliffe, C. A.; Murray, S. G., *J. Organomet. Chem.* **1975,** *88* (2), 171-174.

(275) McCortney, B. A.; Jacobson, B. M.; Vreeke, M.; Lewis, E. S., *J. Am. Chem. Soc.* **1990,** *112* (9), 3554-3559.

(276) Henry, M. C.; Wittig, G., *J. Am. Chem. Soc.* **1960,** *82* (3), 563-564.

(277) Beckett, M. A.; Brassington, D. S.; Coles, S. J.; Hursthouse, M. B., *Inorg. Chem. Commun.* **2000,** *3* (10), 530-533.

(278) Kleerekoper, M., *Endocrin. Metab. Clin.* **1998,** *27*, 441.

(279) Schmidt, R. K.; Müther, K.; Mück-Lichtenfeld, C.; Grimme, S.; Oestreich, M., *J. Am. Chem. Soc.* **2012,** *134* (9), 4421-4428.

(280) Reed, A. E.; Curtiss, L. A.; Weinhold, F., *Chem. Rev.* **1988,** *88* (6), 899-926.

(281) Parks, D. J.; Piers, W. E., *J. Am. Chem. Soc.* **1996,** *118* (39), 9440-9441.

(282) Parks, D. J.; Blackwell, J. M.; Piers, W. E., *J. Org. Chem.* **2000,** *65* (10), 3090-3098.

(283) Beutner, G. L.; Denmark, S. E., *Top. Organomet. Chem.* **2013,** *44*, 55-90.

(284) Koller, J.; Bergman, R. G., *Organometallics* **2012,** *31* (7), 2530-2533.

(285) Liberman-Martin, A. L.; Bergman, R. G.; Tilley, T. D., *J. Am. Chem. Soc.* **2015,** *137* (16), 5328-5331.

(286) Calas, R., *J. Organomet. Chem.* **1980,** *200* (1), 11-36.

(287) Fry, J. L.; Orfanopoulos, M.; Adlington, M. G.; Dittman, W. P.; Silverman, S. B., *J. Org. Chem.* **1978,** *43* (2), 374-375.

(288) Doyle, M. P.; West, C. T.; Donnelly, S. J.; McOsker, C. C., *J. Organomet. Chem.* **1976,** *117*, 129.

(289) Glendening, E. D.; Badenhoop, J. K.; Reed, A. E.; Carpenter, J. E.; Bohmann, J. A.; Morales, C. M.; Weinhold, F., *NBO 5.9*, Theoretical Chemistry Institute, University of Wisconsin, Madison, WI, 2011.

(290) Carmalt, C. J.; Cowley, A. H.; Culp, R. D.; Jones, R. A.; Kamepalli, S.; Norman, N. C., *Inorg. Chem.* **1997,** *36* (13), 2770-2776.

(291) Wade, C. R.; Saber, M. R.; Gabbaï, F. P., *Heteroat. Chem* **2011,** *22* (3-4), 500-505.

(292) Jura, M.; Levason, W.; Reid, G.; Webster, M., *Dalton Trans.* **2008,** (42), 5774-5782.

(293) Wrackmeyer, B.; Dörfler, U.; Milius, W.; Herberhold, M., *Polyhedron* **1995,** *14* (11), 1425-1431.

(294) Appel, A.; Jäkle, F.; Priermeier, T.; Schmid, R.; Wagner, M., *Organometallics* **1996,** *15* (4), 1188-1194.

(295) Aldridge, S.; Bresner, C.; Fallis, I. A.; Coles, S. J.; Hursthouse, M. B., *Chem. Commun.* **2002,** (7), 740-741.

(296) Bresner, C.; Day, J. K.; Coombs, N. D.; Fallis, I. A.; Aldridge, S.; Coles, S. J.; Hursthouse, M. B., *Dalton Trans.* **2006,** (30), 3660-3667.

(297) Butler, I. R.; Cullen, W. R.; Ni, J.; Rettig, S. J., *Organometallics* **1985,** *4* (12), 2196-2201.

(298) Cullen, W. R.; Derek Woollins, J., *Coord. Chem. Rev.* **1981,** *39* (1–2), 1-30.

(299) Hayashi, T.; Kumada, M., *Acc. Chem. Res.* **1982,** *15* (12), 395-401.

(300) Hayashi, T.; Konishi, M.; Fukushima, M.; Mise, T.; Kagotani, M.; Tajika, M.; Kumada, M., *J. Am. Chem. Soc.* **1982,** *104* (1), 180-186.

(301) Mizuta, T.; Imamura, Y.; Miyoshi, K.; Yorimitsu, H.; Oshima, K., *Organometallics* **2005,** *24* (5), 990-996.

(302) Mizuta, T.; Aotani, T.; Imamura, Y.; Kubo, K.; Miyoshi, K., *Organometallics* **2008,** *27* (11), 2457-2463.

(303) Haenel, M. W.; Jakubik, D.; Rothenberger, E.; Schroth, G., *Chem. Ber.* **1991,** *124* (8), 1705-1710.

(304) Marimuthu, T.; Friedrich, H. B.; Bala, M. D., *Acta Crystallogr. E* **2011,** *67* (12), o3319.

(305) Vogl, E. M.; Bruckmann, J.; Krüger, C.; Haenel, M. W., *J. Organomet. Chem.* **1996,** *520* (1–2), 249-252.

(306) Vogl, E. M.; Bruckmann, J.; Kessler, M.; Krüger, C.; Haenel, M. W., *Chem. Ber.* **1997,** *130* (9), 1315-1319.

(307) Kamer, P. C. J.; van Leeuwen, P. W. N. M.; Reek, J. N. H., *Acc. Chem. Res.* **2001,** *34* (11), 895-904.

(308) Kuang, S.-M.; Fanwick, P. E.; Walton, R. A., *Inorg. Chem.* **2002,** *41* (2), 405-412.

(309) Pintado-Alba, A.; de la Riva, H.; Nieuwhuyzen, M.; Bautista, D.; Raithby, P. R.; Sparkes, H. A.; Teat, S. J.; Lopez-de-Luzuriaga, J. M.; Lagunas, M. C., *Dalton Trans.* **2004,** (21), 3459-3467.

(310) de la Riva, H.; Nieuwhuyzen, M.; Mendicute Fierro, C.; Raithby, P. R.; Male, L.; Lagunas, M. C., *Inorg. Chem.* **2006,** *45* (4), 1418-1420.

(311) Partyka, D. V.; Updegraff Iii, J. B.; Zeller, M.; Hunter, A. D.; Gray, T. G., *Dalton Trans.* **2010,** *39* (22), 5388-5397.

(312) Mayoral, M. J.; Ovejero, P.; Criado, R.; Cristina Lagunas, M.; Pintado-Alba, A.; Rosario Torres, M.; Cano, M., *J. Organomet. Chem.* **2011,** *696* (15–16), 2789-2796.

(313) Partyka, D. V.; Teets, T. S.; Zeller, M.; Updegraff, J. B.; Hunter, A. D.; Gray, T. G., *Chem. Eur. J.* **2012,** *18* (7), 2100-2112.

(314) Browne, A. R.; Deligonul, N.; Anderson, B. L.; Rheingold, A. L.; Gray, T. G., *Chem. Eur. J.* **2014,** *20* (52), 17552-17564.

(315) Kiplinger, J. L.; Richmond, T. G., *J. Am. Chem. Soc.* **1996,** *118* (7), 1805-1806.

(316) Harrison, D.; Stacey, M.; Stephens, R.; Tatlow, J. C., *Tetrahedron* **1963,** *19* (12), 1893-1901.

(317) Nunn, M.; Sowerby, D. B.; Wesolek, D. M., *J. Organomet. Chem.* **1983,** *251* (3), C45-C46.

(318) Zhao, X.-F.; Zhang, C., *Synthesis* **2007,** *2007* (04), 551-557.

(319) Neugebauer, W.; Clark, T.; Schleyer, P. v. R., *Chem. Ber.* **1983,** *116* (10), 3283-92.

(320) Bruce, P. G.; Freunberger, S. A.; Hardwick, L. J.; Tarascon, J.-M., *Nat Mater* **2012,** *11* (1), 19-29.

(321) Argyropoulos, D. S., *Oxidative Delignification Chemistry*. American Chemical Society: 2001; Vol. 785, p 548.

(322) Hrncir, D. C.; Rogers, R. D.; Atwood, J. L., *J. Am. Chem. Soc.* **1981,** *103* (14), 4277-4278.

(323) Cleaver, W. M.; Barron, A. R., *J. Am. Chem. Soc.* **1989,** *111* (24), 8966-8967.

(324) Power, M. B.; Ziller, J. W.; Barron, A. R., *Organometallics* **1993,** *12* (12), 4908-4916.

(325) Lewiński, J.; Zachara, J.; Grabska, E., *J. Am. Chem. Soc.* **1996,** *118* (28), 6794-6795.

(326) Lewiński, J.; Zachara, J.; Goś, P.; Grabska, E.; Kopeć, T.; Madura, I.; Marciniak, W.; Prowotorow, I., *Chem. Eur. J.* **2000,** *6* (17), 3215-3227.

(327) Kumar, S. S.; Singh, S.; Roesky, H. W.; Magull, J., *Inorg. Chem.* **2005,** *44* (5), 1199-1201.

(328) Uhl, W.; Jana, B., *Chem. Eur. J.* **2008,** *14* (10), 3067-3071.

(329) Uhl, W.; Jana, B., *Eur. J. Inorg. Chem.* **2009,** *2009* (26), 3942-3947.

(330) Uhl, W.; Halvagar, M. R.; Layh, M., *Chem. Commun.* **2009,** (28), 4269-4271.

(331) Uhl, W.; Reza Halvagar, M.; Claesener, M., *Chem. Eur. J.* **2009,** *15* (42), 11298-11306.

(332) Henthorn, J. T.; Lin, S.; Agapie, T., *J. Am. Chem. Soc.* **2015,** *137* (4), 1458-1464.

(333) Vankar, P. S.; Reddy, M. V. R.; Vankar, Y. D., *Org. Prep. Proced. Int.* **1998,** *30* (4), 373-400.

(334) Davies, A. G., *Tetrahedron* **2007,** *63* (42), 10385-10405.

(335) Razuvaev, G. A.; Brilkina, T. G., *B. Acad. Sci. CH+. 24* (8), 1653-1666.

(336) Satoh, W.; Masumoto, S.; Yamamoto, Y.; Akiba, K.-y., *Heteroat. Chem.* **2001,** *12* (5), 431-443.

(337) Fabre, B.; Lehmann, U.; Schluter, A. D., *Electrochim. Acta* **2001,** *46* (18), 2855-2861.

(338) Herberich, G. E.; Englert, U.; Fischer, A.; Wiebelhaus, D., *Eur. J. Inorg. Chem.* **2004,** (20), 4011-4020.

(339) Sakuda, E.; Funahashi, A.; Kitamura, N., *Inorg. Chem.* **2006,** *45* (26), 10670-10677.

(340) Sun, Y.; Ross, N.; Zhao, S. B.; Huszarik, K.; Jia, W. L.; Wang, R. Y.; Macartney, D.; Wang, S., *J. Am. Chem. Soc.* **2007,** *129*, 7510-7511.

(341) Venkatasubbaiah, K.; Nowik, I.; Herber, R. H.; Jäkle, F., *Chem. Commun.* **2007,** (21), 2154-2156.

(342) Cao, D.; Zhao, H.; Gabbaï, F. P., *New J. Chem.* **2011,** *35*, 2299-2305.

(343) Stephan, D. W.; Erker, G., *Chem. Sci.* **2014,** *5* (7), 2625-2641.

(344) Weicker, S. A.; Stephan, D. W., *Bull. Chem. Soc. Jpn.* **2015,** *88* (8), 1003-1016.

(345) Stephan, D. W.; Erker, G., *Angew. Chem. Int. Ed.* **2015,** *54* (22), 6400-6441.

(346) Stephan, D. W., *J. Am. Chem. Soc.* **2015,** *137* (32), 10018-10032.

(347) Paull, D. H.; Abraham, C. J.; Scerba, M. T.; Alden-Danforth, E.; Lectka, T., *Acc. Chem. Res.* **2008,** *41* (5), 655-663.

(348) Serdyuk, O. V.; Heckel, C. M.; Tsogoeva, S. B., *Org. Biomol. Chem.* **2013,** *11* (41), 7051-7071.

(349) Bouhadir, G.; Bourissou, D., *Chem. Soc. Rev.* **2016,** *45* (4), 1065-1079.

(350) Welch, G. C.; Juan, R. R. S.; Masuda, J. D.; Stephan, D. W., *Science* **2006,** *314* (5802), 1124-1126.

(351) Appelt, C.; Westenberg, H.; Bertini, F.; Ehlers, A. W.; Slootweg, J. C.; Lammertsma, K.; Uhl, W., *Angew. Chem. Int. Ed.* **2011,** *50* (17), 3925-3928.

(352) Devillard, M.; Nicolas, E.; Appelt, C.; Backs, J.; Mallet-Ladeira, S.; Bouhadir, G.; Slootweg, J. C.; Uhl, W.; Bourissou, D., *Chem. Commun.* **2014,** *50* (94), 14805-14808.

(353) Yang, H.; Gabbaï, F. P., *J. Am. Chem. Soc.* **2015,** *137* (41), 13425-13432.

(354) Yang, H.; Gabbaï, F. P., *J. Am. Chem. Soc.* **2014,** *136*, 10866–10869.

(355) Bart van Oort, A.; Budzelaar, P. H. M.; Frijns, J. H. G.; Guy Orpen, A., *J. Organomet. Chem.* **1990,** *396* (1), 33-47.

(356) Smirnova, E. S.; Echavarren, A. M., *Angew. Chem. Int. Ed.* **2013,** *52* (34), 9023-9026.

(357) Whited, M. T.; Rivard, E.; Peters, J. C., *Chem. Commun.* **2006,** (15), 1613-1615.